DESIGN AND SYNTHESES OF DYES FOR BIOLOGICAL APPLICATIONS

A Dissertation

by

CLIFERSON THIVIERGE

Submitted to the Office of Graduate Studies of
Texas A&M University
in partial fulfillment of the requirements for the degree of

DOCTOR OF PHILOSOPHY

May 2011

Major Subject: Chemistry

Design and Syntheses of Dyes for Biological Applications

DESIGN AND SYNTHESES OF DYES FOR BIOLOGICAL APPLICATIONS

A Dissertation

by

CLIFERSON THIVIERGE

Submitted to the Office of Graduate Studies of
Texas A&M University
in partial fulfillment of the requirements for the degree of

DOCTOR OF PHILOSOPHY

Approved by:

Chair of Committee,	Kevin Burgess
Committee Members,	Daniel Singleton
	Karen Wooley
	Andreas Holzenburg
Head of Department,	David Russell

May 2011

Major Subject: Chemistry

ABSTRACT

Design and Syntheses of Dyes for Biological Applications.

(May 2011)

Cliferson Thivierge, B.S., Florida Atlantic University

Chair of Advisory Committee: Dr. Kevin Burgess

The challenges in modern biological imaging applications are two-fold: (i) to develop better methods of imaging, and (ii) to develop dyes that are suitable for these methods. This dissertation deals with the design and synthesis of dyes mainly by modification of known dyes to make them suitable for modern biological applications.

Towards this aim, novel ways of derivatizing BODIPY dyes are explored. One method involves extending the conjugation *via* phenyl acetylene units, pushing fluorescence wavelengths near 600 nm. A different approach deals with C-H functionalization of BODIPY in which the fluors are functionalized with acrylate units, extending their fluorescence to the red. The BODIPY dyes developed are then incorporated in through-bond energy transfer cassettes. We examine the factors affecting energy transfer efficiencies by synthesizing analogs of the cassettes and also studying the electrochemical behavior of the donor and acceptor parts.

The concept of through-bond energy transfer is incorporated into conjugated polymers by random incorporation of BODIPY dyes into polyfluorenes. The ideal ratio of fluorene to BODIPY parts was found to be 4:1. The BODIPY doping agents result in

dispersed emissions when excited at the polyfluorene donors. Concurrently, the polyfluorene backbone acts as an energy harvester for the BODIPY dyes, in effect increasing their molar absorptivities.

Finally the use of BODIPY dyes as photodynamic therapeutic agents was examined. We found that BODIPY dyes are efficient at producing reactive oxygen species when halogens are attached directly on the BODIPY core. Furthermore, the mechanism of cell death by using such agents was elucidated. Attachment of the most promising agent to polyglutamic acid is done to promote the EPR effect. Lastly we develop a potentially new type of PDT agent that absorbs strongly above 800 nm, permitting its use in deep tissue PDT.

DEDICATION

for Johanne and Jacques to whom I owe so much

ACKNOWLEDGEMENTS

I would like to thank my committee chair, Professor Kevin Burgess, and my committee members, Prof. Singleton, Prof. Wooley, and Prof. Holzenburg, for their guidance and support throughout the course of this research. In addition I am grateful for the wealth of advice provided by Prof. Gyula Vigh.

I would also like to thank the Burgess group members (past and present) for providing a great research environment. I would especially like to acknowledge Drs. Rakeshwar Bandichhor and Junyan Han for mentorship and Drs. Liangxing Wu, Aurore Loudet, Yuichiro Ueno, and Jiney Jose for insightful discussions.

Finally, I would like to thank my wife Melissa and my son Didier for much needed love and support.

TABLE OF CONTENTS

CHAPTER Page

LIST OF FIGURES

FIGURE Page

FIGURE Page

FIGURE Page

FIGURE Page

LIST OF TABLES

LIST OF SCHEMES

CHAPTER I

INTRODUCTION

The importance of fluorescent probes in research is ever growing as demonstrated by the 2008 Nobel Prize in Chemistry being awarded to Drs. Osamu Shimomura, Martin Chalfie, and Roger Y. Tsien for the development of bioluminescent tools that exploit the phenomena in the studies of biological systems. The first fluorescent compound discovered was quinine, a naturally occurring blue fluorescent organic dye responsible for the slight blue tinge of tonic water.[1] Ever since, a number of synthetic and naturally occurring fluorescent dyes have been described. These types of organic fluorescent dyes have found widespread applications including: biological molecule labeling, cancer treatments, OLED, and paper additives.

1.1 Fluorescence

Dyes, molecules that absorb light, are ubiquitous in everyday life. Their *modus operandi* is depicted in the Jablonski diagram in Figure 1.1. Generally a dye has a pair of electrons in the singlet ground state, S_0. Upon absorption of a photon of energy equal to the difference in energy between its ground state and an excited state, an electron is promoted to an excited state, preserving its spin in the process. Quick relaxation to the ground vibrational energy level of S_1 usually occurs through a process called internal

---

This dissertation follows the style of the *Journal of the American Chemical Society*.

conversion. This process occurs in the order of 10^{-12} s and is faster than most radiative processes. The dye then dissipates the energy and the electron returns to a vibrational level in S_0.

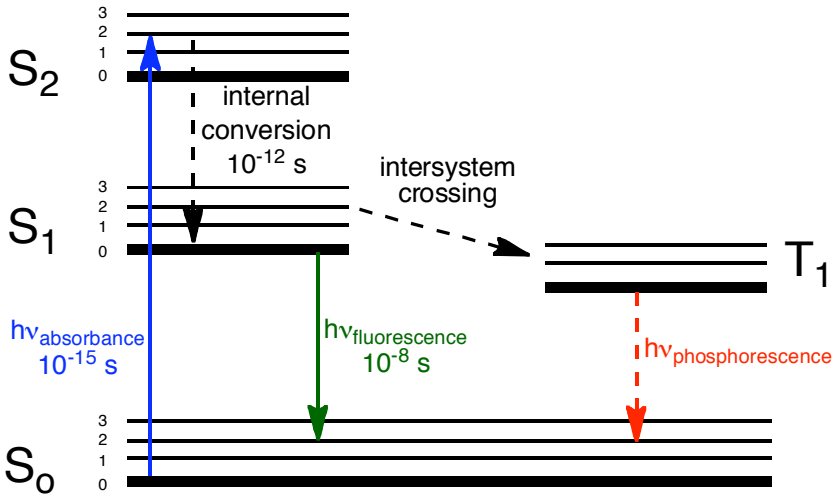

Figure 1.1. Jablonski diagram depicting the processes of absorbance and common radiative relaxations.

In the case of fluorescent dyes, the energy is lost, at least partially, by the emission of a photon through a transition from S_1 to a vibrational state in S_0. This process usually occurs in the order of 10^{-8} s. A slower relaxation pathway also exists through intersystem crossing to the triplet state T_1 where the unpaired electrons in T_1 and S_0 have the same spin. This is a forbidden transition and is therefore much slower than fluorescence. Relaxation back to the ground state through emission is known as phosphorescence and is rare especially for organic dyes because of the time required for intersystem crossing to occur. Introduction of heavy atoms can expedite transitions to

the triplet state and addition of bromine and iodine are common modifications to enhance such transitions in organic dyes.

An important characteristic of fluorescence is that the emitted photon is of lesser energy than the one absorbed. As mentioned above, this is because fast internal conversion occurs to the lowest vibrational level of S_1. A measure of the difference in energy between the absorbed and emitted photons is known as a Stokes shift and is usually expressed in wavenumbers (cm^{-1}).

Not all dyes undergo fluorescence efficiently. In fact, very rarely do all photons absorbed by a dye solution result in the same number being emitted. There are a number of ways relaxation from S_1 to S_0 can occur such as vibrational energy losses and molecular collisions. A measure of the efficiency a dye can fluoresce is known as its quantum yield (Φ_f; commonly shortened to Φ or even ϕ) and is defined as the ratio of photons emitted to the number absorbed. A dye with a quantum yield of 0.5 for example would emit half as many photons as it absorbs. This is usually measured in a relative fashion using a dye of known quantum yield: the amount of absorbance and fluorescence area of the known and unknown dyes can be compared in order to estimate the unknown's quantum yield. Quantum yields ranging from 0.1 - 0.8 are common for dyes considered "fluorescent" although dyes of higher quantum yields are also commonly encountered. Another useful property of fluorescent dyes is their overall brightness and is defined as the product of the quantum yield and the molar absorptivity (ε).

$$brightness = \Phi \times \varepsilon$$

General cellular imaging applications require certain criteria from fluorescent dyes. Typically dyes should fluoresce to the red to near-IR regions to avoid emission overlap with endogenous cellular fluorophores. The fluors should be bright; typically quantum yields higher than 0.10 and molar absorptivities (ε) larger than 40,000 $cm^{-1}M^{-1}$ are preferred. The fluorophores should be photostable to withstand the powerful lasers used in modern microscopy. Quenching can be problematic in cell imaging; it is therefore practical to use dyes that are less prone to aggregation and have fluorescence characteristics that are independent from the local environment of the dye.

Dyes for *in vivo* imaging have the added challenges of water solubility and targeting. The necessity of red emitting dyes is even greater for *in vivo* imaging due to poor tissue penetration of wavelengths below *ca* 600 nm.[2] Tissue penetration is also an important factor for the excitation laser, so a dye should not only emit but also absorb to the red. In fact, lasers that are closer to the blue and ultra-violet regions can damage tissue. One relatively new way to overcome this problem is to use two-photons to promote the fluorophores to an excited state.[3] In this method, two photons are simultaneously absorbed by the dye to promote the chromophore from the ground electronic state to an excited one (Figure 1.2). The two-photons are of lower energy than the 1-photon process but do not necessarily need to correspond to half the energy of the one photon process. In typical 2-photon setups, high intensity lasers are employed to increase the chances of simultaneous two-photon absorption; this is necessary because the TPA process is nonlinear and thus heavily dependent in the laser intensity. A measure of the probability a dye will undergo Two Photon Absorption (TPA) is known as its two-photon cross-

section and is usually expressed in cm^4 s $photon^{-1}$ or simply GM (GM = 10^{-50} cm^4 s $photon^{-1}$).

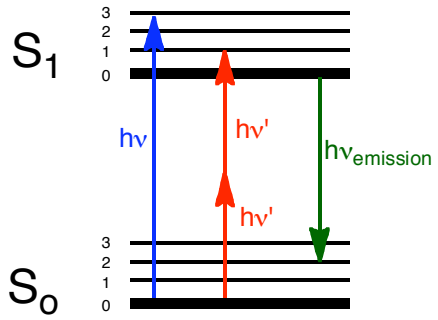

Figure 1.2. Illustration of one-photon (blue) and two-photons (red) absorption processes.

To summarize some of the criteria discussed, ideal fluors should:

(i) fluoresce in the red to near-IR regions

(ii) be bright; have quantum yields higher than 0.10 and molar absorptivities greater than 40,000 $cm^{-1}M^{-1}$

(iii) be photostable

(iv) not be prone to aggregation

(v) have fluorescence characteristics that are independent from the local environment of the dyes

Criteria (i) appears simple, it is well known that extending the conjugation of a dye pushes its absorbance and emission wavelengths to the red.[1] From a design standpoint, it is usually more practical to derivatize a known fluor in order to extend its conjugation than to design a whole new type of fluorescent dye. A common method is by the

introduction of a "push-pull" system where one area of the dye has high electron density while another has low electron density, with the two being electronically conjugated. The difficulty however lies in the synthetic accessibility of such modifications.

Criteria (ii) defined brightness as a critical factor for imaging because of the difficulty in observing low fluorescence signals in biological systems. A common way of improving the molar absorptivity of a dye is by extending its conjugation and an approach that is congruent with criteria (i) could be used. Increasing the quantum yield however first requires an analysis of the dye to determine why its quantum yield is low. Non-radiative decay, usually through rotational energy losses, is a common cause of low fluorescent quantum yields and approaches that minimize the rotational freedom of the dye are effective in this regard.[1] Indeed, rigid dyes tend to have higher quantum yields than ones with many modes of rotation. Of course quenching is also a common reason for low quantum yields and steps to reduce quenching are also helpful.

The photostability of criteria (iii) can be ambiguous and increasing this parameter can be a result of trial and error. Unfortunately, the exists no general principal to predict photostability of a fluor.[1]

Aggregation (iv) of dyes can be problematic because the photophysical properties of the dyes can change upon aggregation, *e.g.* the quantum yields can be lowered and the spectral maxima shifted. The addition of water solubilizing groups such as carboxylic acids, ethers, and amines for example tend to alleviate aggregation.

Finally dyes that are impervious to their microenvironments are desired unless the sensitivity is required for a specific application such as sensing. These sensitivities can

be caused by the protonation (or deprotenation) of functional groups directly attached to the dye core, which alter the electronic properties of the dye. Avoiding these types of functional groups is the best strategy.

Of course in addition to these general guidelines, others that are specific for certain applications may also be desirable. For example, single molecule microscopy generally requires dyes that have a low tendency to photo-blink.♦ Another example that was already discussed are dyes used for *in vivo* imaging needing to absorb in the red region and/or have high two-photon cross-sections to allow tissue penetration of the excitation source.

1.2 Resonance Energy Transfer

When two dyes are in close proximity a different type of relaxation from the excited state is possible.[4] Resonance Energy Transfer (RET) is a process whereby a *donor* dye absorbs a photon in the usual manner but relays the energy an *acceptor* dye resulting in excitation of the acceptor. A requirement for this process is that the emission of the donor dye overlaps with the absorbance of the acceptor dye. The energy is transferred through a dipole-dipole interaction and does not involve the emission of photons from the donor.

♦ Photo-blinking is a process whereby a dyes excited by a laser source ceases to emit photons and essentially enters an "off-state". The process is usually reversible so is not a problem when imaging a population of dyes although problems occur in single molecule imaging.

The efficiency of energy transfer is also dependent on the distance between the donor and acceptor dyes. The rate of RET (k_T) is given as

$$k_T = \frac{1}{\tau_D}\left(\frac{R_0}{r}\right)^6$$

where τ_D is the lifetime of the donor in the absence of the acceptor and r is the distance between the donor and acceptor. R_0 is called the Förster distance and is the distance at which 50 % of the energy from the donor transfers to the acceptor. R_0 not only dependent on the spectral overlap between the donor and acceptor mentioned above but also on an orientation factor in which R_0 becomes larger in circumstances where the transition dipoles of the donor and acceptors are "head-to-tail". In cases where the transition dipoles are perpendicular to each other, R_0 becomes zero and RET does not occur. Overall, the efficiency of energy transfer (E) for a donor and acceptor at a fixed distance is

$$E = \frac{R_0^6}{R_0^6 + r^6}$$

The distance between the donor and acceptor is thus crucial for efficient energy transfer to occur. Typical Förster distances range from 30 to 60 Å. For this reason RET is a commonly used tool to detect bimolecular interactions where one biomolecule is labeled with the donor and a second is labeled with the acceptor. If the biomolecules interact then the proximity of the donor and acceptor becomes favorable for RET and the interaction is easily detected through fluorescence spectroscopy.

1.3 Multiplexing

It is often desirable to study biomolecules through means of multiplexing where each biomolecule is tagged with different fluorescent labels that are excited simultaneously by a laser. The advantage of this "high-throughput" method is that *multiple* biomolecules can be observed *simultaneously* (Figure 1.3). Decreases in sensitivity complicate the method as dyes absorb further away from the excitation source. For this reason, a practical limit exists that restricts the amount of concurrent dyes that can be simultaneously resolved.

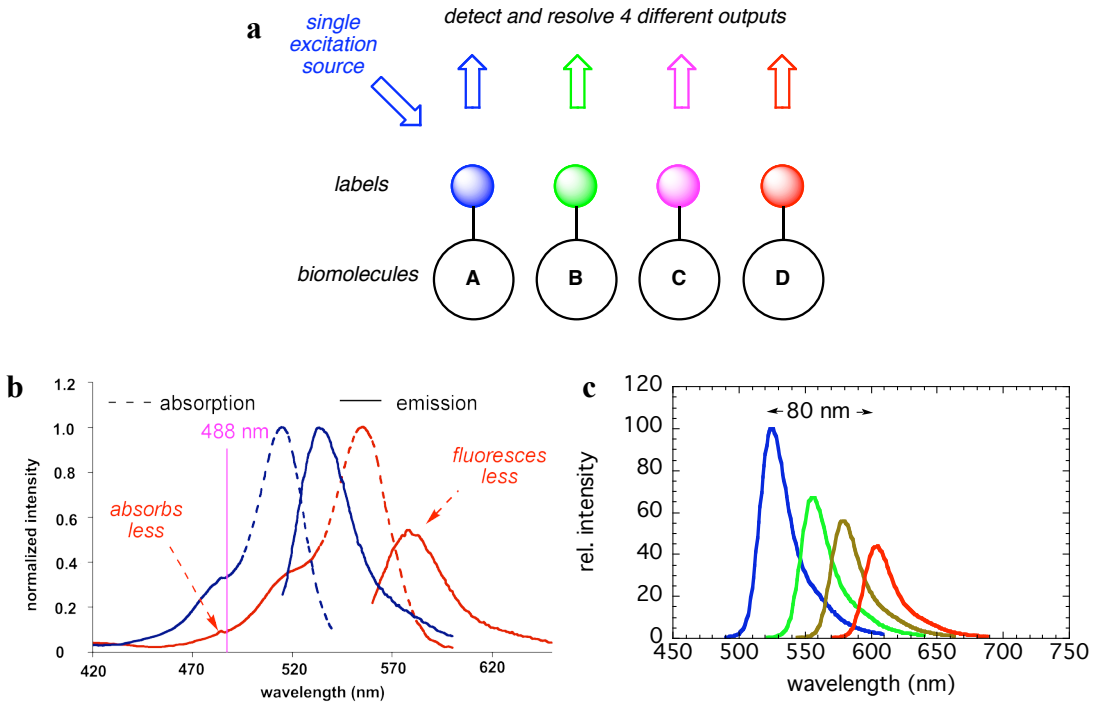

Figure 1.3. **a.** Typical arrangement for multiplexing of biomolecules. **b.** Dyes that absorb away from the excitation wavelength absorb less light and incur a loss of sensitivity. The problem is more pronounced as more dyes are used (c).

Combinations of donor and acceptor dyes that maximize the occurrence of RET is a common way of lessening the sensitivity loss. In these arrangements, a dye absorbing the laser efficiently is used as the donor and covalently linked to acceptor dyes in a way to keep them close enough for RET to occur. Acceptors are chosen so that their absorbance overlaps with the emission of the donor dye, a requirement of RET (see above). Acceptors are also selected to ensure well resolved emissions are obtained. Only a partial improvement in sensitivities using RET are obtained however due to the donor-acceptor overlap requirement in RET. As the donor-acceptor overlap becomes smaller, the energy transfer through RET becomes less efficient as a loss in sensitivity occurs.

1.4 Through-bond Energy Transfer

As discussed above, the requirements of RET are: (i) good overlap between donor emission and acceptor absorbance; and, (ii) favorable transition dipole orientations These requirements make RET difficult to use in certain situations, especially when the donor and acceptors absorb far away from one another. A different type of energy transfer occurs when two dyes (again, a donor and acceptor) are coupled together in *through-bond energy transfer (TBET) cassettes* (Figure 1.4). In TBET cassettes the donor and acceptor dyes are attached together in a way where the donor and acceptor are *twisted* and therefore not acting a one entity. The twist can be induced by a conjugated linker between the two dyes or can be provided by steric interactions if the donor and acceptor are to be directly coupled together. The dyes retain their individual

photophysical properties because the twist prevents them from being electronically conjugated. In TBET, there is no known requirement of spectral overlap between the donor and acceptor. It is therefore possible to create dye dyads with *large virtual Stokes shifts*.

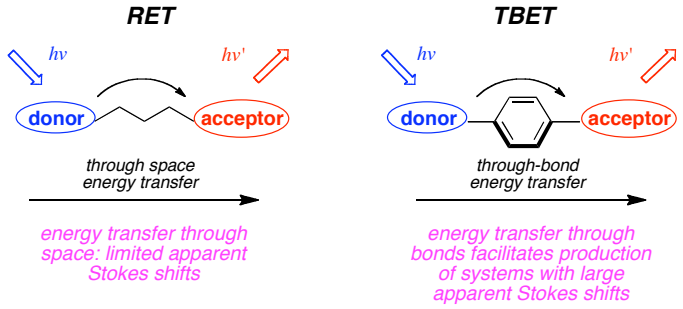

Figure 1.4. Differences between RET and TBET.

TBET systems have been investigated in materials research[5,6] and to model photosynthetic systems;[7-9] Theories describing TBET are vague; TBET may really be a summation of several means of transferring energy (*i.e.* dexter[10], superexchange[11], resonance energy transfers, etc…), although transfer rates in TBET are usually faster than those of just RET; this is conducive to more efficient transfer of energy.

Besides the usefulness of large virtual Stokes shifts in multiplexing applications, TBET cassettes have several other valuable attributes for biotechnology. Quenching of an acceptor dye in RET systems usually results in a "turned-off" state where no fluorescence is observed from either the donor or acceptor. This is because energy transfer still occurs to the quenched acceptor. In TBET, the donor can fluoresce even in

cases where the acceptor is quenched, thus affording "always-on" probes. Finally, if the donor is prone to photobleaching it may be less so in TBET cassettes due to the fast energy transfer from donor to acceptor that often precedes photobleaching processes such as intersystem crossing to T_1 (Figure 1.5)

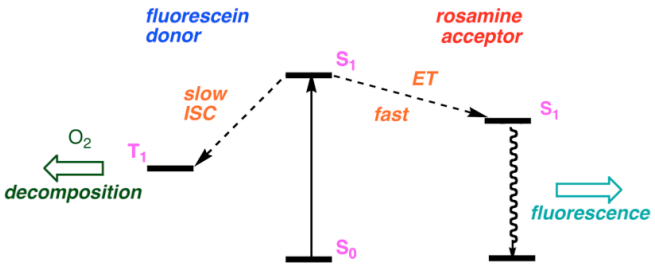

Figure 1.5. Example of fast through-bond energy transfer from a fluorescein donor to a rosamine acceptor leading to an increase in photostability of the fluorescein. (ISC = Intersystem Crossing, ET = Energy Transfer)

Elegant investigations carried out by Lindsey in the 1990s to model energy transfer in photosynthesis serve as the pioneering work in the area of TBET. Lindsey's seminal contribution was to study BODIPY[¤]-porphyrin molecular photonic wire **1** (Figure 1.6) where the energy was absorbed by a BODIPY unit and transferred step-wise from porphyrin to porphyrin and finally to the free base porphyrin that emitted the energy.[9] In this arrangement, the BODIPY is considered the donor, Zn-porphyrin complexes the

[¤] BODIPY dyes, short for BoronDIPYrromethene or 4,4-difluoro-4-bora-3a,4a-diaza-*s*-indacene, will be covered in detail in Chapter II.

linker, and the free-base porphyrin the acceptor. An important observation in the work was that photophysical properties of the donor and porphyrins were preserved. Most interestingly, nearly all of the emission occurred from the porphyrin acceptor (92 %), with minimal occurring from the BODIPY (3 %) and the Zn-porphyrin complexes (5 %). The overall energy transfer efficiency from donor to acceptor was 76 %, 13 times higher than would be predicted of RET in a similar system.

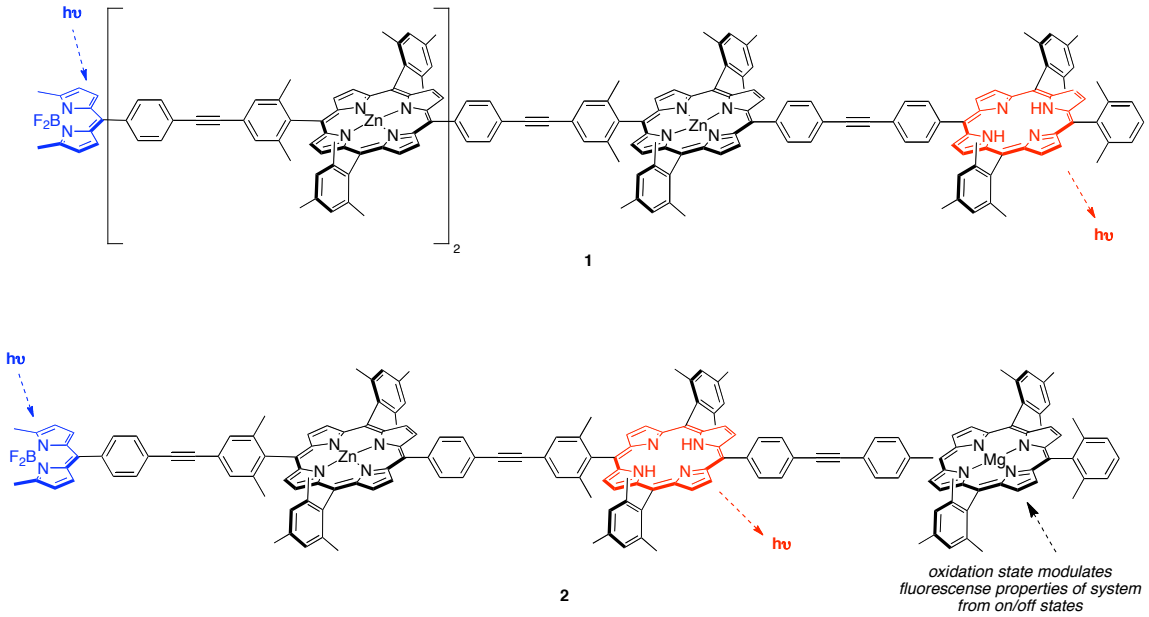

Figure 1.6. Lindsey's TBET systems to study photosynthesis. The BODIPY donors (blue) absorb energy and relay it through bonds to porphyrin acceptors (red).

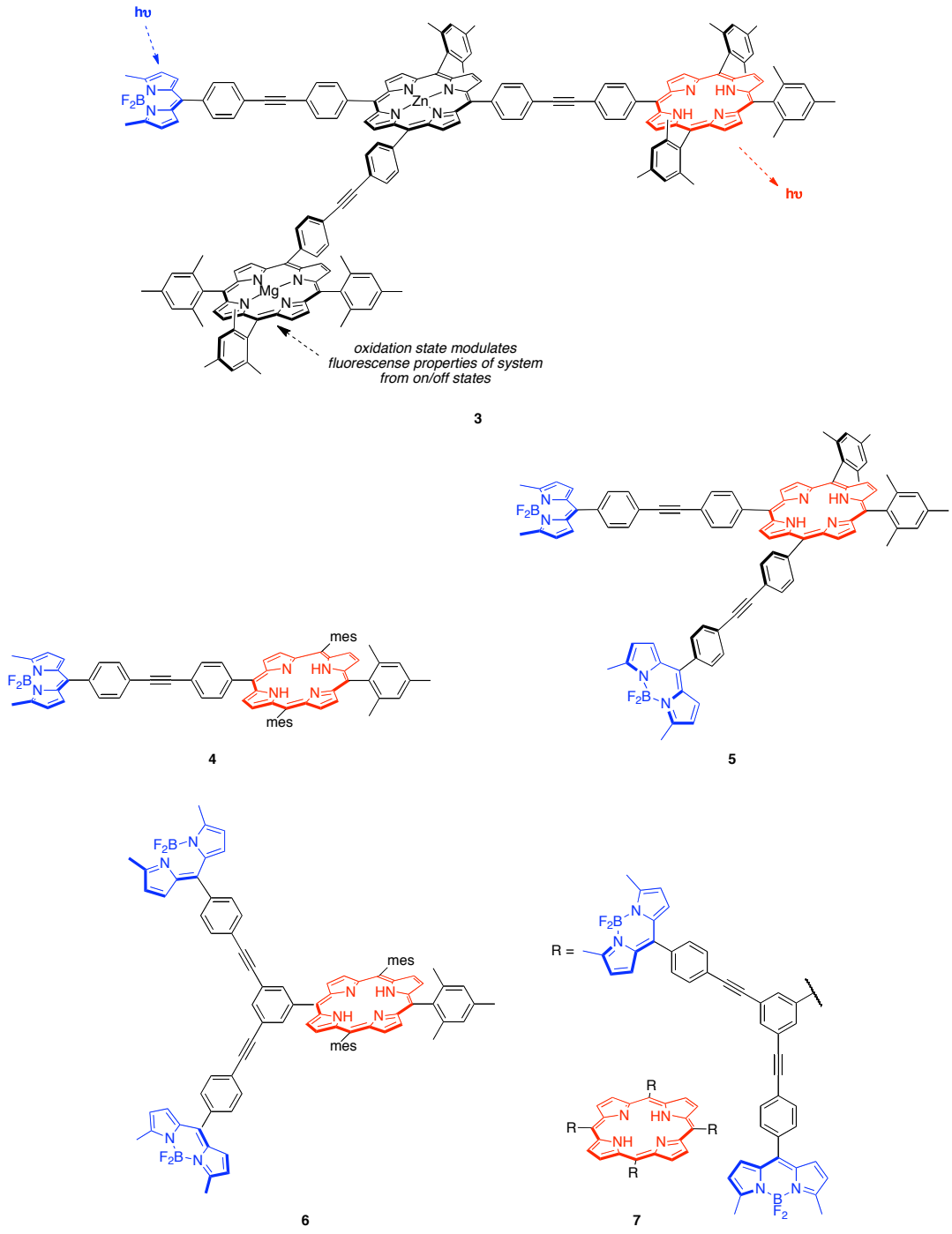

Figure 1.6 Continued.

Lindsey investigated the potential of systems like **1** as "optoelectronic gates" where the fluorescence of the system could be modulated from an "on/off" state by altering the oxidation state of Mg-porphyrins.[8] Systems **2** and **3** have properties similar to **1** where good energy transfer efficiencies (> 80 %) occur from the BODIPYs to the free base porphyrins. Upon oxidation, the Mg-porphyrin quenched the fluorescence of the adjacent free base porphyrin and minimal emissions (3 %) were observed from the acceptors.

Further work by Lindsey examined the effect of multiple donors to a single acceptor (**4** – **7**).[8] Systems containing one and two BODIPY donors exhibit efficient energy transfer to the acceptor (> 95 %) while system **7** with eight BODIPY donors shows a slightly lower albeit still very high (> 85 %) efficiency. In a subsequent publication, Lindsey gives some design guidelines to maximize efficient energy transfer: [12]

(i) linker should be placed in areas of high HOMO electron density on the donor and acceptor

(ii) shorter linkers should be used

(iii) *slight* twists between the donor/acceptor with the linker are better

The criteria can conveniently be applied to potential systems through design and molecular modeling even before synthesis begins. Criteria *iii* is interesting because it suggests that although a twist is needed for TBET systems to operate complete electronic decoupling between the donor and acceptor actually slows down the energy transfer process.

Although Lindsey conducted the investigation described above to study energy transfer in photosynthesis systems, the efficiency of energy transfer in addition to the large virtual Stokes shift involved appeared ideal for multiplexing applications. With this aim in mind the Burgess group looked to design TBET cassettes for high-throughput biological applications such as the detection of protein-protein interactions and DNA sequencing.

TBET Cassettes for Multiplexed Detection of Protein-Protein Interactions

The approach undertaken for multiplexed detection of protein-protein interactions is depicted in Figure 1.7. In order to find which partner(s) protein 1 interacts with, it is labeled with a fluorescent dye, preferably of high molar absorptivity. Potential binding partners to protein 1 are labeled with different TBET cassettes consisting of the same donor that is chosen to optimize RET from the dye labeling protein 1. The acceptors of the cassettes are chosen to have sharp, resolved emissions and high quantum yields. In the example shown in Figure 1.7, upon interaction with protein 1 proteins B and D will be in close enough proximity to 1 for RET to occur between the label on protein 1 and the donors of cassettes on B and D. The energy will then be transferred to the acceptors via TBET and the respective emissions will identify the interacting proteins, in this case B and D.

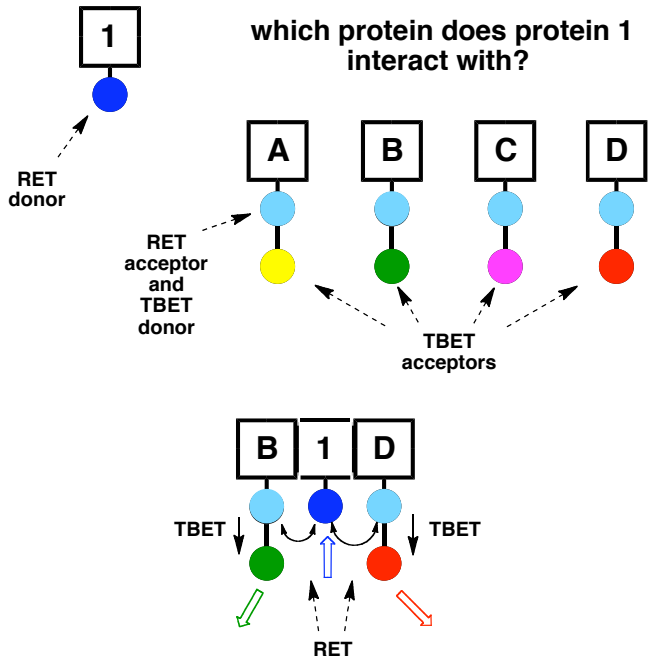

Figure 1.7. Theoretical experimental setup to employ multiplexing to detect protein-protein interactions.

Cassette **8** (Figure 1.8) was constructed to determine if BODIPY-BODIPY cassettes could undergo efficient TBET similar to the ones observed by Lindsey; model compound **8** has no functionality to attach biomolecules.[13] The incorporated BODIPYs preserved their photophysical properties with absorption maxima matching closely to those of the free dyes. Efficient energy transfer was observed from the donor to the acceptor. Encouraged by this, the authors synthesized derivatives **9-11** incorporating carboxylic acid functionalities. Acceptors emitting from 545 to 652 nm were used and energy transfers greater than 90 % were measured for these cassettes. The advantages of systems **9-11** over porphyrin based systems are obvious: BODIPYs have high quantum yields and their emission wavelengths can be tuned by varying the substitution on the

BODIPY. Although **9-11** have ideal photophysical properties, their use as biomolecular labels is precluded by their inherent hydrophobicities.

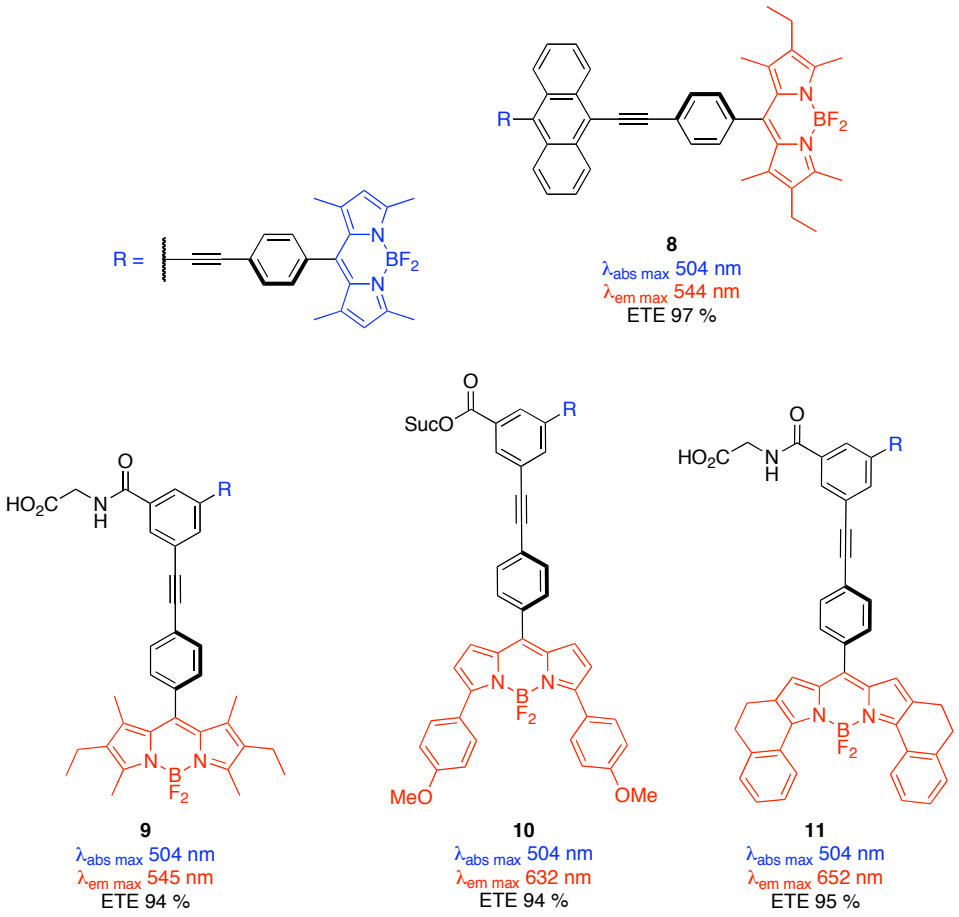

Figure 1.8. First-generation TBET cassettes produced by the Burgess group.

Fluorescein and rhodamine dyes are water soluble under particular conditions and this motivated the development of cassettes **12-15** (Figure 1.9) containing xanthene donors and hydrophilic rosamines derivatives as acceptors.[14] Remarkably, these cassettes display nearly quantitative energy transfer efficiencies and can conveniently be excited by Argon lasers at 488 nm. Furthermore, dispersed emission wavelengths of 78 nm

were achieved in the series. As discussed previously in Figure 1.5, the xanthene donor showed improved photostability when incorporated in the cassettes. Unfortunately, despite the addition of cationic functionality, the cassettes again proved too hydrophobic for the detection of protein-protein interaction although they did find use as DNA label (*vide infra*).

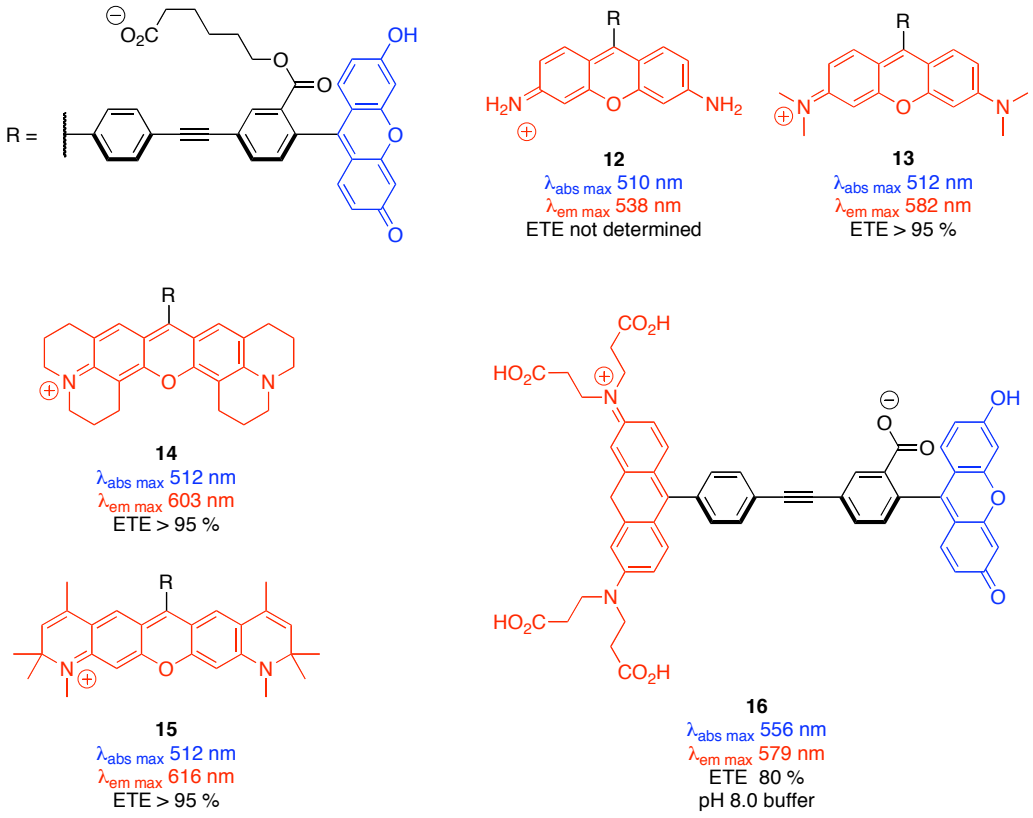

FIGURE 1.9. Xanthene-rosamine cassettes.

Cassette **16** is a water soluble version of **13** that was made by the incorporation of tetraacids on the rosamine part.[15] The absorbance maximum at 556 nm is markedly red-shifted compared to **13** perhaps due to the presence of the acid on the phenyl group attached to xanthene which is known to equilibrate between a closed-lactone and open

forms. This equilibrium is affected by pH and consequently the photophysical properties of **16** are pH dependent. The emission maximum is 579 nm and an ETE of 80 % was reported in pH 8.0 buffer. Mouse acyl-coenzyme A binding protein (ACBP) was labeled with **16**. The cassettes did not impede natural binding of or misfold the protein. The photophysical properties of the cassette did change upon binding to ACBP, an indication that the photophysical properties of **16** are affected by its microenvironment. An ACPB-**16** conjugate was imported inside COS-7 cells via Chariot carrier. The energy transfer in cells appeared to be good with little fluorescence from the donor and intense emission from the acceptor when exciting at xanthene. Although **16**'s water solubility is a remarkable improvement over previous TBET cassettes, the pH sensitivity coupled with the lack of clear strategies to obtain series of similar cassettes with dispersed emission wavelengths make it difficult to employ for multiplexing.

TBET Cassettes for Other Biological Applications

TBET cassettes have been used for other biotechnological applications besides multiplexing. Akkaya has developed cassettes that act as metal sensors. Cassette **17** (Figure 1.10) displayed near quantitative ETE in organic solvents.[16] The emission wavelength of the acceptor shifted from 680 to 630 nm upon addition of Ag(I) while other metals such as Mn(II), Fe(II), Hg(II), and Co(II) had no such effect. The shifts in emission wavelengths made it possible to ratiometrically detect metal concentrations through calibration curves. Interestingly, the energy transfer of the cassette remained high even in the presence of Ag(I).

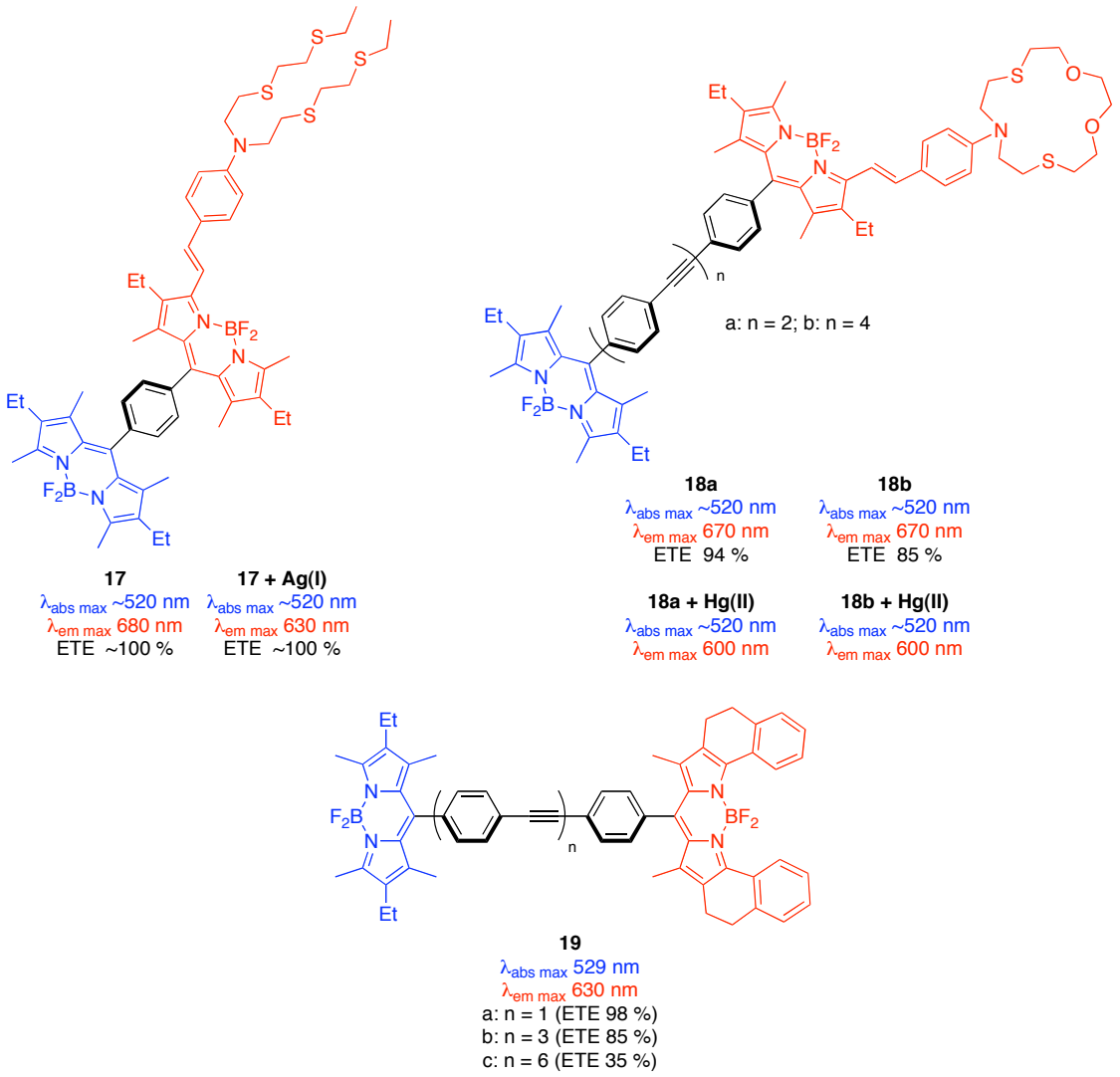

Figure 1.10. Akkaya's Ag(I) **17** and Hg(II) **18** sensing TBET cassettes and Diederich's BODIPY donor and acceptor TBET cassette.

Cassettes **18** were designed as Hg(II) sensors.[17] Similar modulations in photophysical properties as **17** occurred upon binding to mercury, mainly a hypsochromic shift from 670 to 600 nm in emission wavelength of the acceptors. Unfortunately a slight, albeit

significant, response to Ag(I) was also obtained although sensitivity to Hg(II) was *ca* 7 times greater; no other metals had appreciable effects on the fluorescence of **18**. Also notable is the decrease in ETE from 94 % to 85 % of **18b** compared to **18a** respectively, resulting from the increase in the length of the phenylacetylene linkers. This seems to corroborate Lindsey's criteria (see above) that longer linker lengths tend to impede efficient TBET. Akkaya *et al.* assert that the energy transfers in **17** and **18** occur through RET although such an exclusive transfer pathway is unlikely. Water-soluble versions of these systems would be more desirable but hydrophilic systems are considerably more challenging to synthesize.

The observed drop in energy transfer efficiency concurrent with linker length increases corroborates work by Diederich *et al.* on cassettes **19**.[18] The authors correlated the decrease in ETE with length between the donors and acceptors as measured by the boron-boron distances. Cassette **19a** showed an excellent ETE of 98 % at a donor-acceptor distance of 19 Å while **19b** had an ETE of 85 % at 32 Å. Amazingly, in the case of **19c**, the ETE dropped to a mere 35 % at a donor-acceptor distance of 53 Å. In the same manuscript, the authors used these findings to design an elegant light activated molecular switch although this work is beyond the scope of a discussion on TBET since the switch did not represent a TBET cassette.

TBET cassettes have also been explored as fluorescent tags for DNA. There are numerous advantages in tagging DNA in such a way; the absorbance wavelengths of the tagged bases are red-shifted away from the unlabeled bases, the molar absorptivities of the bases increase as a result of the added conjugation, and finally acceptors that emit far

from the excitation source can be used thus simplifying the detection process. Cassettes **20**-**22** feature extended thymidine donors and xanthene acceptors (Figure 1.11). First a deoxynucleoside analog of **20** was made.[19] This analog showed an absorption maximum from the donor at 320 nm in contrast with thymidine that absorbs near 260 nm. The energy transfer efficiency to the acceptor was near 100 % and fluorescence from the acceptor occurred at 520 nm. Oligonucleotides incorporating **20** were synthesized by solid phase syntheses[20] and the cassette was not significantly quenched in either single or double stranded conformations. Thermal denaturation studies showed that the presence of **20** in ds-oligonucleotides did not significantly decrease the stability of the chains, less so in fact than A-A mismatches. Circular dichroism studies also demonstrated that **20** did not perturb the ds-oligonucleotide B-form. Dideoxythymidine triphosphate-cassette conjugates were constructed from compounds **20**-**22**.[21] Taq polymerase was used in an attempt to incorporate the modified nucleotides into DNA. The rate of incorporation was ddTTP > 6-TAMRA-ddTTP > ddTTP-**22** > ddTTP-**21** > ddTTP-**20**, with the later two showing little to no incorporation (TAMRA ddTTP is a common dye used in sequencing and was included for comparison). The leading hypothesis for this trend is that longer donors separate the acceptors from the nucleotides affording more room for the polymerase to operate. Although the cassette conjugates showed slower incorporation, their favorable photophysical properties still lend to their potential applications in DNA labeling so long as a linker of suitable length is used.

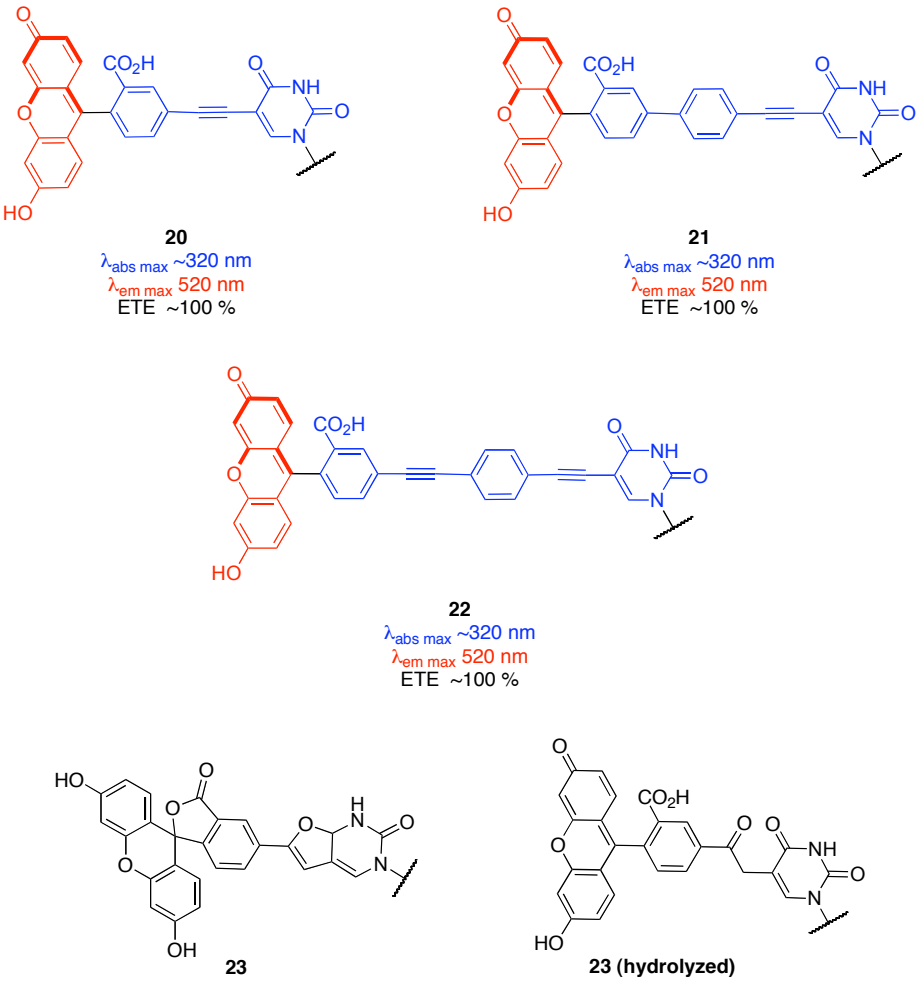

Figure 1.11. Cassettes studied as DNA labels.

A serendipitous discovery of side product **23** was observed upon synthesis of cassette **20**.[22] The time and temperature of a Sonogashira coupling step was critical as longer reaction times and higher temperatures tended to favor formation of **23**. Melting experiments with oligonucleotides containing **23** revealed that the modified nucleobase is a better mimic for thymine than other nucleobases. The use of cassettes of type **23** in

DNA is complicated due to their tendency to readily hydrolyze to the corresponding saturated ketones.

Cassettes as possible fluorescent labels for Sanger sequencing were also investigated.[23] Common dyes available from ABI for Sanger sequencing are FAM, JOE, TAMRA, and ROX and emit from 520 to 620 nm compared to **12**-**15**-primers conjugates that emit from 519 to 641 nm. The cassettes were attached to DNA primer R931. Although incorporation and thus chain termination appeared to have occurred as would be expected in Sanger sequencing, the analysis software complicated the utilization of cassettes **12**-**15** for sequencing.

The Burgess group has investigated an intriguing use of TBET in which a chemiluminescent, as opposed to a fluorescent dye, is used as a donor.[24] Just as in traditional TBET cassette systems, upon excitation the donor transfers the energy to the fluorescent acceptor; the difference in these systems being the initial donor excitation occurs by *chemical reactions rather than light*. Two compounds containing a luminol donor, and xanthene (**24**) and Nile Red (**25**) acceptors were prepared (Figure 1.12). Luminol is activated in the presence of oxidants while the acceptors would otherwise not be affected by such conditions. In systems **24** and **25**, no luminescence was observed from the luminol donor upon oxidation and emission occurred only from the acceptors at 524 and 634 nm respectively.* Interestingly, upon excitation of **24** and **25** by light, the

* There is some ambiguity in whether compound **25** is acting as a true TBET cassette or an extended Nile Red with luminol functionality; the required twist for TBET in this system is not evident. Nile reds are particularly sensitive to their microenvironments causing significant fluctuations in their photophysical properties[25] making a determination based solely on absorbance and emission spectra difficult. This is trivial

emission wavelengths shifted to the blue by 6 nm in both cassettes compared to chemiluminescent activation, something that cannot easily be explained but may be an artifact of the slight change in microenvironment caused by the addition of the oxidant. Potential uses of chemiluminescent cassettes include cellular oxidant sensing which could help the study of cell signaling pathways[26], and **24** and **25** could be used in conjunction with horseradish peroxidase's Enhanced ChemiLuminescence (ECL) method of enhancing chemiluminescent signals for biological applications.

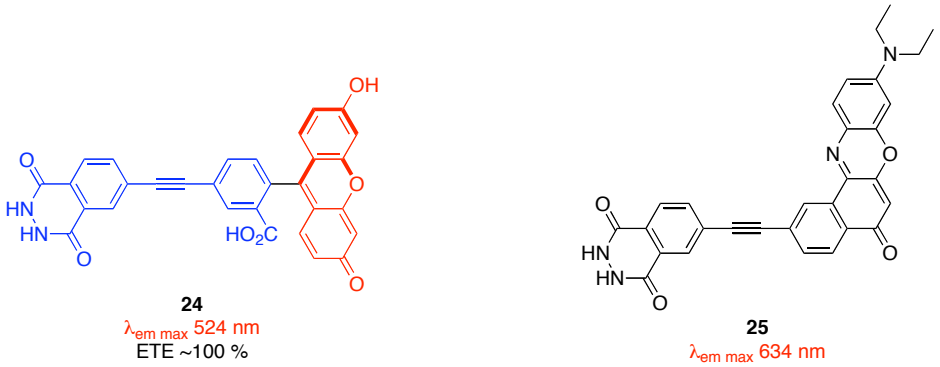

Figure 1.12. Chemiluminescent systems incorporating TBET.

---

in the case of chemiluminescence since the properties of the cassettes versus the extended dyes would be similar.

Other TBET Cassettes

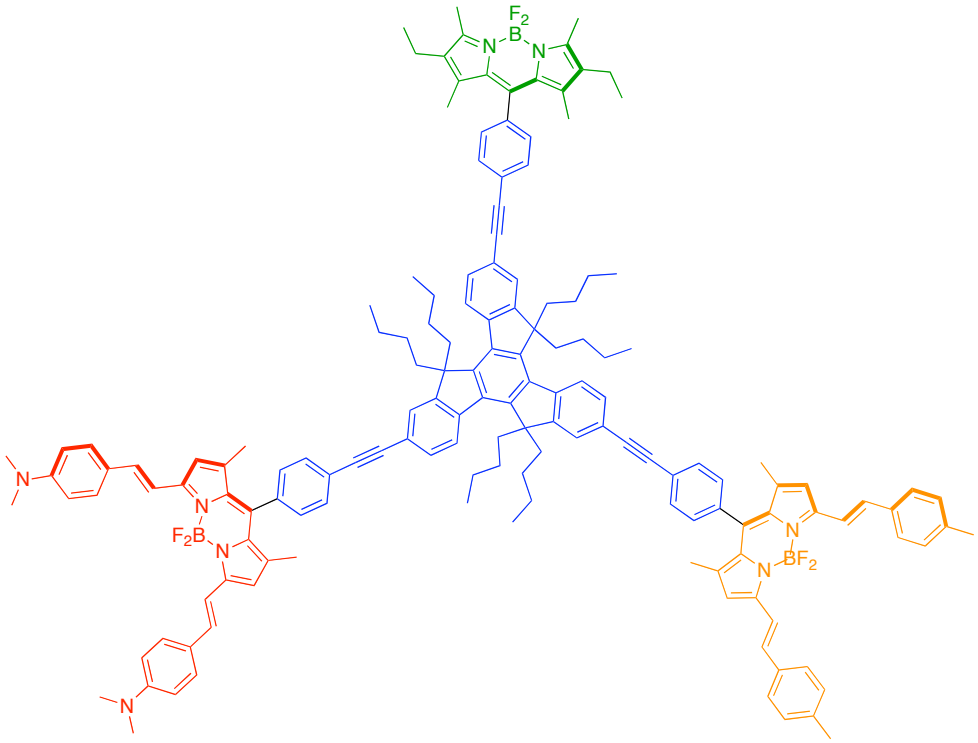

Figure 1.13. Ziessel's star-shaped multichromophoric system that absorbs most wavelengths of the visible spectrum. Donors (blue, green, and orange) all relay energy to the acceptor (red).

TBET cassettes have also been studied for solar cell applications. The concurrent harvest of energy by multiple donor dyes at many wavelengths is the premise of such systems. Ziessel et al. designed cassette **26** with one truxene and two BODIPY donors that absorb light from 300 to 636 nm while a BODIPY acceptor expands the absorbance of the system to 750 nm and emits at 767 nm (Figure 1.13).[18] In the context of a TBET cassette, **26** is interesting in so far as it has three different donors. Irradiation at each of the donors produces emissions primarily from the acceptor with minimal leakage from the other donors. Mechanistically, the energy absorbed by the truxene is quickly transferred to the BODIPYs, indicative of TBET. The energy from the BODIPYs is then transferred, perhaps in a step-wise fashion, to the acceptor through slower energy transfer processes in good agreement with theoretical RET calculations. It is unclear why inter-BODIPY energy transfer occurs through RET although the arrangements of the BODIPYs around the truxene (acting as a linker after it quickly passes off its energy) could be the reason since it is unclear if multiple energy transfers can simultaneously occur through a single linker.

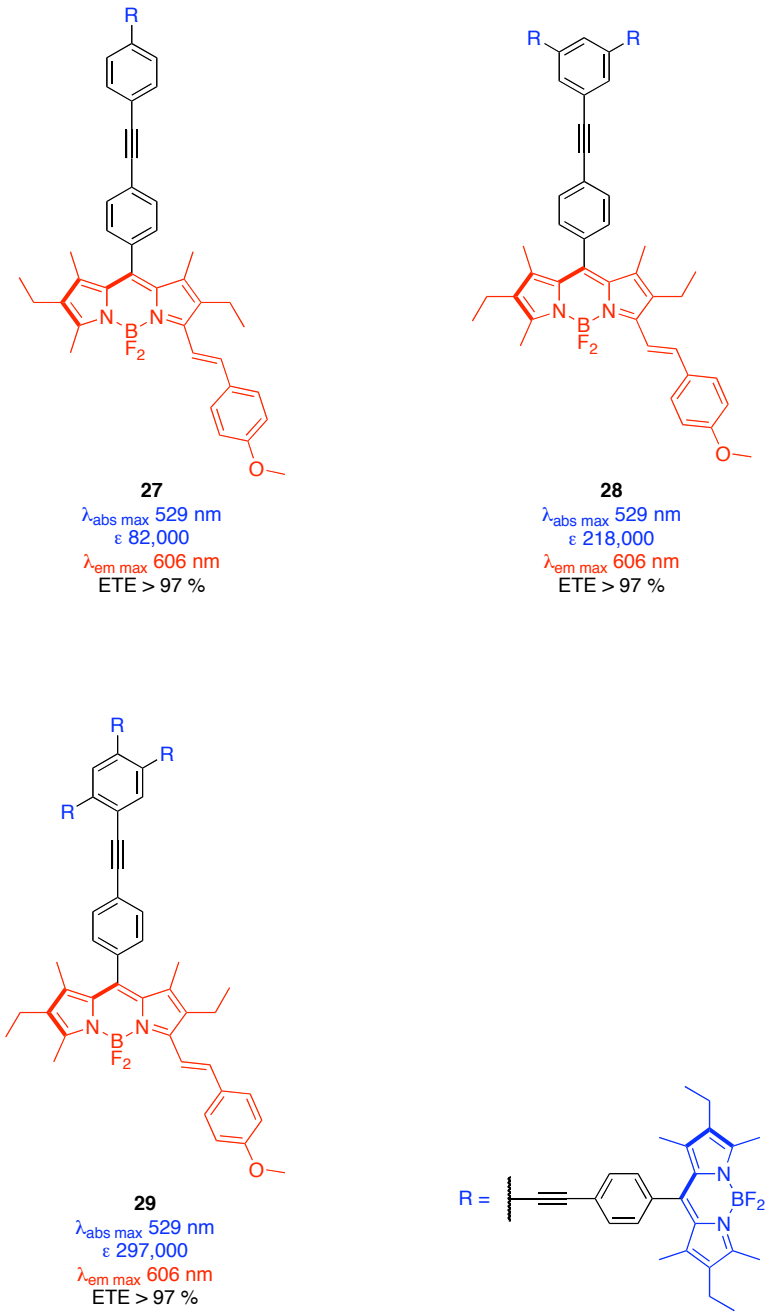

Figure 1.14. BODIPY TBET cassettes with differing donor to acceptor ratios. The molar absorptivities do not increase linearly with the amount of donors.

Further work by Akkaya investigated cassettes **27-29**[27] designed with donor to acceptor ratios greater than 1 (Figure 1.14). The ETE remained high for all cassettes in the series, even as three donors to one acceptor were incorporated. This is congruent with work discussed above by Lindsey (Figure 1.6) where a drop in ETE occurred only as eight donors to one acceptor where incorporated. Perhaps the most remarkable part of the work is the non-linear increase in molar absorptivities as the number of donors was increased; the incorporation of two donors increased the molar absorptivity by 2.7 times (compare **27** and **28**) demonstrating the potential of TBET cassettes as bright fluorescent probes.

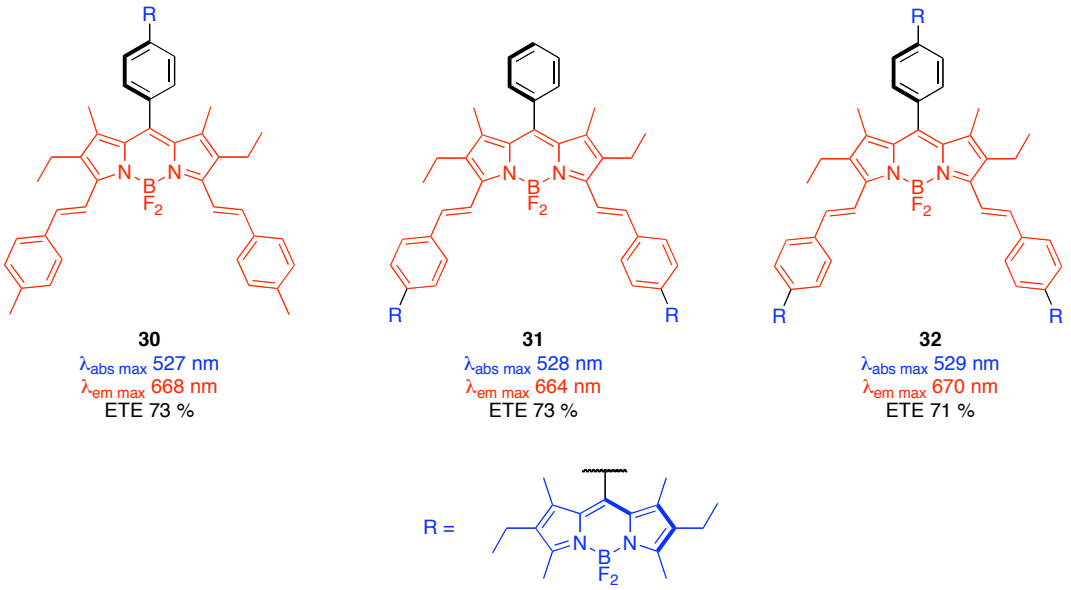

Figure 1.15. TBET systems with donors attached on different parts of the cassette. The ETEs where not reported by the authors but where calculated here by taking the ratio of the quantum yield when exciting at the donor to the one when exciting at the acceptor (see Chapter III for a detailed explanation)

Akkaya (Figure 1.15) described similar studies using a deep red emitting acceptor.[28] The ETE remained high even as three donors were used, something that is notable considering the pseudo-Stokes shift of these systems: the absorbance of the cassettes was near 528 nm with emissions at *ca* 668 nm. The molar absorptivities in this series did increase in a near-linear fashion as opposed to cassettes **27** and **28**. An interesting aspect of these cassettes is that the donors all retained the same photophysical properties even though they were incorporated in different parts of the molecule indicating a strong electronic decoupling produced by the molecular twists. This, the authors argued, was an indication that the mechanism of energy transfer occurred through RET although the aforementioned twist is also a requirement for fast TBET and in fact both processes may be occurring simultaneously.

Optimization of TBET

Burgess *et al*. tested the effect of the relative placement of donors and acceptors as well as the nature of the molecular twist on the energy transfer rates (these rates are usually proportional to ETE).[29] In these systems an anthracene donor was attached in different arrangements to a BODIPY acceptor; no linker was present on these systems (Figure 1.16). It is easy to explain the photophysical properties[#] (especially absorbance and emission wavelengths) of the cassettes based on the nature of the molecular twist

[#] The photophysical properties described in Figure 1.16 do not match those in the referenced paper[29]. There appears to be some disagreement between Table 2 and Figure 4 in the manuscript. Consequently, the photophysical properties reported herein are from the raw, original, data that is included in Appendix A.

between the donor and acceptor. Understanding the position of the molecular twist in these systems is important as the photophysical properties depend heavily on these. Cassettes **33**, **34**, and **36** for example are twisted only at the junctions of the BODIPYs and phenylacetylene units. In these cases, the phenylacetylene and anthracene parts are electronically conjugated and the absorbance wavelengths of the anthracenes are red-shifted compared to that of free anthracene; these whole units in essence become the donors. The absorbance of anthracene in **34** is further red-shifted by the introduction of bromine. It is interesting to note that systems attached at the *meso* position of BODIPY (**33** and **34**) appear to be more electronically decoupled from the BODIPY than those attached at the *C-2* position (**35** and **36**). This is indicated by the emission wavelengths of the BODIPYs where **33** and **34** match the emissions of the free acceptor while **35** and **36** are greatly red-shifted. This difference can be explained in terms of the steric interactions between the BODIPY core and the donor. Substituents at the *meso* position encounter greater steric strain thus locking them in a near perpendicular orientation relative to the BODIPY core. This orthogonal arrangement fundamentally breaks the electronic conjugation between the two systems. The steric constraints at the *C-2* position appear to be less; this is corroborated by X-ray crystallography.

Ultra-fast relaxation time measurements of the anthracene donors were measured and are good indications of the rates of energy transfer within the cassettes. Lindsey revealed that cassettes with greater electronic conjugation between the donor and acceptor have generally faster energy transfer rates (*vide supra*). It is therefore not surprising that cassettes **35** and **36** have faster relaxation rates than **33** and **34** supporting

the above assertion that the formers are have better electronic conjugation between the donors and acceptors.

Cassettes **37** and **38** have virtually no steric constraints between the donor and acceptor and spectrographically they behave nearly as one entity with bathochromic shifts in both the absorbance of the anthracenes and the emission of the BODIPYs. The anthracene and BODIPY units still do appear to retain some of their photophysical properties, for example in the case of **37** and **38** both BODIPY and anthracene absorbance peaks are present though the anthracene one is relatively weak and deformed (anthracenes generally have “triplet” absorbance spectra while the ones in these cassettes are broad singlets).

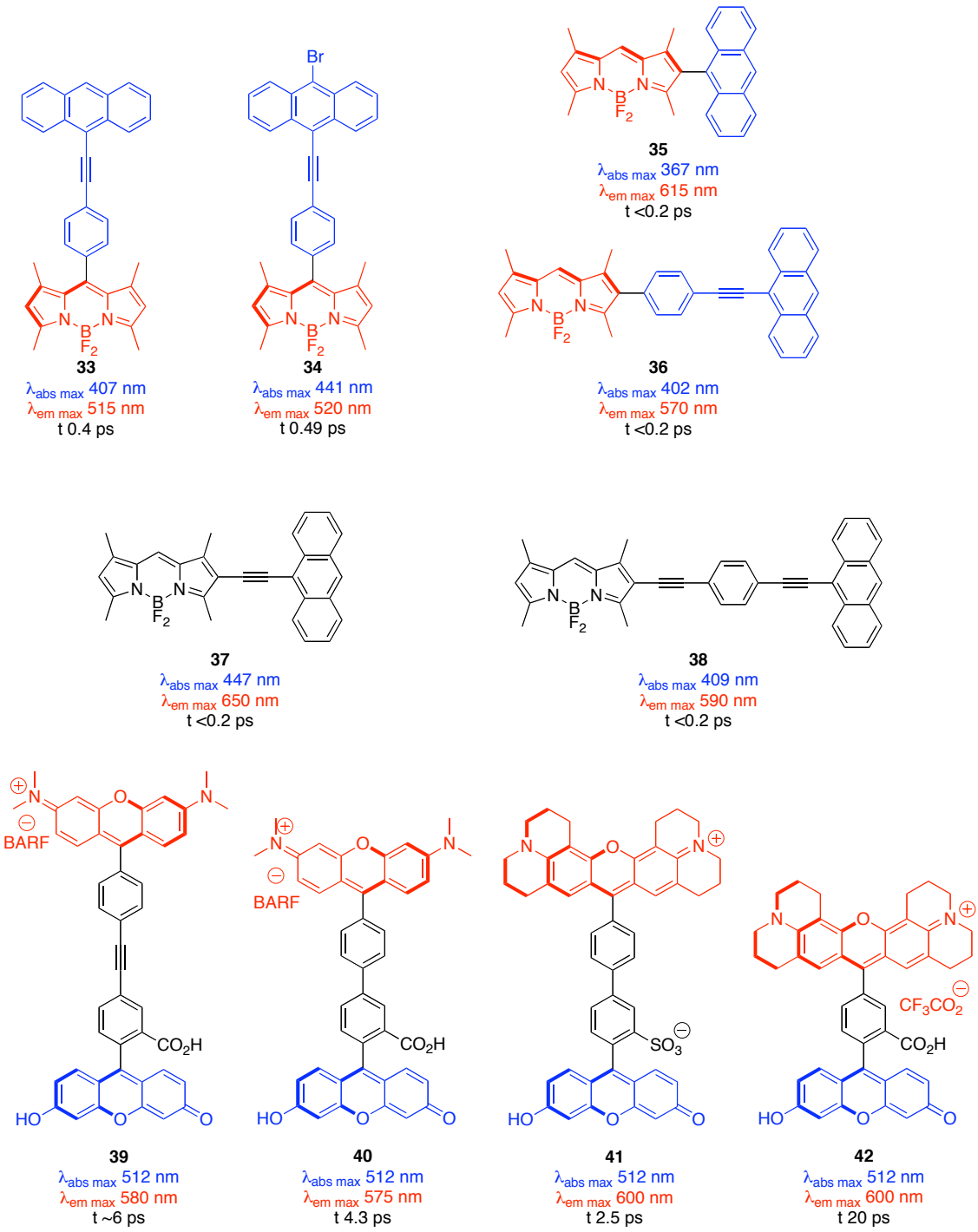

Figure 1.16. Structures and basic photophysical properties of cassettes to study various aspects of energy transfer. All ETE are > 95 % and t is the time for the energy transfer process (see note in text about the wavelengths reported here).

A subsequent publication by Burgess *et al*. correlated the rates of energy transfer with respect to the $S_1 \leftrightarrow S_0$ transition moments of the donors and acceptors (Figure 1.17).[30] Their findings indicated that fastest energy transfer (*ca* 200 fs) occurred when the donor and acceptor transition moments were parallel to one another, representative of compounds **35** and **36**. The next fastest energy transfer (*ca* 420 fs) occurred when the donor and acceptor had perpendicular transition moments such as cassettes **33** and **34**. Finally the introduction of linkers slowed the energy transfer process considerably. Cassettes **12**-**15** and **39**-**42** for example have energy transfer rates ranging from 2.5 to 20 ps. Interestingly, in some circumstances, as the length of the linker increased the rate of energy transfer became faster. Cassettes **14** for example displayed an energy transfer rate of 6 ps while analog **35**, with a shorter linker, had an energy transfer rate of 30 ps. Notably this contradicts observations of cassettes **18** and **19** in which shorter linker lengths gave more efficient energy transfers as well as Lindsey's observations for faster energy transfer. Several factors seemed to indicate that TBET and not RET was the primary energy transfer mechanism in these cassettes:

(i) RET should not occur when the donor and acceptor are locked in an arrangement in which their transition dipoles are perpendicular to one another

(ii) as the distance between the donor and acceptor increased the energy transfer rates either did not change or actually became faster

(iii) no correlation between the transfer rates and the nature of the acceptor was found, a correlation would be expected in RET due to the spectral overlap requirements for efficient transfer of energy

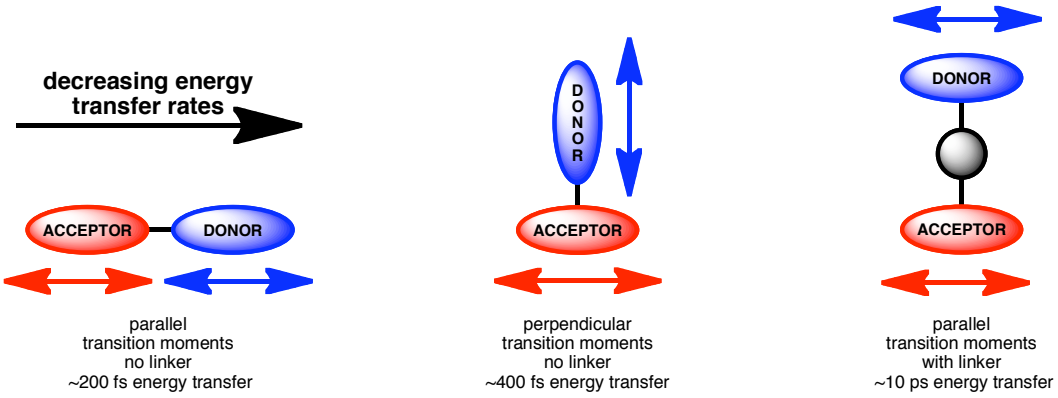

Figure 1.17. Correlation of donor-acceptor transition moment with energy transfer rates.

1.5 Goals and Aims

The focus of this dissertation is on the development of new fluorescent molecules for labeling of proteins to visualize their locations and/or study their interactions with other biomolecules by:

(i) developing ideal acceptor dyes for incorporation in TBET cassettes (Chapter II)

(ii) synthesizing new TBET cassettes (Chapter III)

(iii) examining the potential use of bright polymer based TBET systems and nanoparticles made from them (Chapter IV)

Another part of this dissertation deals with the development of dyes for PhotoDynamic Therapy (PDT) that have potential for cancer treatment; this will be discussed in Chapter V.

CHAPTER II

MODIFICATIONS OF THE BODIPY CORE

2.1 Introduction

BODIPYs© (BOronDIPYrromethene or 4,4-difluoro-4-bora-3a,4a-diaza-*s*-indacene) are good imaging dyes for numerous reasons.[31,32] BODIPYs are compact fluors and therefore have minimal impact on biomolecular conformations upon binding. Furthermore, BODIPYs are highly conjugated owing to their nitrogen-to-nitrogen push-pull system leading the high molar absorptivities. The boron chelate holds the dyes rigid while also preventing photo-isomerization processes; consequently BODIPYs possess high fluorescence quantum yields. BODIPY dyes are relatively photostable and are used for a variety of biological imaging applications.[33-38] The BODIPY core is generally insensitive to pH or solvent environments. Overall BODIPYs' brightness, photostabilities, and insensitivities to their environments meet criteria ii, iii, and v of ideal imaging dyes discussed in section 1.1. The drawbacks of simple BODIPYs are their blue-green emissions and hydrophobicities, which complicates their use as acceptors in TBET cassettes for biological imaging applications.

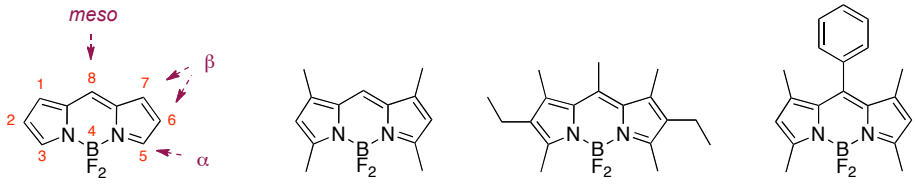

Figure 2.1. BODIPY core and commonly encountered BODIPY dyes

BODIPY dyes were discovered in 1968 by Treibs *et al.*[39] although the parent unsubstituted BODIPY core **A** remained unsynthesized until recently.[40-42] Some general photophysical trends are apparent from Figure 2.1; as the substitution on BODIPY increases, so do the absorbance and emission wavelengths. Not surprisingly, since these substituents can easily rotate, the quantum yields are negatively affected. Unfortunately, even the fully substituted BODIPY **C** fluoresces near 550 nm and is therefore of limited value for fluorescence imaging or as an acceptor for TBET cassettes.

General syntheses of BODIPYs are shown in Scheme 2.1. BODIPYs can be categorized into ones with *meso*-substituents and those without. For *meso*-substituted BODIPYs, the synthesis usually involves the condensation of the corresponding pyrrole with a benzaldehyde derivative (Scheme 2.1).[37] This gives a dipyrrole intermediate that is oxidized and subsequently treated with base in the presence of BF_3•OEt_2 to yield the BODIPY dye. The oxidation step can be avoided by initial condensation of the corresponding pyrrole with acyl chlorides instead of aldehydes though these reactions tend to be harder to purify.[43,44]

The syntheses of *meso*-unsubstituted BODIPYs are accomplished via condensation of the pyrrole with the corresponding pyrrole-2-carbaldehyde under acidic conditions, followed by treatment with BF_3•OEt_2 in the presence of base (Scheme 2.2).[39] A more recent procedure involves the condensation of 2 equivalents of pyrrole-2-carbaldehydes in the presence of phosphorous oxychloride[45] followed by chelation to boron. This method is generally cleaner and higher yielding and is now the preferred method to

synthesize symmetrical *meso*-unsubstituted BODIPYs though it was not yet discovered at the start of this dissertation.

a

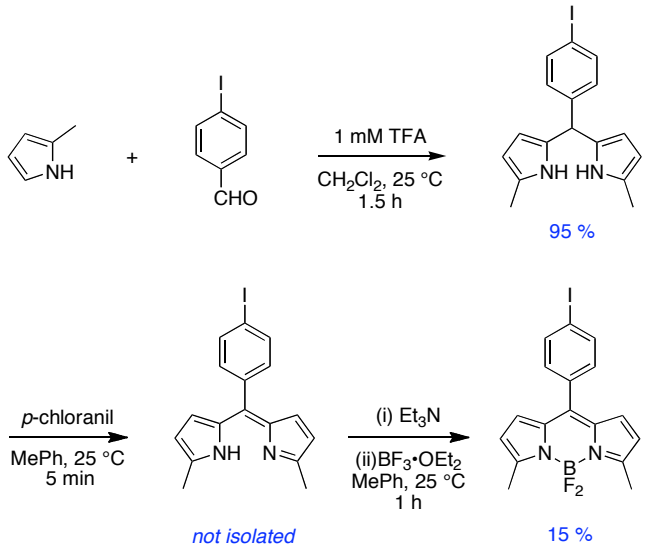

Scheme 2.1. Examples syntheses of **a.** *meso*-substituted BODIPYs

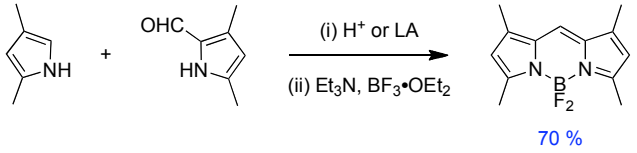

Scheme 2.2. Examples syntheses of unsubstituted BODIPYs.

Prior to the start of the work described in this dissertation, few red emitting (> 600 nm) BODIPYs were known (Figure 2.2). Emissions of type **E** systems are modestly red-shifted to 609 nm by the modification of the BODIPY with isoindoles though syntheses of such compounds require multiple steps and their quantum yields tend to be low.[46,47] BODIPYs of Types **F**-**I** possess aryl groups on the α-positions. The simplest, compound

F[48,49] has freely rotatable α-aryl groups and emits at 626 nm with a quantum efficiency of 0.42. Compounds **G**-**I** possess even deeper red emissions by restricting the rotation of the α-aryl groups, increasing the overall conjugation of the α-aryl groups with the BODIPY core.[38,50,51] An α-distyryl BODIPY derivative (**K**) has also been reported and emits at 642 nm with a very high quantum yield of 0.84.[52] Unfortunately BODIPYs **F-I,K** are inconvenient to make since the α-functionality needs to be introduced on the pyrroles prior to BODIPY formation; this extends and complicates the syntheses of such compounds. The introduction of nitriles on the *meso*-position of type **J** BODIPYs also red-shifts the emissions though syntheses of these are cumbersome and not generalized.[39,53] A general approach to *modify existing BODIPY cores* was therefore warranted to avoid the lengthy or difficult syntheses of the pyrroles for compounds of type **E-K**. A condition developed by Akkaya *et al*. was known to adequately red-shift BODIPY dyes by modifying the BODIPY core and was the only known example at the time of this work (Scheme 2.3).

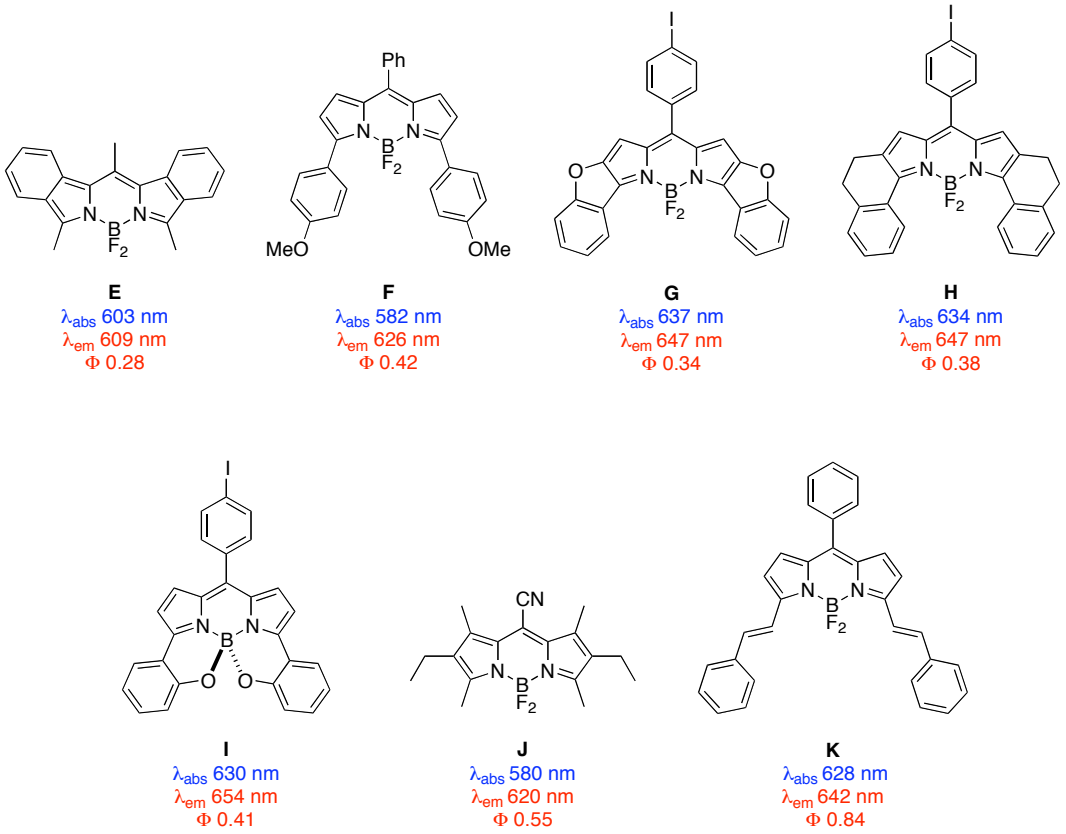

Figure 2.2. Known red-emitting BODIPYs prior to start of dissertation work.

Akkaya's modification involved Knoevenagel condensation of **D** with 4-dimethylaminobenzaldehyde yielding BODIPY **L** that fluoresced at 672 nm (Φ 0.58) in THF though photophysical properties were heavily dependent on solvent due to the presence of aniline functionality.[54] For example, in acetonitrile **L** fluoresced at 731 nm with a quantum yield of 0.13 while it emitted at 672 nm with a quantum yield of 0.58 in tetrahydrofuran. Another drawback was that only mono-condensation was obtained and in low yields (24 %). Therefore the goal of this chapter deals with the exploration of

novel ways of modifying BODIPY cores to extend their emission wavelengths into the red to use these dyes as acceptors for TBET cassettes in multiplexing applications.

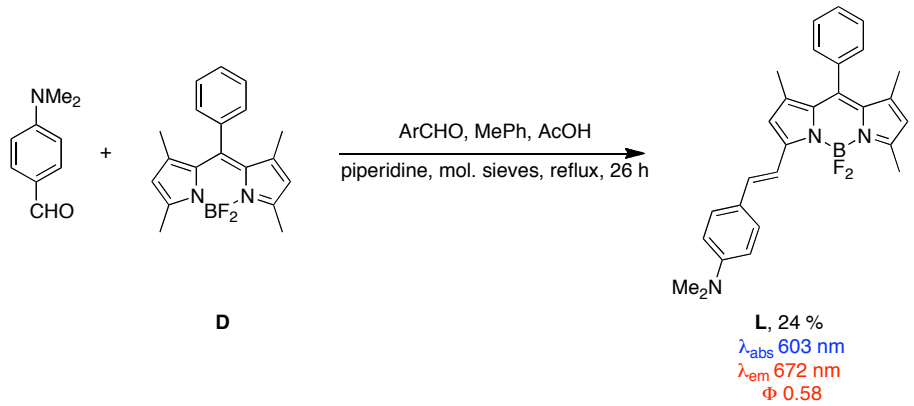

Scheme 2.3. Modification of BODIPY core to obtain **L**.

2.2 Phenylacetylene-BODIPY Derivatives

We hypothesized that compounds of type **43**, in which the conjugation of the BODIPY core are extended by the addition of phenylacetylene units, should have red-shifted emission wavelengths and the rigidity of such systems should not negatively impact quantum yields (Scheme 2.4). Furthermore, derivative **43** contains no functionality that should increase the pH or solvent dependence versus those of simple BODIPYs.

Synthesis began with standard Vilsmeyer Haack formylation of 2,4-dimethylpyrrole to yield **44** in 98 % yield. Condensation of **44** with 2,4-dimethylpyrrole under Lewis acid conditions followed by treatment with triethylamine and BF_3•OEt_2 yielded BODIPY **B** in 51 % yield. Diiodination of **B**[55] with iodine and iodic acid[56] gave BODIPY **45** in 88 % yield. Diiodide **45** was subjected to Sonogashira coupling with phenylacetylene to give BODIPY **43** albeit in low yields (12 %).

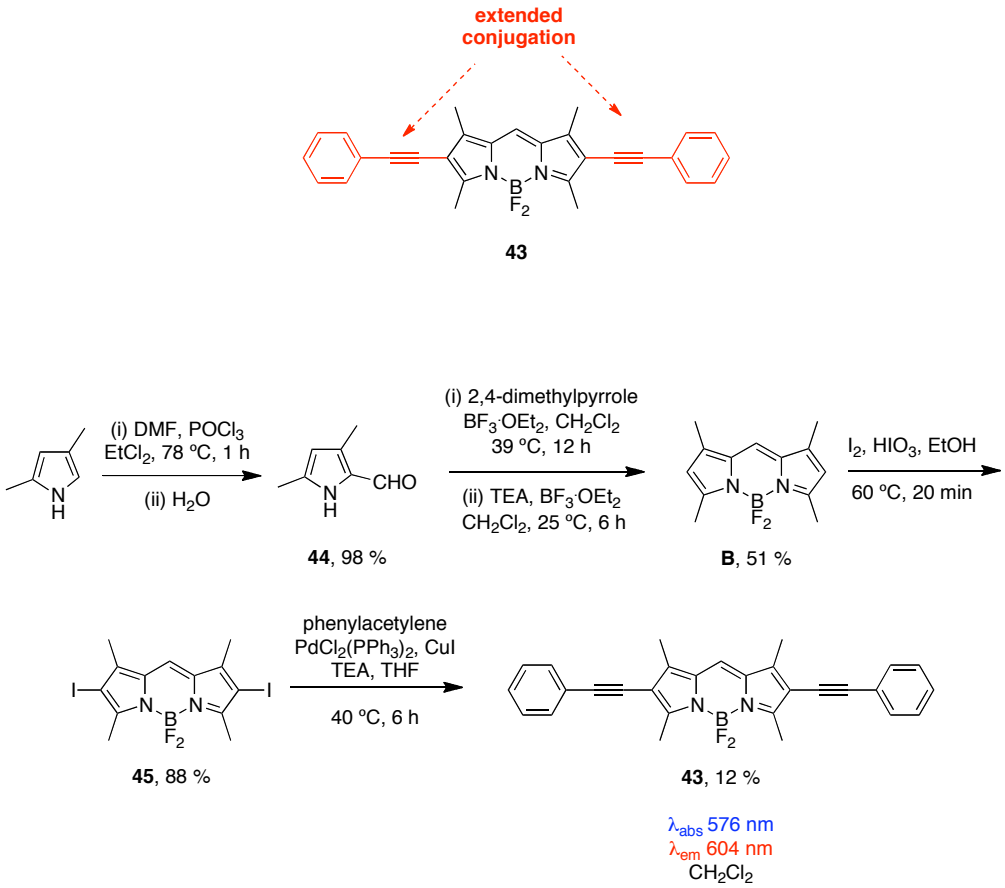

Scheme 2.4. Synthesis of BODIPY **43**.

We were pleased that **43** had red-shifted absorbance at 576 nm and emission at 604 nm compared to parent compound **B** which absorbs at 505 nm and emits at 516 nm. Furthermore **43** displayed a bigger Stokes shift which is a quality that can be useful for imaging purposes. Unfortunately, **43** was nearly insoluble in every solvent tested which prevented us from measuring other photophysical properties. Furthermore, **43** lacked functionality to attach to biomolecules. We theorized that the addition of an aliphatic chain would help solubility in organic solvents and the inclusion of carboxylic acid functionality would allow for conjugation to biomolecules; for these reasons compound

46 was investigated (Scheme 2.5). Synthesis of **46** was accomplished by condensation of 2,4-dimethylpyrrole with succinic anhydride under Lewis acid conditions followed by addition of triethylamine and BF_3•OEt_2 to yield BODIPY **47** in 18 % yield. BODIPY **47** was diiodinated using iodine and iodic acid though the yields tended to be modest (54 %) due to a side reaction involving formation of the methyl ester derivative of **46**. Finally Sonogashira coupling of **48** with phenylacetylene gave acceptor **46** in moderate yield (55 %).

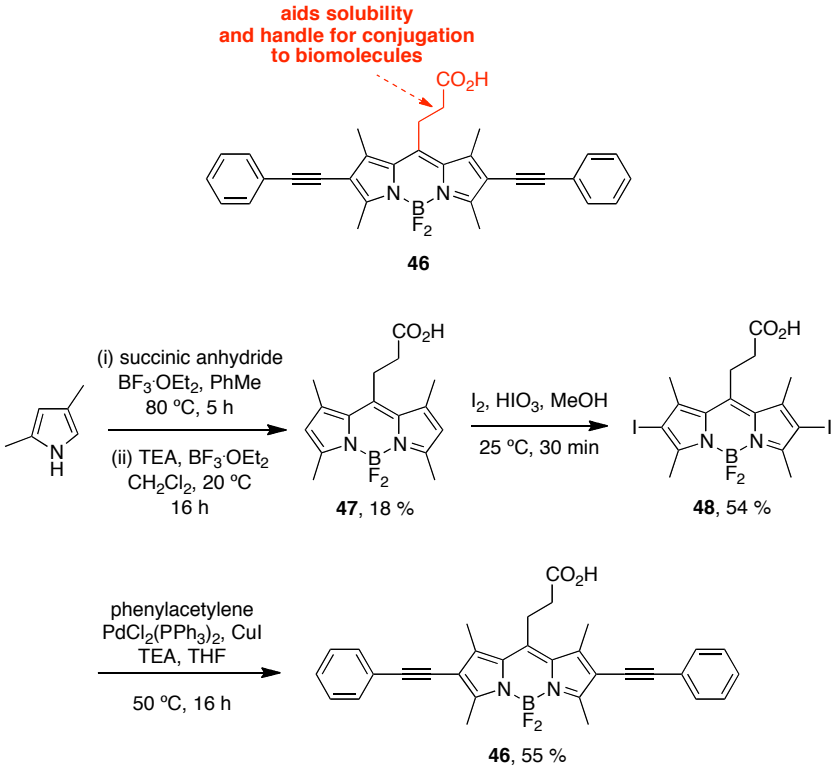

Scheme 2.5. Synthesis of BODIPY **46**.

Table 2.1. Photophysical properties of compounds **46** and **49**.

Cmpd	base[a]	λ_{abs} (nm) / ε x 10^{-4}	λ_{em} (nm)	fwhm (nm)	Φ[b]
B[57]	_	505 / 8.0	516	22	0.80
46	_	560 / 2.6	587	41	0.72
46	+	559 / 2.6	587	41	0.71
49	_	565 / 0.9	593	46	0.46
49	+	563 / 1.0	592	43	0.61

Absorption data recorded at 1 x 10^{-5} M. Emission data taken at 1 x 10^{-6} M. [a] With Bu_4NOH at a concentration of 8 x 10^{-5} M. [b] Rhodamine 101 (Φ = 1.0 in ethanol)[58] was the standard for **46** - **49**. FWHM is "Full-Width at Half Maximum" and is a measure of the sharpness of emission signals.

BODIPY **46** emitted at 587 nm (Table 2.1), displayed a favorable quantum yield (Φ 0.73), had greater solubility in organic solvents than **43**, and its fluorescence properties were not affected by the presence of base. Solubility of **46** in aqueous solvent however was poor and this led to significant fluorescence quenching due to aggregation in such media. We attempted to increase water solubility of **46** through addition of carboxylic acids on the phenylacetylene parts while being mindful that such modifications could increase the pH dependence of the compound. For this purpose compound **49** was made via Sonogashira coupling of **48** and **50** (Scheme 2.6) This BODIPY was obtained in 13 % yield reflecting the difficulty in purifying the compound through preparatory HPLC. Emission of **49** was slightly red-shifted compared to compound **46** (Table 2.1) and fluoresced near 600 nm. Interestingly, **49** did not exhibit pH-dependent fluorescence

properties and this characteristic is attractive for imaging applications. Furthermore, **49** is soluble in alkaline aqueous conditions which further adds to its potential as not only a fluorescent label but as an acceptor for TBET cassettes.

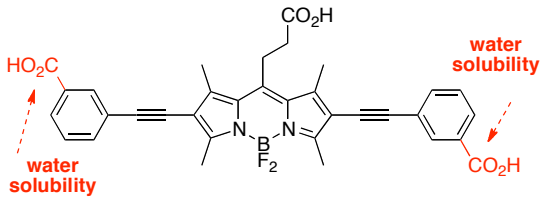

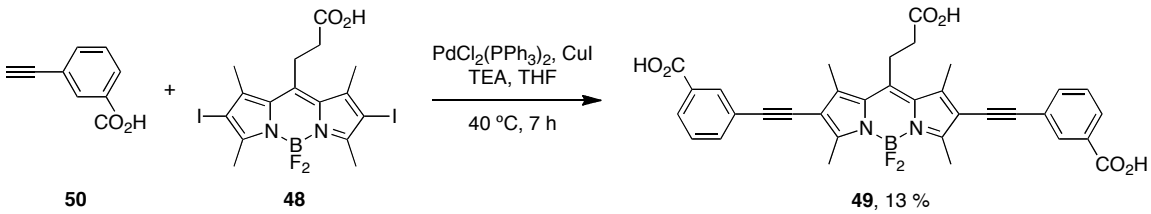

Scheme 2.6. Synthesis of BODIPY **49**.

After completion of the work above, Ziessel *et al*. looked into similar phenylacetylene extended BODIPYs with the aim of extending their emissions to the red (Figure 2.3) and published their findings in 2008.[59] Compound **M** fluoresced near 600 nm, similar to the emissions of compounds **43**, **46**, and **49**. BODIPY **N** displayed a remarkable emission bathochromic shift compared to emissions of other phenylacetylene BODIPYs, emitting at 700 nm but unfortunately possessed a quantum yield below 0.01. Addition of acid to **N** caused hypsochromic shifts in the emission wavelength to 584 nm and also increased the quantum yield to 0.53. This pH sensitivity precludes the use of such compounds for general imaging applications.

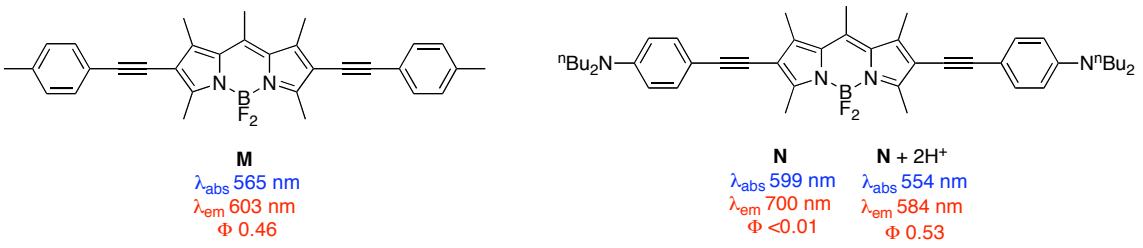

Figure 2.3. Phenylacetylene BODIPYs published by Ziessel after completion of the work described in this chapter.

In summary, compounds of type **43**, **46**, and **49** fluoresce near 600 nm with good quantum yields. Overall, the compounds show promise as acceptors for TBET cassettes and their incorporation into cassettes will be explored in Chapter III.

2.3 C-H Functionalization on BODIPYs

While compounds **43**, **46**, and **49** showed promise as TBET acceptors we were originally interested in developing acceptors that could be conveniently made from derivatizations of the BODIPY core. While this was partially achieved for the phenylacetylene-BODIPY derivatives **43**, **46**, and **49**, the BODIPYs first needed to be diiodinated before derivatization, which could be inconvenient and difficult on more complicated BODIPY systems.

It has been demonstrated that palladium can activate aromatic compounds, particularly pyrroles[60-62] and indoles[63-65], towards C-H functionalization reactions (Figure 2.4a-b) We hypothesized that similar types of reactions could be performed on BODIPY cores due to their nucleophilicities. We were particularly interested in metal catalyzed

functionalizations of BODIPYs with electron withdrawing acrylates to disperse emissions into the red (Figure 2.4c).[66]

a

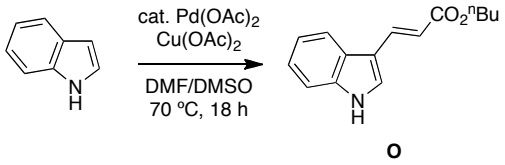

b

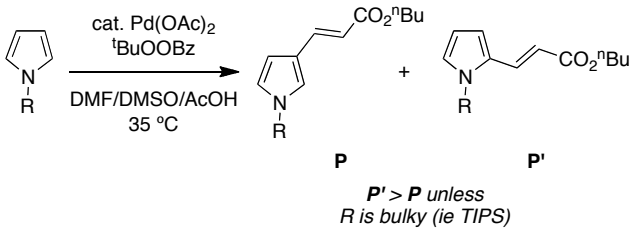

c

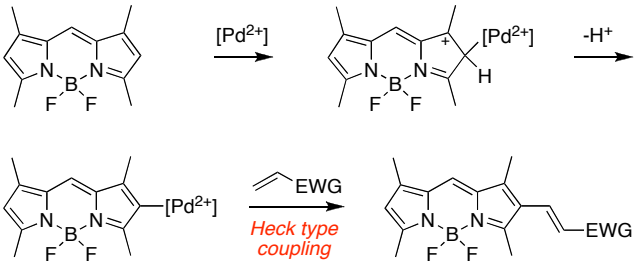

Figure 2.4. C-H functionalization of **a.** indoles and **b.** pyrroles developed by Gaunt *et al.*. **c.** Guiding hypothesis for producing BODIPY dyes with extended conjugation in a single reaction.

The Heck-type coupling shown in Figure 2.4c liberates HPdX(2+) species that disproportionate to Pd(0) and HX; consequently, reoxidants are required to make the reaction catalytic in palladium. Two sets of conditions were explored to bring this about. Method A in Table 2.2 features *tert*-butyl benzoyl peroxide as a reoxidant in a

mixed solvent system. These conditions were devised by Gaunt[62,65] based on Larock's discovery that solvent systems containing DMSO ligate palladium zero preventing formation of insoluble aggregates.[67-69] Method B is a minor modification by us, based on other conditions originating from Larock and Gaunt, but with microwave irradiation.

Table 2.2 indicates method A gave good overall yields when the EWG group was an ester, and that mixtures of mono- (**50**) and di- (**51**) substitution were formed. These were easily separable via flash chromatography (entries 1 and 2). Functionalization with acids was of particular interest to label biomolecules. Entry 3 shows that the predominant product **50c** arose from mono-substitution when an α,β-unsaturated acid was the electrophile. A very low yield of the monosulfonated product **50d** was isolated in entry 4. Diminished yield in this reaction reflects difficulties encountered in the isolation procedure for the sulfonic acid, and perhaps some attenuation of alkene electrophilicity associated with the negatively charged sulfonate form.

Table 2.2. Oxidative functionalization of tetramethyl-BODIPY.

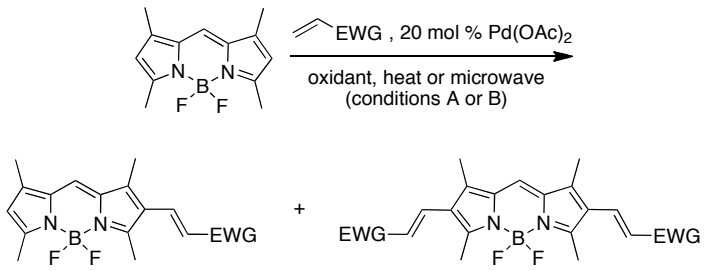

50a - d **51a - d**

entry	EWG	method	isolated yield (%) 50	51
a	CO_2Me	A	61	30
b	CO_2Bu	A	56	28
c	CO_2H	A	29	trace
d	SO_3H	B	2	0

Method A: 20 mol % $Pd(OAc)_2$, ^tBuOOBz, AcOH:dioxane:DMSO, 35 ºC, 5 d. Method B: 20 mol % $Pd(OAc)_2$, $Cu(OAc)_2$, DMF:DMSO, microwave (200W, cooling, 80 ºC, 30 min) .

The fact that both mono- and disubstituted products were formed in some cases gave a good dispersion of UV absorbance and fluorescence emissions for the series as a whole (Figure 2.5). Further, the molar absorptivities of the dyes are comparable to the starting material.[35] Their quantum yields tend to be excellent, ranging from 0.51 to 0.73 for the esters and 0.42 for the carboxylic acid **50c**, though the quantum yield of sulfonic acid **50d** was lower (0.25). Brightness of dyes is a function of absorbance and quantum

yields (see section 1.1), thus it is unsurprising that compounds **50** and **51** are colorful to the eye, and brilliant when irradiated (Figure 2.4c). Spectral data for all the dyes in EtOH is collected in Table 2.3. The sharpness of the fluorescence emissions, characterized as the width of the emission peak at half the fluorescence intensity (full width at half maximum; fwhm), was comparable to the parent 1,3,5,7-tetramethyl-BODIPY (22 nm) but tended to become slightly broader with increased conjugation. This is somewhat unfortunate since dyes ideally need sharp emissions to be used as acceptors in TBET cassettes to obtain well-resolved signals for multiplexing applications (see sections 1.3 and 1.4).

a

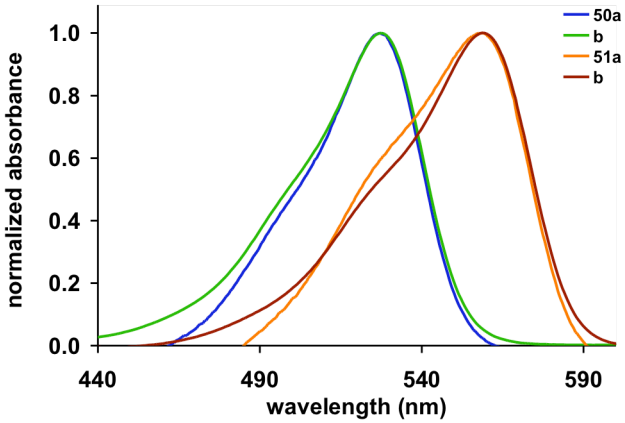

Figure 2.5. Normalized **a.** absorbance; and, **b.** emission spectra of dyes **50a** - **b**, **51a** – **b** in EtOH (1.23 x 10^{-5} M, excited at the respective λ_{max}) with the exception of **51a** which was measured in EtOAc due to poor solubility in EtOH. **c.** Photograph of the dyes **51a**, **51b**, **50b**, **50a**, **53f**, **53e**, **52f**, and **52e** (in that order) under UV irradiation.

b

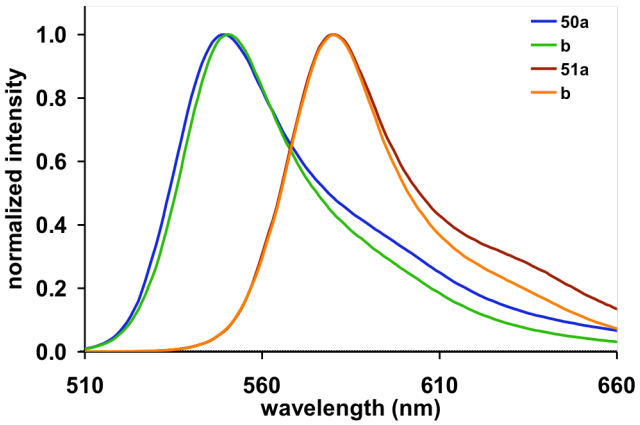

c

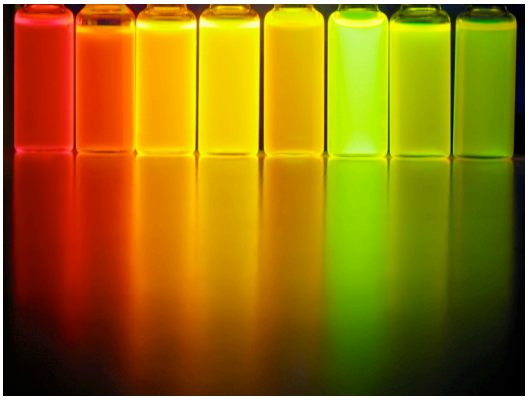

Figure 2.5 Continued.

Table 2.3 Spectral Properties Measured in Ethanol

	λ_{max} (nm)	$\log(\varepsilon_{max})$	λ_f (nm)	fwhm (nm)[a]	Φ_f
50a	527	4.80 ± .01	549	40	0.73 ± .01
51a	559[b]	4.13 ± .01	580	45	0.51 ± .02
50b	528	4.79 ± .01	551	39	0.73 ± .01
51b	560	4.48 ± .01	580	37	0.52 ± .01
50c	531	4.43 ± .02	570	58	0.42 ± .02
50d	529	-[c]	560	50	0.25 ± .01
52e	518	4.37 ± .02	525	24	0.72 ± .01
53e	530	4.86 ± .01	539	25	0.92 ± .05
52f	517	4.80 ± .01	527	25	0.78 ± .01
53f	529	4.74 ± .01	540	24	0.89 ± .01

[a] Full width at half-maximum height: a measure of the sharpness of the fluorescence peaks. [b] Measured in ethyl acetate. [c] Quantity isolated too small for accurate measurement

At the time of this work, there were relatively few water soluble BODIPY dyes, and even fewer that had well documented synthetic procedures to make them.[44,70] In the context of TBET cassettes, water solubility is important to avoid quenching of the dyes by intercalation in biomolecules and also to aid the labeling process, however since the use of dyes **50** and **51** in cassettes is precluded by their emission wavelengths we chose to shift the focus of these BODIPYs as simple biomolecule labels. Fluorescent labels also need to be water soluble to avoid aggregation effects and to aid the labeling process;

and functionality should be present for labeling purposes. Dye **50c** is slightly water soluble, and has a carboxylic acid that could be activated with water solubilizing groups, *e.g.* a sulfonated *N*-hydroxysuccinimide. Consequently, it has potential for covalent linking to biomolecules. BODIPY **50d** is water soluble, and could find other applications where fluorescence in aqueous media is required. For these reasons, we chose to study these two dyes in aqueous buffers at different pH values (Figure 2.6). **50c-d** show no sensitivity to pH range of 6.05 – 8.04 where the emissions vary by only 3 nm. This is a marked contrast to fluorescein dyes for which equilibria between xanthene and ring-closed-lactone forms cause the emissions wavelengths and intensities to vary greatly over a similar pH range. [71]

a

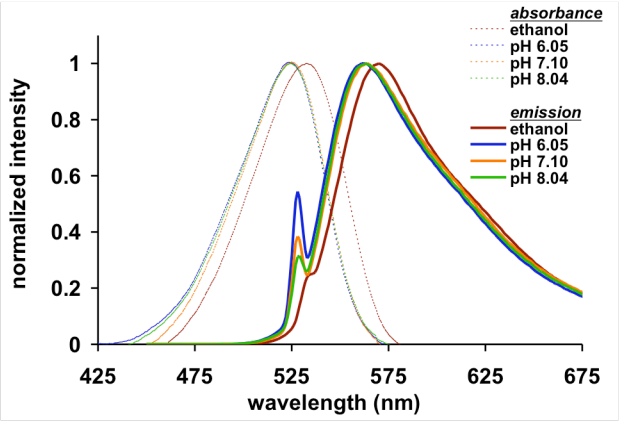

Figure 2.6. Normalized absorbance and emission spectrum of **1c** (**a**) and **1d** (**b**) in various solvents (1.23 x 10^{-5} M in ethanol and 1.00 x 10^{-5} M in buffer). Buffers used were: pH = 2.19 citric acid; pH = 6.05 MES/LiOH; 7.10 bis-tris/H_3PO_4; 8.04 HEPES/LiOH

b

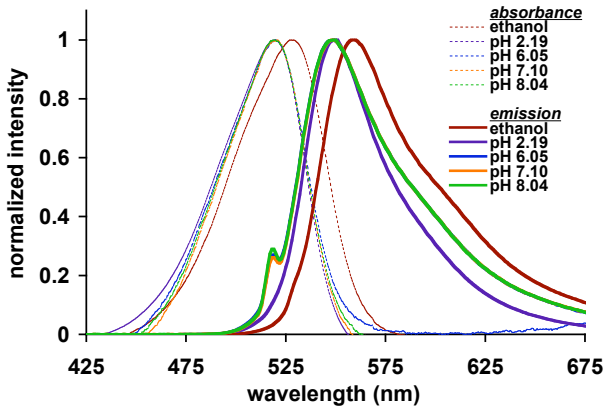

Figure 2.6 Continued.

Mechanistically, C-H functionalization was thought to proceed first by ligand exchange between the BODIPY and $Pd(OAc)_2$ yielding a BODIPY-Pd-OAc intermediate (Figure 2.7). The substituted BODIPY then undergoes Heck-type migratory insertion between the BODIPY and acrylate followed by β-hydride elimination. To test this mechanistic hypothesis we tried the functionalization reaction on cyclic substrates lacking *syn* β-hydrides that would otherwise allow for elimination producing alkenes in conjugation with BODIPY.

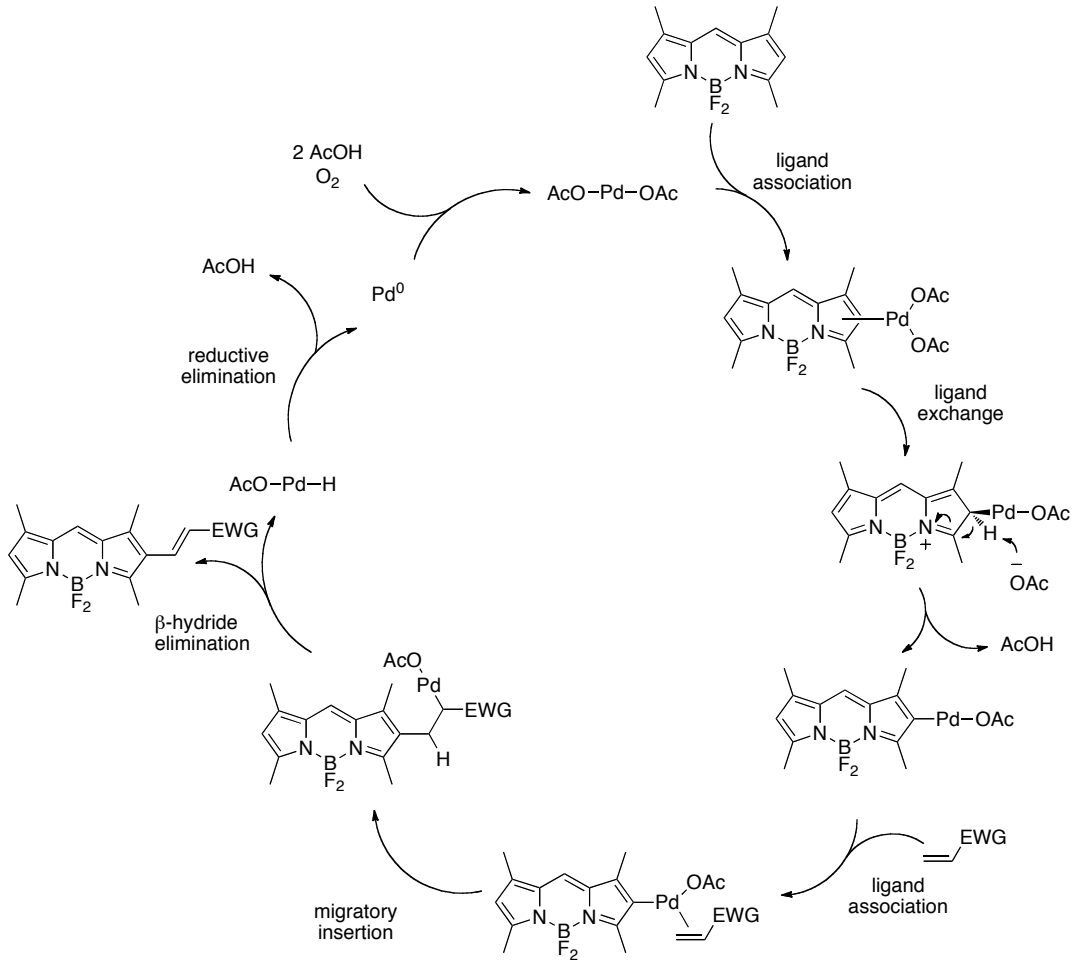

Figure 2.7. Hypothesis for mechanism of C-H functionalization.

Reaction 1 (Figure 2.8) shows the C-H functionalization process applied to two α,β-unsaturated esters, **Q** and **R**. As before, mono- and disubstituted products were isolated (**52** and **53**, respectively), but the alkene double bond was shifted out of conjugation with the BODIPY core. Migratory insertion of intermediates like **S** cannot undergo β-elimination to form an alkene in conjugation with the BODIPY part; the only hydrogen available on the same face of the carbocyclic ring is the one marked H^{β} below, which takes the alkene out of conjugation. The products **53** are probably mixtures of

diastereomers, but the two chiral centers are so far apart that the NMR data is as if this were essentially one compound.

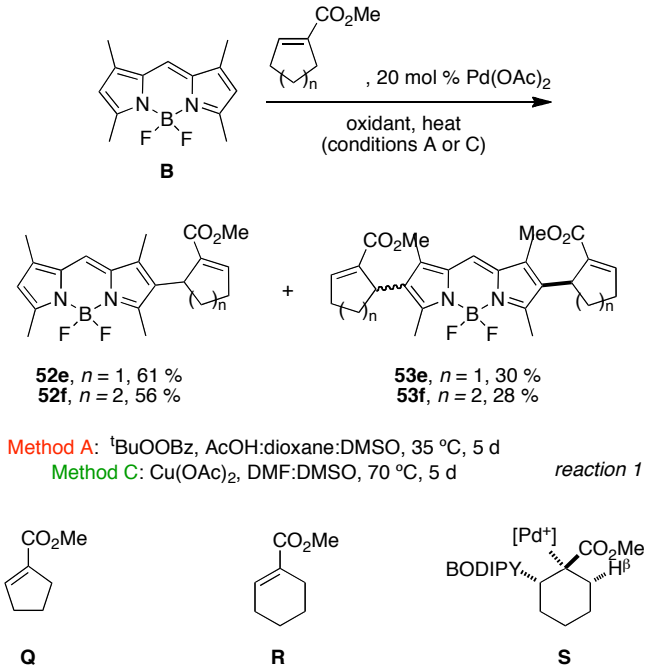

Figure 2.8. C-H functionalization of **B** with carbocyclic unsaturated esters that lack β-hydride that can eliminate to give a conjugated product with the BODIPY core.

In summary, palladium mediated C-H functionalization reactions provide a direct way to extend the conjugation of BODIPY **B**. The strategy does not require that halogenated or metallated intermediates be isolated prior to the coupling reaction. Mono- and disubstituted products can be obtained; these have brilliant fluorescence with emissions that span 525 – 580 nm. Further the methodology has potential for syntheses of systems with handles for bioconjugation and inclusion of water-solubilizing groups. The

fluorescence wavelengths and large FWHM however are not conducive towards use of the compounds as acceptors for TBET cassettes.

2.4 Conclusions

Functionalizing the BODIPY core provides direct methods of shaping BODIPY dyes for specific uses. There have been numerous modifications to BODIPY cores to increase both emission wavelengths and water solubilities since the work described herein.

C-H activation[72-76] has potential for functionalizing BODIPYs since otherwise unreactive C-H bonds could potentially be functionalized and regioselectivities can be different than other methods. Boronic esters are valuable intermediates since they undergo many transformations including Suzuki couplings[77], Heck-type couplings[78], oxidations to alcohols, and deprotections to boronic acids.[79] For this purpose we explored the C-H activated borylation of BODIPY **B** (Scheme 2.7a). Unfortunately, the BODIPY proved unreactive towards C-H borylation reactions, though similar borylation was subsequently achieved by others on less substituted BODIPYs (Scheme 2.7b).[78] The differences in reactivity between our attempt and theirs can be ascribed to steric hindrances since these types of C-H borylation reactions tend to be highly sensitive to such interactions; this also explains β-selectivity of such borylation reactions since α-selectivity are favored electronically.[72] Unfortunately, borylated BODIPY **T** was obtained in low yield and as a mixture with mono-activated product **U** although the authors found that the borylation step could be more conveniently carried out at earlier

stages of BODIPY synthesis. The authors utilized the borylated BODIPY intermediates for Heck-type coupling reactions to acrylates (Scheme 2.7c) to obtain products similar to BODIPYs **50** and **51**. Comparable reactions with dienoates where also attempted but the yields were low (not shown).

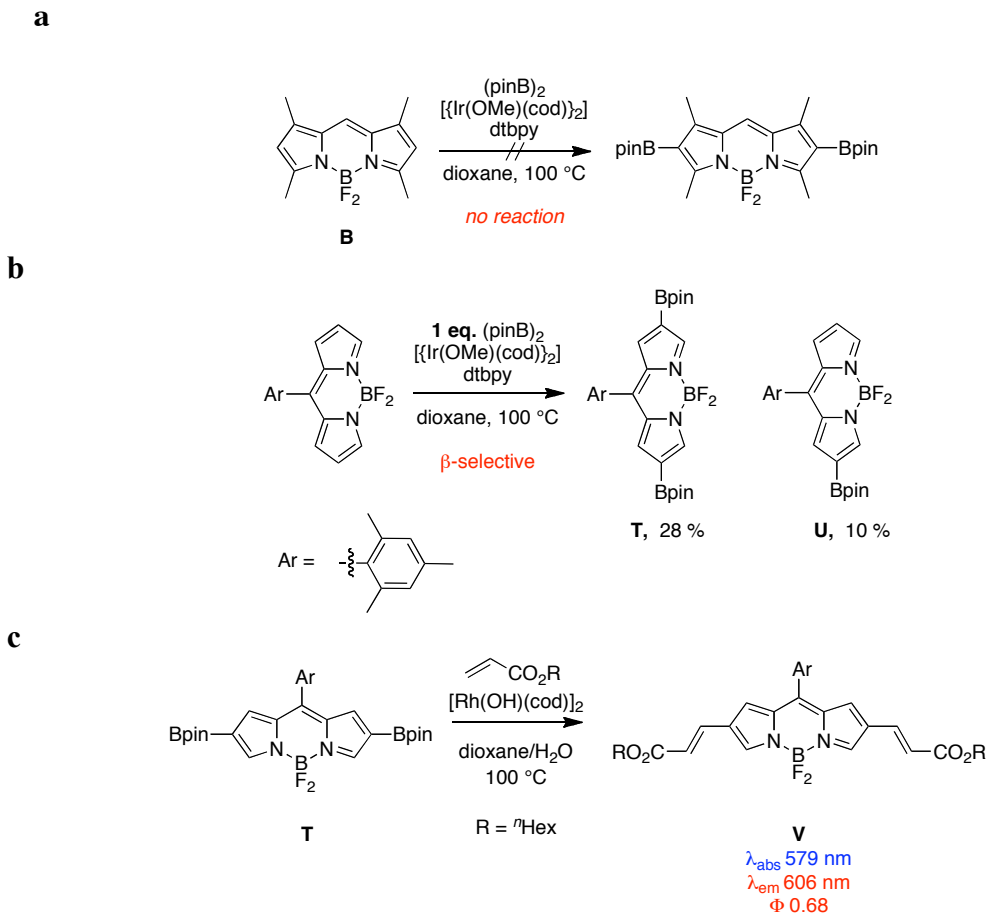

Scheme 2.7. C-H activated borylation of the BODIPY core.

Although modifications described so far focused on functionalization to increase emission wavelengths, modifications of the BODIPY core can be performed for other purposes. The BODIPY core is nucleophilic and therefore reacts with a variety of

electrophiles.[31] Vilsmeier–Haack formylation provides a convenient way to add carbonyl functionality to electron rich aromatic systems. Once the functionality is introduced the oxidation state of the carbonyl can be adjusted to yield alcohols by reduction, and esters and acids by oxidations. For this reason we sought to formylate BODIPY using standard Vilsmeier–Haack conditions. Unfortunately only mono-formylation was obtained. Oxidation to the acid using perchromates tended to react in poor yields often leading to decomposition of the BODIPY. Although this work was never published the results were briefly mentioned in a review published in 2007.[31]

Subsequent work by Jiao *et al*. expanded formylation of BODIPYs to *meso*-aryl substrates and found that these could also be mono-formylated.[80] The authors further explored Knoevenagel condensation of the aldehydes with nucleophiles such as malononitrile and found the reactions to proceed in good yields (Scheme 2.8). Surprisingly, only modest emission bathochromic shifts were obtained upon these condensations; for example formylated BODIPY **W** emitted at 516 nm while extended BODIPY **X** emitted at 543 nm.

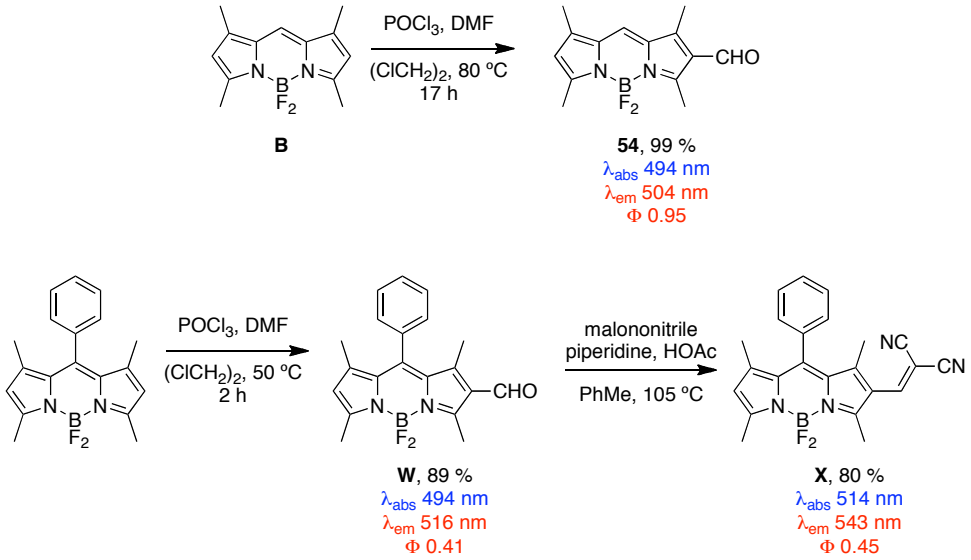

Scheme 2.8. β-selective formylation of the BODIPY core by us and others.

Other than extending the emission wavelengths, perhaps the most important modifications of the BODIPY core are ones that increase water solubility. Although water solubility can be an important factor for imaging application, there are relatively few known water-soluble analogs of BODIPYs.[44,70,81-88] Sulfonation of the BODIPY core provides a convenient way of increasing water solubility without affecting photophysical properties. Sulfonation is usually performed by the reaction of the BODIPY with chlorosulfonic acid, followed by base hydrolysis (Figure 2.9a). [86,87] Using this method probes like **Z** have been synthesized and attached to proteins (Figure 2.9b). Unfortunately, compounds like **Z** do not fluoresce very far to the red. In practice it becomes harder to modify the BODIPY core to simultaneously enhance water solubility and emission wavelengths. It is not hard to image dyes such as the one in Figure 2.9c that would be ideal as both acceptors and fluorescent probes due to their water

solubilities, red emissions, and possession of functionality to attach biomolecules. However, such dyes are difficult to make and a balance must exist between the complexity of dyes and the cost and time needed to make them. Overall, in TBET cassettes, an opportunity exists to spread the needed modifications unto the donor and acceptors. Such examples will be presented in Chapter III and in the concluding chapter. In this regard, even non-ideal dyes such as compounds **46** and **49** have scope as acceptors in TBET cassettes.

a

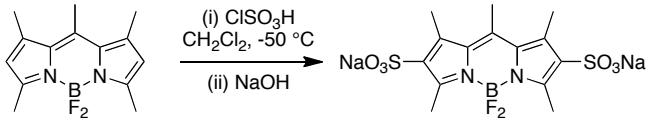

Y, 40 %
λ_{abs} 492 nm
λ_{em} 533 nm
Φ 0.73 (H_2O)

b

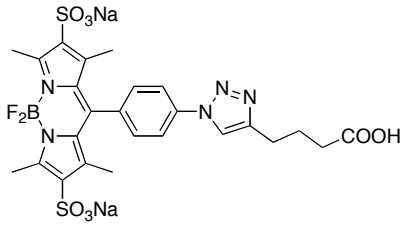

Z
λ_{abs} 498 nm
λ_{em} 511 nm
Φ 0.49 (H_2O)

Figure 2.9. a. Example of sulfonation of BODIPYs to increase water solubility. **b.** Example of probes that have been made from such sulfonations. **c.** Example of an "ideal" acceptor that could be made from derivatizations of the BODIPY core.

c

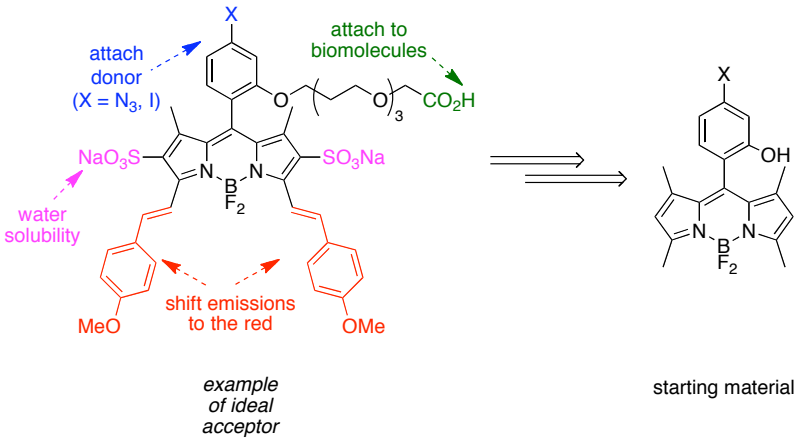

Figure 2.9 Continued.

CHAPTER III

THROUGH-BOND ENERGY TRANSFER CASSETTES WITH PHENYLACETYLENE-BODIPY ACCEPTORS

3.1 Introduction

TBET cassettes were discussed in detail in Chapter I so only a brief overview will be reviewed here. When two dyes are connected together in a way that prevents the two from being co-planar with each other or with a conjugated linker (if one is used) fast energy transfer can occur through-bonds (Figure 3.1). The advantage of such an arrangement is that large virtual Stokes' shifts are accessible because the energy transfer efficiency from donor to acceptor is not governed by any known spectral overlap of the donor and acceptor, a requirement of RET.

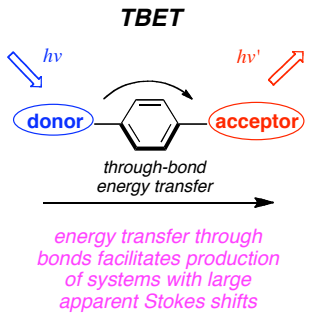

Figure 3.1. Basic concept of TBET cassettes. See Chapter I for a detailed explanation.

Although BODIPY dyes are ideal imaging fluors due to their photostabilities, high quantum yields, and favorable molar absorptivities, most lack functionality to attach to biomolecules and fluoresce in the blue-green region. Furthermore they are usually

lipophilic and have a tendency to intercalate in hydrophobic portions of biomolecules. For these reasons derivatives of BODIPYs that: (i) fluoresce to the red, (ii) contain biomolecular handles, and (iii) are water soluble, were explored in Chapter II. In this chapter, some of the dyes developed in Chapter II will be incorporated in TBET cassettes in attempts to study protein-protein interactions, and used as pH probes.

Preliminary Work

Of the dyes developed in Chapter II, **46** and **49** showed promise as acceptors for TBET cassettes because they emitted near 600 nm and contained a handle to attach to proteins and other biomolecules (Figure 3.2). Since **46** is not water-soluble and **49** is only so under basic conditions we decided to convey water solubility on to the donors. Donors for TBET do not need to absorb or fluoresce far to the red and therefore compound **A** was ideal for our purposes. It has been observed by others that increasing the number of donor dyes in cassettes simultaneously increased the molar absorptivities, increasing brightness of the cassette in the process.[27] For this reason we designed cassette **55**, with two peripheral sulfonated BODIPY donors (corresponding to **A**) and a diphenylacetylene BODIPY acceptor (corresponding to **46**). The twist in such cassettes should be afforded by the steric interactions at the *meso*-position on the BODIPY donors. It is also noteworthy that there is no linker in this cassette design.

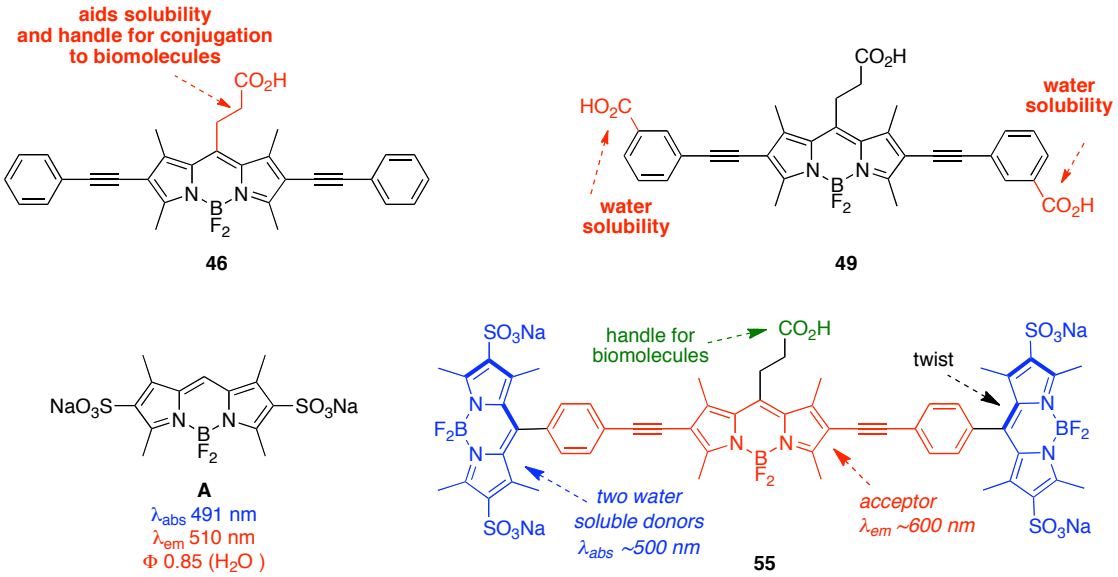

Figure 3.2. Design of TBET cassette **55**.

Synthetically it is generally more difficult to work with polar, hydrophilic compounds than lipophilic ones. For this reason we wished to add polar functionality in late stages of the synthesis. To briefly summarize our efforts to obtain cassette **55** (Scheme 3.1), our first attempt involved the Sonogashira coupling between acetylene BODIPY **57** with diiodoBODIPY **59** to yield cassette **60**. The idea was to first hydrolyze the methyl ester **60** and then sulfonate the free acid four times with chlorosulfonic acid. Strangely, **60** did not hydrolyze under various conditions and more rigorous methods decomposed the starting material. Comparable hydrolysis of diiodoBODIPY **59** did yield the acid though the reaction time had to be carefully monitored to avoid decomposition (not shown). After much effort we theorized that hydrolysis of sulfonated cassette **62** might be more successful, mindful that purification of intermediate **62** could be difficult. However, Sonogashira coupling between the sulfonated *p*-iodophenylBODIPY **B** and

diacetyleneBODIPY **61** was not successful. We then attempted Sonogashira coupling of free acid BODIPY **48** with sulfonated donor **63** but this too failed produce the desired product. We finally synthesized cassette **64** with the intent of sulfonating it to obtain cassette **55**, unfortunately the reaction yielded complex mixtures and mass spectrometry failed to confirm presence of **55**.

a

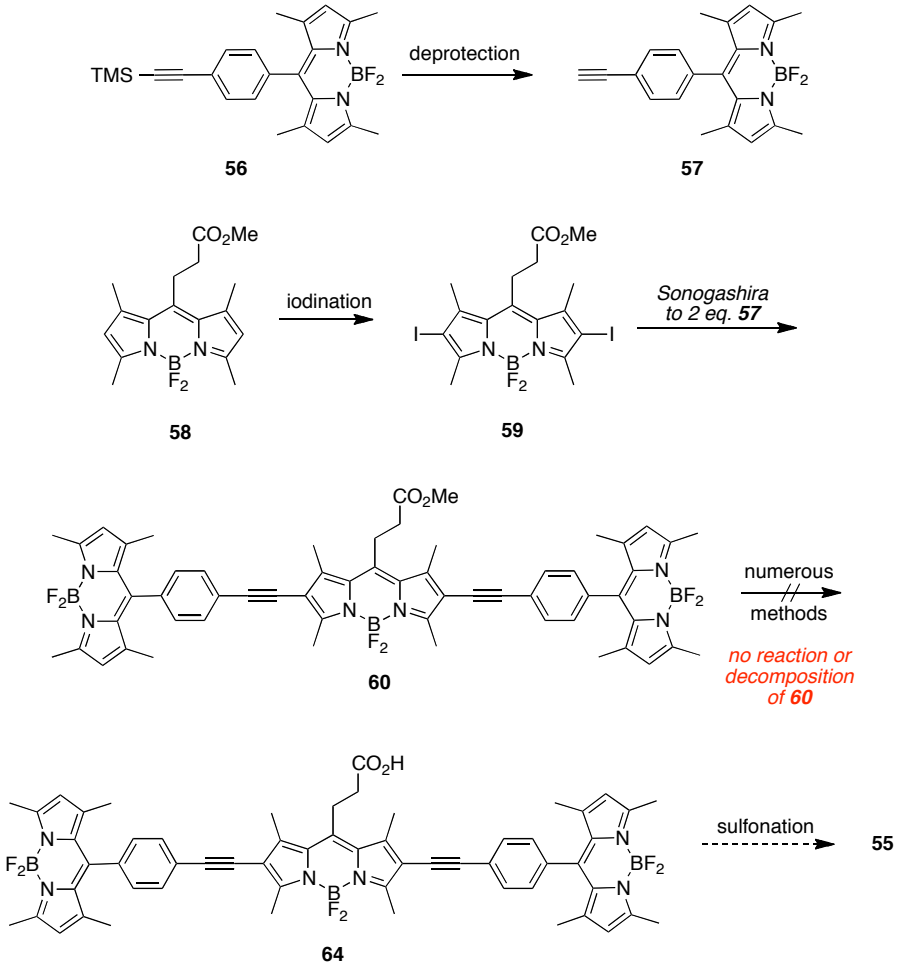

Scheme 3.1. Attempted syntheses of cassette **55**.

b

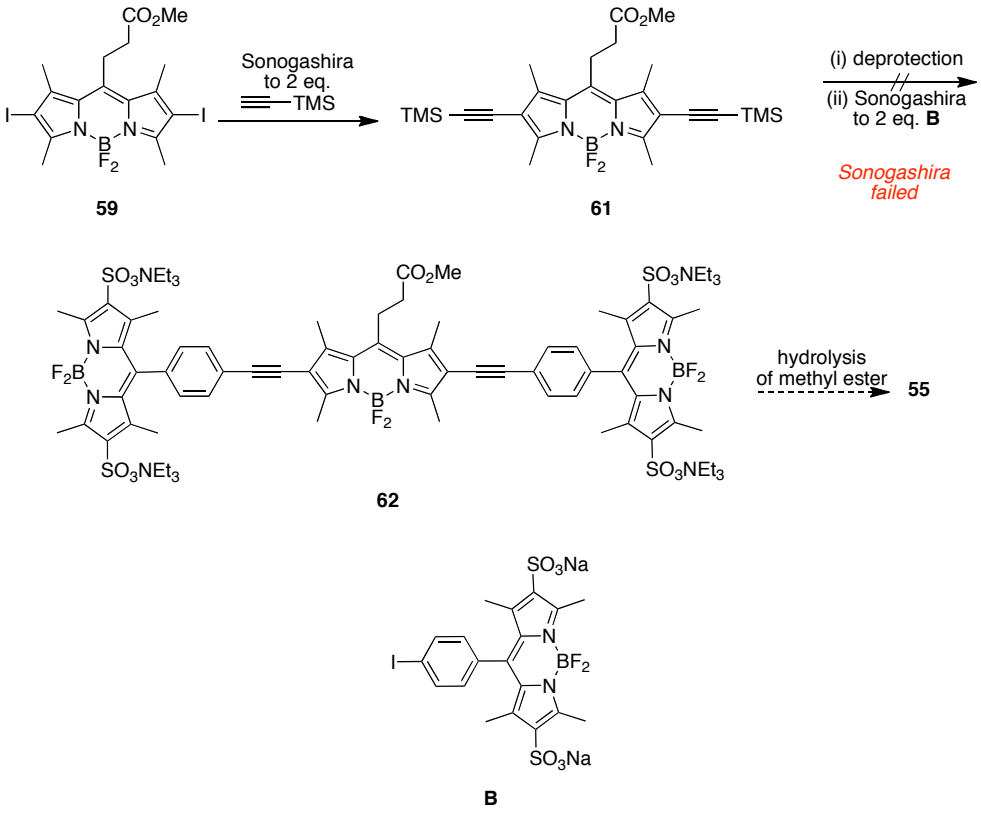

c

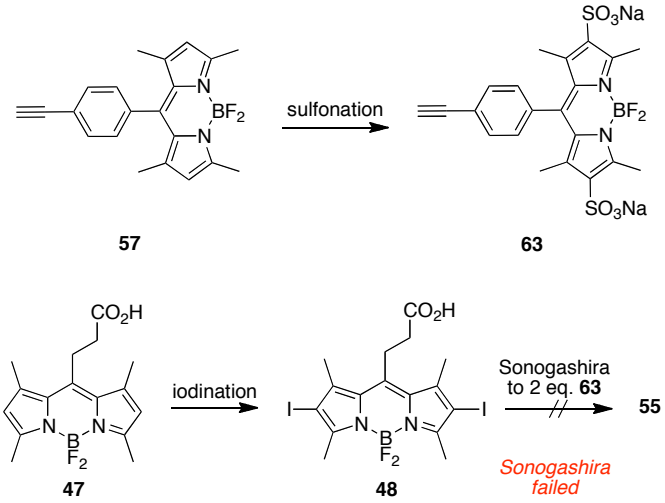

Scheme 3.1 Continued.

d

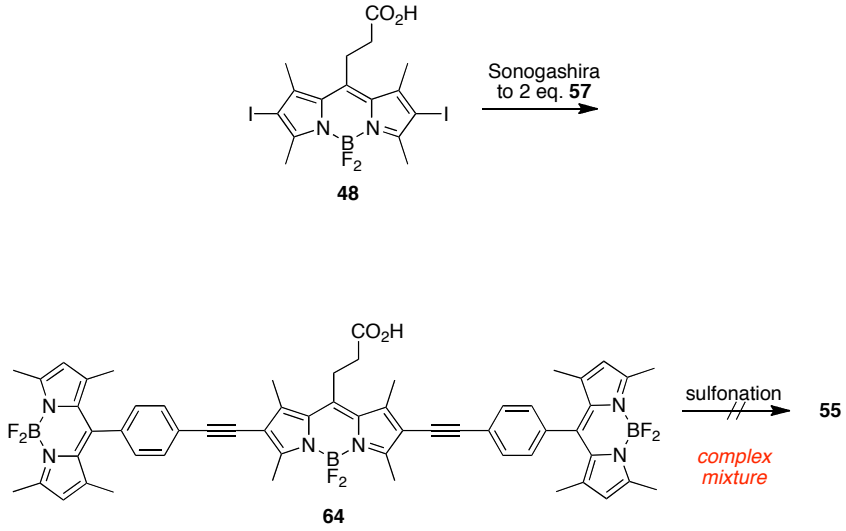

Scheme 3.1 Continued.

Although compound **55** would have been interesting for cellular imaging, its synthesis was becoming time and resource consuming. For this reason we the reconsidered synthesis of **55** and looked into the use of lipophilic compound **64** as an alternative. Photophysical properties of **64** in methylene chloride are adequate for imaging, the donors absorb at 502 nm with a molar absorptivity of 110,000 $cm^{-1}M^{-1}$. The emission of the acceptor part at 588 nm was slightly blue shifted compared to free acceptor **46**. Cassette **64** displayed excellent energy transfer, only <5 % of the total fluorescence of the cassette was attributed to donor emission when the cassette was excited at the donor.

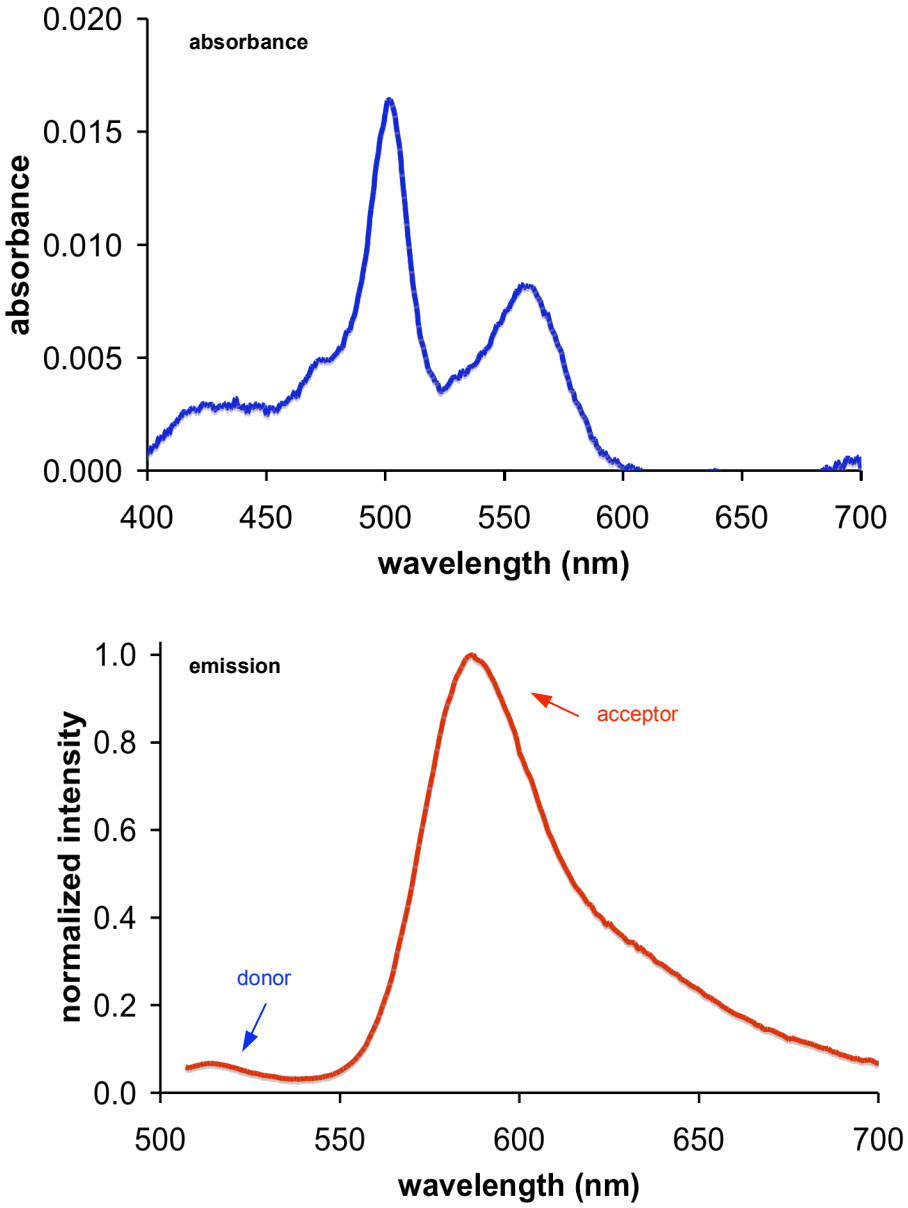

Figure 3.3. Absorbance and emission spectra of **64** in CH_2Cl_2 at 10^{-5} M.

Encouraged by the energy transfer properties of **64** we wanted to test if these favorable characteristics were retained after labeling to protein. For this purpose we chose Avidin for no other reason than its availability. Labeling was accomplished by first activating

the acid on **64** with sulfo-NHS in the presence of DIC (Figure 3.4a) This activated intermediate was then used to label lysines on Avidin. The absorbance of the labeled protein in water confirmed the presence of the cassette and the spectrum is not significantly different than the free cassette in organic solvents (Figure 3.4b). The emission of cassette on Avidin however was weak compared to the free cassette and the emission came from mostly the donor parts. This suggests poor energy transfer possibly due to intercalation of the cassette in the protein. Further experiments carried out in collaboration with Robin Hochstrasser's lab involved the absorption of the labeled protein on glass (Figure 3.4c). In these experiments the cassette showed similar fluorescence characteristics as the cassette on Avidin in water. Interestingly, when labeled Avidin was bound to PalmitoylOleoylPhosphatidylCholine (POPC) bilayer, better energy transfer was observed. This could be because the cassette intercalates less when the protein is introduced to a hydrophobic environment. POPC bilayers have been found to be suitable models of the matrix of endoplasmic reticulum[89] hinting at the potential of cassette **64** as a labeling agent of membranes. However, its use to label proteins especially to study protein-protein interactions is limited.

a

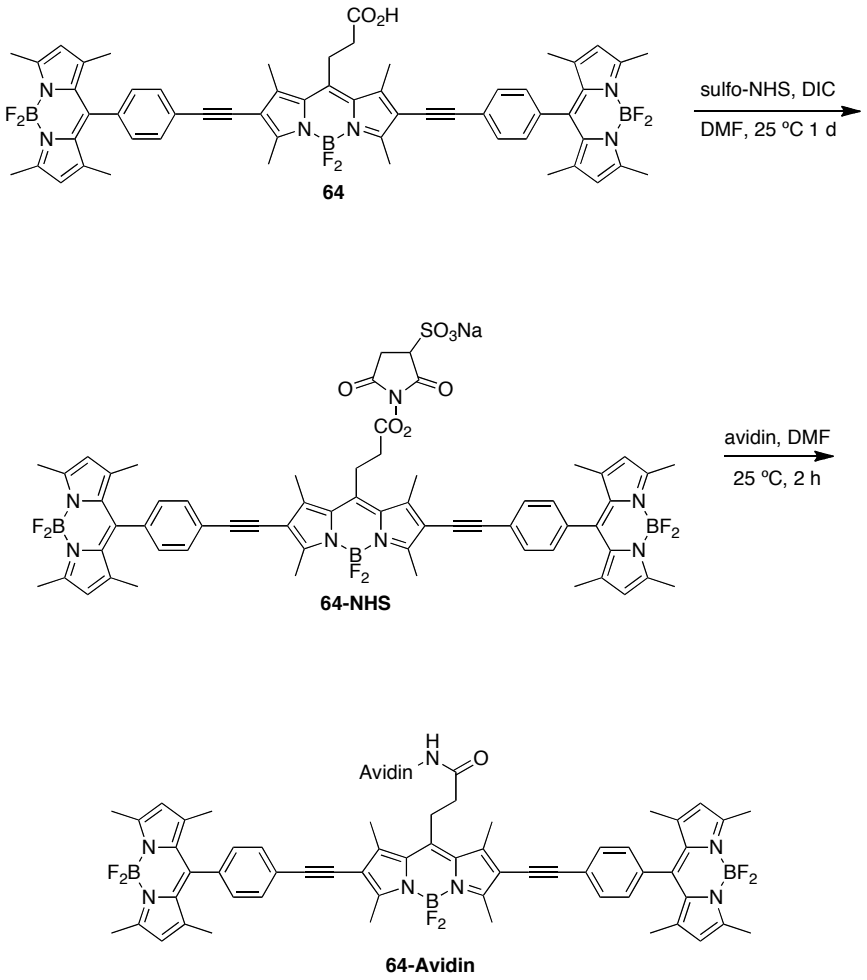

Figure 3.4. a. Attachment of **64** to protein. **b.** Absorbance and emission spectra of **64-avadin** conjugate in water. **c.** Energy transfer studies of **64-avidin** absorbed on glass and bound to POPC. Excitation and detection wavelengths used: D->D = λ_{ex} 488 nm and λ_{det} 510-600 nm; A->A = λ_{ex} 568 and λ_{det} 590-650 nm; D->A = λ_{ex} 488 and λ_{det} 590-650 nm.

b

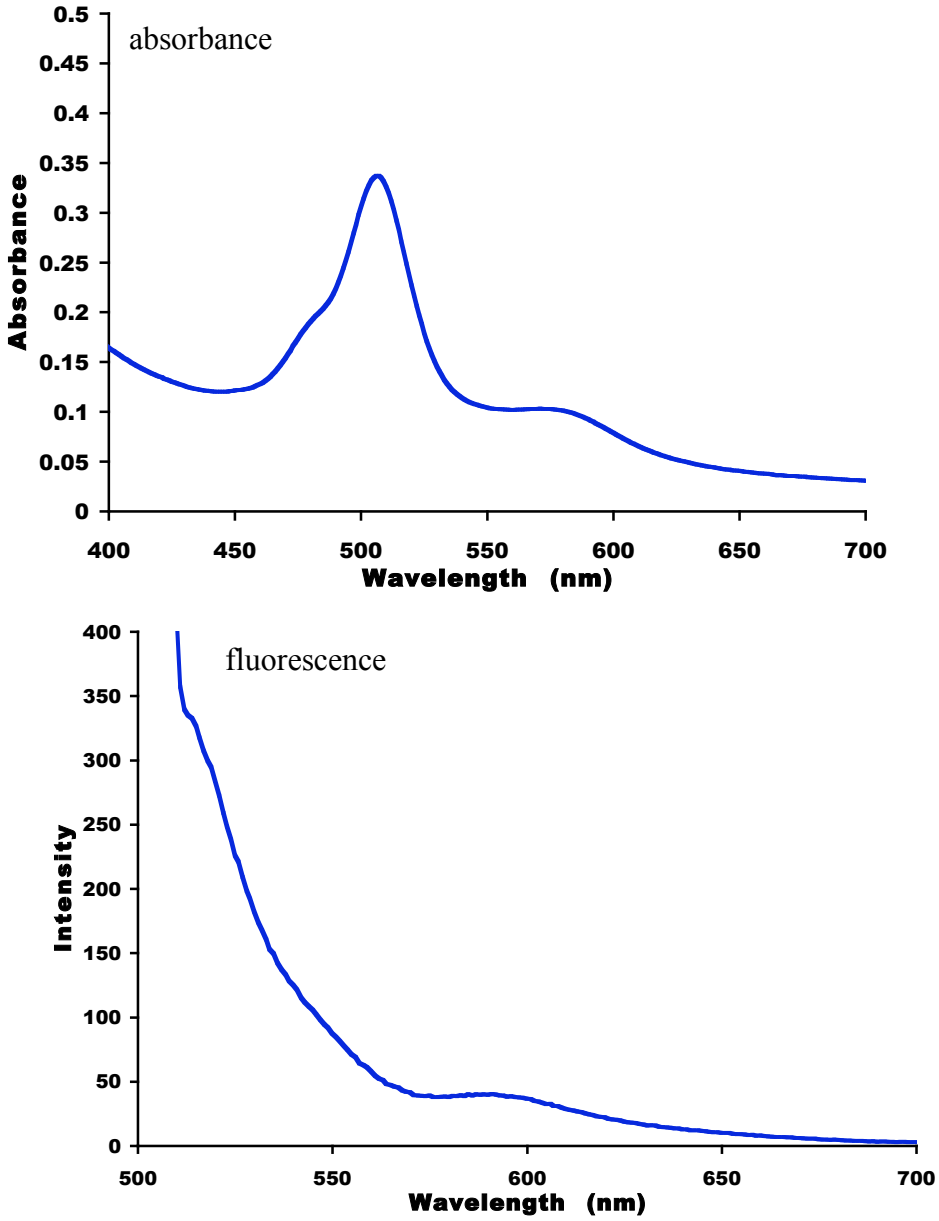

Figure 3.4 Continued.

c

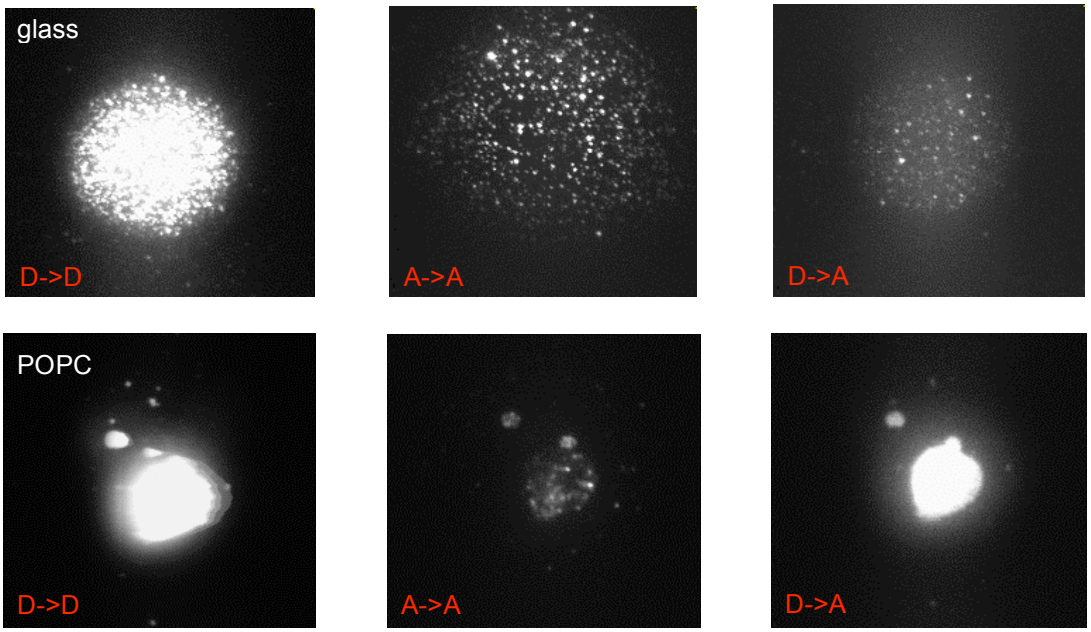

Figure 3.4 Continued.

Concurrent to the work outlined above, others in our lab looked into using dyes of type **46** and **49** as acceptors for TBET cassettes. For example cassette **C** is based on acceptor **49** with the addition of a triethylene glycol linker for increased water solubility (Figure 3.5). Cassette **C** further differs from **64** in the use of xanthene donors rather than BODIPYs. Interestingly, energy transfer properties of **C** showed remarkable sensitivity to pH. Efficient energy transfer occurred in acidic pHs with emission primarily at ~600 nm while poor transfer arose under basic conditions leading to green emission at 525 nm. Neutral conditions produced simultaneous emission from the donors and acceptor. Although pH sensitivity is not a property associated with ideal imaging dyes, the use of such systems as pH probes is, at the very least, intriguing.

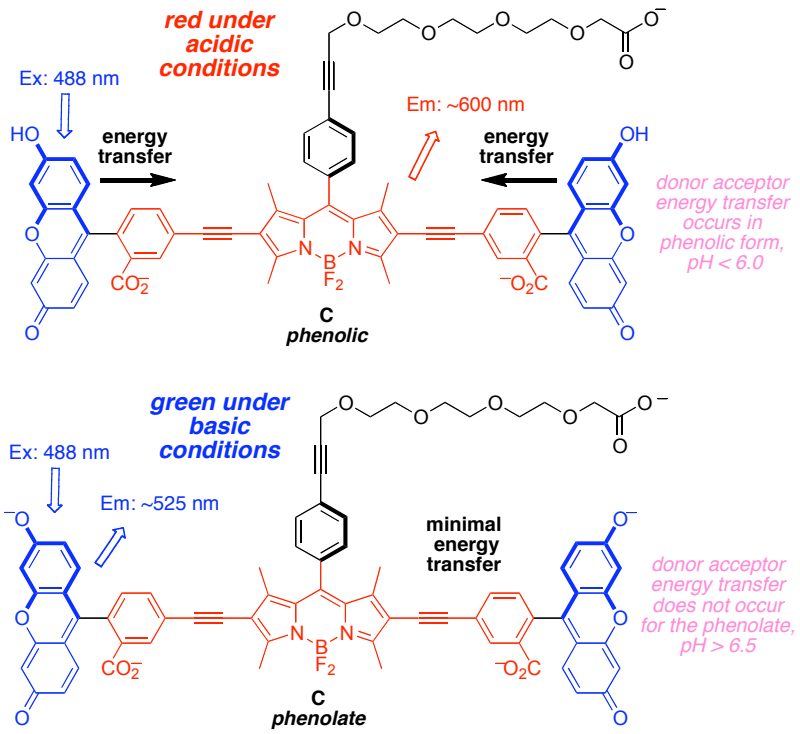

Figure 3.5. Structure and pH sensitivity of **C**.

Fluorescent sensors are widely used for detection of protons and metals in several applications,[90,91] especially intracellular imaging.[92] Types of indicators may be divided into three: (i) ones that are insignificantly fluorescent in the absence of analyte, but are much more emissive when it is present; (ii) the inverse, where fluorescence of the probe is quenched by the analyte; and, (iii) sensors which have observable spectroscopic differences when the analyte is present compared to when it is absent. The third type of sensor is "always on"; this is a significant advantage because it is clear that the probe is present even if the analyte is not (Figure 3.6).

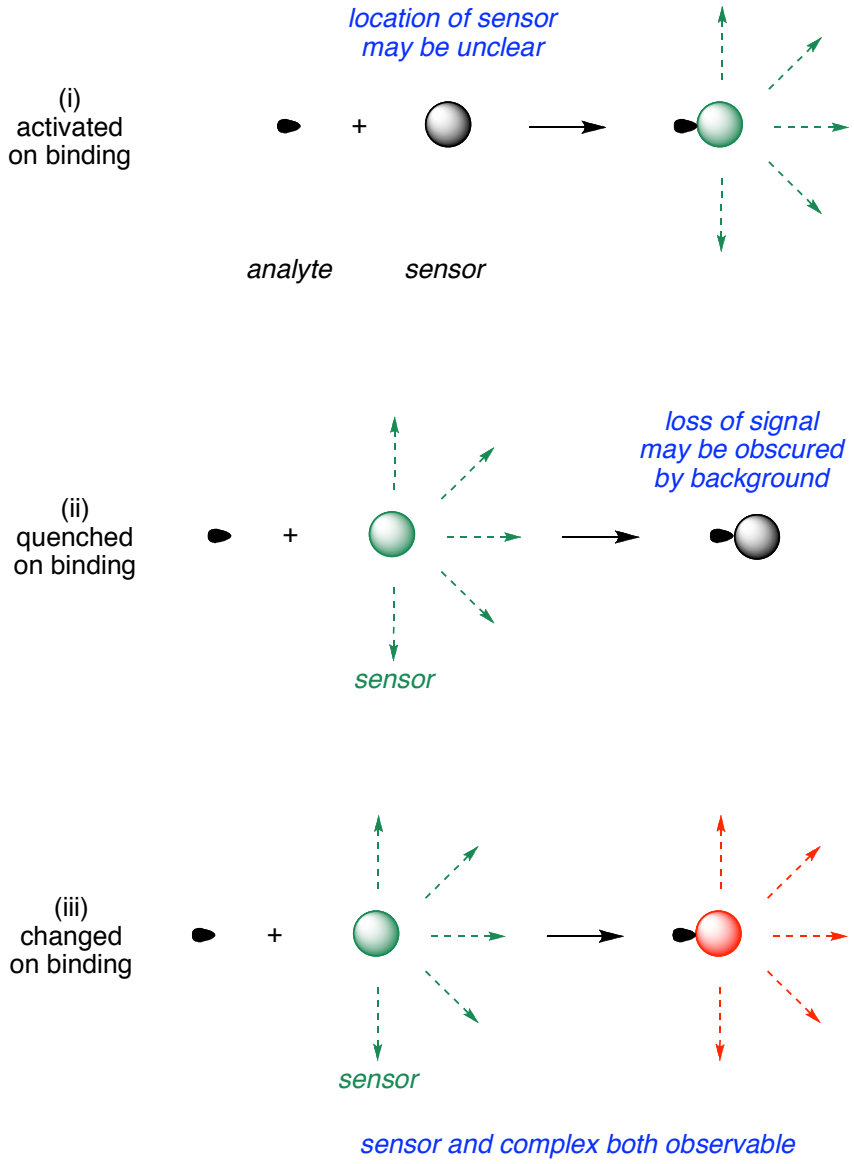

Figure 3.6. Fluorescent sensors may be activated (i) or quenched (ii) by analytes; ones that are "always on" (iii) but change wavelength of fluorescence emissions on binding.

Intracellular pH (pH_i) is a fundamental property that correlates with many events in cell biology. To measure this, researchers tend to rely on subtle changes in sensors that

are "always on";[93-101] for instance, they observe emission intensities as a function of excitation wavelength.[71,101-103] However, these sensors do not change emission wavelength maxima as the pH is varied; if they did, they would be far easier to use. That is why we were excited to realize cassette **C** is always fluorescent at pH ranges around the physiological region, but with emission maxima that varying over a very significant spectral region, ca 530 and 600 nm. Probe **C** compared favorably with commercial pH sensors such as carboxySNARF-1 (Invitrogen), insofar as its pH response range is complementary, and its quantum yields are higher. Further, probe **C** exhibits a greater wavelength difference (~80 nm) between the two ratiometric emission peaks than carboxySNARF-1. It also has acid functionality to conjugate to proteins while carboxySNARF-1 does not.

Endosomes within cells are markedly more acidic (pH 5.0 – 5.5) than the cytosol (*ca* pH 7.4).[104] We have observed that when the non-covalently bound carrier peptide "Pep-1"[105] imports dye labeled proteins into COS-7 cells the protein-dye conjugates tend to be encapsulated in endosomes.[106] Consequently, it was anticipated that when **C-BSA** was imported into cells using Pep-1, it would localize in endosomes and, in that acidic environment the probe would emit around 600 nm. When **C-BSA** was imported into COS-7 cells using Pep-1, irradiation at 488 nm resulted predominantly in red fluorescence localized in punctate vesicular structures (Figure 3.7a).

A discovery from our laboratories shows that Pep-1 mediated import into COS-7 cells tends to deposit the dye-labeled protein cargoes *into the cytosol when the experiment is performed at 4 °C*.[106] Thus, **C-BSA** under these conditions would be expected to fluoresce with diminished red-to-green ratios. The fluorescence intensity for **C-BSA** is distributed within the cytosol, hence the images in Figure 3.7b appear to be deceptively weak relative to situations (*e.g.* Figure 3.7a) where the probe is concentrated in punctates.

Quantitative data for pH measurements in cells were obtained via a calibration experiment. A curve generated with the calibration experiment (Figure 3.7c) was used to determine pH values for the endosomes and the cytosol for the experiments shown in Figure 3.6a and b. The pH values, obtained from the red/green ratio, were 5.4 and 7.4 and were in good agreement with those expected for such intracellular regions, matching very closely to values obtained from commercially available sensors (not shown).

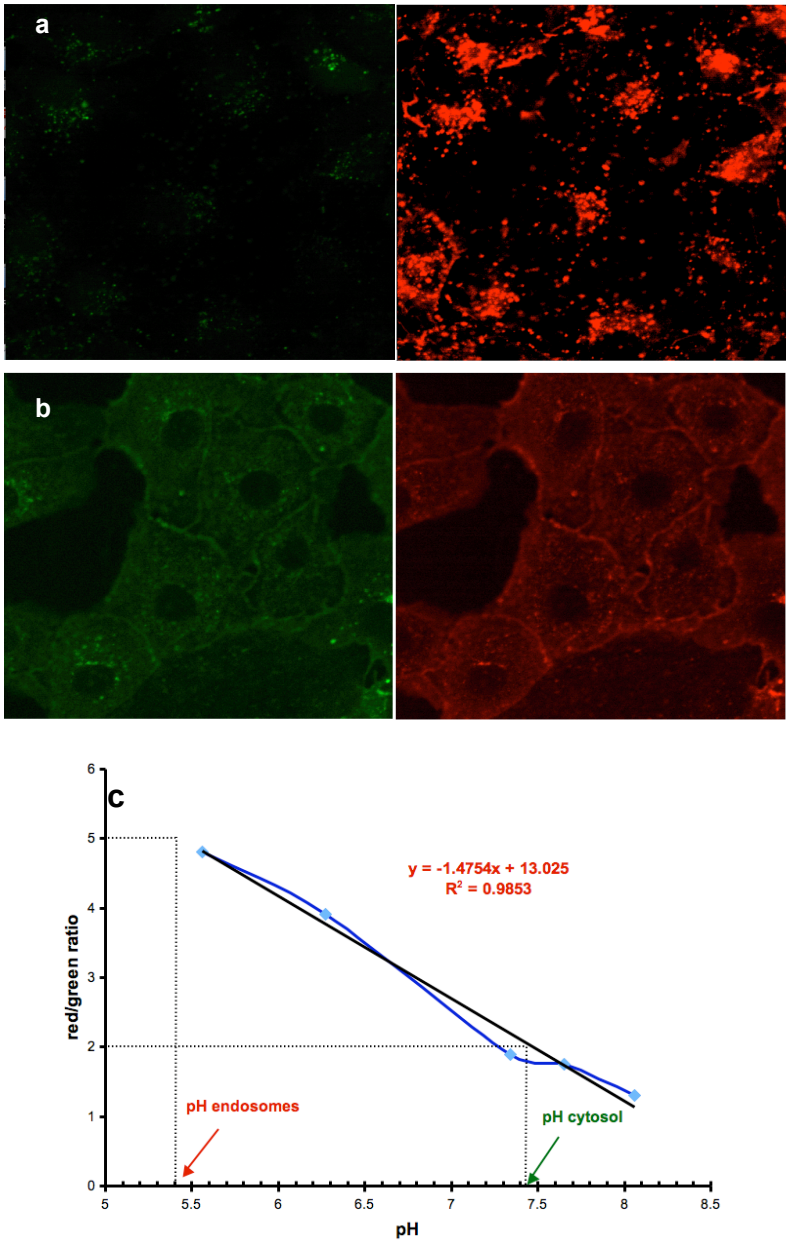

Figure 3.7. Pep-1 mediated cellular uptake of **C-BSA** into COS-7 cells after 1h incubation at **a.** 37 °C and **b.** 4 °C. The cells were irradiated at 488 nm and fluorescence from donor (503-553 nm) and acceptor (575-625 nm) was detected respectively. **c.** *ex-vivo* calibration curve with pH values corresponding to those observed within endosomes (red/green = 5.03; import at 37 °C) and the cytosol (red/green = 2.03; import at 4 °C).

Fluorescent Proton Sensors Based On Energy Transfer[*]

Research described in this chapter was undertaken to explore how the photophysical properties of energy transfer cassettes correlate with their structures, and specifically try to explain the difference in energy transfer between compounds **64** and **C**.[107] As already mentioned, it is generally easier to work with lipophilic compounds than polar, hydrophilic ones. We therefore opted to work with *tert*-butyl protected compound **65** (Figure 3.8) rather than free acid **C**.

Nagano has published on the photoinduced electron transfer (PeT) between *meso*-phenyl groups and BODIPY cores.[108] These PeT processes can negatively impact the fluorescence quantum yields of BODIPYs and we therefore set out to prepare cassette **66**, a modification of **65** wherein the *meso*-phenyl functionality is absent. For comparison, cassettes **67** and **64** were also targeted; these maintain the basic design, two donors perpendicularly aligned to the same central BODIPY[31,32,109,110]-acceptor. However, they are fundamentally different insofar as the donors are also BODIPY-based, and there was no obvious reason to suspect transfer of energy from the donors in these molecules to the acceptors should be pH dependant. These were envisaged as reference compounds for comparison of the extent of energy transfer in these systems.

[*] The work described forth in this chapter is the result of an equal collaboration with Dr. Junyan Han. In general, Dr. Han was responsible for compounds **65** and **67** and no further distinction between his efforts and mine will be provided.

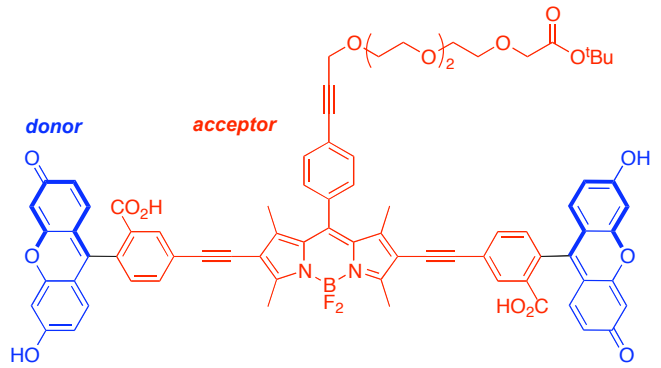

65

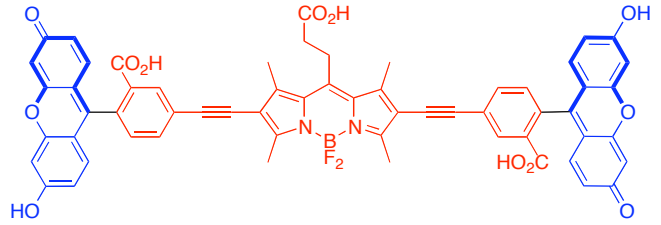

66

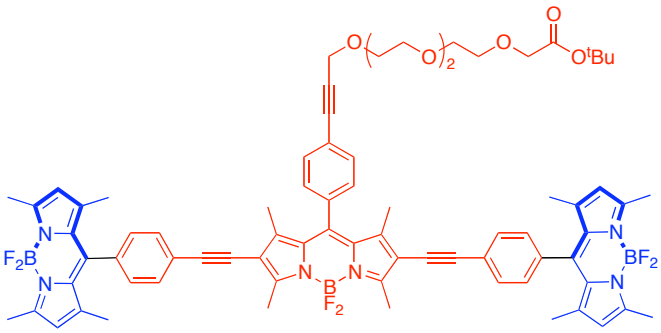

67

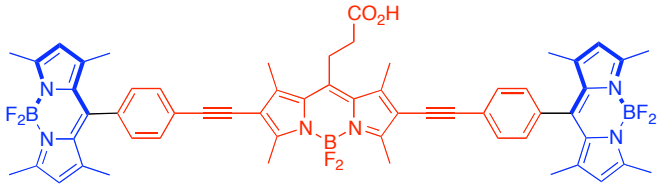

64

Figure 3.8. Cassettes targeted in this study.

In outline, the research described here investigates: (i) syntheses of the cassettes; (ii) effects of changing of the *meso*-substituent on the central BODIPY {acceptor} fragment represented by the difference between cassettes **65** and **66** and between **67** and **64**; (iii) changes of donor fragment from xanthene to BODIPY represented by the structural differences between **65** or **66**, and **67** or **64**. Comparison of the cassettes is made on the basis of photophysical and electrochemical data measured at different pH levels. The latter measurements are related to orbital levels in the donor and acceptor fragments.

3.2 Results and Discussion

*Syntheses of the Cassettes **64** - **67**.*

Two key diiodinated BODIPY intermediates were prepared to make the cassettes featured in this chapter. The first, compound **69** (Scheme 1a), was designed to have a triethylene glycol linker that would somewhat separate the dye from the protein as well as increase solubility in polar solvents. Conditions for the diiodination reactions shown in Scheme 1 were based on work from Nagano *et al.*[56] The second, compound **48** (Scheme 1b), was formed via a route that is analogous to one used for a homolog formed from glutaric anhydride.[111] Synthons **69** and **48** lead to cassettes with different *meso* substituents: aryl and alkyl functionalities.

a

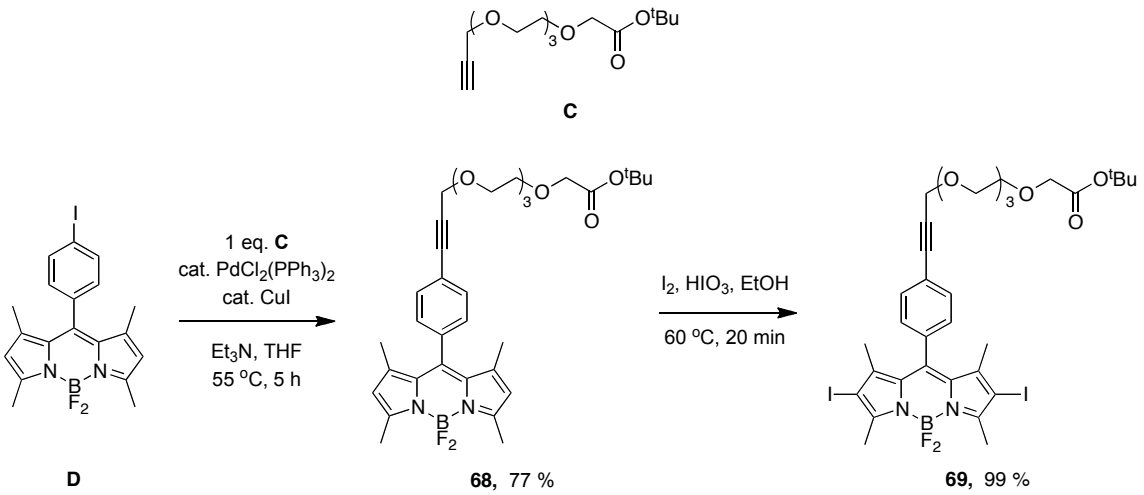

b

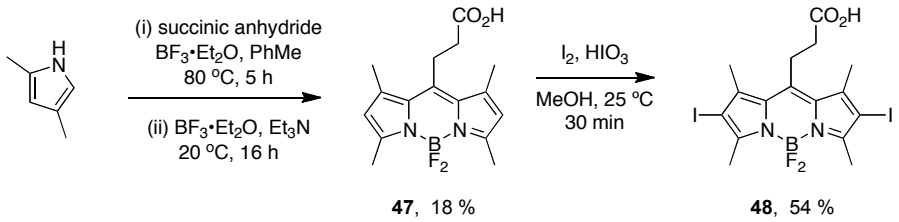

Scheme 3.2. Syntheses of pivotal diiodinated synthons: **a** BODIPY **69**; and, **b** BODIPY **48**.

Sonogashira reactions[59,112] were used to assemble the cassettes from the acceptor components **69** and **48**, and the fluorescein-based and BODIPY-based donor components **E**[21,24] and **F**[13] (Scheme 3.3). The diacetate intermediate **70** is of some importance because this compound has been shown to be cell permeable, and hydrolyzes in the cytosol to give green fluorescence.[113] The fluorescein-based cassettes **65** and **66** are soluble in lower alcohol solvents giving pink solutions.

a

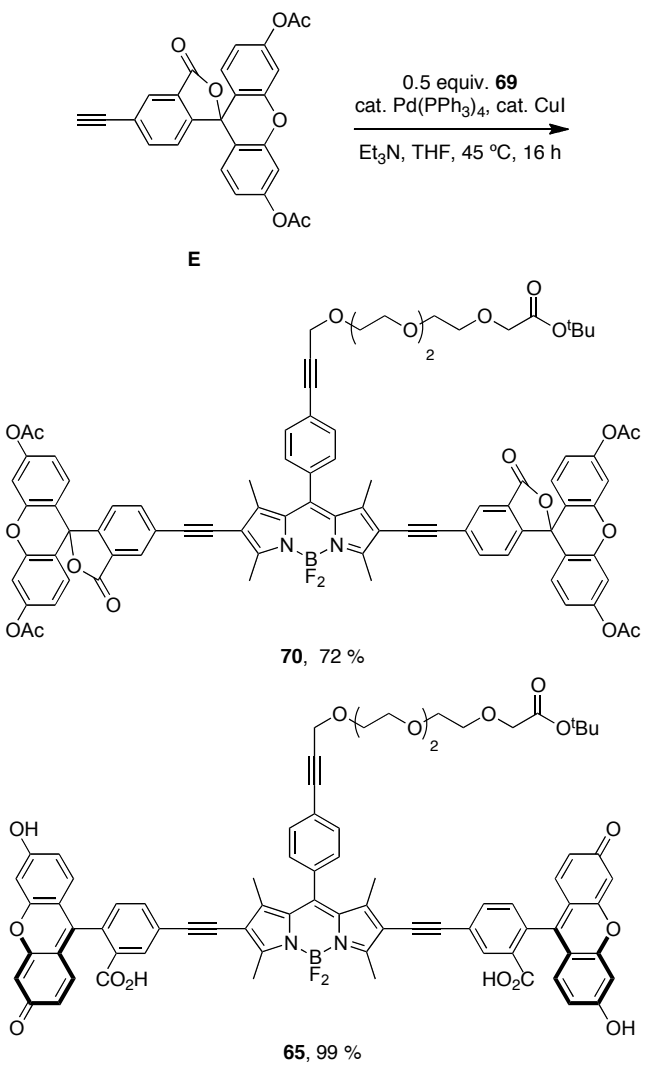

Scheme 3.3. Syntheses of cassettes: a. **65**; and, b. **67**.

b

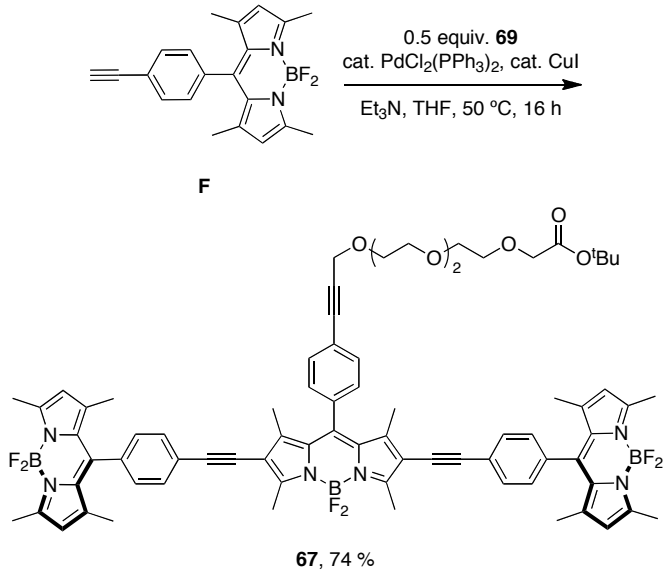

Scheme 3.3 Continued.

Cassette **66** (Scheme 3.4) was difficult to purify. Flash chromatography did not give pure material, but the compound was isolated via preparative reverse phase HPLC in 4 % yield. Both cassettes **67** and **64** are soluble in lipophilic solvents like CH_2Cl_2, and give strongly colored pink or red solutions.

a

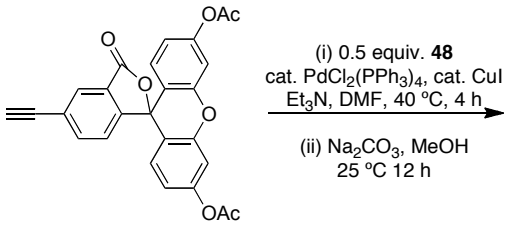

E

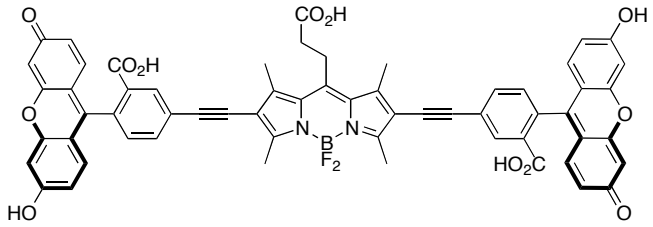

66, 4 %

b

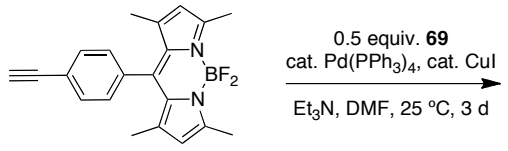

F

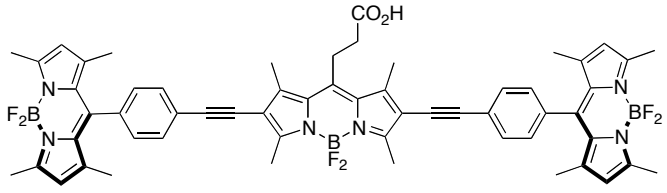

64, 53 %

Scheme 3.4. Syntheses of cassettes: a. **66**; and, b. **64**.

The methyl ester of cassette **64**, compound **60**, was crystallized for single crystal X-ray diffraction studies (Figure 3.9). They show the BODIPY donor fragments resting perpendicular to the acceptor part. In part, it is this molecular twist that differentiates

cassettes from planar dyes consisting of a single conjugated chromophore. Interestingly, the molecule appears to "sag" around the central BODIPY fragment, because the alkyne parts are not exactly in the same plane; an ideal linear arrangement would give a 180° angle, but the observed angle was 168.2 degrees. This parameter may have some relevance because if the angle were 180° and rigid then the transition dipoles of the BODIPY acceptor and the two donor fragments (which are aligned with their long axes)[30] would be exactly perpendicular in any conformation about the alkyne. In that orientation there can be no dipole-dipole coupling hence fluorescence resonance energy transfer (RET) could not occur. The fact that the molecule is not perfectly linear means that RET cannot be completely excluded because rotation about the alkyne bond could place the BODIPY donors in conformations in which weak dipole-dipole coupling could occur. However, the "sag-angle" is small, and conformations that allow dipole-dipole coupling also take the phenyl group out of conjugation with the rest of the acceptor; consequently, energy transfer via this mechanism[1] is unfavorable.

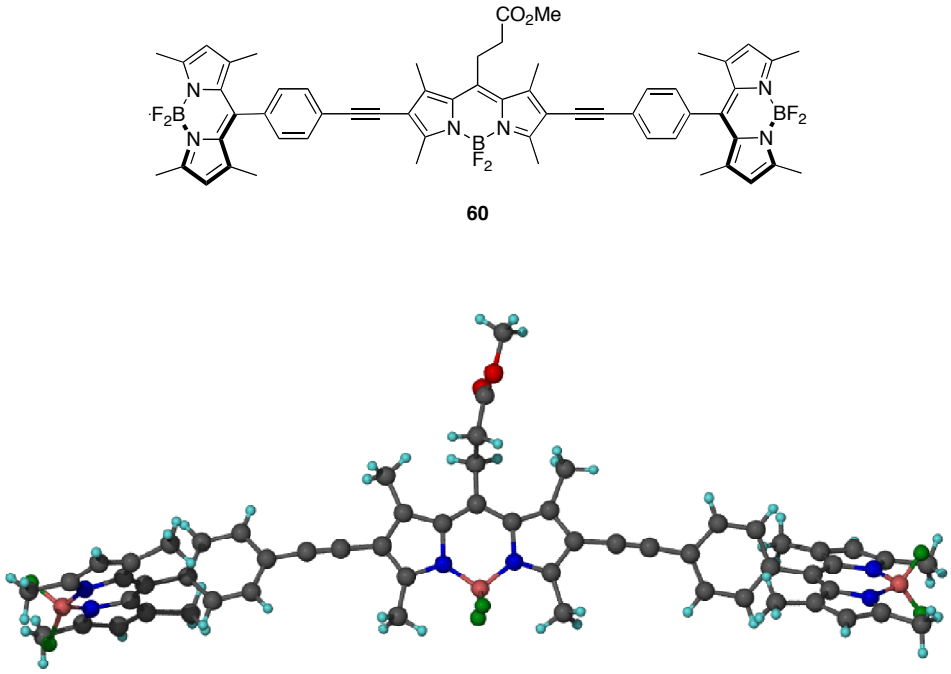

60

Figure 3.9. Single crystal X-ray structure of **60**.

An important set of new acceptor fragments **46**, **49**, **108**, and **109** and known BODIPY **G**[39] and xanthene **H**[114] reference compounds were also generated for this study. Photophysical and electrochemical properties in cassettes tend to be accurately represented by the individual donor and acceptor fragments.[12] Consequently, electrochemical studies were performed on these constituents, thus avoiding the need for destructive experiments (electrochemistry) on the valuable cassette samples. Syntheses of the new materials are outlined in APPENDIX D.

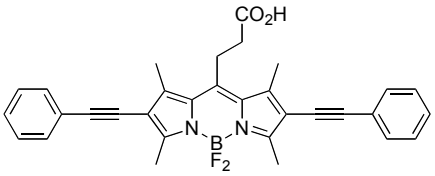

46

an acceptor mimic

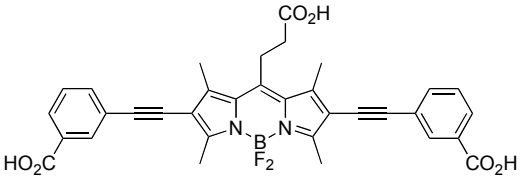

49

an acceptor mimic

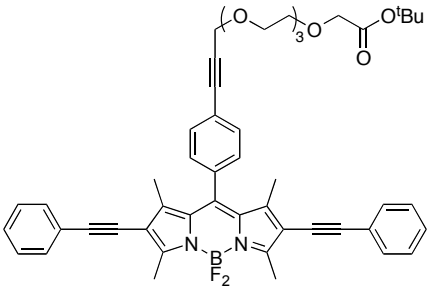

108

an acceptor mimic

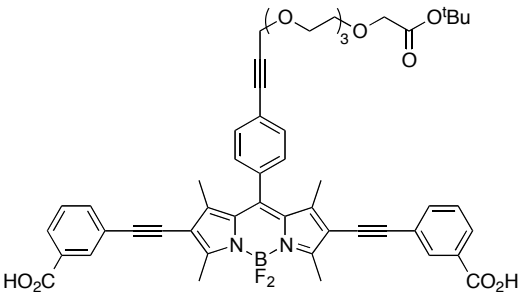

109

an acceptor mimic

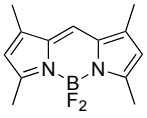

G

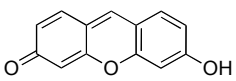

H

donor fragments

Photophysical Properties

Salient photophysical properties of the cassettes are shown in Table 3.1. The acceptor fragment is formed by the 2,6-(alkyne-aryl) substituents because these impose a dramatic red-shift on the absorbance and fluorescence properties of the BODIPY core.[59] The fluorescein and BODIPY donor parts exhibit characteristically large molar absorptivities, and absorb/fluoresce at wavelengths that are characteristic of the free dye fragments (see Table 3.2 below).

Through bond energy transfer cassettes are usually designed to absorb light at the donor excitation wavelength, relay it to the acceptor part, then emit fluorescence from there. The term "energy transfer efficiency" (ETE %) quantifies this, it is defined as follows:

$$\text{ETE \%} = \frac{\text{quantum yield of the acceptor fragment in the cassette excited at the donor}}{\text{quantum yield of the acceptor fragment in the cassette excited at the acceptor}} \times 100$$

ETE % is a measure of the quantum yield of the cassette when irradiated at the donor. It reflects the extent of energy transfer including the negative effects of non-radiative loss in the transfer process. The product of the molar absorptivity of the donor in the cassette and the ETE give a measure of the brightness of the acceptor in the system.

Values of the ETE % for the cassettes **64** – **67** are shown in Table 3.1. Several important observations are clear. First, the fluorescein-based cassettes **65** and **66** have moderate ETE values in the absence of base, but not when Bu_4NOH is added. Second,

the BODIPY-based cassettes **67** and **64** have excellent ETE values, and these are *not* influenced by base.

Table 3.1. Photophysical properties of **64** - **67** in 1:1 ethanol:CH_2Cl_2.

		absorption[b]		fluorescence[c]					
cmpd	base[a]	$\lambda_{max\ donor}$ (nm) / $\varepsilon \times 10^{-4}$	$\lambda_{max\ acceptor}$ (nm) / $\varepsilon \times 10^{-4}$	$\lambda_{max\ donor}$ (nm)	$\lambda_{max\ acceptor}$ (nm)	$\Phi_{acceptor}$ excited at acceptor[d]	$\Phi_{acceptor}$ excited at donor[e,j]	ETE (%)[f]	Φ_{donor}[g]
65	-	505 / 5.6	575 / 3.5	521	600	0.30[i]	0.15	51	0.05
65	+	505 / 11	578 / 3.0	529	-	0.01[i]	-	< 5	0.09
66	-	506 / 3.7	560 / 1.9	528	579	0.24[j]	0.09	38	0.07
66	+	505 / 13	561 / 2.8	529	-	0.01[j]	-	< 5	0.08
67	-	502 / 14	566 / 6.6	513	606	0.62[i]	0.58	93	-[h]
67	+	502 / 14	566 / 6.6	516	604	0.66[i]	0.60	92	-[h]
64	-	502 / 11	561 / 4.7	521	588	0.84[j]	0.79	94	-[h]
64	+	502 / 11	560 / 5.2	515	588	0.93[j]	0.85	91	-[h]

[a] with $^nBu_4NOH$ at a concentration of 8×10^{-5} M. [b] At 1×10^{-5} M. [c] At 1×10^{-6} M. [d] Quantum yield of acceptor when excited at the acceptor. [e] Quantum yield of acceptor while excited at the donor. [f] Energy transfer efficiency calculated with the quantum yield of the acceptor with excitation at donor divided by that with excitation at the acceptor. [g] Fluorescein (Φ = 0.92 in 0.1 M NaOH)[115] was used as a standard. [h] Donors in these cassettes show no significant fluorescence emission. [i] Rhodamine 101 (Φ = 1.00 in EtOH)[58] was used as a standard. [j] Rhodamine B (Φ = 0.97 in EtOH)[115] was used as a standard.

Effects of base on the cassettes are probably best visualized from their absorbance and fluorescence spectra (Figures 3.10). Addition of $^nBu_4NOH$ to cassettes **65** and **66** increases the absorption corresponding to the fluorescein component relative to that from the BODIPY acceptor part. This is logical because addition of base forces the

fluorescein donor into its ring-opened phenolate carboxylate form. Absorbance spectra of cassettes **67** and **64** are almost completely insensitive to base, as would be predicted since the electronic spectra of BODIPY dyes are not significantly affected by pH.

In the absence of base, excitation of the fluorescein donor of cassettes **65** and **66** leads to significant fluorescence from the BODIPY acceptor. However, no significant fluorescence is observed from the BODIPY part when base is added to the same solutions (Figure 3.10a and b). Conversely, addition of base has no significant effect on the extent of energy transfer for the cassettes **67** and **64** that have BODIPY donors. Thus in 1:1 ethanol/CH_2Cl_2 the fluorescein donor parts of cassettes **65** and **66** are, at least partially, protonated, and energy transfer to the BODIPY acceptor occurs. Energy transfer is *quenched* when the fluorescein donors are completely deprotonated. Cassettes **67** and **64** have BODIPY, not fluorescein, donor parts, but they are otherwise identical to **65** and **66**.

a

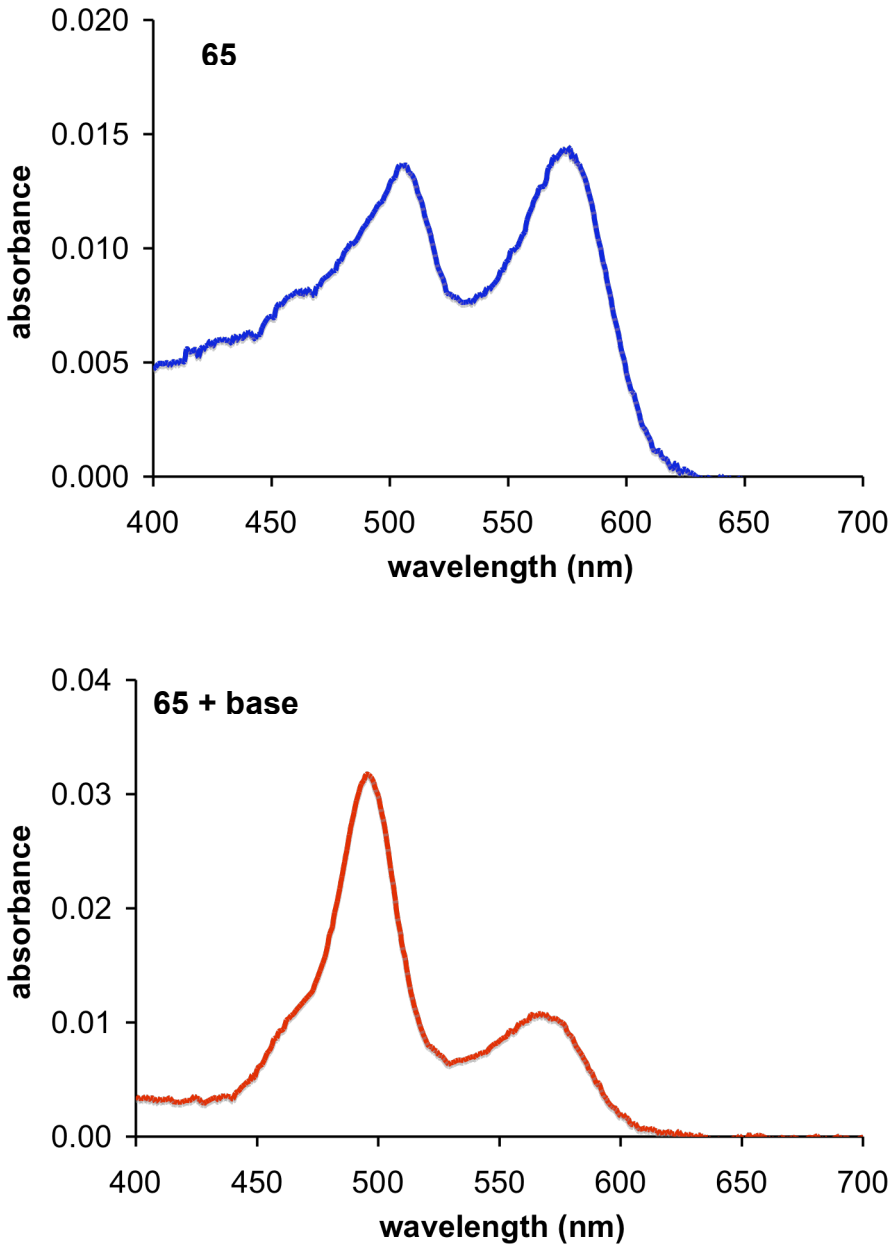

Figure 3.10. **a.** Absorbance spectra of **64** – **67** (10^{-5} M conc. in 1:1 ethanol/CH_2Cl_2) with and without $^{n}Bu_4NOH$ (concentration of 1 x 10^{-4} M). **b.** Fluorescence spectra of cassettes **64** - **67** (1 x 10^{-6} M in 1:1 ethanol/CH_2Cl_2), spectra recorded without added base are shown in blue, and with $^{n}Bu_4NOH$ (concentration of 1 x 10^{-4} M) are shown in red.

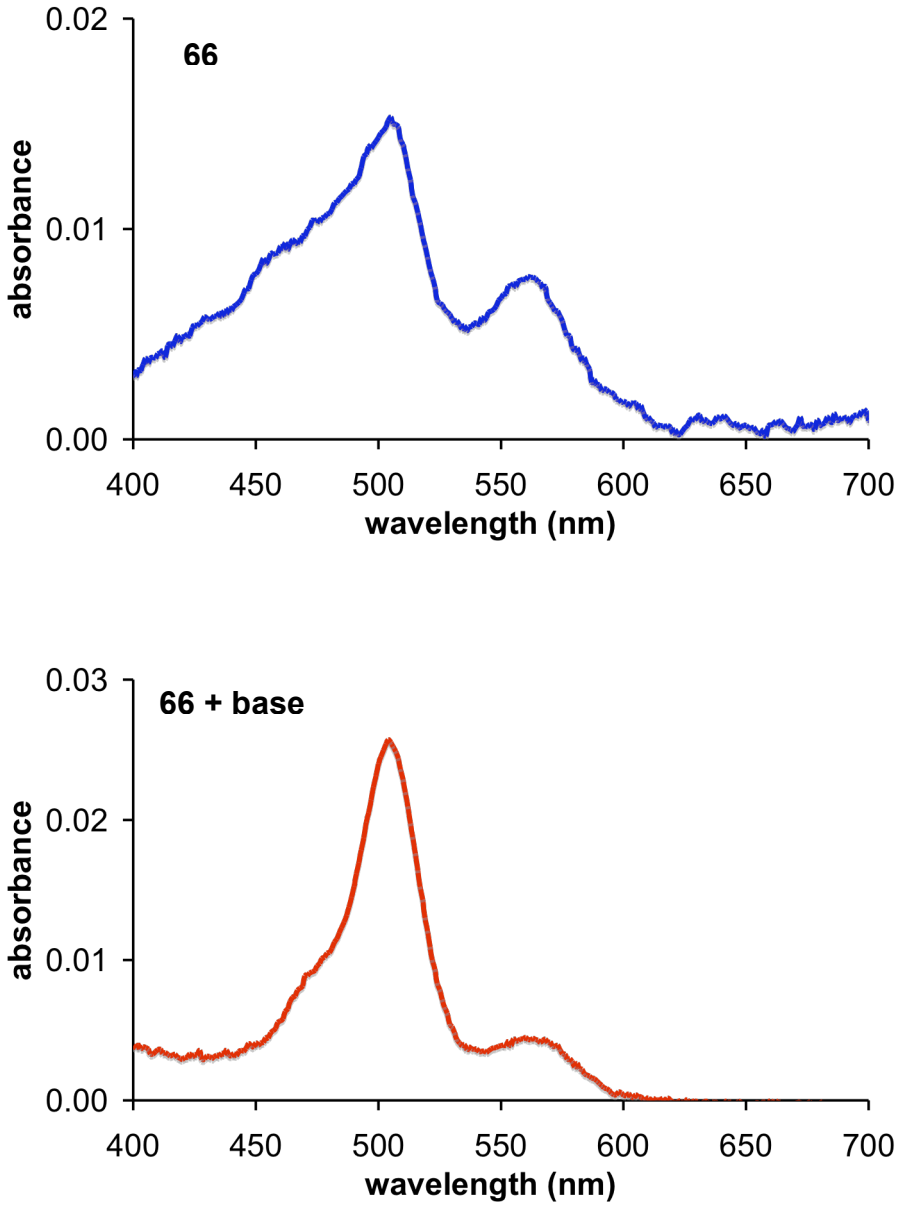

Figure 3.10 Continued.

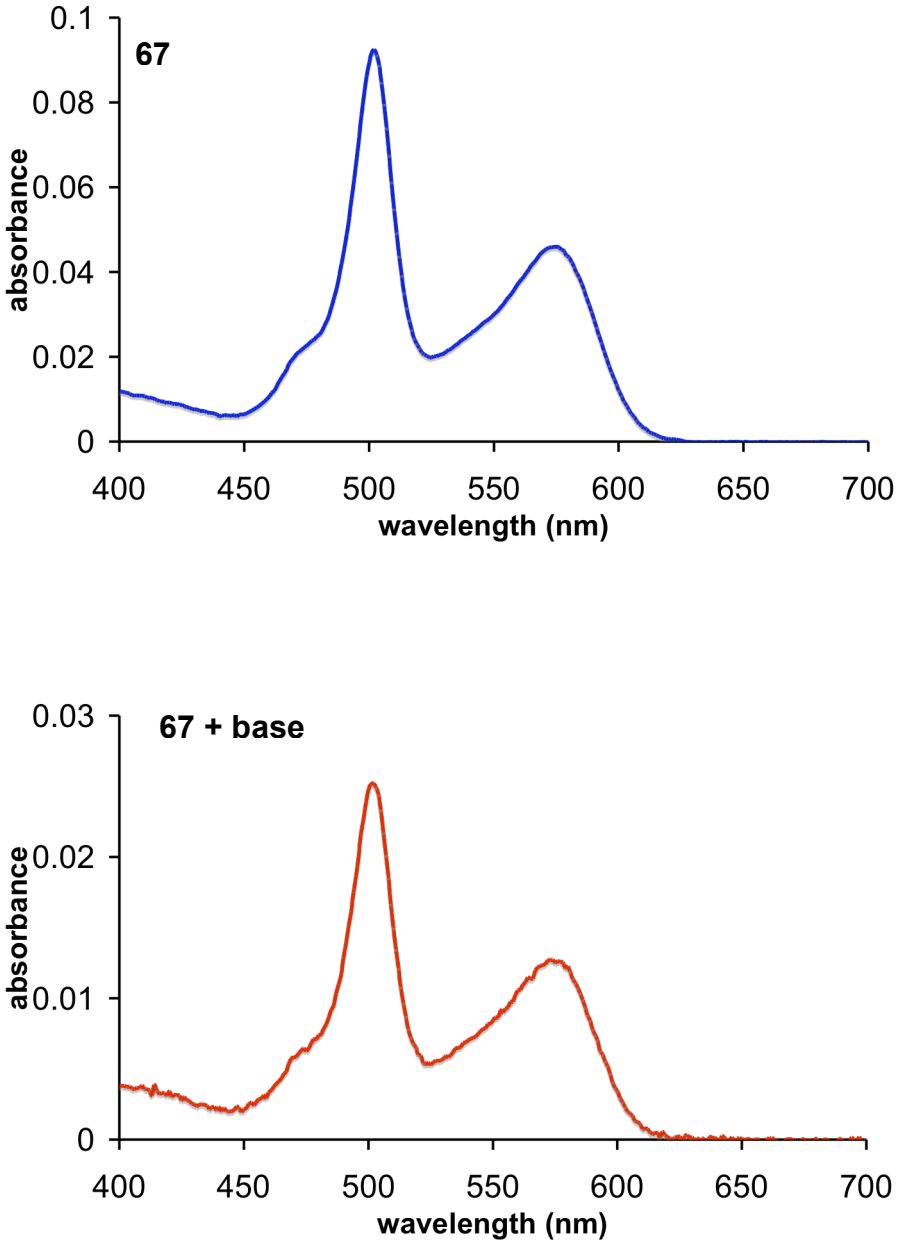

Figure 3.10 Continued.

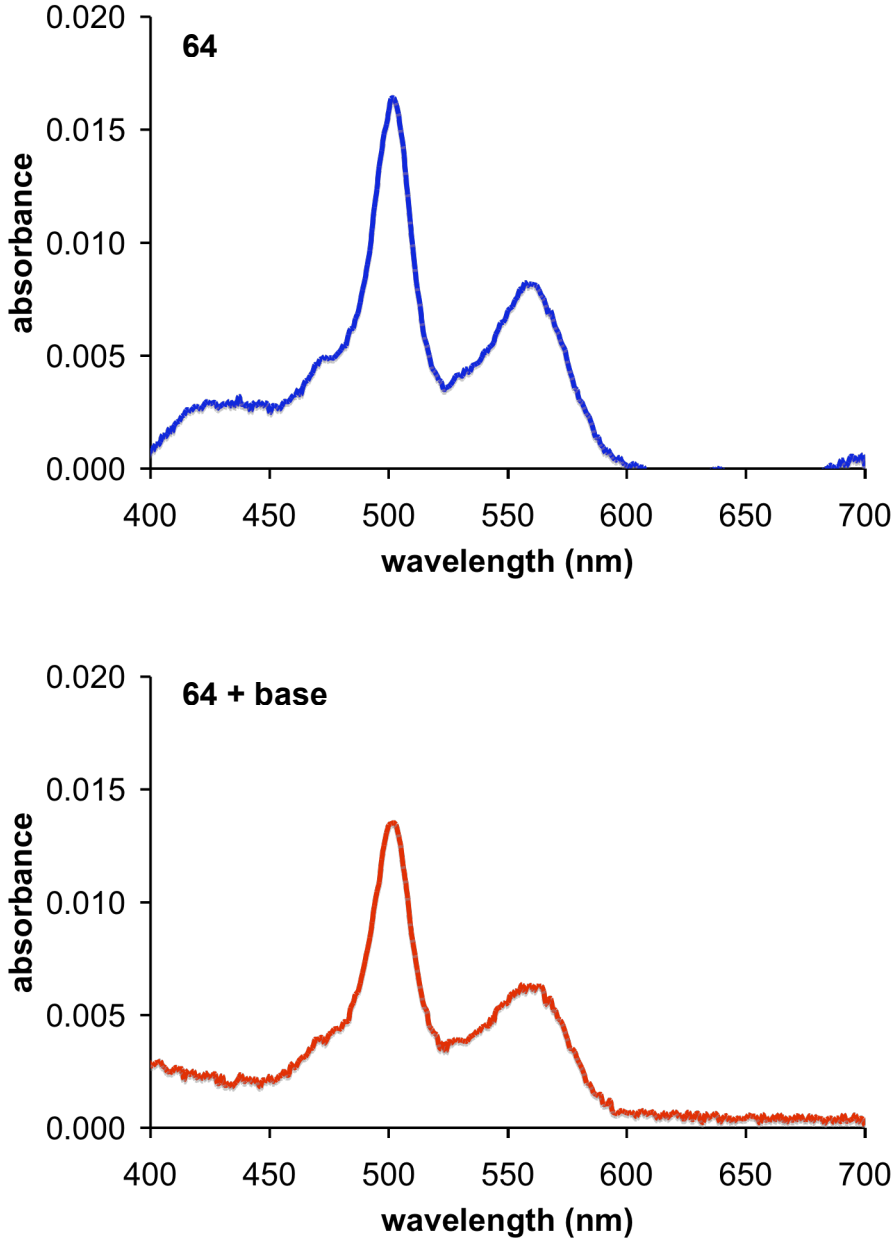

Figure 3.10 Continued.

b

*cassette **65** (fluorescein donor)*

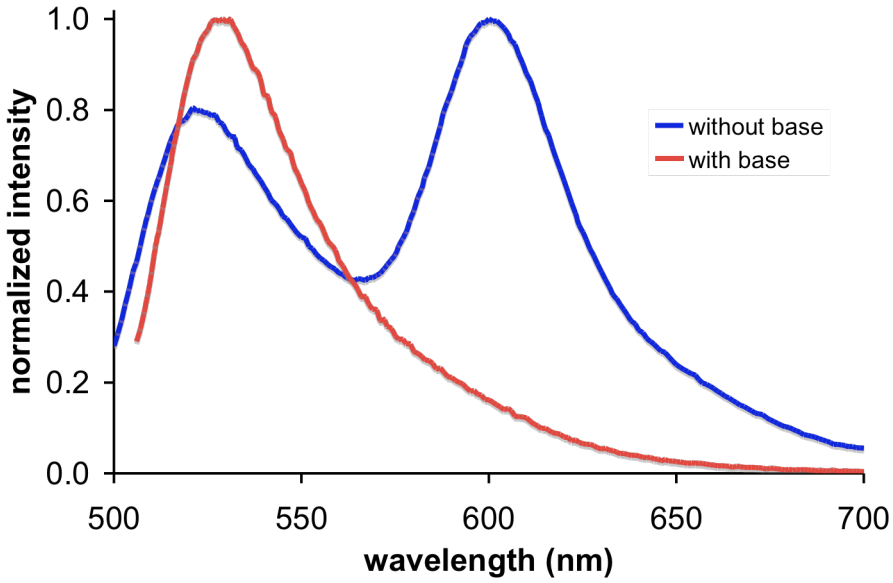

*cassette **66** (fluorescein donor)*

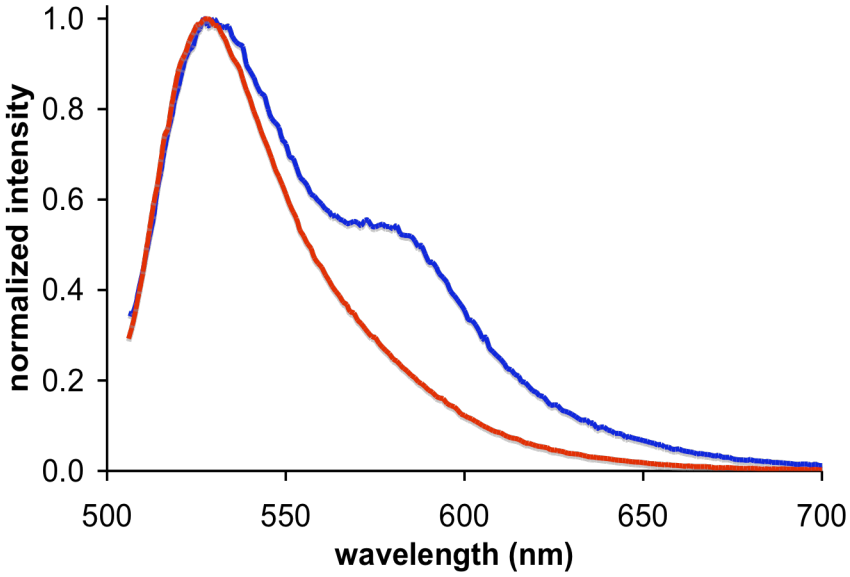

Figure 3.10 Continued.

*cassette **67** (BODIPY donor)*

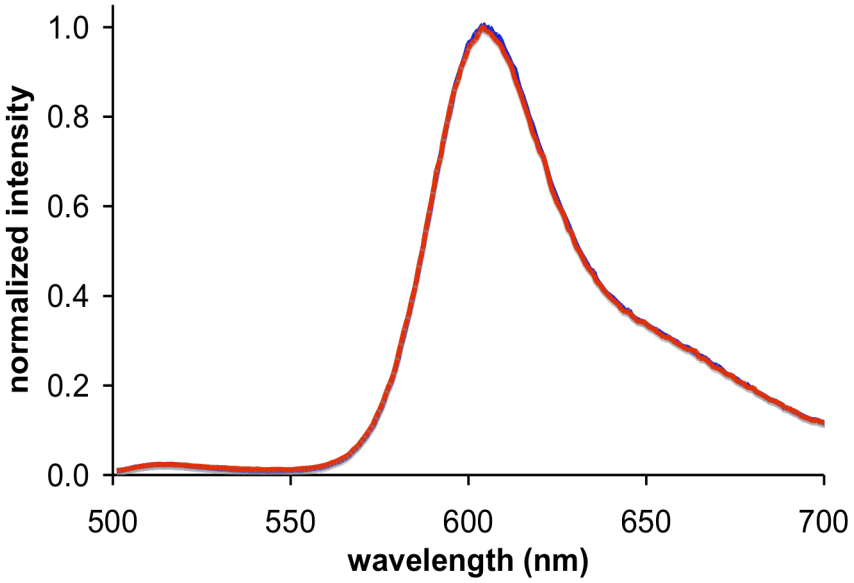

*cassette **64** (BODIPY donor)*

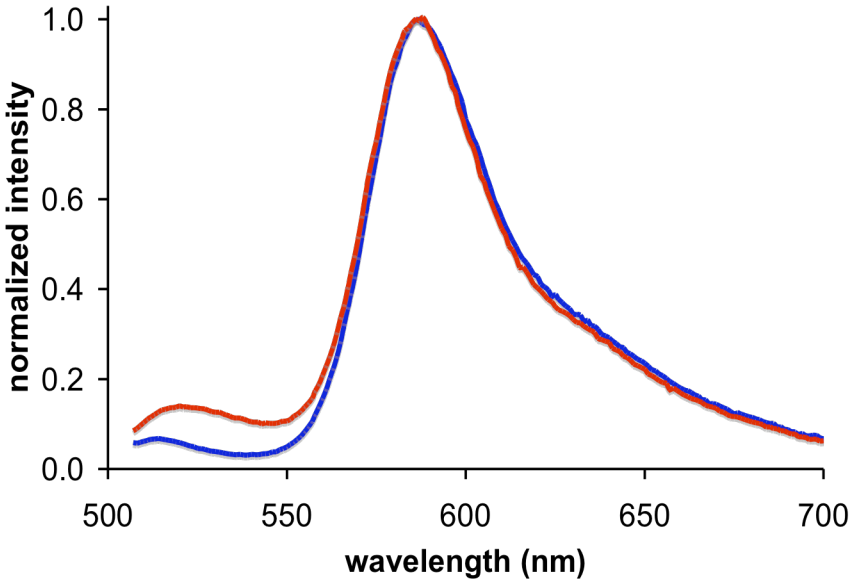

Figure 3.10 Continued.

Table 3.2 shows photophysical properties for the reference compounds **46, 49, 108, 109, G**, and **H**. None of the building blocks that were assembled to give cassettes **64** – **67** have fluorescence characteristics that are significantly changed by added base. The largest change in quantum yield is seen for the dicarboxylate **109** and xanthene **G**: for these compounds a 25 % increase in the presence of base. There are no appreciable shifts in λ_{abs}, λ_{em}, or even the peak width values when these fragments are compared without and with base.

None of the reference compounds can undergo changes like that shown in equilibrium 1, but this has been comprehensively studied for fluorescein in aqueous media.[71] These data show that the quantum yield of fluorescein is highest in its dianion state. However, Table 3.1 shows that the quantum yield of the donor part in the fluorescein-based cassettes **65** and **66** are less than 0.1, with or without base. Without base there is significant energy transfer to the acceptor, so some quantum yield reduction is anticipated. With base, however, less of the energy transferred between the donor and acceptor is emitted as acceptor fluorescence. Further, the xanthene quantum yields in the cassettes are much less than for fluorescein in any of the accessible protonation states, or for the xanthene **G**. Thus, integration of the xanthene donors in cassettes **65** and **66** reduces their quantum yields relative to the parent fragments.

Table 3.2. Photophysical properties of reference compounds in 1:1 ethanol/CH_2Cl_2

cmpd	base[b]	λ_{abs} (nm) / ε x 10^{-4}	λ_{em} (nm)	fwhm (nm)	Φ[a]
46	_	560 / 2.6	587	41	0.72
46	+	559 / 2.6	587	41	0.71
49	_	565 / 0.9	593	46	0.46
49	+	563 / 1.0	592	43	0.61
108	_	574 / 3.2	606	44	0.52
108	+	574 / 3.2	605	53	0.54
109	_	573 / 2.3	612	53	0.42
109	+	578 / 2.5	613	52	0.44
G	_	506 / 8.7	511	16	0.98
G	+	506 / 8.7	511	17	0.90
H	_	508 / 7.4	517	26	0.76
H	+	508 / 11	517	25	0.95

Absorption data recorded at 1 x 10^{-5} M. Emission data taken at 1 x 10^{-6} M. [a] Rhodamine 101 (Φ = 1.0 in ethanol)[58] was the standard for **46**, **49**, **108**, and **109** and fluorescein (Φ = 0.92 in 0.1 M NaOH)[115] for **G** and **H**. [b] with Bu_4NOH at a concentration of 8 x 10^{-5} M.

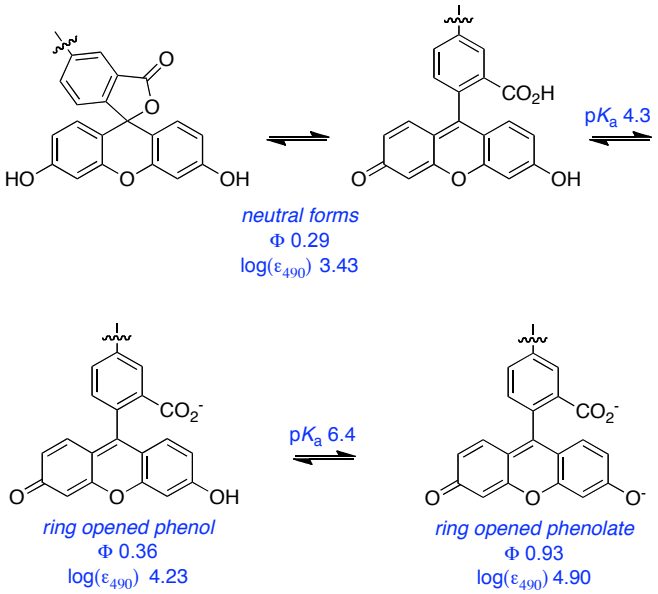

equilibrium 1

Electrochemical Studies

Oxidation and reduction potentials were measured for the reference fragments **G**, **H**, **108, 109**, and for cassette **67** relative to the ferrocene/ferrocinium couple. The electrochemical measurements provide an approximation of the band gap magnitude. The HOMO and LUMO energies were estimated based on the *onset* of REDOX events as described by Reynolds *et al.*[116] BODIPY **108** shows a reversible reduction wave, while for **109** and **G** the wave is *quasi*-reversible for the first reduction events. For **H** and $\mathbf{H}_{Na}$ the first reduction wave is irreversible. The oxidation events for all compounds are irreversible. In a method similar to the one used by Reynolds *et al.*[116] the ferrocene/ferrocenium couple in Volts is estimated to an orbital level of 5.15 eV and 5.16 eV relative to vacuum in DMF and CH_2Cl_2, respectively.[117,118] Thus energy levels of

HOMO and LUMOs can be pegged relative to this reference point. The same data was acquired for compounds **46** and **49** (see Appendix D).

Figure 3.11a plots HOMO and LUMO energy levels for the reference BODIPY **E** and the acceptor mimic **108** that represent cassette **67** (BODIPY donor and acceptor). The LUMO levels of the donor and acceptor parts are close in energy with the latter 0.35 eV lower. This corresponds to the system for which high ETE was observed (93 %), and for which no pH dependence was observed or expected. Figure 3.11b and c shows data corresponding to the pH dependant cassette **65**. Under conditions favoring protonation of the phenolic-*O* atoms the two LUMO levels are also close in energy (0.1 eV), and again, significant ETE was observed. However, for the same cassette but under conditions wherein the phenol groups would be completely deprotonated, poor energy transfer corresponds with a large energy gap between the donor and acceptor LUMO levels.

Table 3.3. Electrochemical data for reference compounds **G**, **H**, **108, 109**, and cassette **67**.

cmpd	$E_{onset,ox}$ (V)	HOMO (eV)	$E_{onset,red}$ (V)	LUMO (eV)	E_g (eV)
G[a]	+0.68	5.84	-1.32	3.84	2.00
H[b]	+0.33	5.48	-1.03	4.12	1.36
$\mathbf{H}_{Na}$[b, d]	+0.04	5.19	-1.67	3.48	1.71
108[a]	+0.99	6.15	-0.91	4.48	1.87
109[b]	+0.49	5.64	-0.93	4.22	1.42
109[c]	+0.49	5.64	-0.92	4.23	1.41
67[a]	+0.99	6.15	-0.92	4.24	1.91
			-1.18	3.98	2.17

Cyclic voltammograms were recorded using a glassy carbon working electrode (A = 0.071 cm^2) referenced to Fc/Fc^+ and a Pt counter electrode at a scan rate of 200 mV/s. All potentials are reported vs. Fc/Fc+ and all HOMO and LUMO energies are derived from electrochemical results based on Fc/Fc^+ = 5.15 eV (DMF) and 5.16 eV (CH_2Cl_2) *vs.* vacuum. All solvents were flushed with $Ar_{(g)}$ before use. [a] In CH_2Cl_2. [b] In DMF. [c] In DMF and 0.1 M pyridine. [d] Xanthene was first reacted with NaOH to obtain the sodium salt.

a

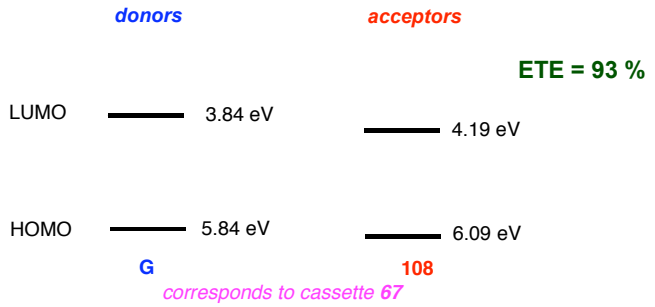

b

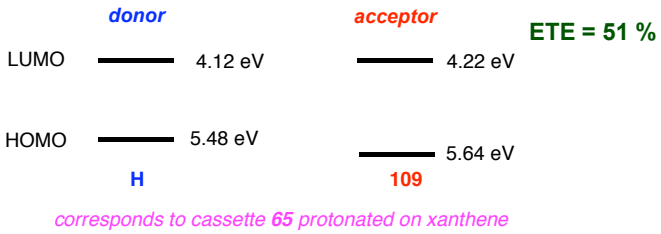

c

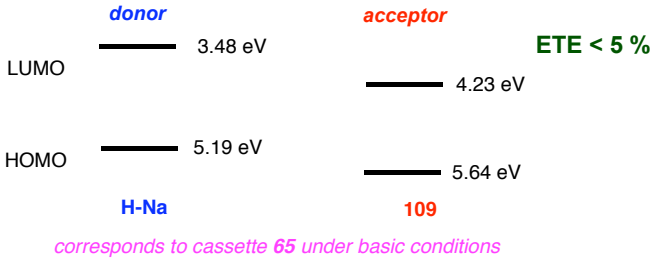

Figure 3.11. a HOMO and LUMO levels of the reference compounds representing cassettes: **a**, **67**; **b**, **65** (under neutral conditions); and, **65** (basic conditions).

3.3 Conclusions

Rapid and efficient energy transfer may be possible when a fluorescent donor is joined to an acceptor in such a way that the two fragments would be electronically conjugated if

they became planar, but are sterically prevented from doing so.[14,119-121] The fact that they cannot easily achieve planarity means that the absorption spectra of the cassette resembles the sum of the donor and acceptor parts. However, the donor part will not fluoresce when it is excited in an efficient energy transfer cassette; instead the energy will be rapidly transferred to the acceptor that will then fluoresce (Figure 8).[23,29,30,122-130]

Previous studies from these laboratories provided evidence that energy transfer mechanisms besides RET can be dominant in cassettes like the ones described in this paper. Specifically, energy transfer rates between anthracene (donor) and BODIPY (acceptor) fragments were much faster than would be expected from a RET mechanism.[23,29,30] Further, some of those cassettes have the donor and acceptor parts oriented in ways that should largely *exclude* the possibility of RET, yet fast transfer rates were observed. Others in this field had documented similar effects for energy transfer cassettes.[10,12,131,132]

In this work, we do *not* profess to know the mechanisms by which energy is transferred between the donor and the acceptor. It seems highly probable that all possible mechanisms compete; these include dipole-dipole coupling (RET), electron transfer, and processes in which relaxation of energy from the donor excited state leads to excitation of the acceptor via through-bond mechanisms that rely on orbital overlap. Moreover, the proportions of each energy transfer mechanism operative will be influenced by the protonation state of the donor, at least for the xanthene dyes. Comparisons with the all-BODIPY donor-acceptor systems **108** and **109** reveal that the relative orbital energy levels between the donor and acceptor fragments in these

cassettes are comparable to those in the pH-sensitive systems **65** and **66** in protonation states where efficient energy transfer is observed. Moreover, the *meso*-aromatic substituent of **65** and **67** has no significant effect on the photophysical properties of these cassettes; this can be inferred from the data collected for **66** and **64** which have only aliphatic groups in that position.

Communication between the donor and the acceptor in these systems, by whatever mechanisms, does appear to be impacted by the relative energies of the frontier orbitals involved. Electrochemical studies as described here are therefore valuable in elucidating what these orbital energy levels are.

The work described here may represent the beginning of a new paradigm in which electronically coupled dye pairs can be used to sense analytes in biomedical applications. There is considerable scope for molecular modifications in this series because the donor, acceptor, and linker fragments[133] could all be modified to give sensors.

CHAPTER IV

BRILLIANT BODIPY-FLUORENE COPOLYMERS WITH DISPERSED ABSORPTION AND EMISSION MAXIMA

4.1 Introduction

It is important to have bright fluors that are easily discernible from endogenous fluorophores when imaging cells. Likewise, *in vivo* imaging necessitates probes whose fluorescence intensities are suitable for detection through tissue. As discussed in Chapter I, brightness of a fluorophore is the product of its quantum yield and molar absorptivity. For this reason probes that have high quantum yields and strong absorptivities tend to have advantages over other probes for imaging applications. Although quantum yields and molar absorptivities can generally be optimized by structural modifications of a dye's core, these modifications can be synthetically challenging and often unpredictable requiring trial and error; for these reasons a systematic way of increasing either the quantum yield or molar absorptivity of fluors would be of great value.

Our lab[134] and others[27,28] have observed that molar absorptivity of TBET cassettes (see chapter I) increases with the inclusion of two or more donors to acceptors (Figure 4.1a). In these cases two or more donor parts absorb light more efficiently than a single one and relay the energy to the acceptor part that emits the energy. Theoretically, the photophysical properties of the acceptor are independent from those of the donors so the quantum yield of the acceptor should not be negatively affected by an increase in the

number of donors. It has been shown however that energy transfer efficiency can diminish in cases where extreme ratios (8:1) of donors to acceptor are used.[8] We theorized that polymerization of donors with random incorporation of acceptors throughout the polymer would be conducive to bright TBET systems because of the large harvest of energy afforded by the donors, fast TBET to the acceptors, and favorable fluorescence quantum yields from those acceptors (Figure 4.1b).[135]

a

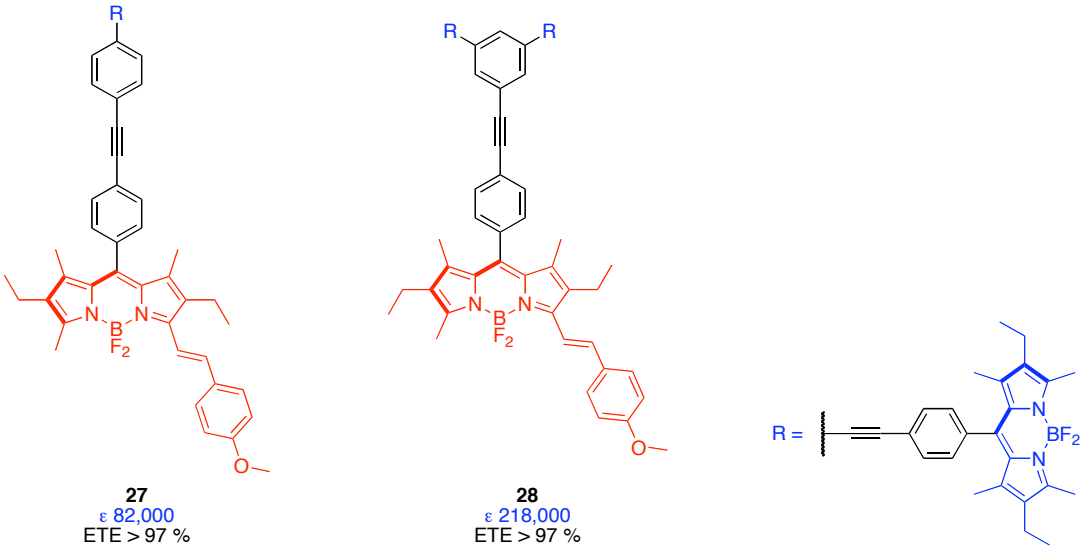

Figure 4.1. **a.** Increase in molar absorptivities resulting from increases in the number of donors (compare **27** to **28**). Addition of too many donors can decrease ETE as in compound **7**. **b.** Model of polymer harvesting energy to acceptor.

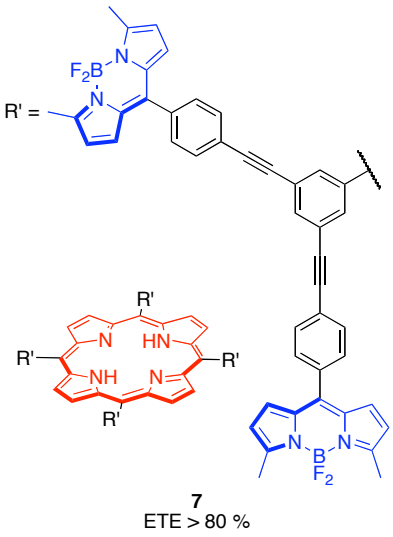

7
ETE > 80 %

b

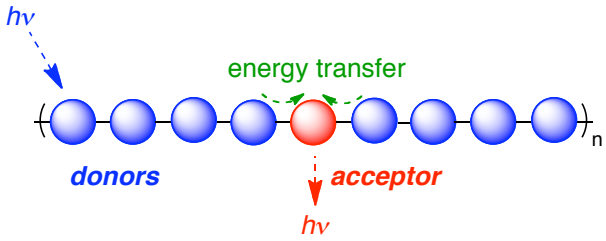

Figure 4.1 Continued.

The choice of acceptor in these types of polymers should be ones that possess high quantum yields and can easily be tunable to different fluorescent wavelengths. BODIPY dyes[31,32,110] meet these criteria and were therefore chosen for these studies. A recent trend in the research of BODIPY dyes has been to polymerize them to concentrate multiple fluor units in single molecules,[136-139] hence to form bright particles for materials or for imaging biological systems. Polymers of this kind tend to have desirable properties for those applications because they concentrate several fluorescent groups in one molecule. Brightness-per-fluor in *homo*polymeric-dye systems is not necessarily greater than the free dye, and scope for manipulation of spectroscopic properties is limited; consequently it is logical to research similar polymers from two or more

components such as the case discussed in Figure 4.1b. This strategy allows donor fragments that absorb light of a desirable wavelength to collect and transfer energy to fluors that then fluoresce. In this paradigm, donor:acceptor ratios may be adjusted to optimize the brightness-per-fluor (*note* brightness-per-fluor = absorption cross-section of the donor parts x quantum yield of the fluor in the polymer).

To the best of our knowledge this has not been attempted; all the BODIPY-containing polymers reported to date are homopolymeric or BODIPY-bridge-BODIPY-bridge... (*i.e.* ABAB) composites (Figure 4.2).[136-146] There are none of the type $(donor)_m$-BODIPY-$(donor)_n$-BODIPY-... in which the acceptor fluors is "doped" into the donor-polymer backbone. This is significant because donor-rich polymers could have extremely high UV absorption cross sections, and accommodate fast, efficient, energy transfer to the BODIPY fluors, affording bright probes with excellent separations of absorption and emission wavelengths.

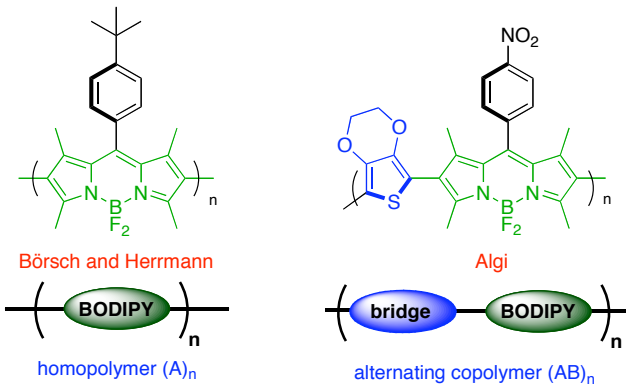

Figure 4.2. Examples of BODIPY homo- and co-polymers done by others.

This chapter describes donor-rich polymers **70** designed to maximize energy transfer to BODIPY or related acceptor fragments (Figure 4.3). Fluorene donor parts were chosen because of their photostabilities, large molar absorptivities, high two-photon cross-sections, and ease of syntheses.[147-149] Violet-blue fluorescence emissions from polyfluorenes are *not* ideal for cellular or *in vivo* imaging, but we hypothesized that appropriately designed BODIPY-doped polyfluorene polymers could be excited at the donor parts, and would emit brightly at much longer wavelengths characteristic of the acceptor parts. Another design attribute of these systems is that variations of the acceptors would enable tuning of fluorescence outputs. Data described here shows that in fact such polymers could be made and optimized for emission via the acceptor. Further, representative systems were cast into particles of around 50 nm that were shown to permeate into Clone 9 rat liver cells where they could be imaged.

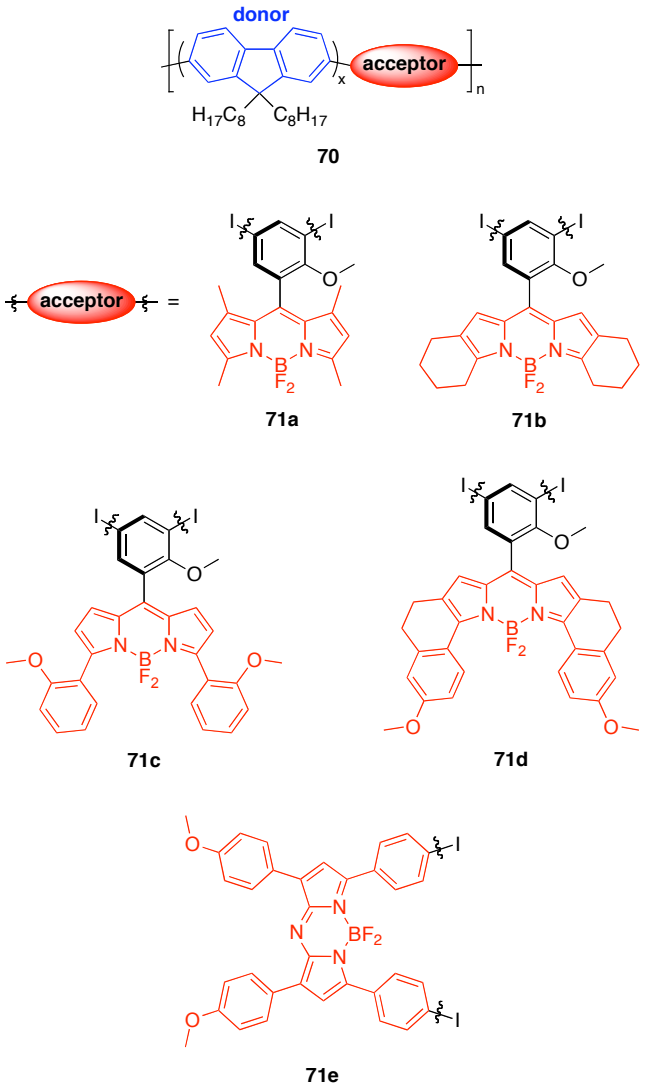

Figure 4.3. Design of BODIPY-doped polyfluorenes and structure of BODIPY acceptors.

4.2 Results and Discussion

Synthesis

Acceptors **71** were chosen to have dispersed emissions of about 30-40 nm ranging from 520 to 700 nm. Two iodines present on BODIPYs provide the means for polymerization *via* Suzuki reaction. Incorporation of methoxy group on the *meso*-phenyl of **71a-d** restricts rotation of the phenyl group thereby avoiding large decreases in quantum yields. BODIPYs **71a-d** were synthesized by acid catalyzed condensation of corresponding pyrroles **72a-d** with 3,5-diiodo-2-methoxybenzaldehyde **74** followed by oxidation with chloranil to yield dipyrromethenes **75a-d**. Chelation of BF_2 was achieved by subsequent addition of triethylamine and BF_3•OEt_2 to obtain BODIPYs **72a-d** in 25–75% yields (Scheme 4.1). AzaBODIPY **72e** was synthesized according to literature procedures.[150]

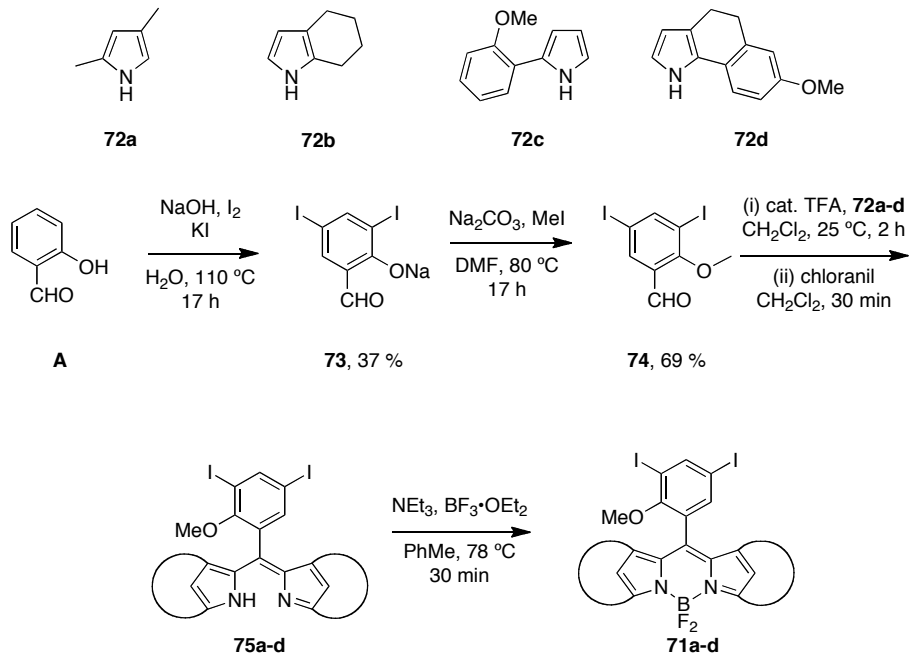

Scheme 4.1. Syntheses of BODIPY acceptors **71a-d**.

Synthesis of the polymers was achieved by Suzuki polymerization of fluorenes **B** and **C** with the appropriate acceptors using $Pd(PPh_3)_4$ and K_2CO_3 in DMF at 80 ºC (Scheme 4.2). The polymers were purified by precipitation from the medium used for the Suzuki couplings (toluene) by addition to methanol. Low molecular weight impurities were subsequently removed via multiple acetone washes, each over an extended period.

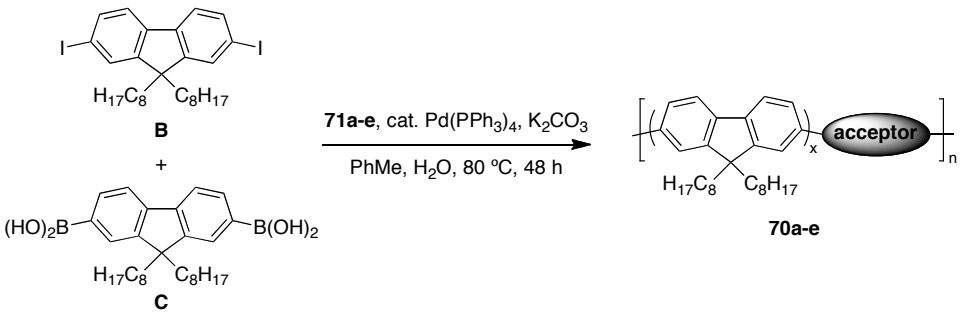

Scheme 4.2. Syntheses of the polymers **70a-e**.

Photophysical Properties

Acceptors have emissions that are dispersed at intervals of about 30 to 40 nm, from 520 to 700 nm (Table 4.1). BODIPY **71b** has an extremely high molar absorptivity and an exceptional quantum yield, and **71c** shows an unusually large Stokes' shift (*i.e.* 1565 cm^{-1}). Acceptor-precursors **71a-d** have *ortho*-methoxy-substituents on their *meso*-aryl groups to minimize radiation-less decay via rotation.

Table 4.1. Spectroscopic properties of fluorene and acceptors in CH_2Cl_2

	$\lambda_{abs\ max}$ (nm)	$\varepsilon \times 10^{-4}$ ($cm^{-1} \bullet M^{-1}$)	$\lambda_{em\ max}$ (nm)	Φ	fwhm[a] (nm)	Stokes Shift (cm^{-1})
fluorene	266	14.7	308	0.28[b]	26	5126
71a	510	8.0	521	0.36[c]	26	414
71b	556	12.0	573	1.0[d]	32	534
71c	556	5.6	609	0.48[d]	46	1565
71d	667	15.0	685	0.46[e]	37	394
71e	678	6.0	710	0.05[e]	47	665

[a] Fluorescence full width at half maximum peak height [b] Naphthalene in cyclohexane as standard (Φ = 0.92)[151] [c] Fluorescein in 0.1M NaOH as standard (Φ = 0.92)[115] [d] Rhodamine B in EtOH as standard (ϕ = 0.65)[152] [e] Zinc phthalocyanine in pyridine as standard (Φ = 0.30)[153]

We hypothesized that energy transfer would increase with greater amounts of acceptor and therefore a measurement of the minimum amount of acceptor necessary for good energy transfer was necessary. This was done by varying the amount of acceptor in the polymerization while at the same time adjusting the amount of **C** to keep a constant 1:1 ratio of diiodinated to boronic acid monomers. Acceptor **71a** was chosen for this study and was copolymerized in 0.05 - 0.67 equivalents (Table 4.2). NMR studies show that BODIPY was incorporated in 6 – 21 mol % in the polymer.

Table 4.2. Physical properties of polymer with varying amounts of acceptor **71a**

eq. acceptor in polymerization	mol % acceptor in polymer[a]	M_n (kDa)[b]
0.05	6.1	5.5
0.14	6.9	6.1
0.27	12.6	7.6
0.40	14.4	8.5
0.54	18.7	9.6
0.67	21.1	9.8

[a]Determined by proton NMR. [b]M_n determined by GPC in THF.

Table 4.3 lists the photophysical properties of the polymers in dichloromethane. The absorbance wavelength of the polymers goes down with increasing amounts of acceptor; this is indicative of random placement of the acceptor throughout the polymer, breaking the polyfluorene repeats. No significant changes in either the absorbance or emission wavelengths were observed for the acceptor when increasing its concentration in the polymer. As predicted, significant increases in ETE % and ET % were obtained with higher amounts of acceptor. This increase was offset by a simultaneous decrease in quantum yield of the polymer as the amount of acceptor increased. Taking both factors into account, an amount of 19 mol % acceptor was found to give the brightest polymers (Figure 4.4).

Table 4.3. Photophysical properties of polymer with varying amounts of acceptor **71a**

mol % acceptor[a]	$\lambda_{abs\ fluorene}$ (nm)	ETE %[b]	ET %[c]	$\Phi_{acceptor}$ (%)[d]	$\Phi_{polymer}$ (%)[e]	ε x 10^{-5}	brightness x 10^{-4}
6.1	366	25±5	28±2	26±6	6.31±0.03	2.7±0.2	1.7±0.1
6.9	362	38±1	51±3	25±1	9.5±0.6	2.8±0.2	2.7±0.4
12.6	363	55±7	73±5	28±3	15.2±0.6	2.9±0.8	4±1
14.4	352	61±1	86±2	20±1	12±1	3.5±0.3	4.2±0.7
18.7	342	70.8±0.5	92±2	15.6±0.2	11.0±0.2	4.3±0.7	4.7±0.9
21.1	336	73.8±0.5	95±1	12.2±0.2	9.09±0.07	4±1	4±1

[a] Determined by proton NMR. [b] Energy transfer efficiency, a measure of how efficiently energy absorbed by the fluorenes is transferred to BODIPY (see Table 2). [c] Percent of energy transferred between fluorene and BODIPY. [d] Fluorescein in 0.1M NaOH as standard (Φ = 0.92). [115] [e] Quantum yield of polymer calculated as the product of ETE and the quantum yield of the acceptor.

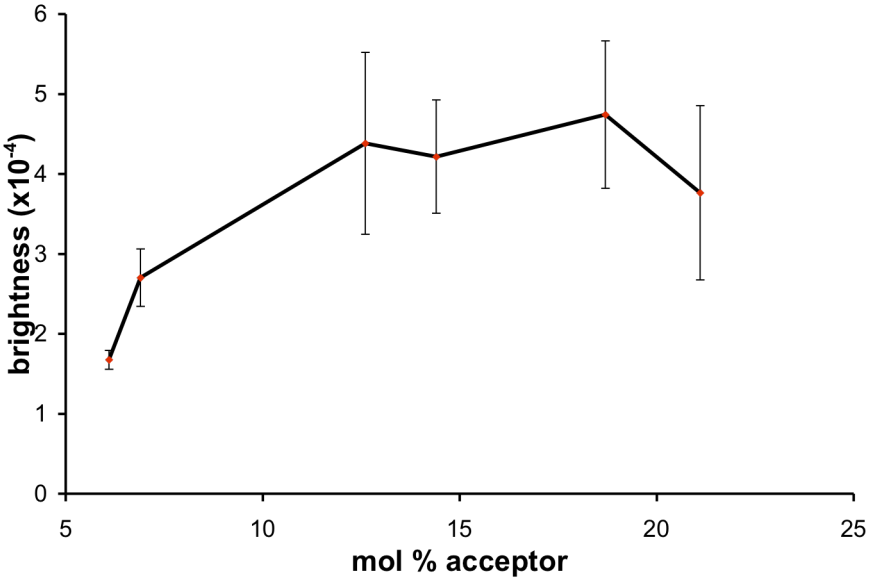

Figure 4.4. Optimization of amount of acceptor in polyfluorene.

Overall the observations described above motivated us to make a series of polymers that contained *ca* 0.19 equivalents of the acceptor monomers; this was achieved using 0.54 equivalents of the BODIPY acceptor. A 48 h polymerization run was used; shorter times gave less brilliant polymers (Figure 4.5). Table 4.4 gives the essential parameters of polymers **70a** – **e** formed via the conditions mentioned above.

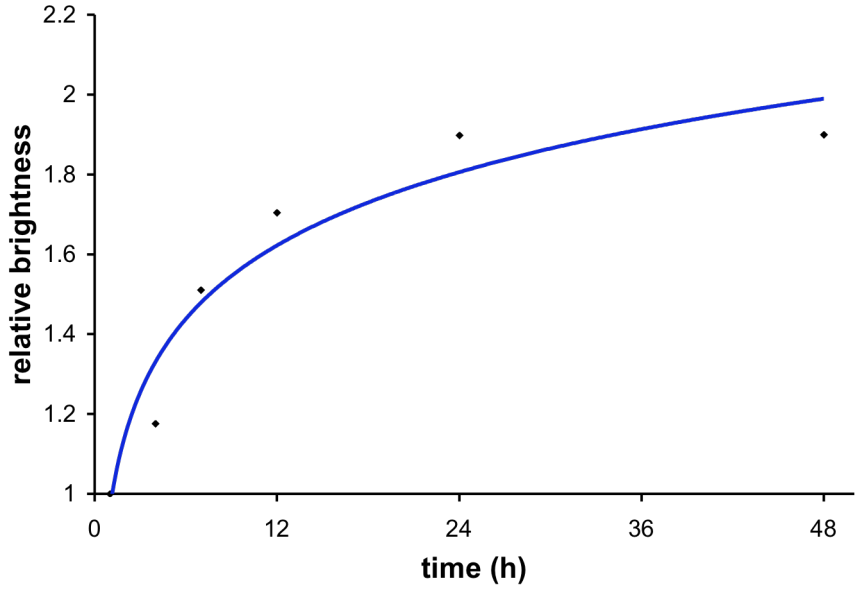

Figure 4.5. Relative brightness of polymer as a function of reaction time

Table 4.4. Physical properties of polymer with different acceptors

polymer	M_n[a]	M_w[a]	PDI[a]	mol % acceptor[b]
1a	8.8	11.3	1.29	18.7
1b	7.3	9.2	1.27	26.7
1c	9.9	14.7	1.49	22.2
1d	6.1	8.2	1.34	25.0
1e	5.8	7.0	1.21	40.0

[a]M_n determined by GPC in THF. [b]Determined by proton NMR.

Emissions from the polymers occur mainly from the acceptors with ET % ranging from 86-98 % (Table 4.5). The emission maxima of polymers **70a-d** emit at wavelengths slightly lower to that of the free acceptors **71a-d**. For example, polymer **70d** has an emission maximum at 685 nm while acceptor **71d** has a maximum at 677 nm. Polymer **70e** shows a considerable increase (43 nm) in its emission wavelength compared to acceptor **71e**. This could be because the phenyl groups on azaBODIPYs in **70e** can adopt conformations that are more planar with the heterocyclic core than the *ortho*-substituted *meso*-aryl groups of **70a** - **d**. In other words, polymerization with fluorene extends the conjugation of the azaBODIPY.

Table 4.5. Photophysical properties of polyfluorenes incorporated with acceptors in CH_2Cl_2

polymer	mol % acceptor[a]	λ_{abs} fluorene (nm)	λ_{abs} bodipy (nm)	λ_{em} (nm)[b]	ETE %[c]	ET %[d]	$\Phi_{acceptor}$	$\Phi_{polymer}$[h]	molar absorptivity x 10^{-5} ($cm^{-1}\bullet M^{-1}$)
70a	19	343	505	517	70.8±0.5	90.5±0.6	0.147±0.002[e]	0.104±0.002	5.1±0.9
70b	27	343	549	566	60±2	97.2±0.3	0.24±0.01[f]	0.14±0.05	5.74±0.07
70c	22	344	547	602	48±8	95.9±0.5	0.13±0.02[f]	0.06±0.02	5.18±0.03
70d	25	347	657	677	37±3	98±1	0.25±0.07[g]	0.09±0.03	4.3±0.3
70e	40	336	703	753	49.4±0.3	86±2	0.002[g]	0.001	4.58±0.07

[a] Estimated by NMR. [b] Emission maximum when excited at 358 nm (fluorenes) [c] Energy transfer efficiency (ETE) was calculated by dividing the quantum yield of acceptor when excited at fluorene donor by the quantum yield of acceptor when excited at acceptor. [d] Percent of the total fluorescence being emitted by the acceptor. [e] Fluorescein in 0.1M NaOH as standard (Φ = 0.92).[115] [f] Rhodamine B in EtOH as standard (Φ = 0.65)[152] [g] Zinc phthalocyanine in pyridine as standard (Φ = 0.30)[153] [h] Quantum yield of polymer calculated as the product of ETE and the quantum yield of the acceptor.

a

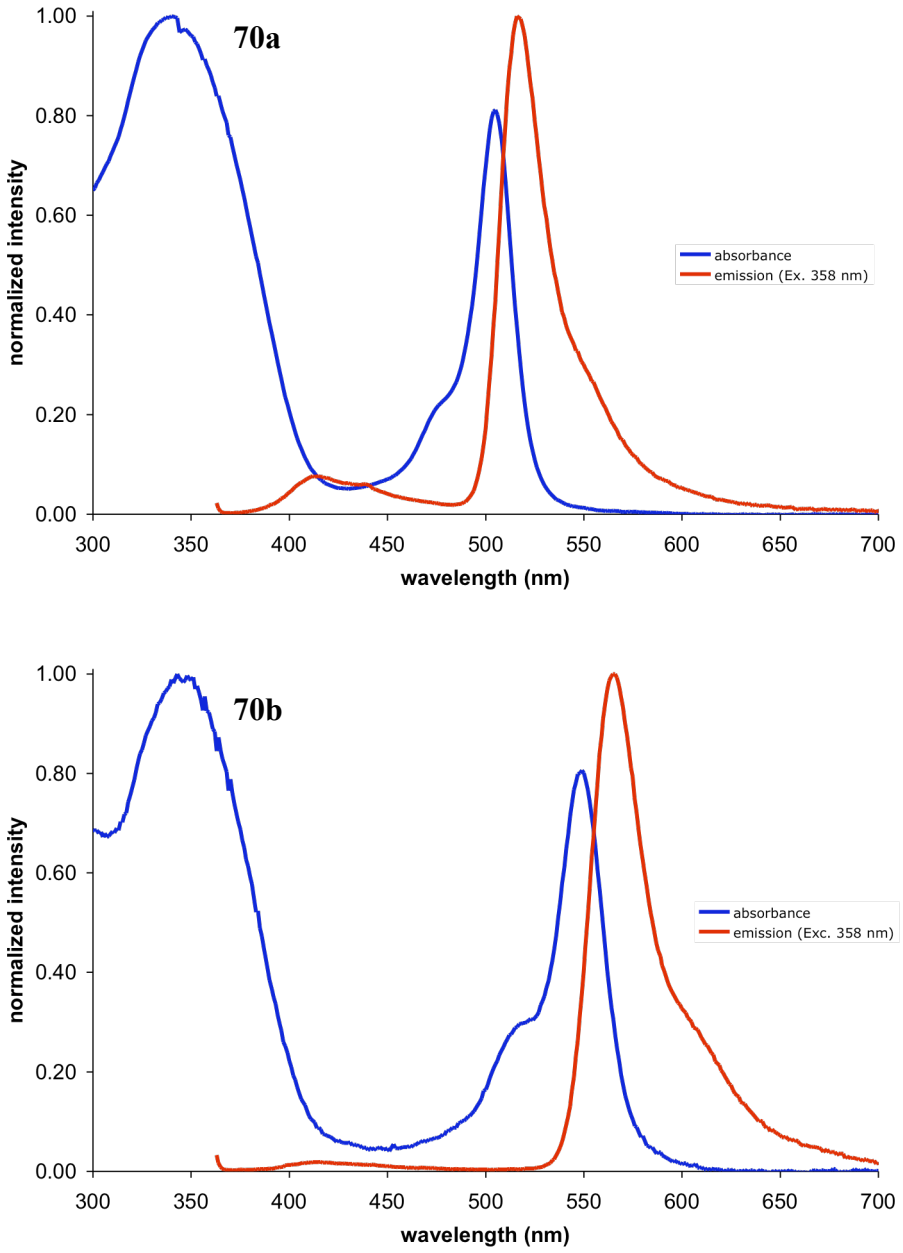

Figure 4.6. a. Absorbance (10^{-5} M) and emission (10^{-6} M) spectra of **70** in CH_2Cl_2. **b.** Combined normalized fluorescence of **70** in CH_2Cl_2 at 10^{-6} M excited at 358 nm. **c.** Photograph of polyfluorene and **70** in CH_2Cl_2 under UV lamp irradiation.

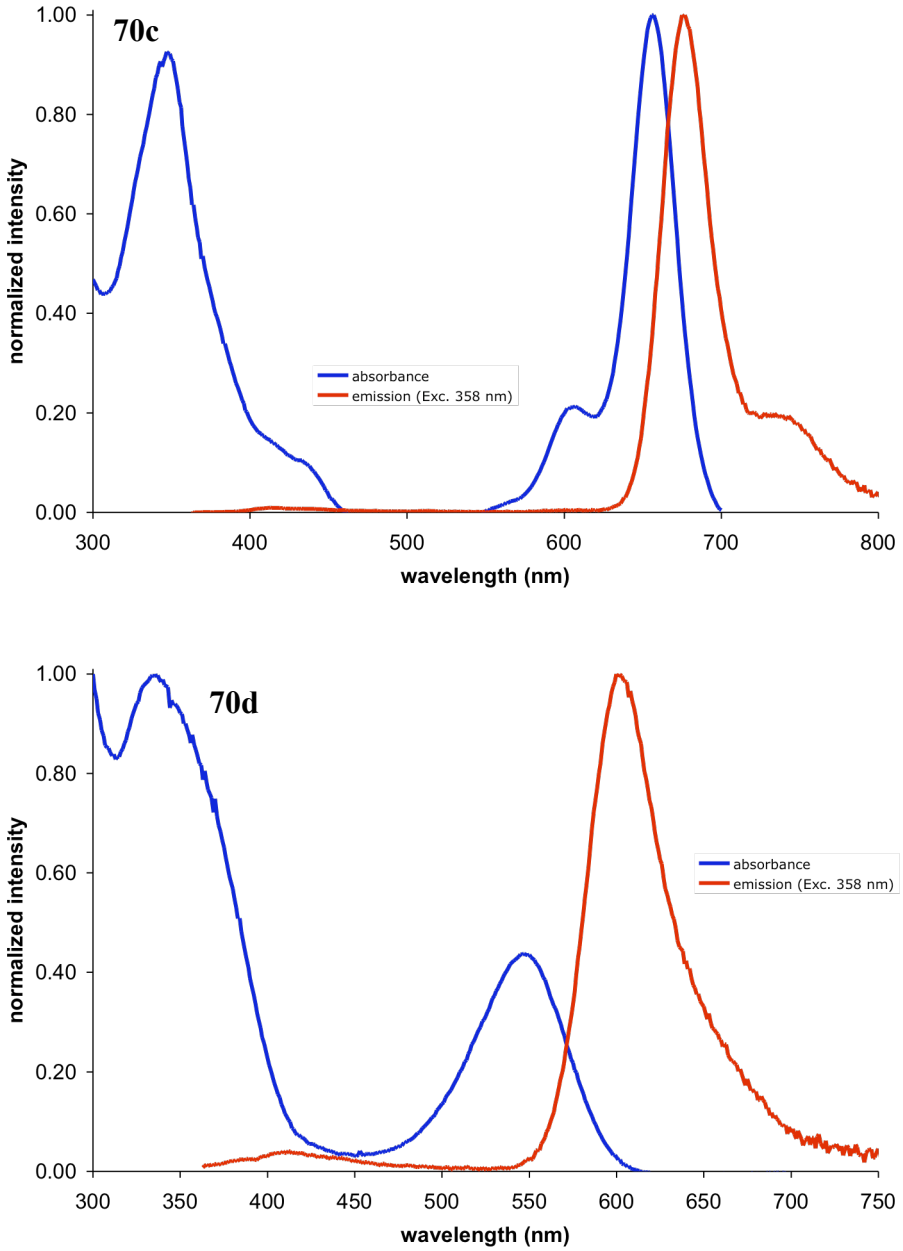

Figure 4.6 Continued.

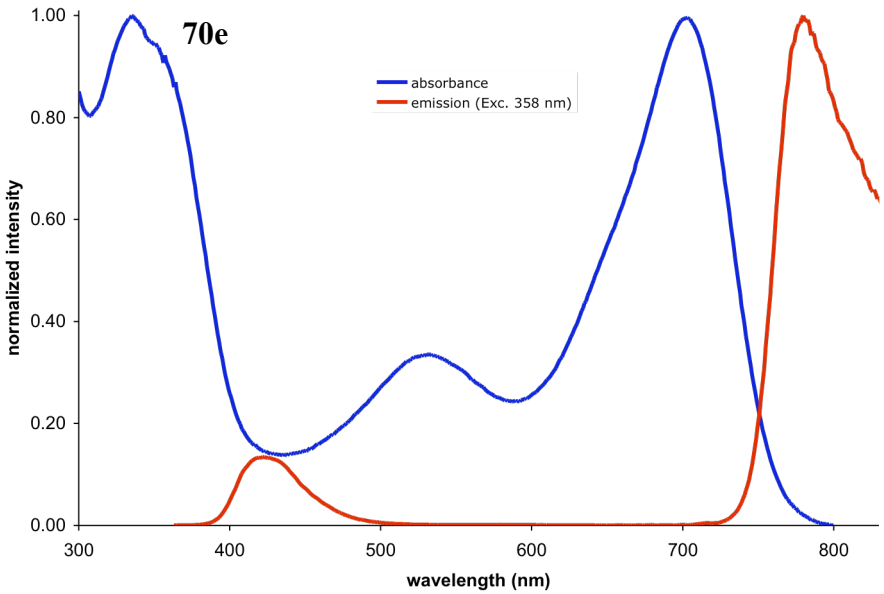

b

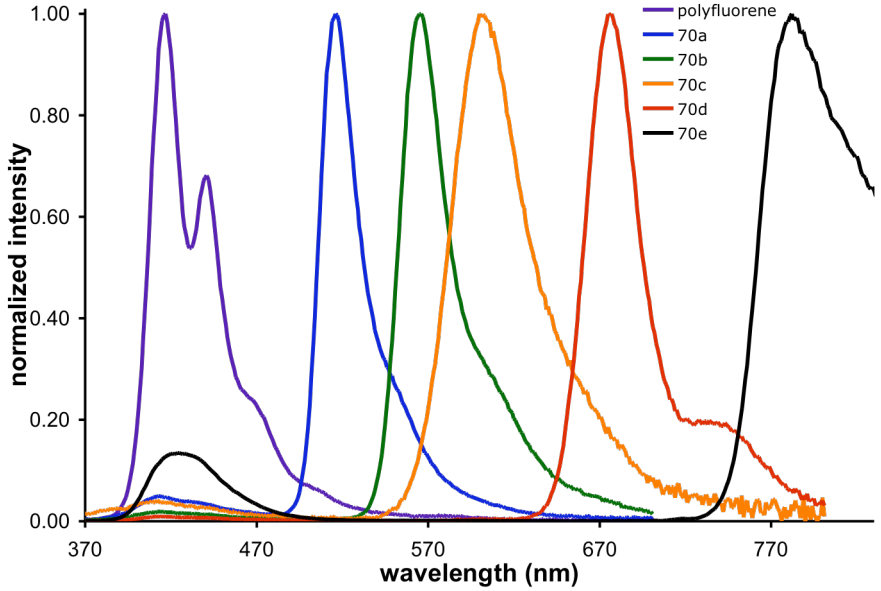

Figure 4.6 Continued.

c

Figure 4.6 Continued.

Cell Imaging via Nanoparticles Fabricated from Polymers

McNeill *et al*. have reported efficient generation of organic nanoparticles from polyfluorene and similar systems.[154-164] We investigated whether comparable nanoparticles could be constructed from doped polymer **70**. In the event, slight modifications were found to be more suitable for these polymers; slower addition rate of a more dilute THF solution of the polymer to water gave particles of 48.4 ± 13.3 nm by dynamic light scattering in the case of **70b** (Figure 4.7). TEM investigations of particles made from **70a-d** led to aggregation before the analysis though smaller particles averaging 20 to 60 nm could be seen (see Appendix E).

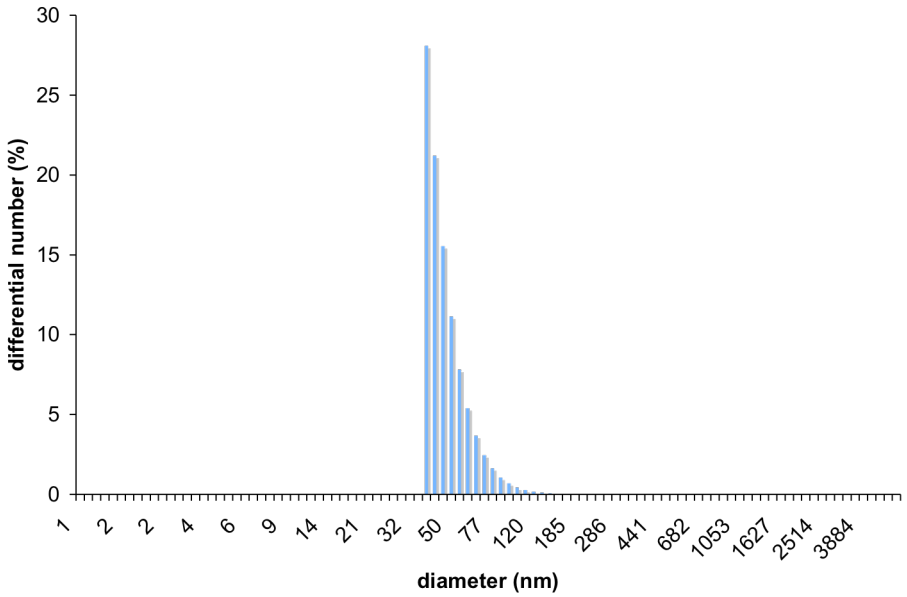

Figure 4.7. DLS and analysis of particles made from **70b** averaging 48.4 ± 13.3 nm.

Uptake of the organic nanoparticles from **70** was studied on normal rat liver cells (Clone 9). After 40 h incubation at 37 °C in Ham's + 5% fetal bovine serum (FBS) culture medium, the nanoparticles were observed as bright dots inside the cells (Figure 4.8); they did not specifically target organelles. Polymers incubated under same conditions did not enter the cells.

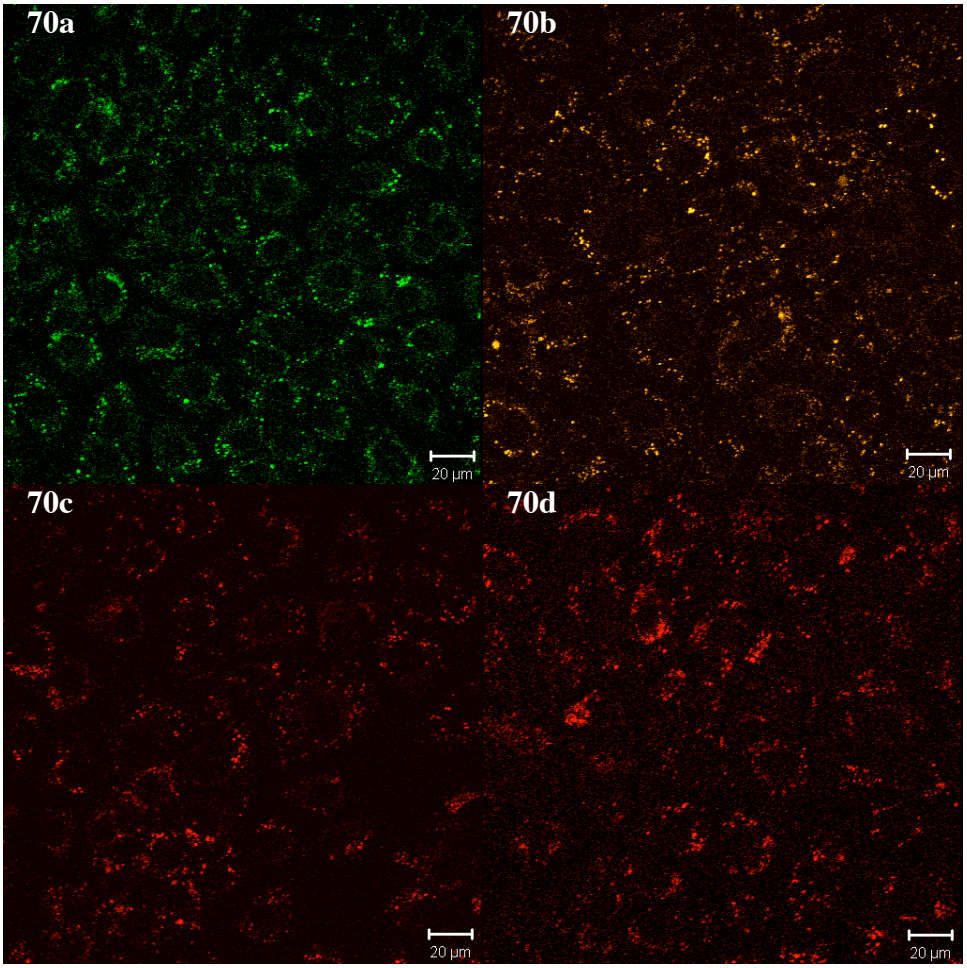

Figure 4.8. Confocal imaging of Clone 9 rat liver cells with polymeric nanoparticles **70a-d**.

4.3 Conclusions

The work reported here features cassettes with donor and acceptor fluors joined via linkers that would allow conjugation if the molecules became planar.[9,13,14,28-30,165] However, the twist between these fragments "insulates" the donor and acceptor parts so that the overall emission characteristics of the composites mirror those of the free acceptor. This makes it possible to design of materials with predictable fluorescence

emission wavelengths. This property coupled with the fact that there are several donors per acceptor part, offers potential for fluorescent probe design, OLEDs and lasing materials.

Further work is needed to address two important issues: (i) lack of water-solubility of the polymers and; (ii) quenching of the acceptors. Luckily the first issue appears trivial since water-soluble analogs of polyfluorene are known. For example, ammoniums[166,167], carboxylic acids[168], sulfonic acids[169], phosphonic acids[170], amino acids[171], crown ethers[172], and sugars[173] have all been used to increase water solubility of polyfluorenes. It should be noted however that complications could arise in the synthesis of such polymers due to the hydrophilicities and hydrophobicities of the donors and acceptor respectively. It may be necessary, for instance, to mask the water-solubilizing groups until after isolation of the polymers or incorporate water solubility on the BODIPY acceptors as well, making both parts hydrophilic.

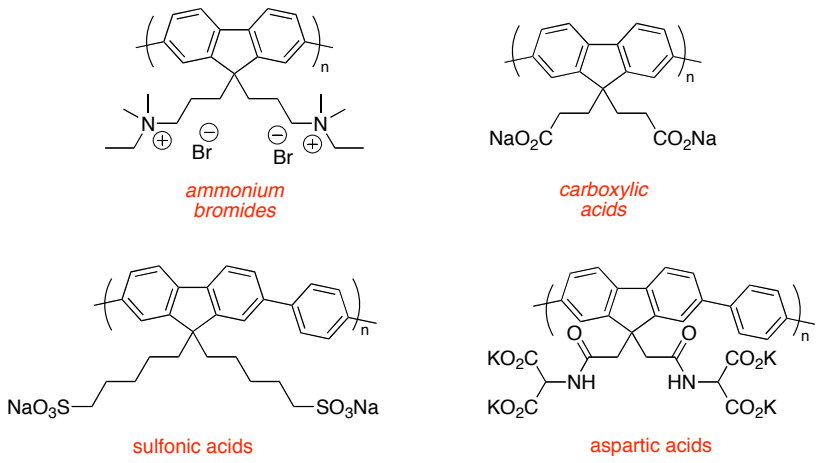

Figure 4.9. Examples of water-soluble polyfluorenes.

The issue of self-quenching of the acceptors can be addressed by decreasing the amount of acceptor used. It is known that incorporation of electron withdrawing aromatics can have drastic effects on the emissive properties of polyfluorenes, mainly shifting the $\lambda_{max\ emiss}$ to the red (Figure 4.10a).[138,158-164] These types of electron withdrawing groups could be doped in polyfluorenes and act as electronic "bridges" that modulate the flow of energy in such polymers leading to increases in ETE; increases that could potentially offset the lowered ETE consequential from the decrease in acceptor. An example of how such a system could be designed for *in vivo* imaging is shown in Figure 4.10b. Compound **76** would possess water solubility needed for *in vivo* imaging, have bright emissions into the red due to the energy bridges facilitating energy transfer from donors to acceptors, and also possess targeting ligands to bind cancer cells.

a

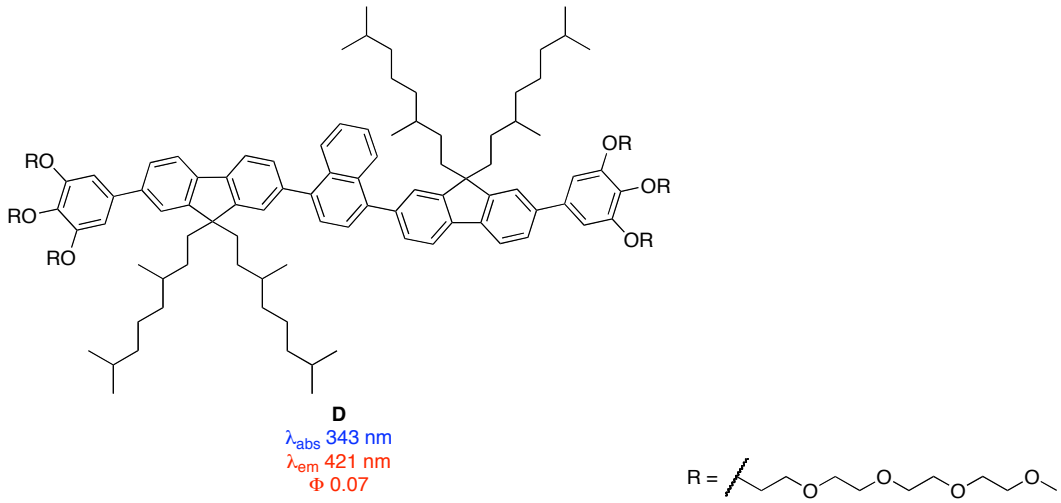

Figure 4.10. **a.** Electron withdrawing rings can affect the photophysical properties of fluorene. **b.** Example of how we can use electron-withdrawing rings to increase energy transfer efficiency in BODIPY doped polyfluorenes for *in vivo* imaging.

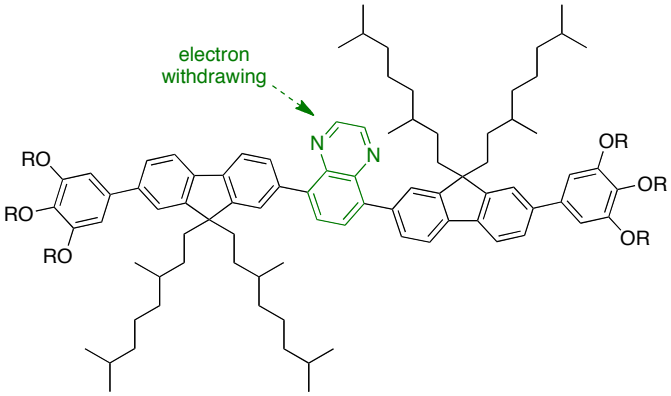

E
λ_{abs} 333 nm
λ_{em} 519 nm
Φ 0.50

b

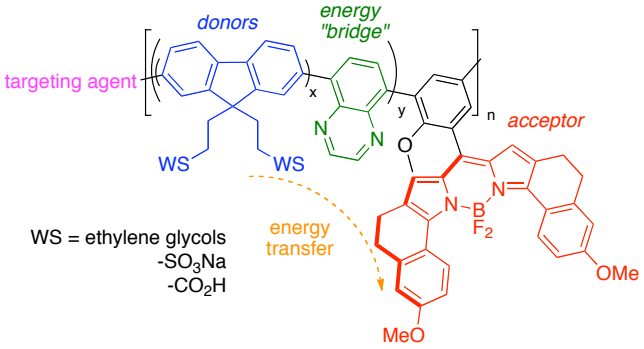

76
potential target
for *in vivo* imaging

Figure 4.10 Continued.

CHAPTER V

DYES FOR PHOTODYNAMIC THERAPY

5.1 Introduction

Cancer is an ever-present threat that accounts for 1 out of every 4 deaths and was the second leading cause of death in the United States in 2010.[174] Indeed, it is no surprise that much research is currently aimed at discovering cures. One relatively new approach to combat cancer is through the use of PhotoDynamic Therapy (PDT). PDT agents are dyes that are non-cytotoxic unless, ideally, they are activated by light. Phototoxicity is caused by the generation of Reactive Oxygen Species (ROS) inside of cells.[175,176] In practice, the PDT agent is either injected or applied topically to the cancer patient. Once the agent has localized in the tumor, it is selectively irradiated with powerful lasers, killing the irradiated cells in the process.

The advantage of such an approach over other types of treatments is that only the cancer is irradiated and theoretically only these cells should be killed, as opposed to chemotherapeutic drugs that often target normal cells. In spite of this, only a few PDT agents have been approved; these are for treatment of skin, gynecological, gastro-intestinal, and some head and neck cancers.[177] Photofrin® was the first and its structure is derived from hematoporphyrin (HpD) (Figure 5.1). Unfortunately, Photofrin is isolated as an oligomeric mixture so batch reproducibility is problematic and, in fact, the most active component of Photofrin is ambiguous.[178] Furthermore, Photofrin lacks selectivity for cancer cells and can stay in the body for up to two months after treatment.[176] Foscan®

is a synthetic analog of Photofrin though its structure is based of the chlorin rather than porphyrin. Furthermore, unlike Photofrin, Foscan is a single component and batch reproducibility is not problematic.

Unfortunately, Photofrin and Foscan are not selective to tumor cells; once the agents are introduced in the blood stream they localized throughout the body. This is problematic because activation due to exposure to sunlight can occur. A clever approach towards selectivity was achieved in the development of Levulan® in which a prodrug, 5-aminolevulinic aid (ALA), is applied topically over the tumor. The body absorbs ALA and produces an active PDT agent. Importantly, the agent is mostly localized near the point of application of the prodrug as opposed to rapid dispersal throughout the host. The process tends to be only effective for cancers near the skin surface because ALA has to reach the tumor.

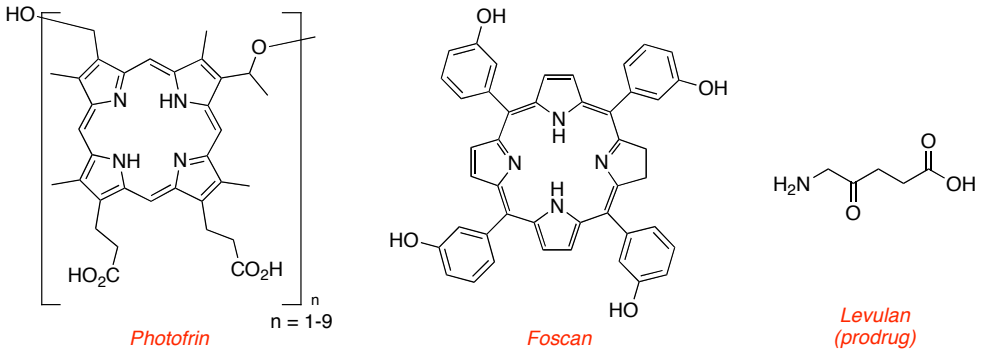

Figure 5.1. Commonly clinical PDT agents encountered.

Besides the tetrapyrrolic agents, naturally occurring dyes have also been investigated as PDT agents. Nile Blue, Nile Red, and the chalcogenopyrylium class of

photosensitizers have all shown promise but have undesirable dark cytotoxicities. A relatively new class of PDT agents is those derived from the BODIPY chromophore. BODIPYs are discussed in detail in Chapter II and they possess several attributes attractive for PDT including: (i) high molar absorptivities, (ii) high fluorescence quantum yields, (iii) relatively low sensitivity to environment, and (iv) resistance to photobleaching. Despite these encouraging properties, the uses of BODIPYs for PDT remain scarce. Nagano *et al.* investigated a simple diiodinated BODIPY as a PDT agent and found it to be efficient at producing singlet oxygen presumably due to the heavy atom effect induced by the iodines (Figure 5.2).[56] Similarly, Akkaya *et al.* studied dibrominated BODIPYs with extended conjugation at the α-positions.[179] These were also effective agents and have the added advantage of absorbing above 650 nm, alleviating problems of tissue penetration by incident light. Our aim for this work was two-fold, (i) further investigate the scope of simple BODIPYs as PDT agents; and (ii) use the information from the first aim to design a new class of PDT agents that absorb in the near-IR region.

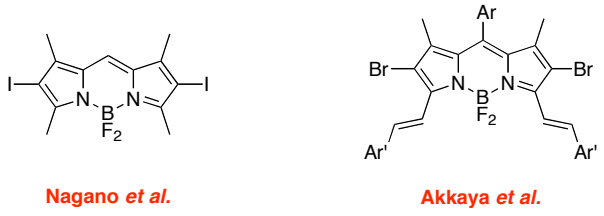

Figure 5.2. Previously studied BODIPYs for PDT.

5.2 *In Vitro* and *In Vivo* Photocytotoxicity of BODIPY Derivatives for PDT

The work described in this section✪ is aimed at understanding how structural variations affect the PDT properties of BODIPY.[180] For this purpose we studied many of the dyes produced in Chapter II and compound **77** (Figure 5.3) that was synthesized by diiodination of **B** using iodine and iodic acid in methanol.

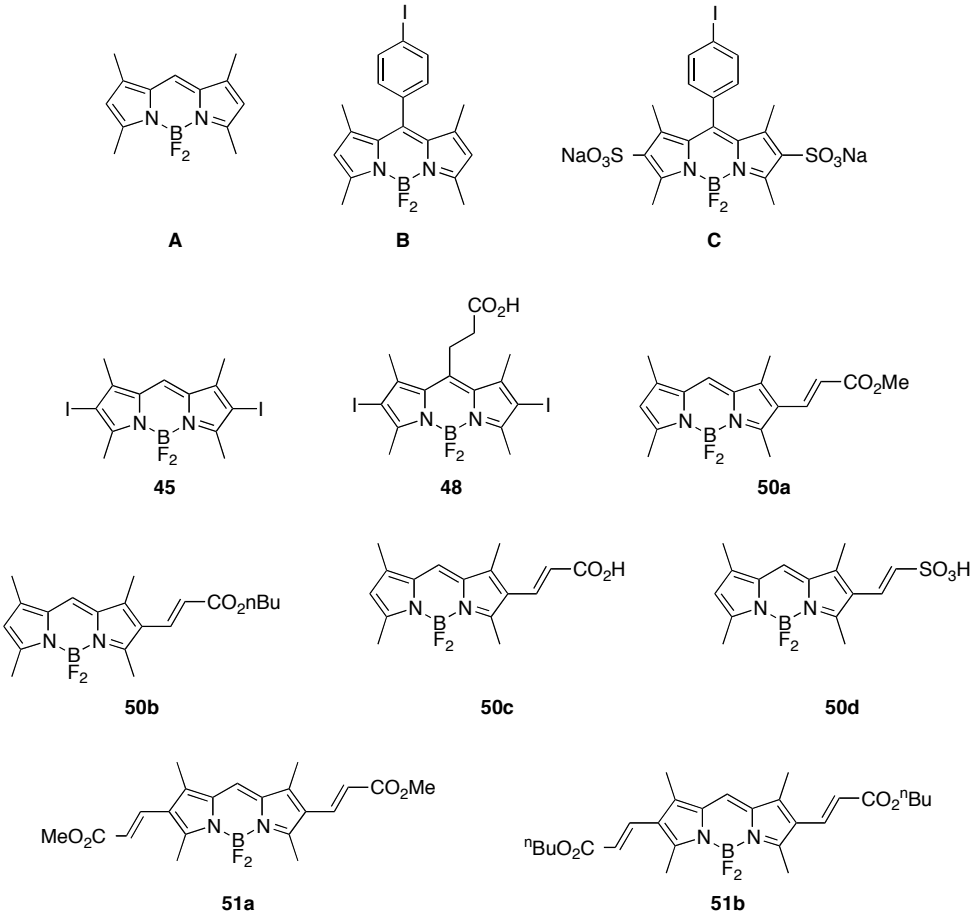

Figure 5.3. Potential PDT agents studied here.

✪ The biological data presented in section 5.2 is mainly from a collaboration with the Boon research group in Malaysia.

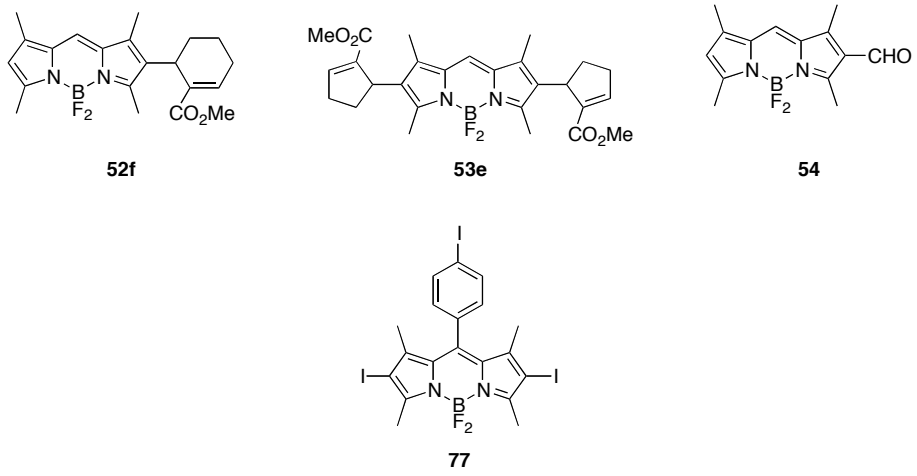

Figure 5.3 Continued.

Structural Variations and Photophysical Properties

Two structural variations around the BODIPY core of compound **A** were investigated in this study (Figure 5.4). The first (compounds **B**, **C**, **77**, **48**, **45**) investigated the effectiveness of various iodinated derivatives in order to maximize the "heavy atom effect". To fine-tune the activity of iodinated BODIPY based structures, additional functionalizations such as *meso*-substitution with alkyl or aryl groups as well as sulfonation to improve hydrophilicity were tested. Compound **48** contains a carboxylic acid handle and could be easily attached to other molecules later if required. For the second variation (compounds **50**-**54**), the effect of extended conjugation at the 4-pyrrolic position was examined. Extended conjugation at the 4-pyrrolic positions increases the absorption wavelength of the compounds to the red, permitting the use of longer

excitation wavelength that penetrates deeper into biological tissues for effective treatment.

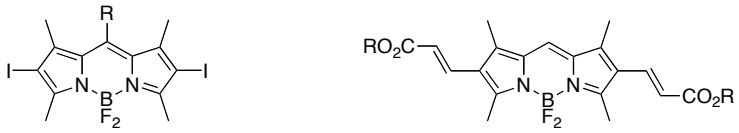

Figure 5.4. Structural variation of BODIPYs studied here.

Table 5.1 summarizes the photophysical data of the compounds studied for PDT. The absorption and emission wavelengths of the series of BODIPYs range from 500 to 600 nm. As expected for dyes **50**-**53**, extending the conjugation with an acrylate shifts the $\lambda_{abs\ max}$ to the red by 20-30 nm while attaching two acrylates red-shifts the $\lambda_{abs\ max}$ by 50-60 nm, compared to compound **A**. The $\lambda_{abs\ max}$ values for iodinated compounds **77**, **48**, and **45** are also red-shifted compared to compound **A** but not for compounds **B** and **C**, which are aryl-iodinated at the *meso*-position. In addition, all compounds have high extinction coefficients and high quantum efficiencies of fluorescence except for a few structures. Among the exceptions, compounds **77**, **48**, and **45** have much lower fluorescence quantum efficiency and a correspondingly higher singlet oxygen generation rate (Table 5.2) compared to the other BODIPYs studied here, probably as a result of the enhanced intersystem crossing efficiency from the lowest singlet excited state to the triplet state contributed by the internal heavy-atom effect.

Table 5.1. Photophysical properties of BODIPY derivatives

Compound	$\lambda_{abs\ max}$ (nm)	ε (x 10^{-6})	$\lambda_{em\ max}$ (nm)	Φ	Ref [a]	solvent
A	505	8.3	516	0.80	1	EtOH
B	504	8.2	510	0.64	1	$CHCl_3$
77	537	8.9	552	0.05	2	CH_2Cl_2
C	498	10	509	0.34	1	H_2O
48	525	9.3	540	0.03	2	EtOH
45	539	9.1	555	0.04	3	CH_2Cl_2
54	494	8.1	504	0.95	1	EtOH
50c	531	2.7	570	0.42	2	EtOH
50d	529	-[b]	560	0.25	2	EtOH
50a	527	6.3	549	0.73	2	EtOH
51a	559	1.3	580	0.51	3	EtOH
50b	528	6.2	551	0.73	2	EtOH
51b	560	3.0	580	0.52	3	EtOH
52f	517	6.3	527	0.78	2	EtOH
53e	530	7.2	539	0.92	2	EtOH

[a] Reference dyes used for quantum yield determination (solvent, Φ): 1. fluorescein (0.1 M NaOH, 0.92), 2. rhodamine 6G (EtOH, 0.94), 3. rhodamine B (EtOH, 0.97); [b] value not determined.

As in the case of the $\lambda_{abs\ max}$ values above, compounds **B** and **C** which contain a *para*-iodoaryl group at the meso position did not demonstrate the same loss in fluorescence yields or the same increase in singlet oxygen generation rate as compounds **77**, **48**, and

45 probably because in the former group, first, the iodine atom is not directly attached to the BODIPY core and, second, the iodoaryl plane is twisted relative to the BODIPY plane[49], overall causing the aryl iodine atom to only, at most, elicit an intramolecular external heavy-atom effect.[181]

In Vitro *Photocytotoxic and Comparative Singlet-Oxygen*

The *in vitro* photocytotoxic activity of all the compounds against a promyelocytic leukemia cell line (HL-60), an oral squamous carcinoma cell line (HSC-2), and a nasopharyngeal carcinoma cell line (HK1) following irradiation with 4.1 J/cm^2 of a broad spectrum light was determined by the Boon group using a modified methylthiazolyldiphenyltetrazolium bromide (MTT) assay. Parallel assays without light irradiation were also carried out to determine cytotoxicity in the dark. Results were expressed as IC50, the concentration of compound (in μM) that inhibits proliferation rate by 50 % compared to control untreated cells. The parent compound, denoted as **A**, was also prepared and tested for comparison (Table 5.2). From the assay, all compounds had negligible or undeterminable un-irradiated cytotoxicities up to 100 μM. Upon irradiation with 4.1 J/cm^2 of light, compounds **A-C**, **45**, **48**, **77**, **50a-b**, and **51-53** demonstrated photosensitized cytotoxicities with IC50 values in the submicromolar to tens of micromolar range. Compounds **48** and **45**, which have two iodine atoms directly attached to the BODIPY core, showed the highest activity among the analogues, with IC50 values that are up to 100 times lower than that of compound **A** (0.045 μM vs. 4.4

μM in HL-60). In contrast, compounds **54** and **50c-d** displayed poor activity with undeterminable IC50 up to 100 μM.

The influence of the iodine atom on the photocytotoxic activity of the compounds was evident from studying compounds **A-C**, **45**, **48**, and **77**. *Meso*-substitution with a *para*-iodoaryl group in compound **B** does not alter the photocytotoxicity significantly compared to compound **A**, while further substitution with iodine atoms on the two pyrrolic 4-carbon to yield either compound **77** from **B** or compound **45** from **A** improved the activity by 10- and 100-fold, respectively, in all three cell lines, alluding to the importance of iodine atom substitution on the pyrrolic carbons rather than on the *meso*-aryl position. Compound **48**, which has an additional carboxylic acid tether at the meso position, has similar to marginally better activity than compound **45** in all three cell lines. An attempt to improve the water solubility of compound **B** by substituting with sodium sulfonate to yield compound **C** resulted in 10 times loss in activity.

Table 5.2. Comparative singlet oxygen generation and i*n vitro* photo cytotoxicity induced by BODIPY. [a] Comparative singlet oxygen generation of photosensitizers in relative to methylene blue. [b] IC_{50}, the concentration of compound, which inhibits the proliferation rate by 50% as compared with control untreated cells. Values represent the mean ± SD of three determinations assessed 24 h using standard MTT assay. Cells were incubated with compound for 2 h prior to irradiation with 9.6 J/cm^2.

Cmpd	Singlet oxygen generation relative rate[a]	Activity IC_{50} (μM)[b]					
		HL60		HSC2		HK1	
		0 J/cm^2 (dark)	9.6 J/cm^2	0 J/cm^2 (dark)	9.6 J/cm^2	0 J/cm^2 (dark)	9.6 J/cm^2
A	0.48	>100	4.4±0.4	>100	8.7±2.0	76.8±10.6	6.2±1.2
B	0.15	>100	2.7±1.2	>100	5.1±0.8	>100	5.7±0.1
77	13.9	10	0.42±0.06	10	0.5±0.1	95.5±7.9	0.69±0.08
C	0.07	>100	54.3±8.3	>100	59.4±6.2	>100	59.0±7.1
48	24.6	>100	0.045±0.004	>100	0.10±0.06	55.8±0.8	0.57±0.1
45	23.9	3.34±0.37	< 0.01	54.5±6.0	0.083±0.014	75.4	0.052±0.01
54	0.07	>100	>100	>100	>100	>100	>100
50c	0.01	>100	>100	>100	>100	>100	>100
50d	0.00	>100	>100	>100	>100	>100	>100
50a	0.57	>100	4.8±0.7	>100	5.4±0.6	>100	5.3±0.6
51a	0.41	>100	5.2±0.6	>100	11.1±7.4	>100	8.5±0.5
50b	0.73	>100	0.49±0.07	>100	0.6±0.1	99.6±0.6	1.1±0.6
51b	0.17	>100	57.7±6.6	>100	37.7±15.7	>100	>100
52f	0.24	>100	4.9±0.6	>100	4.1±0.2	>100	5.0±0.6
53e	0.29	>100	3.8±0.7	-	-	>100	4.8±0.9

For the effect of extended conjugation at 4-pyrrolic positions on photocytotoxic activity of BODIPYs, compounds **50**-**53** were studied. Extending the 4-pyrrolic carbon with a single aldehyde **54** or the hydrophilic allylic carboxylic acid **50c** and allylic sulfonic acid **50d** resulted in loss of activity of greater than 100 μM IC50 values. Single extensions at the 4-pyrrolic position with acrylate esters affected the activity differently depending on the length of the alkyl ester group, where the methyl compound **50a** showed no change in activity while ^{n}butyl compound **50b** demonstrated 10-fold improvement in activity compared to compound **A**. For compounds with double extension with the same groups at the 4-pyrrolic positions, the methyl compound **51a** displayed comparable activity to compound **A**, but interestingly, the ^{n}butyl compound **51b** showed 10-fold loss in activity compared to **A** or 100-fold loss compared to the singly extended counterpart **50b**. The explanation for the reversal in structure-activity relationship of the ^{n}butyl acrylate esters compared with the methyl acrylate esters from the single to the double-extension (compounds **50a** and **50b** compared with compounds **51a** and **51b**) is not obvious and could just be due to the poorer solubility of the doubly extended ^{n}butyl derivative **51b**. Compounds **52f** and **53e**, which were failed attempts to prepare the analogous ring-constrained conjugated structures, were also tested and showed similar activities compared to compound **A**, further suggesting the minor role that 4-pyrrolic extended conjugation or the lack of it plays in modulating the photocytotoxicity of the BODIPY structures.

Subsequently, the relative rate of singlet oxygen generation was measured for all the compounds by monitoring the reaction of known singlet oxygen acceptor 1,3-

diphenylisobenzofuran (DPBF) with photosensitizers generated singlet oxygen.[182] This was achieved by following the loss of DPBF absorbance at 410 nm at an initial concentration of 50 μM over a period of 1 h. A light source filtered at 510 nm wavelength was used to minimize the photobleaching of DPBF. As a result, this would have caused an underestimation of singlet oxygen generation rate of the compounds with $\lambda_{abs\ max}$ lower than 510 nm, as the light transmission through the filter begins to drop below 510 nm. Each of the compounds was tested at an equivalent concentration of reference sensitizer methylene blue. The results from this study ranged from 0.01- to over 24-fold of singlet oxygen generation rate compared to that of methylene blue. Importantly, the rate of reactive oxygen generation measured generally correlated with the potency of these compounds and may be a main factor affecting the photocytotoxicity of these BODIPYs.

Photosensitizer Cellular Localization

To ascertain the intracellular localization of the BODIPYs, compound **48**, owing to its good potency data, was chosen and examined by spinning disk confocal microscopy using dual staining techniques (Figure 5.5). Co-staining images and topographic profiles of HSC-2 cell line loaded with compound **48** and a mitochondria-specific dye rhodamine 123 (Rh123) revealed an almost identical overlap, suggesting that compound **48** localized particularly well in mitochondria (Figure 5.5B,C). In comparison, compound **48** displayed only partial colocalization with endoplasmic reticulum and lysosomes, according to the confocal images and topographic profiles of compound **48** with ER-

Tracker (Figure 5.5D,E) and with LysoTracker (Figure 5.5F,G), respectively. Staining of the cytoplasmic or nuclear membrane by compound **48** was not detected, indicating that it does not react nonspecifically with biological membranes. Furthermore, the nucleus remained free of compound **48** (dark nuclear area), signifying that this class of compounds would not be expected to directly damage DNA.

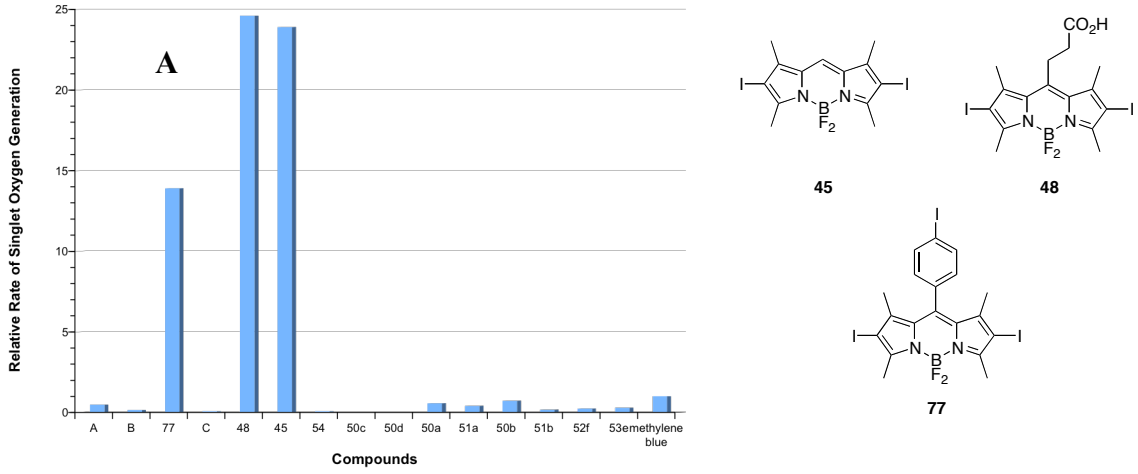

Figure 5.5. Relative rates of singlet oxygen generation for agents **45**, **48**, and **77** (A) and intracellular localization of compound **48** in HSC-2 cells. Spinning disk confocal images (B, D, F) and fluorescence topographic profiles (C, E, G) of HSC-2 cells double-stained with 100 nM compound **48** and respective organelle probes. (B, C) Mitochondria were labeled with 100 nM Rh123 and excited at 494 nm. (D, E) Endoplasmic reticulum were labeled with 100 nM ER-Tracker and excited at 365 nm. (F, G) Lysosomes were labeled with 500nM of LysoTracker and excited at 365 nm. Compound **48** was excited at 575 nm. Line indicates the longitudinal transcellular axis analyzed to generate the topography fluorescence profiles. Objective magnification is 63.

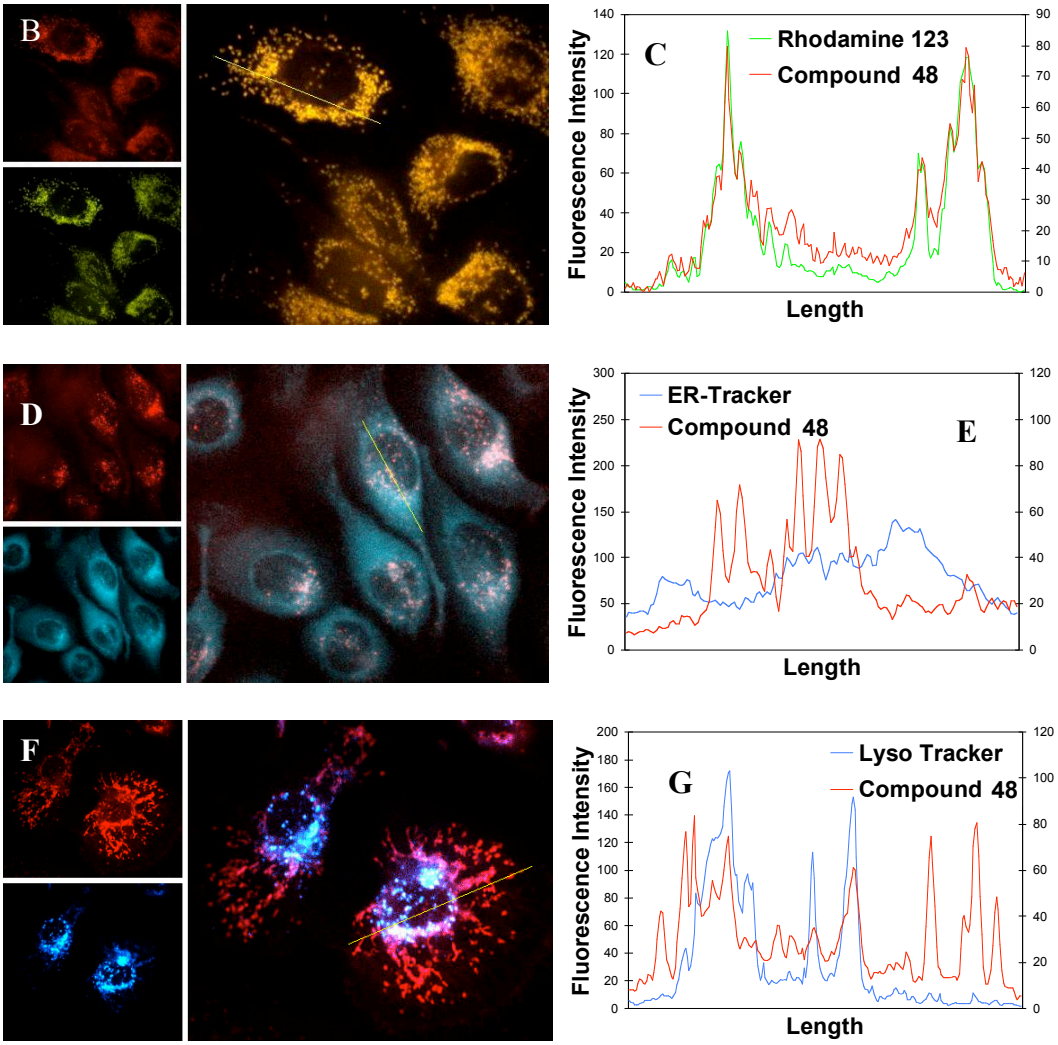

Figure 5.5 Continued.

Mitochondria perform vital cellular functions and are involved in multiple signaling cascades in regulation of metabolism, cell cycle control development, and cell death.[183] In PDT, mitochondria are an important target. During mitochondria-photosensitization in PDT, cytochrome c is released from mitochondria to directly effect rapid cell death through downstream effector pathways of apoptosis, bypassing other upstream apoptotic signaling pathways that require synthesis of new proteins. This mechanism of action is

particularly useful in the treatment of cancer types that are chemoresistant because of mutations in upstream proapoptotic signaling pathways.[184]

Cell Cycle Arrest and Apoptosis

To study the mechanism of action of compound **48** that contributed to its photocytoxicity, the effect of compound **48** on cell cycle and apoptosis of HSC-2 cells was investigated by the Boon group using flow cytometric method. The cell cycle profile of HSC-2 cells treated with compound **48** was analyzed in a time course experiment. At 0.25 μM, compound **48** was found to induce G2/M arrest in HSC-2 cells as early as 2 h following light irradiation (Figure 5.6a). HSC-2 cells in G2/M phase gradually increased from 26.1% in the control group to 39.8 %, 48.4 %, 55.5 %, respectively, at 2, 4, and 6 h after light irradiation. Concomitant with the increased proportion of G2/M phase cells, HSC-2 cells in the G1 phase were reduced from 57.7 % to 46.3 %, 33.8 %, and 26.4 % while the proportion of HSC-2 cells in S phase remained fairly constant. At 8 and 12 h, the proportion of cells arresting in the G2/M phase was reduced to 48.8 % and 26.0 %, respectively, after light irradiation. Following the reduction of the proportion of cells arresting in G2/M phase, an increase of sub-G1 cells population from 8 to 12 h (from 4.4 % to 10.6 %) was observed. The proportion of cells treated with compound **48** without irradiation remains unchanged compared to control.

a

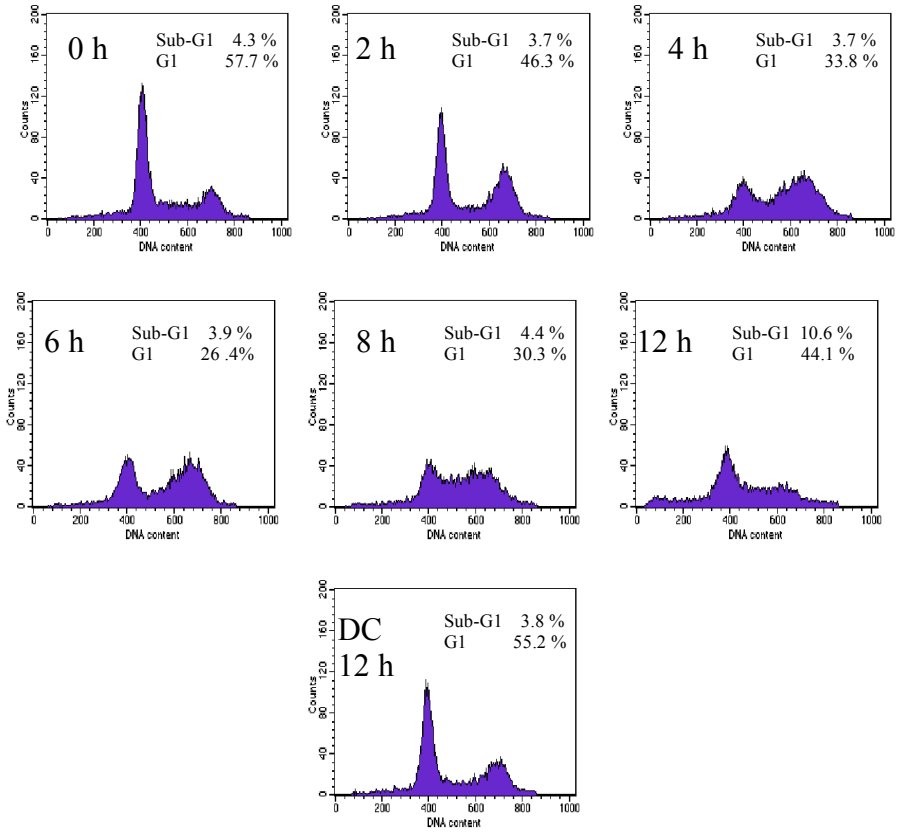

Figure 5.6. a. Effects on HSC-2 cell cycle phase at various intervals post irradiation analyzed using flow cytometry after treatment with 0.25 μM compound **48** and irradiated with a light dose of 4.1 J/cm^2. DC represents unirradiated dark control. **b.** Representative histograms of the event of annexin V-fluorescein isothiocyanate (FITC) binding to phosphatidylserine as an indicator of apoptosis in HSC-2 cells treated with 0.5 μM compound **48** and irradiated with a light dose of 4.1 J/cm^2. M1 represents viable cell population, M2 represents apoptotic cell population, and DC represents unirradiated dark control.

b

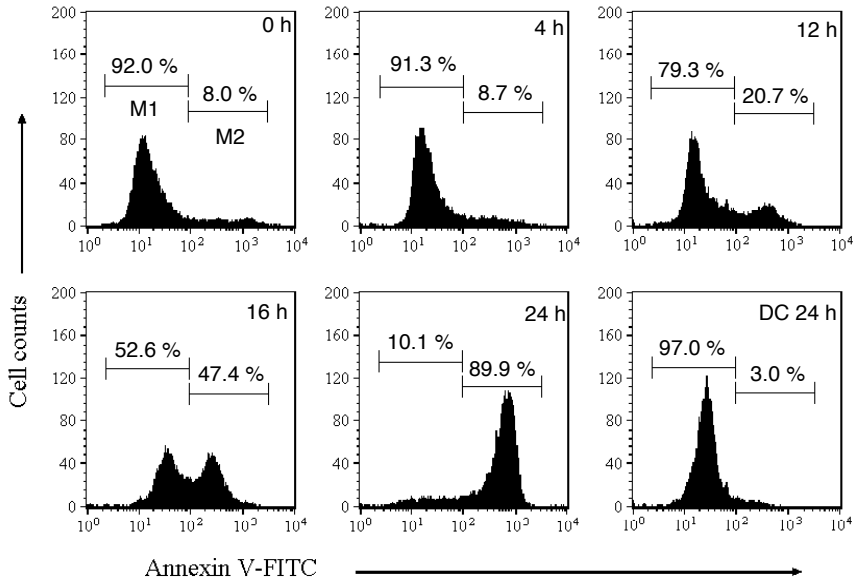

Figure 5.6 Continued.

In the present study, the maximal level of G2/M cell cycle arrest was observed at 6 h after PDT. Thereafter, the recovery of the cell cycle profile to one with a reduced G2/M peak may be due to the redistribution of cells to sub-G1, indicating the onset of apoptosis of arrested cells. A similar G2/M arrest was also observed in hypericin-based PDT, a naturally occurring photosensitizer currently undergoing research.[185,186] Photosensitization of Hela cervical cancer cells with hypericin resulted in phosphorylation of mitochondria Bcl-2 that correlated with G2/M cell cycle arrest, followed by the onset of apoptosis.[186]

In addition to cell cycle analysis, the onset of apoptosis was also quantified in flow cytometry experiments by measuring the externalization of membrane

phosphatidylserine through annexin V-FITC staining, an event that is considered characteristic of cells undergoing apoptosis (Figure 5.6b). Flow cytometric analysis of HSC-2 cells treated with 0.5 μM compound **48** showed the onset of apoptosis by 12 h following irradiation with 20.7% of the cells stained positive for annexin V compared to less than 10% at 0 or 4 h time points. The proportion of cells undergoing apoptosis continued to increase rapidly to 47.4% by 16 h, and at 24 h the apoptotic cell proportion was at 89.9%.

PDT-Induced Vascular Occlusion

One of the ways PDT causes damage during cancer treatment is by shutdown of blood vessels feeding the tumor.[187] Hence, the ability of compound **48** to exert *in vivo* vasculature disruption was investigated using the *in ovo* CAM model. In the present study by the Boon group, the ability of compound **48** to induce occlusion of blood vessels in the CAM by PDT was performed at 3.5-7.0 nmol/embryo with a light dose of 20-40 J/cm^2. The degree of vascular occlusion was scored 24 h after treatment according to Table 5.3. The score for photosensitized-mediated PDT-induced vascular occlusion is shown in Figure 5.7, and the angiograms representing the vascular occlusion score are shown in Figure 5.8. As expected, the degree of vascular occlusion increased with drug and light dose.

Table 5.3. The damage score of PDT-induced vasculature network occlusion.

Occlusion score	Findings
0	No occlusion
1	Partial closure of capillaries of diameter < 10 μm
2	Closure of capillary system, partial closure of blood vessel of diameter < 30 μm and size reduction of larger blood vessels
3	Closure of vessels of diameter < 30 μm and partial closure of larger blood vessels
4	Total closure of vessels of diameter < 70 μm and partial closure of larger vessels
5	Total occlusion of vessels in the irradiated area

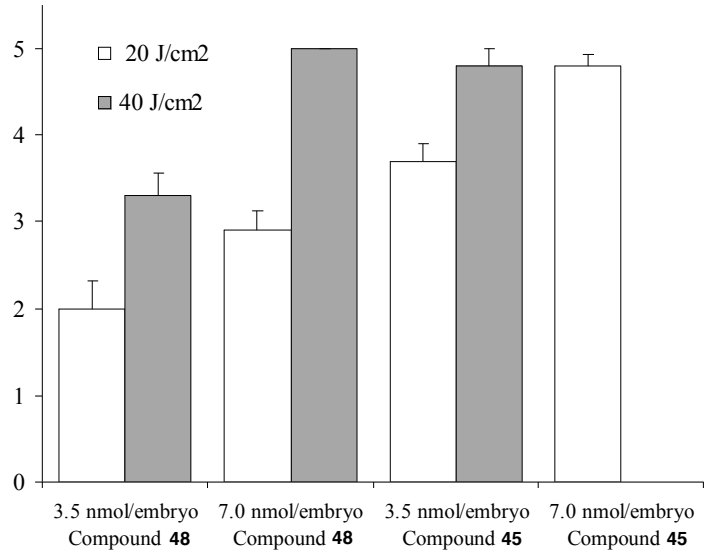

Figure 5.7. Effects of drug concentration and light dose on vascular occlusion efficacy of compound **48** in the CAM model. Error bars represent standard error mean from at least 10 embryos.

The average CAM vasculature damage score when irradiated at 20 J/cm^2 on embryos treated with 3.5 and 7.0 nmol/embryo of compound **48** was approximately 2 and 3, respectively. When the light dose increased to 40 J/cm^2, the damage score increased accordingly to 3.5 and 5. Meanwhile, the control eggs that received 20 μL of vehicle (cremophor EL 2.5%, EtOH 2.5% in saline) and exposed to a similar light dose showed no detectable vascular alteration in the treated area. This indicated that the vascular occlusion observed in embryos treated with compound **48** was neither caused by the vehicle components nor was it thermally induced. Finally, treatment with compound **48**

alone without irradiation did not induce any vascular occlusion, as non-irradiated areas remained perfused after 24 h.

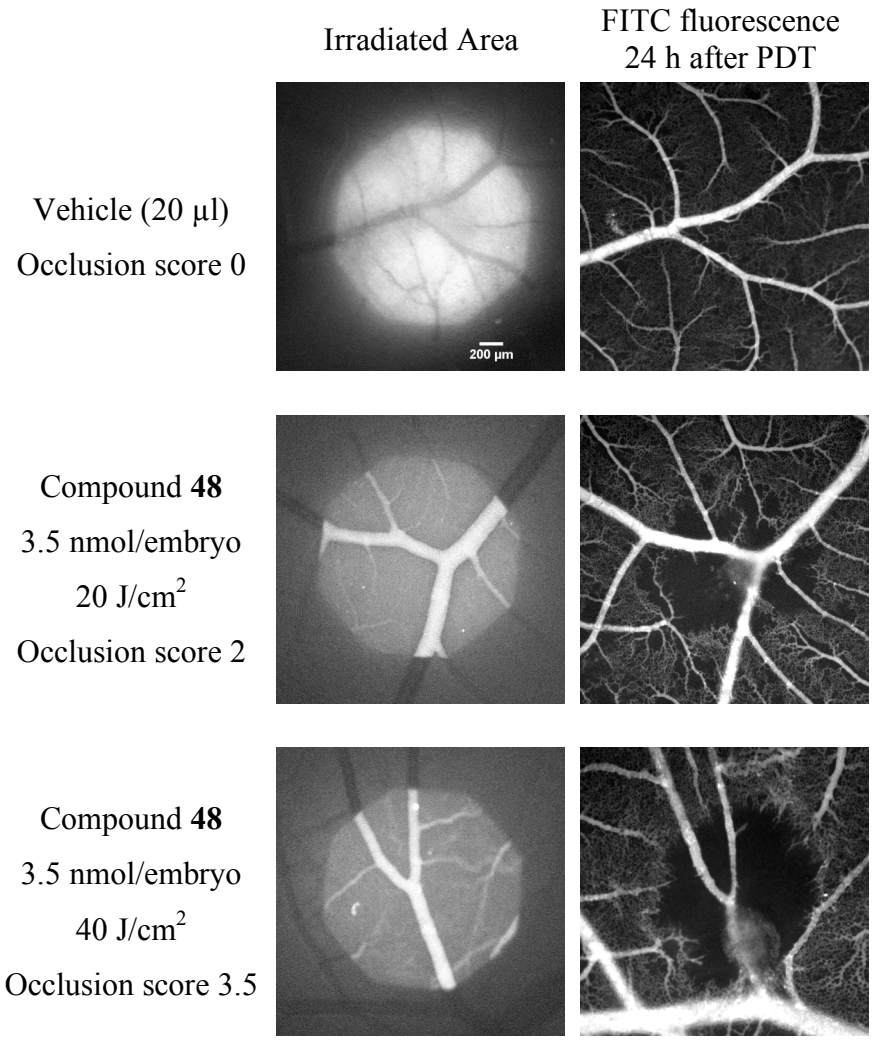

Figure 5.8. Representative angiographies of blood vessels supplying the CAM at beginning and 24 h after PDT, illustrating the vascular occlusion efficacy induced by compound 5 at 3.5-7 nmol/embryo. Irradiation was performed at 510-560 nm of excitation with 20-40 J/cm^2 light dose. Cremophor EL (2.5%) and EtOH (2.5%) in saline were used as a control vehicle. Objective magnification is 4.

Compound **48**
7.0 nmol/embryo
20 J/cm^2
Occlusion score 3.0

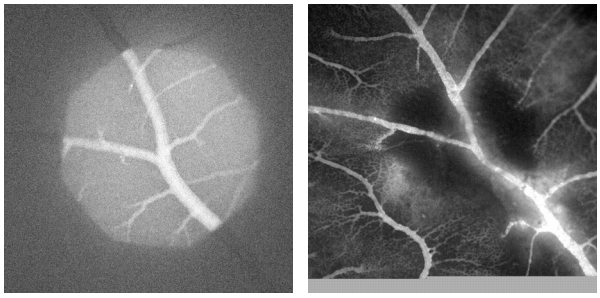

Compound **48**
7.0 nmol/embryo
40 J/cm^2
Occlusion score 5.0

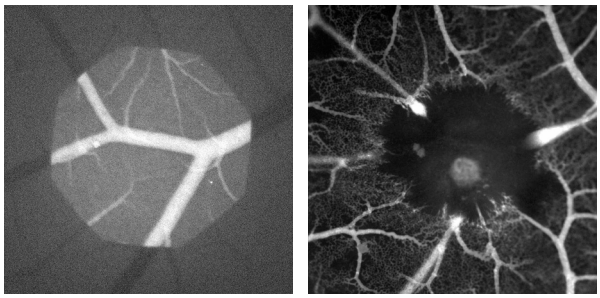

Figure 5.8 Continued.

As the main respiratory organ of the chick embryo, CAM is a well-vascularized membrane that is suitable as a model for PDT. It is easily accessible, inexpensive, and relatively easy to handle for photosensitizer administration, light irradiation, fluorescence analysis of administered photosensitizer, and microscopy examination of PDT-induced vascular damage.[188,189] CAM is a viable model that has been successfully used to evaluate the photodynamic-induced vascular occlusion efficacy of some photosensitizers that are in clinical trials as well as those that are already clinically approved such as palladium bacteriopheophorbide, porfimer sodium, lutetium texaphyrin, 5-aminolevulinic acid, and verteporfin.[190,191] For example, a PDT experiment in the CAM model using verteporfin at a dose that is similar to the recommended clinical

dosage for the treatment of age related macular degeneration has been shown to cause complete occlusion of the large neovessels, an observation that correlates well with clinical setting.[188] In addition, in a BALB/c mouse model where PDT treatment by verteporfin resulted in suppression of tumor growth, antivascular effects were also observed, whereby a decrease in the blood volume at the tumor site was noted.[192,193] The results from the study demonstrated that compound **48** was able to induce complete closure of larger vessels, which is considered favorable in PDT treatment of cancer.

*PDT Agent **48** for Enhanced Permeability and Localization (EPR) Effect*

It has been demonstrated that lager molecules tend to localize inside of tumor cells more readily than in normal ones.[194] This phenomenon is known as the EPR effect and is a result of cancer cells' promiscuity towards nutritional supplies to meet the demands of rapid growth of the tumor. In PDT, agents that localize preferably in tumor cells over normal ones are desirable since the agents can stay inside the host for several hours to even days after initial therapy. In these cases, exposure to sunlight can produce undesirable "side effects" if the PDT agents are localized without specificity.

Polyglutamic acid (PGA) has been shown to be an effective promoter of EPR effect.[195,196] We envisioned an approach in which BODIPY **48** is attached to PGA, enhancing its localization inside tumor cells, may promote its use as a PDT agent. BODIPY derivative **78** was targeted as a key precursor that would covalently bind to PGA *via* amide bond formation (Scheme 5.1). Synthesis of **78** was accomplished first by condensation of 2,4-dimethylpyrrole with 4-chlorobutanoyl chloride yielding alkyl chloride functionalized BODIPY **79** in 32 % yield. Azide functionality was introduced by reacting alkyl chloride **79** with sodium azide yielding **80** in 99 % yield. Azide intermediate **80** was diiodinated with iodine and iodic acid to yield diiodinated BODIPY **81** in 75 % yield. The azide functionality of **81** was reduced *via* Staudinger reduction and the crude product was reacted with **PGA-H** in the presence of 0.1 eq. of DCC* and catalytic amount of DMAP to yield the **PGA-78** conjugate. The conjugate was first precipitated from the reaction medium (DMF) by addition of chloroform, filtered, and subjected to sodium bicarbonate to convert the unlabeled carboxylic acids on the conjugate to the carboxylate form. Conjugate **PGA-78** was further purified by dialysis in water and was isolated as pink fibers after lyophilization. The carboxylate form of **PGA-78** displays good solubility in water, a desirable property for *in vivo* work.

* Equivalents here are calculated as moles of DCC to moles of carboxylic acids in PGA-H. This number is important since similar polymers that were made with 0.2 eq. of DCC proved to be insoluble in water presumably do the hydrophobicities of these conjugates.

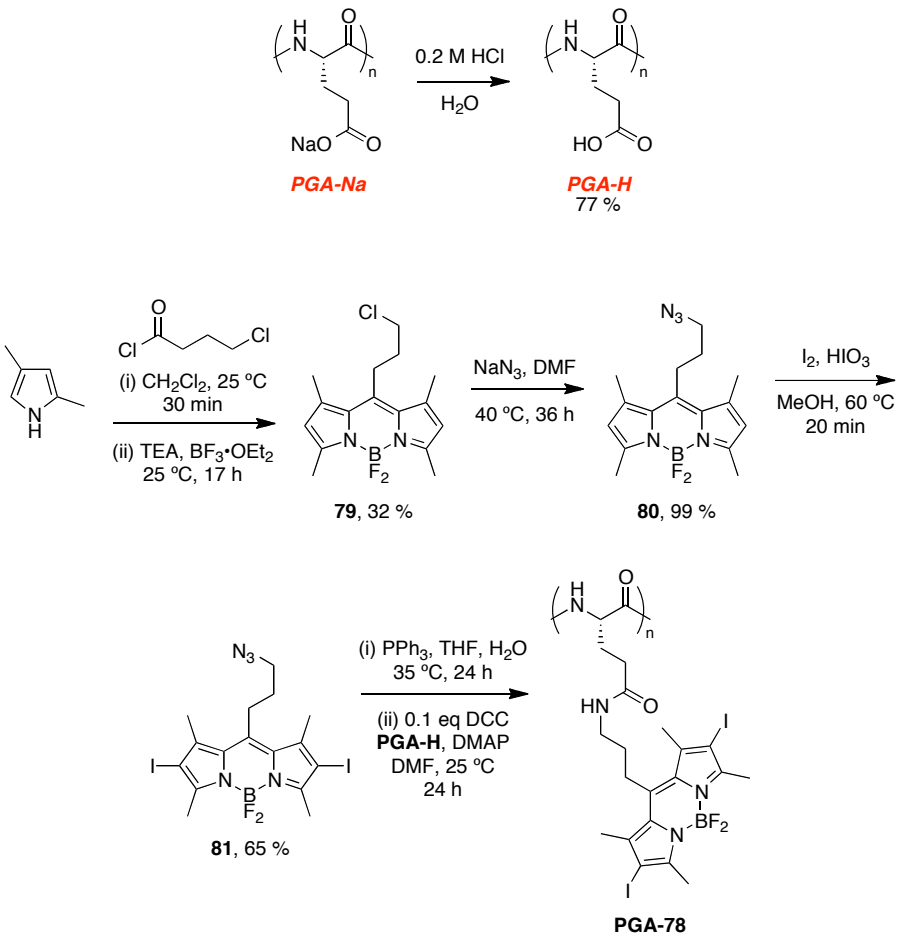

Scheme 5.1. Synthesis of **PGA-78** conjugate.

Basic photophysical properties of the conjugate were measured in pH 7.4 PBS buffer (Figure 5.9). The conjugate possesses a $\lambda_{abs\ max}$ at 533 nm corresponding to the BODIPY and at 285 nm ascribable to an overlap of absorption from BODIPY and carboxylic functionality of the polymer. Interestingly, no fluorescence is observed when the conjugate is excited at the $\lambda_{abs\ max}$ of the BODIPY suggesting good internal conversion to the triplet state and/or quenching of the fluorescence due to the polar environment. The loading of BODIPY on PGA was calculated as 2.5 mol of BODIPY to mol of polymer

through the use of absorption spectroscopy. This number reflects the difficulty in the coupling reaction and indeed different loadings were obtained for different batches. Unfortunately, at the time this dissertation is written, testing of **PGA-78** as an *in vivo* PDT agent remains in progress.

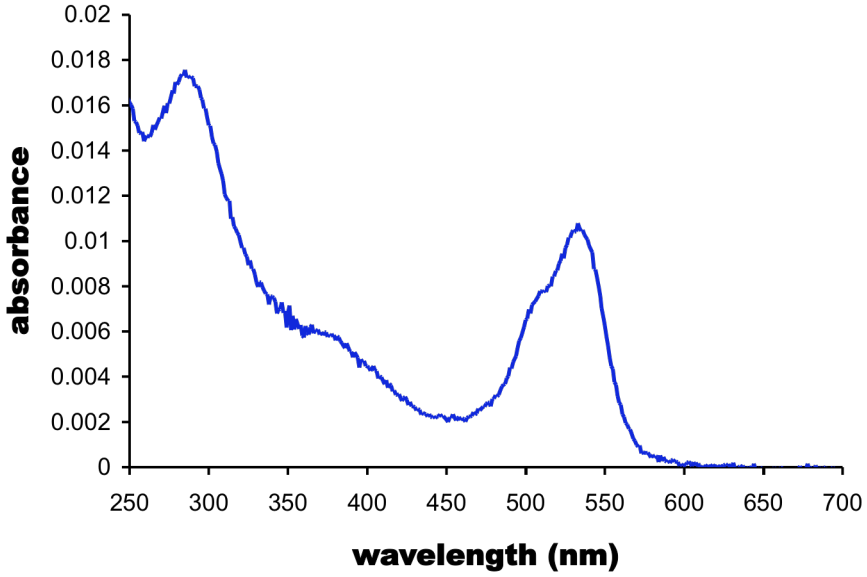

Figure 5.9. Absorbance spectrum of **PGA-78** conjugate in pH 7.4 PBS buffer.

In conclusion, we have demonstrated the *in vitro* photocytotoxic activity of BODIPY derivatives against cell lines from leukemia and two types of solid tumor. Structure-activity relationship study indicated the importance of having iodine atoms directly substituted on the BODIPY pyrrolic carbon-4 position rather than at the *meso*-aryl position, in accordance with the high singlet oxygen generation rate of these compounds. Extended conjugation at the 4-pyrrolic positions shifts the $\lambda_{max\ abs}$ to the red but did not

confer extra potency except for the compound with a single ^{n}butyl acrylate ester [183]. Hydrophilic analogues substituted with groups such as carboxylic acid, sulfonic acid, or sodium sulfonate generally drastically diminished the activity to the comparable compounds without these groups. An exception here was the doubly iodinated compound **48** with an aliphatic carboxylic acid which showed up to 100-fold lower IC50 value in HL-60 compared to the parent compound **A**, perhaps because of the structural difference where the carboxylic acid group is not directly conjugated with the BODIPY core. Fluorescence microscopy studies showed that compound **48** localized exclusively within the mitochondria. This, together with data from cell cycle analysis and onset of apoptosis studies, suggests that compound **48** probably induced cell death through mitochondria-dependent apoptosis rather than through damage to nucleic materials. In addition, an emulsion of compound **48** was able to occlude the vasculature network in the CAM *in vivo* model, further showing its potential as an effective PDT agent.

Although photosensitizers with > 600 nm excitation wavelengths allow deeper access into biological tissues for effective treatment of abnormal tissues of bigger volume, the shorter absorption wavelength of the BODIPY-based photosensitizers studied here, such as compound **48**, may be preferred in the treatment of superficial tissues. In a clinical PDT of cancer in the esophagus and bronchi with porfimer sodium II, treatment regime with light corresponding to the 514 nm excitation wavelength exhibited similar effectiveness as that with 630 nm in terms of tumor eradication but, significantly, with less damage of the deep tissue which could cause perforation in the esophagus.[197]

Overall, our results suggest that BODIPY structures, especially compound **48**, have potential to be explored as a clinically useful agent for PDT of cancer.

5.3 Design and Synthesis of Near-IR PDT Agents

Though we were encouraged by the favorable activities of PDT agents such as **48**, their absorbance wavelengths precludes their use for deep skin cancer treatments due to poor tissue penetration of wavelengths below 600 nm.[2] This led us to search for near-IR dyes that could potentially be used as PDT agents. PyrroloPyrrole Cyanines (PPCy) are a relatively new class of near-IR fluorophores developed by the Zumbusch lab. [198-202] These dyes are remarkable not only for their absorbance wavelengths that extend far beyond 700 nm, but also for their high molar absorptivities and fluorescence quantum yields. Though high fluorescence quantum yield is desirable in imaging applications, it is indicative of efficient conversion of energy as fluorescence and not other pathways that could lead to ROS production.

We have seen in the study of BODIPY dyes (Section 5.2) that introduction of heavy atoms such as iodines on BODIPY's core is an efficient method to promote ROS production. We hypothesized that a similar method could be used to promote ROS pathways in PPCy dyes. To this end we targeted compounds of type **82** as potential PDT agents. Our hopes were that compounds of type **82** would have ROS production efficiencies similar to **46**, absorb at wavelengths greater than 800 nm for deep tissue penetration, and do so with high molar absorptivities.

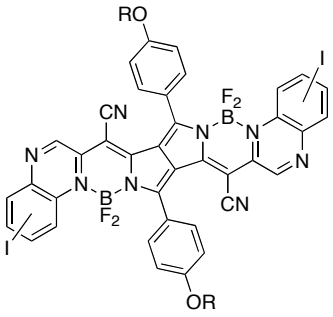

82
targets for near-IR PDT agents

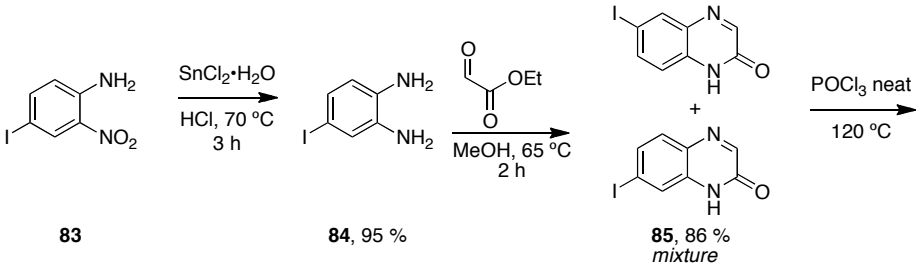

83 **84**, 95 % **85**, 86 % *mixture*

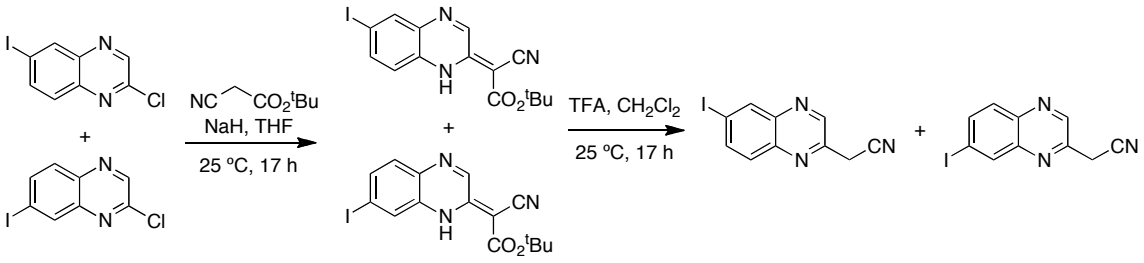

86, 96 % *mixture* **87**, 72 % *mixture* **88a** 1:1 mixture 40 % **88b**

Scheme 5.2. Synthesis of PPCy **82**.

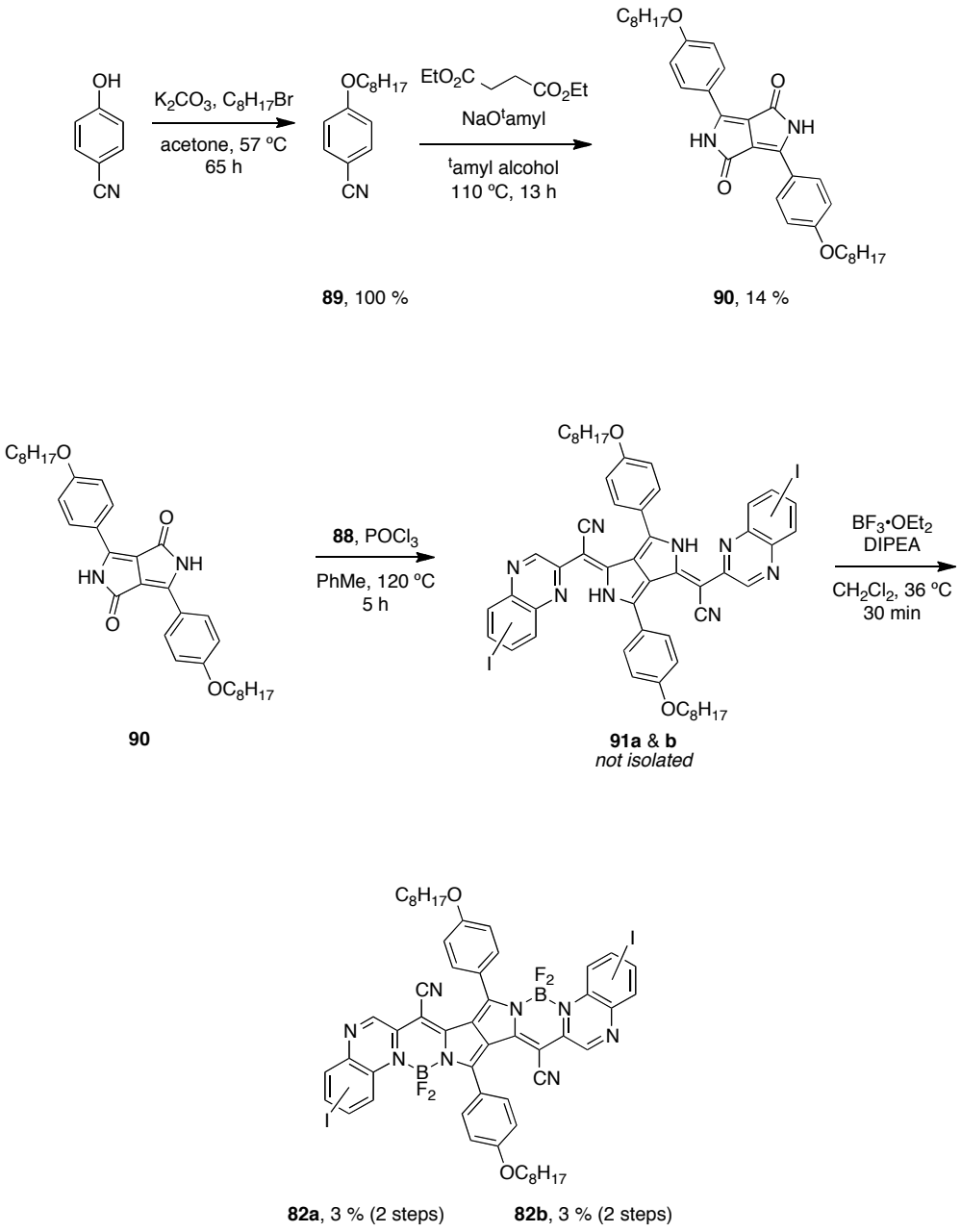

Scheme 5.2 Continued.

The key reaction for synthesis of **82** is the condensation between DPP dye **90** and quinoxaline **88** (Scheme 5.2). Unfortunately, to our knowledge, there is no detailed procedure in the literature for the synthesis of **88**. Our route began with tin mediated reduction of 4-iodo-2-nitroaniline **83** under acidic conditions to yield 4-iodobenzene diamine **84** in 95 % yield. Diamine **84** was condensed with ethyl 2-oxoacetate in methanol resulting in cyclization to form a regioisomeric mixture of iodoquinoxalinones **85** (86 %) that could not be conveniently separated due to poor solubility of the mixture in all solvents attempted. Quinoxalinone mixture **85** was chlorinated by reacting with neat phosphorus oxychloride at reflux to yield the dihalogenated quinoxaline mixture **86** in 96 % yield. ^{t}Butyl 2-cyanoacetate was deprotonated with sodium hydride and reacted with mixture **86** to yield the isomeric mixture of quinoxalinylidene **87** in 72 % yield. Mixture **87** was subjected to trifluoroacetic acid first resulting in the ^{t}butyl cleavage of the ester and subsequent decarboxylation to yield a 1:1 mixture of isomers **88** in 40 % yield, which are conveniently separable *via* flash chromatography. The structures of isomer **88a** and **88b** were assigned based on X-ray crystallography.

DPP (1,4-Diketo-3,6-diarylpyrrolo{3,4-c}pyrroles)[203] intermediate **90** was synthesized by alkylation of 4-hydroxybenzonitrile to give octyloxybenzonitrile **89** in quantitative yield. Benzonitrile **89** was subjected to a one-pot, double condensation-cyclization to yield DPP dye **90** in 14 % yield. Unfortunately, syntheses of, perhaps, more interesting DPPs such as the ones in Figure 5.10 failed at the DPP formation stage. Reaction of **92** with diethyl succinate yielded complex mixtures that were not easily separable. The

same reaction with **93** failed to yield any products, presumably due to deprotenation on α-carbon of the ^{t}butyl ester.

PPCy formation occurred by two sequential substitutions on DPP **90** with either isomer of **88** in the presence of phosphorous oxychloride. Crude intermediate **91** was obtained upon removal of the reaction solvent and treated with BF_3•OEt_2 in the presence of Hunig's base to yield either isomer of **82** in 3 % yield (2 steps). Interestingly, although neither isomer is extremely soluble in organic solvents, **82b** was so insoluble that routine ^{1}H NMR analysis was complicated though its presence was confirmed by mass spectrometry. This lack of solubility makes its use as a PDT agent difficult and is not considered for that purpose hereafter. ^{1}H NMR of **82a** was obtainable under normal conditions and normal phase HPLC was used to confirm purity.

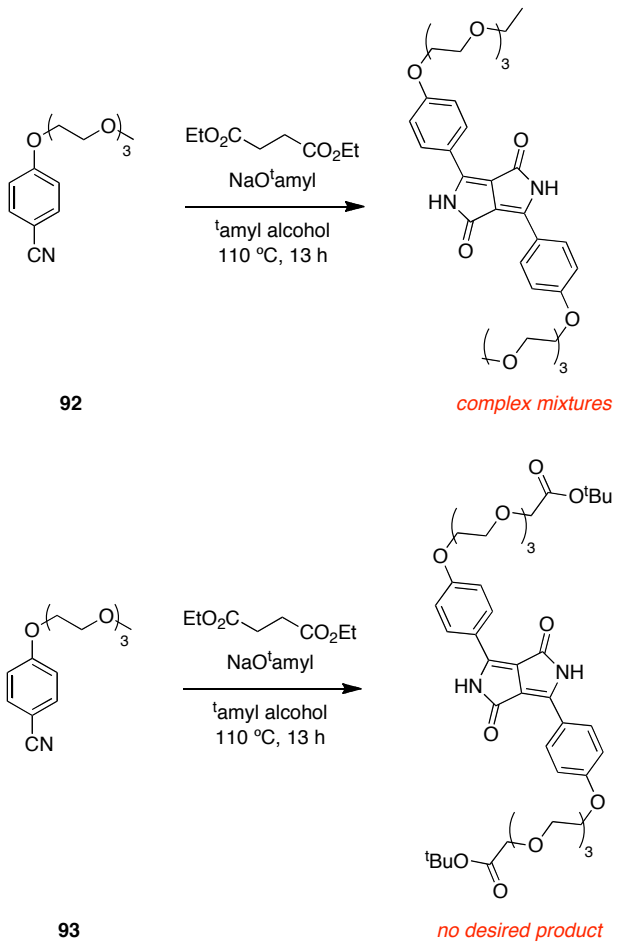

Figure 5.10. Failed syntheses of polar DPP dyes as PPCy precursors.

Absorbance and emission spectra for both compounds were recorded in CH_2Cl_2 (Figure 5.11). We were excited to see that compound **82a** absorbs strongly above 800 nm with a molar absorptivity of 156,000 $cm^{-1}M^{-1}$ at maximum. Fluorescence of **82a** occurs at 823 nm though the quantum yield could not be confidently measured with our instrumentation or any instrumentation easily accessible due to the high wavelength of fluorescence. Compound **82b** has a maximum absorbance at 801 nm and the molar

absorptivity could not be accurately measured due to the aforementioned solubility problems of this compound. Dye **82b** exhibits an emission maximum at 820 nm.

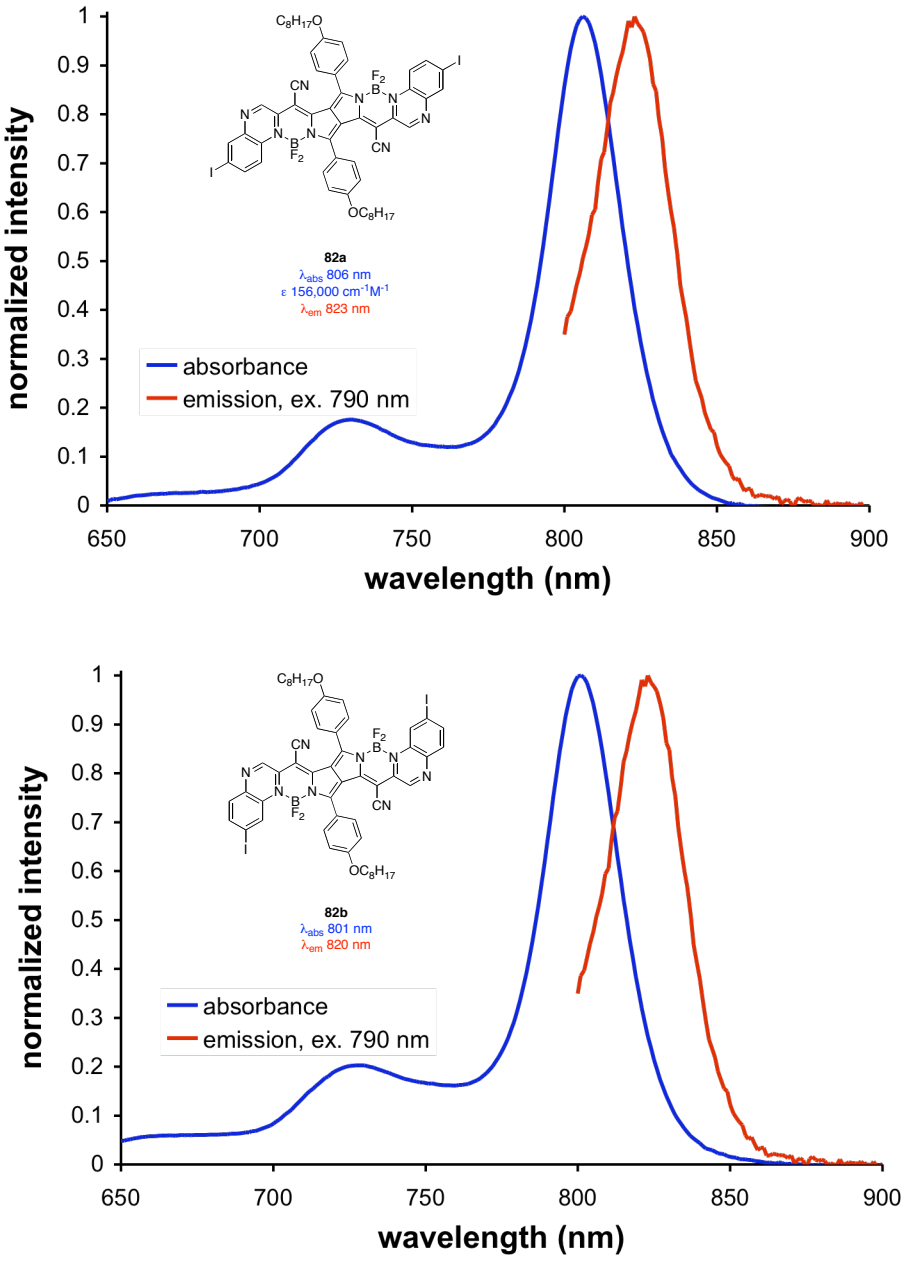

Figure 5.11. Absorbance and fluorescence spectra of **82** in CH_2Cl_2.

5.4 Conclusions

In this work we studied simple BODIPYs and found that ones with iodines directly attached to the BODIPY core tend to have good activities for PDT. We then derivatized a relatively new type of near-IR fluorophores with iodines to make them suitable PDT agents. Studies are currently underway on PPCy **82a** to assay its ROS production and the depth of tissue activation. If these studies show **82a** to be favorable for PDT, *in vivo* assays will then be conducted.

Modifications of **82a** could be attempted to make it more suitable for PDT if preliminary *in vitro* and *in vivo* testing of **82a** show promise. Compounds similar to **94** (Figure 5.12) with ethylene glycol linkers and sulfonic acids should considerably increase the hydrophilicities of such compounds and the carboxylic acids could be used to attach targeting agents and/or macromolecules that promote EPR effect. Although similar compounds have already been attempted (Figure 5.10), an approach could be taken to add the problematic polar functionality at the PPCy stage, thus circumventing tricky DPP formations.

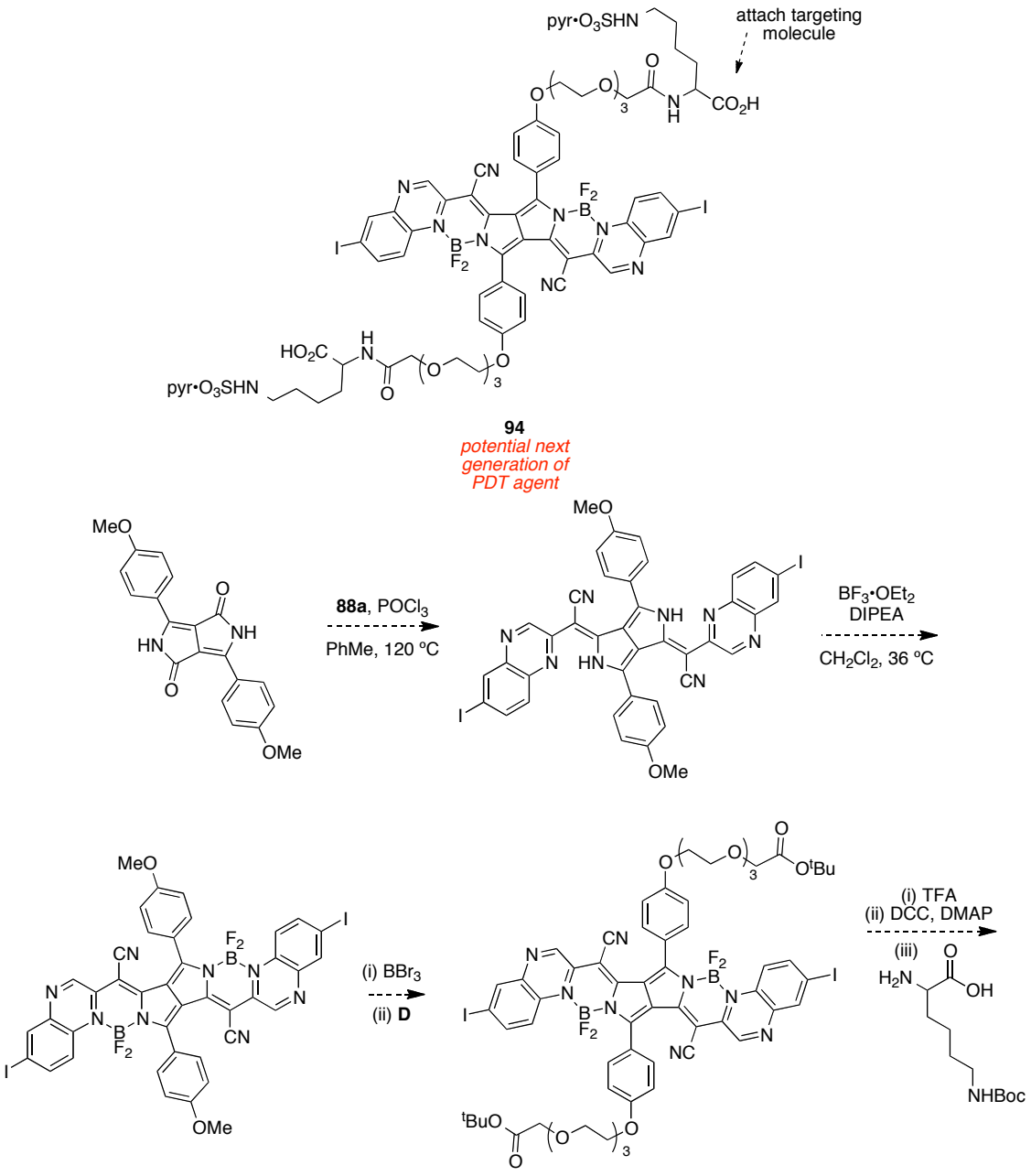

Figure 5.12. Potential next generation of PDT agents.

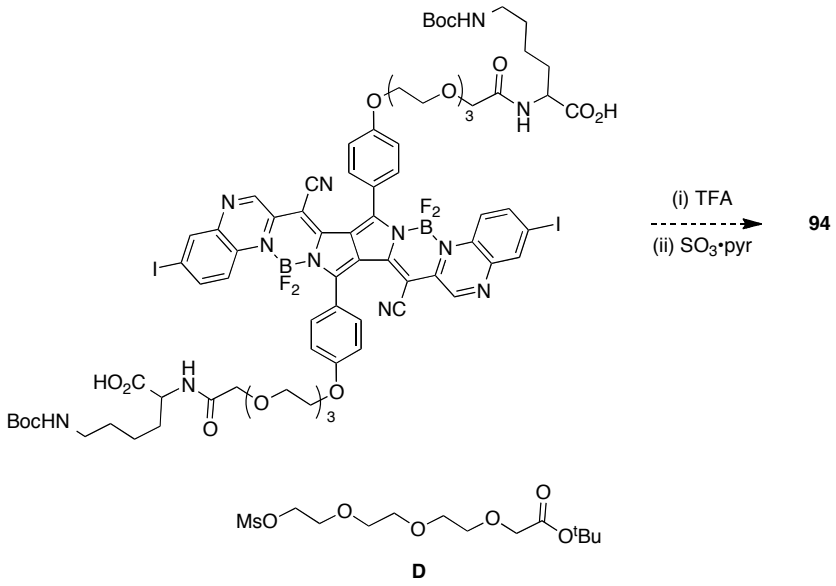

Figure 5.12 Continued.

CHAPTER VI

CONCLUSIONS

Overall this dissertation examined numerous ways in which dyes could be modified to make them more suitable for a variety of biological applications such as imaging, detection of protein-protein interactions, and as PDT agents. In this chapter closing remarks for the work discussed in this dissertation are given.

Concurrent to the work done in Chapter III on TBET cassettes, others in the Burgess group explored different approaches to design systems suitable for detection of protein-protein interactions. *Water-soluble* TBET cassettes **95**–**99** were reported by Burgess and coworkers and[204-206] have favorable photophysical properties even in aqueous solutions (Figure 6.1a). Cassettes **95**-**97** share a common BODIPY donor and differ in BODIPY acceptors, each of which emit above 595 nm. BODIPY **95** possesses a handle to label biomolecules on the acceptor part while **96** and **97** have handles on the linker portion of the cassette. Cassette **96** has additional water solubility provided by the ethylene glycol linker. Overall, these cassettes show promise for biomolecular labeling and multiplex detection of protein-protein interactions as discussed in Chapter I.

Cassettes **96** and **97** were utilized to monitor three-component interactions, (via RET and TBET) as illustrated in Figure 6.1b. This model mimics typical experiments to detect protein-protein interactions using such cassettes. A RET donor (Atto425 attached to BSA-biotin) was mixed with **96**-streptavidin and **97**-avidin conjugates, and the interactions between (strept)avidin and biotin were monitored by observing emissions

from **96** and **97** upon excitation at 458 nm.[205] These cassettes allow increased dispersion of fluorescence emissions from a single excitation source.

a

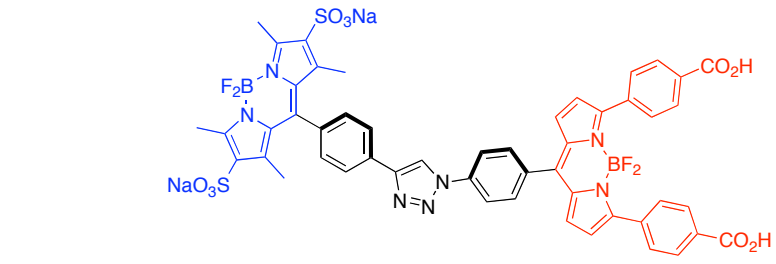

95
λ_{abs} *ca* 495 nm
λ_{em} *ca* 595 nm
ETE 85 %
pH 7.4 phosphate buffer

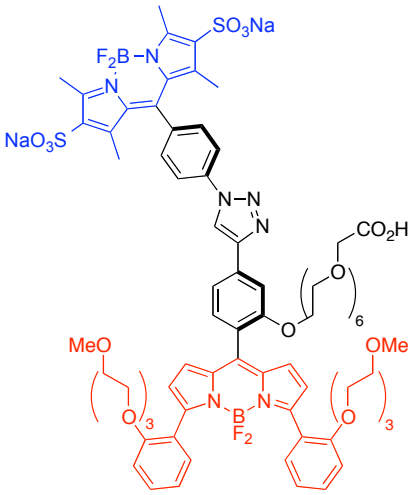

96
λ_{abs} 499 nm
λ_{em} 599 nm

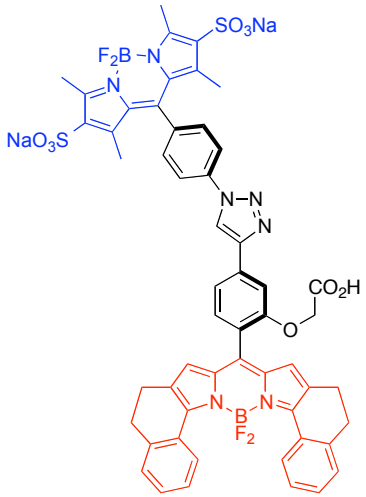

97
λ_{abs} 501 nm
λ_{em} 645 nm

Figure 6.1. **a.** Water soluble TBET cassettes developed by the Burgess group. **b**. Depiction of how cassettes **96** and **97** can be used in multiplex experiments to detect protein-protein interactions.

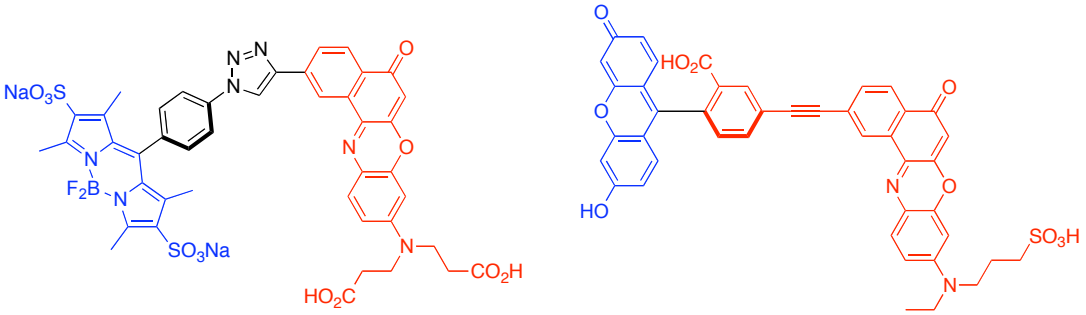

b

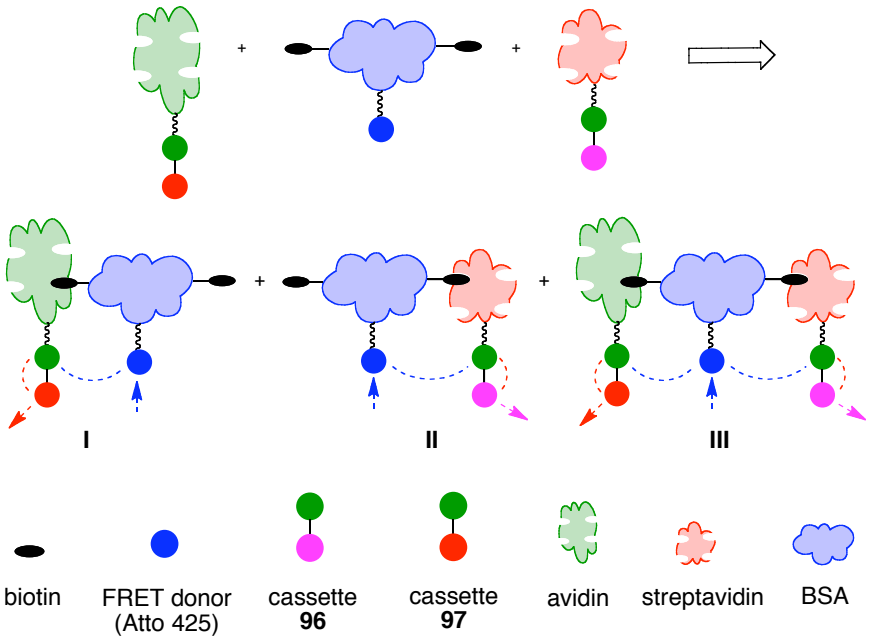

Figure 6.1 Continued.

Cassettes **98** and **99**[206] both possess Nile Red acceptors but differ in numerous ways. The Nile Red acceptor in **98** emits at 632 nm and contains two carboxylic acids that could conveniently label proteins and other biomolecules. The donor of **98** is a disulfonated BODIPY that absorbs at 501 nm. The Nile Red acceptor of cassette **99** is

slightly extended in conjugation owing to the phenylacetylene portion and consequentially emits at a higher wavelength (648 nm) than cassette **98**. The donor portion of cassette **99** is a pH sensitive xanthene that absorbs at 498 nm. Overall cassettes **98** and **99** have good energy transfer efficiencies of 81 % and 77 % respectively, and are promising as biological fluorescent labels.

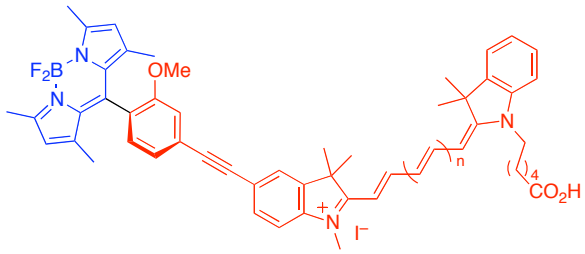

n = 0 **a**, 1 **b**, 2 **c**

100	**100** (encapsulated)
λ_{abs} 504 nm	λ_{abs} 504 nm
λ_{em} **a**; 590, **b**; 687 **c**; 794 nm	λ_{em} **a**; 592, **b**; 687 **c**; 793 nm
ETE **a**; > 88 % **b**; > 88 %, **c**; 43 %	ETE **a**; > 88 % **b**; > 89 %, **c**; 41 % pH 7.4 phosphate buffer

Figure 6.2. Examples of hydrophobic cassettes encapsulated in nanoparticles, in this case calcium phosphate, to make them suitable for work in aqueous media.

Although we were pleased that water-soluble cassettes could successfully label biomolecules and retain their favorable photophysical properties in aqueous environments, a general way of conferring water-solubility unto hydrophobic cassettes was still lacking. For this purpose, the Burgess group attempted to encapsulate cassettes like **100** within calcium phosphate[207] and silica to form nanoparticles (Figure 6.2). Theoretically, the shell of such particles should prevent the hydrophobic cassettes from

encountering the polar solvent environment when the particles are suspended in water. Indeed, when cassette **100** was encapsulated inside of calcium phosphate its photophysical properties compared well as a suspension in aqueous buffer with those of the free cassette in organic solvent (ethanol). This implies efficient encapsulation of the hydrophobic cassette and suggests a general method of solubilizing other hydrophobic TBET cassettes. Interestingly, when calcium phosphate nanoparticles of **100** were imported inside of clone 9 rat liver cells, the cargo inside the nanoparticles seemed to dictate localization of the particles within the cell. An unfortunate drawback of such an approach however is the difficulty in attaching the nanoparticles to biomolecules without disrupting their functionalities.

Others have had findings similar those described in this dissertation. For example, Lin *et al*. have reported a ratiometric pH sensitive TBET cassette (**101)** consisting of a coumarin donor and rhodamine acceptor (Figure 6.3).[208] The donor of the cassette absorbs near 400 nm with an emission maximum is at 465 nm. The rhodamine acceptor emits at 587 nm. Like cassettes **65** and **66**, probe **101** can measure the pH of its environment by calculating the ratio of emission intensities at 465 and 587 nm. Under acidic conditions, efficient energy transfer from donor to acceptor was observed while the opposite was true in basic conditions.

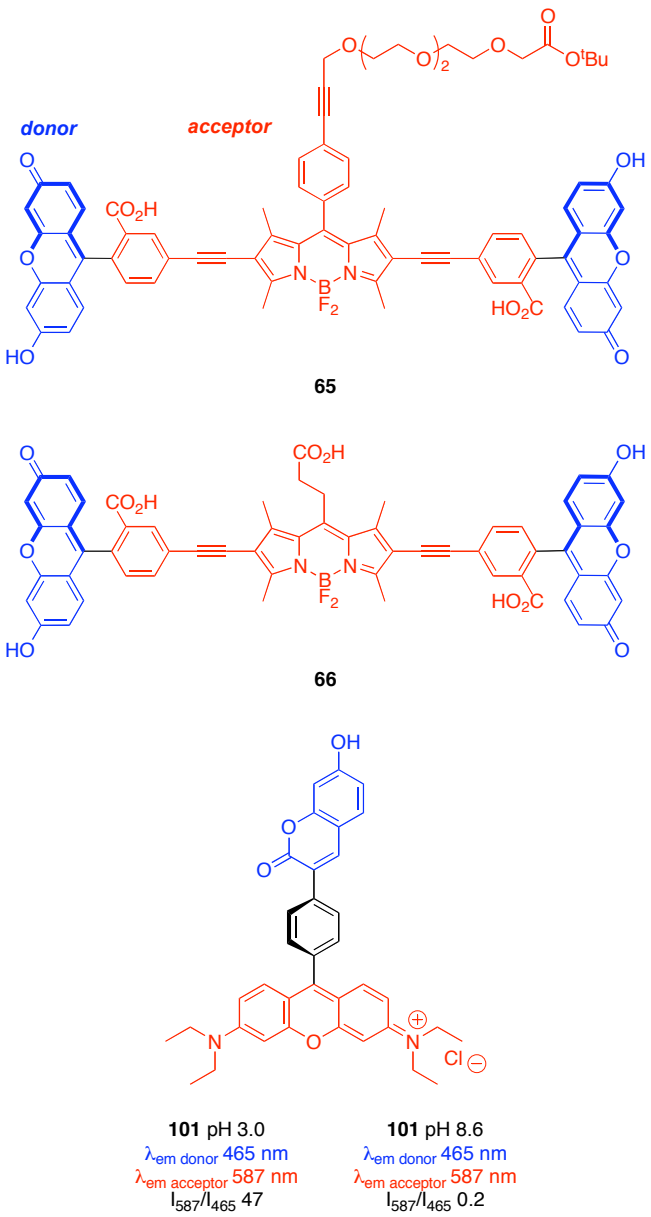

Figure 6.3. Ratiometric pH probes based on TBET.

Jaschke *et al.* recently reported an elegant use of TBET cassettes to monitor intracellular biocatalytic Diels-Alder reactions.[209] Water-soluble versions of cassette **33** were used for this purpose by sulfonating the BODIPY acceptor. Upon undergoing

Diels-Alder reactions on the anthracene donor, the photophysical properties of cassette **102** change dramatically. In fact, it is possible to differentiate free cassette with those bound to DAse (an enzyme that catalyzes Diels-Alder reactions), the Diels-Alder product bound to DAse, and the free products of type **103** in intracellular settings. Most importantly, in each of these states the *probes remain fluorescent and the probes locations can be ascertained.*

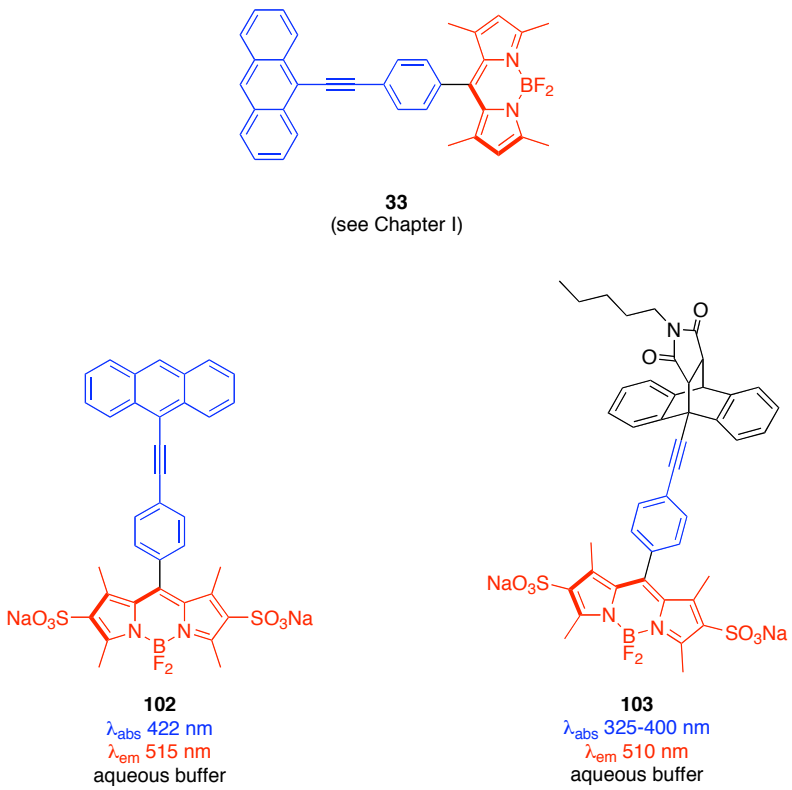

Figure 6.4. Water-soluble TBET cassette used to monitor intercellular Diels-Alder reactions.

Other examples of TBET cassettes are xanthene-BODIPY cassettes **104** and **105** reported by Akkaya *et al.*.[210] These cassettes share commonality with cassettes **65** and

66 although the authors reported no pH sensitivity and **104** and **105** are hydrophobic and lack functionality to attach to biomolecules. The proximity of the two BODIPY units of **105** resulted in significant excimer emission. Unfortunately, the authors did not study these compounds in the context of TBET cassettes and therefore details such as the absorbance wavelength of xanthene and the ETE % are not mentioned. Interestingly, contrary to cassettes synthesized in Chapter III, probes **104** and **105** are composed of two acceptors to one donor. A comparative study of the brightness of such systems to ones with multiple donors to acceptor would be interesting.

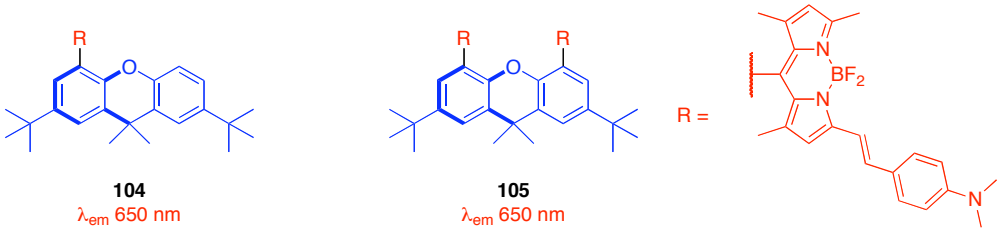

Figure 6.5. Other examples of TBET cassettes developed by the Akkaya group.

The polymer work described in Chapter IV leads to many possibilities. The Achilles' heel of systems of type **70** is the concurrent quenching of acceptors as the amount of acceptors increases in the polymers, placing a limit on attainable brightness. One possible remedy concerning "energy bridges" was already discussed in the conclusion of Chapter IV. An alternative to using polymers could be the use of well-defined oligomers as opposed to polymeric systems. It was proved in Chapter IV that energy transfer remained efficient with 4:1 donor to acceptor ratios. Compounds such as **106** could be constructed to maximize molar absorptivity of the oligomers thus increasing overall

brightness, while avoiding the counteracting intramolecular quenching of the acceptor (Figure 6.6).

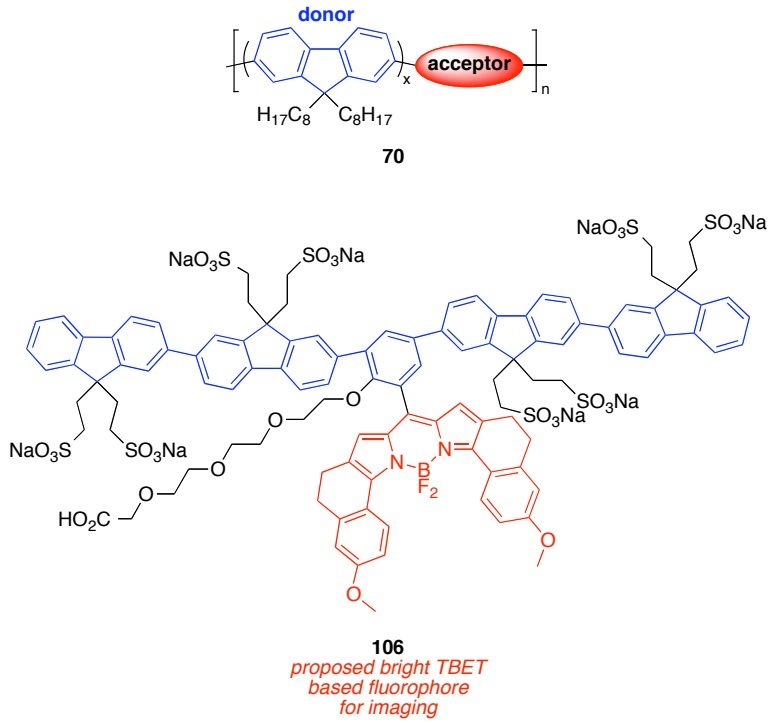

Figure 6.6. Proposed highly brilliant probe for imaging and multiplexing applications.

It is harder to make conclusions on the PDT work of Chapter V since testing is, at the time of this dissertation, still ongoing. It is obvious that if PPCy dyes of type **82** are efficient at producing ROS without significant dark cytotoxicities then water-soluble versions would be of immediate interest. A possible way of conferring water-solubility in such dyes was discussed in the conclusion of Chapter V. The PDT activity of **48** however has been established and current work deals with making it suitable for *in vivo* therapy. A method of promoting the EPR effect, by attaching **48** to polyglutamic acid,

was attempted in Chapter V and the results are still pending. Another method could be to attach **48** to water-soluble polyfluorenes (Figure 6.7). The advantage of polyfluorene versus other polymers such as polyglutamic acid is the large amounts of light that can be collected by polyfluorene using two-photon excitation. The energy would then conceivably be funneled *via* RET to the PDT agent. Of course testing would be necessary to assure that ROS produced do not significantly degrade the polymer before damaging tumor cells, and also quantification of the promotion of the EPR effect by polyfluorenes is, to the best of our knowledge, unknown.

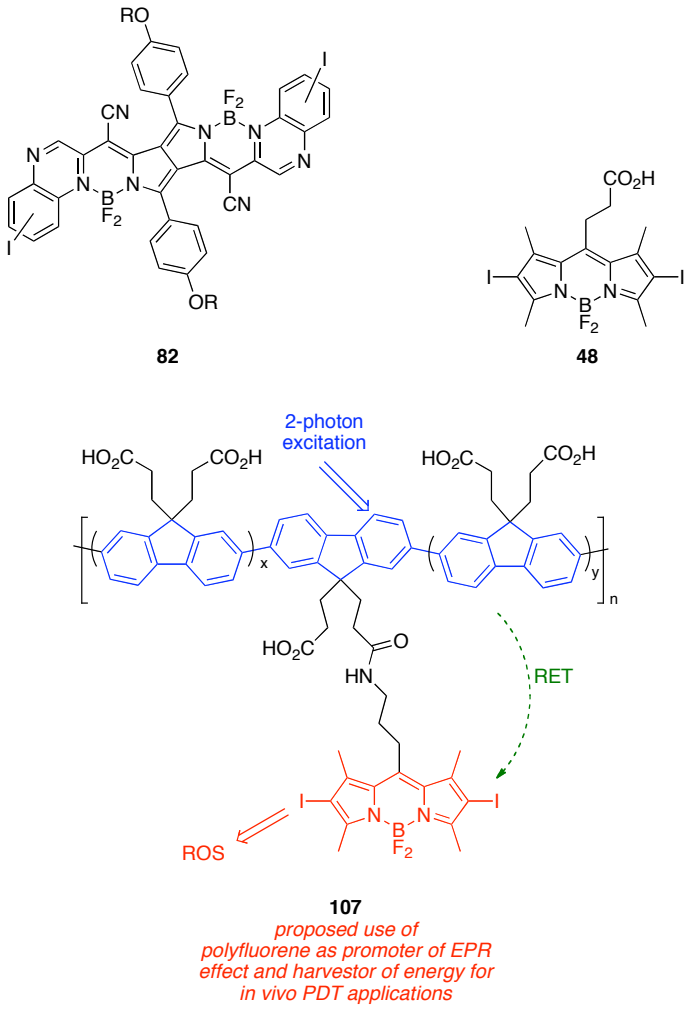

Figure 6.7. Proposed polyfluorene as both a promoter of the EPR effect and an efficient two-photon harvester of energy that can readily transfer energy *via* RET to PDT active agents such as **48**.

The use of through-bond energy transfer cassettes for biological applications appears to be spreading throughout the research community though overall still remains small. Factors antagonizing the growth in this area of research are undoubtedly the ambiguity

of the militating factors controlling the energy transfer and the complexity and cost of synthesizing these rather complex molecules. These obstacles however are not insurmountable with proper research. It remains to be seen what impact TBET systems have in long-term biological research.

REFERENCES

(1) Lakowicz, J. R. *Principles of Fluorescence Spectroscopy*; 3rd ed.; Springer: New York, 2006.

(2) Ghoroghchian, P. P.; Therien, M. J.; Hammer, D. A. *Wiley Interdisciplinary Reviews: Nanomedicine and Nanobiotechnology* **2009**, *1*, 156.

(3) Helmchen, F.; Denk, W. *Nat Meth* **2005**, *2*, 932.

(4) Forster, T. *Discussions of the Faraday Society* **1959**, *No. 27*, 7.

(5) Bunz, U. H. F. *Chem. Rev.* **2000**, *100*, 1605.

(6) Tour, J. M. *Chem. Rev.* **1996**, *96*, 537.

(7) Van Patten, P. G.; Shreve, A. P.; Lindsey, J. S.; Donohoe, R. J. *J. Phys. Chem. B* **1998**, *102*, 4209.

(8) Li, F.; Yang, S. I.; Ciringh, Y.; Seth, J.; Martin, C. H.; Singh, D. L.; Kim, D.; Birge, R. R.; Bocian, D. F.; Holten, D.; Lindsey, J. S. *J. Am. Chem. Soc.* **1998**, *120*, 10001.

(9) Wagner, R. W.; Lindsey, J. S. *J. Am. Chem. Soc.* **1994**, *116*, 9759.

(10) Dexter, D. L. *J. Chem. Phys.* **1953**, *21*, 836.

(11) Anderson, P. W. *Physical Review* **1950**, *79*, 350.

(12) Holten, D.; Bocian, D.; Lindsey, J. S. *Acc. Chem. Res.* **2002**, *35*, 57.

(13) Burghart, A.; Thoresen, L. H.; Chen, J.; Burgess, K.; Bergstrom, F.; Johansson, L. B.-A. *Chem. Commun.* **2000**, 2203.

(14) Jiao, G.-S.; Thoresen Lars, H.; Burgess, K. *J. Am. Chem. Soc.* **2003**, *125*, 14668.

(15) Bandichhor, R.; Petrescu, A. D.; Vespa, A.; Kier, A. B.; Schroeder, F.; Burgess, K. *J. Am. Chem. Soc.* **2006**, *128*, 10688.

(16) Coskun, A.; Akkaya, E. U. *J. Am. Chem. Soc.* **2005**, *127*, 10464.

(17) Coskun, A.; Akkaya, E. U. *J. Am. Chem. Soc.* **2006**, *128*, 14474.

(18) Azov, V. A.; Schlegel, A.; Diederich, F. *Angew. Chem. Int. Ed.* **2005**, *44*, 4635.

(19) Jiao, G.-S.; Kim, T. G.; Burgess, K. *Org. Lett.* **2004**, *6*, 1701.

(20) Jiao, G.-S.; Burgess, K. *Bioorg. Med. Chem. Lett.* **2003**, *13*, 2785.

(21) Thoresen, L. H.; Jiao, G.-S.; Haaland, W. C.; Metzker, M. L.; Burgess, K. *Chem. Eur. J.* **2003**, *9*, 4603.

(22) Jiao, G.-S.; Burgess, K. *Chem. Commun.* **2004**, 1304.

(23) Jiao, G.-S.; Thoresen, L. H.; Kim, T. G.; Haaland, W. C.; Gao, F.; Topp, M. R.; Hochstrasser, R. M.; Metzker, M. L.; Burgess, K. *Chem. Eur. J.* **2006**, *12*, 7816.

(24) Han, J.; Jose, J.; Mei, E.; Burgess, K. *Angew. Chem. Int. Ed.* **2007**, *46*, 1684.

(25) Jose, J.; Burgess, K. *Tetrahedron* **2006**, *62*, 11021.

(26) Miller, E. W.; Tulyathan, O.; Isacoff, E. Y.; Chang, C. J. *Nat Chem Biol* **2007**, *3*, 263.

(27) Bozdemir, O. A.; Cakmak, Y.; Sozmen, F.; Ozdemir, T.; Siemiarczuk, A.; Akkaya, E. U. *Chem. Eur. J.* **2010**, *16*, 6346.

(28) Barin, G.; Yilmaz, M. D.; Akkaya, E. U. *Tetrahedron Lett.* **2009**, *50*, 1738.

(29) Wan, C.-W.; Burghart, A.; Chen, J.; Bergstroem, F.; Johansson, L. B. A.; Wolford, M. F.; Kim, T. G.; Topp, M. R.; Hochstrasser, R. M.; Burgess, K. *Chem. Eur. J.* **2003**, *9*, 4430.

(30) Kim, T. G.; Castro, J. C.; Loudet, A.; Jiao, J. G. S.; Hochstrasser, R. M.; Burgess, K.; Topp, M. R. *J. Phys. Chem. A* **2006**, *110*, 20.

(31) Loudet, A.; Burgess, K. *Chem. Rev.* **2007**, *107*, 4891.

(32) Ulrich, G.; Ziessel, R.; Harriman, A. *Angew. Chem. Int. Ed.* **2008**, *47*, 1184.

(33) Haugland, R. P. *Handbook of Fluorescent Probes and Research Chemicals*; 6th ed.; Molecular Probes: Eugene, OR, 1996.

(34) Metzker, M. L.; (Baylor College of Medicine, USA). WO, 2003; Vol. WO Patent 2003066812, p 50 pp.

(35) Karolin, J.; Johansson, L. B.-A.; Strandberg, L.; Ny, T. *J. Am. Chem. Soc.* **1994**, *116*, 7801.

(36) Yee, M.-c.; Fas, S. C.; Stohlmeyer, M. M.; Wandless, T. J.; Cimprich, K. A. *J. Biol. Chem.* **2005**, *280*, 29053.

(37) Wagner, R. W.; Lindsey, J. S. *Pure Appl. Chem.* **1996**, *68*, 1373.

(38) Tan, K.; Jaquinod, L.; Paolesse, R.; Nardis, S.; Di Natale, C.; Di Carlo, A.; Prodi, L.; Montalti, M.; Zaccheroni, N.; Smith, K. M. *Tetrahedron* **2004**, *60*, 1099.

(39) Treibs, A.; Kreuzer, F. H. *Liebigs Ann. Chem.* **1968**, *718*, 208.

(40) Tram, K.; Yan, H.; Jenkins, H. A.; Vassiliev, S.; Bruce, D. *Dyes Pigm.* **2009**, *82*, 392.

(41) Arroyo, I. J.; Hu, R.; Merino, G.; Tang, B. Z.; Pena-Cabrera, E. *J. Org. Chem.* **2009**, *74*, 5719.

(42) Schmitt, A.; Hinkeldey, B.; Wild, M.; Jung, G. *J. Fluoresc.* **2009**, *19*, 755.

(43) Boyer, J. H.; Haag, A. M.; Sathyamoorthi, G.; Soong, M. L.; Thangaraj, K.; Pavlopoulos, T. G. *Heteroat. Chem.* **1993**, *4*, 39.

(44) Shah, M.; Thangaraj, K.; Soong, M. L.; Wolford, L.; Boyer, J. H.; Politzer, I. R.; Pavlopoulos, T. G. *Heteroat. Chem.* **1990**, *1*, 389.

(45) Wu, L.; Burgess, K. *Chem. Commun.* **2008**, *40*, 4933.

(46) Kang, H. C.; Haugland, R. P.; Molecular Probes, Inc.; Eugene, OK, United States, 1995; Vol. US Patent 5,433,896.

(47) Wu, Y.; Klaubert, D. H.; Kang, H. C.; Zhang, Y.-z.; (Molecular Probes, Inc., USA). Application: US, 1999; Vol. US Patent 6005113, p 20 pp.

(48) Thoresen, L. H.; Kim, H.; Welch, M. B.; Burghart, A.; Burgess, K. *Synlett* **1998**, 1276.

(49) Burghart, A.; Kim, H.; Welch, M. B.; Thoresen, L. H.; Reibenspies, J.; Burgess, K.; Bergstroem, F.; Johansson, L. B. A. *J. Org. Chem.* **1999**, *64*, 7813.

(50) Coskun, A.; Akkaya, E. U. *Tetrahedron Lett.* **2004**, *45*, 4947.

(51) Ikeda, C.; Maruyama, T.; Nabeshima, T. *Tetrahedron Lett.* **2009**, *50*, 3349.

(52) Rurack, K.; Kollmannsberger, M.; Daub, J. *New J. Chem.* **2001**, *25*, 289.

(53) Sathyamoorthi, G.; Boyer, J. H.; Allik, T. H.; Chandra, S. *Heteroat. Chem.* **1994**, *5*, 403.

(54) Rurack, K.; Kollmannsberger, M.; Daub, J. *Angew. Chem. Int. Ed.* **2001**, *40*, 385.

(55) Bandichhor, R.; Thivierge, C.; Bhuvanesh, N. S. P.; Burgess, K. *Acta Chrystallogr., Sect. E* **2006**, *E62*, o4310.

(56) Yogo, T.; Urano, Y.; Ishitsuka, Y.; Maniwa, F.; Nagano, T. *J. Am. Chem. Soc.* **2005**, *127*, 12162.

(57) Vos de Wael, E.; Pardoen, J. A.; Van Koeveringe, J. A.; Lugtenburg, J. *Recl. Trav. Chim. Pays-Bas* **1977**, *96*, 306.

(58) Karstens, T.; Kobs, K. *J. Phys. Chem.* **1980**, *84*, 1871.

(59) Bonardi, L.; Ulrich, G.; Ziessel, R. *Org. Lett.* **2008**, *10*, 2183.

(60) Rieth, R. D.; Mankad, N. P.; Calimano, E.; Sadighi, J. P. *Org. Lett.* **2004**, *6*, 3981.

(61) Bowie, A. L.; Hughes, C. C.; Trauner, D. *Org. Lett.* **2005**, *7*, 5207.

(62) Beck, E. M.; Grimster, N. P.; Hatley, R.; Gaunt, M. J. *J. Am. Chem. Soc.* **2006**, *128*, 2528.

(63) Zhang, H.; Ferreira, E. M.; Stoltz, B. M. *Angew. Chem. Int. Ed.* **2004**, *43*, 6144.

(64) Lane, B. S.; Brown, M. A.; Sames, D. *J. Am. Chem. Soc.* **2005**, *127*, 8050.

(65) Grimster, N. P.; Gauntlett, C.; Godfrey, C. R. A.; Gaunt, M. J. *Angew. Chem. Int. Ed.* **2005**, *44*, 3125.

(66) Thivierge, C.; Bandichhor, R.; Burgess, K. *Org. Lett.* **2007**, *9*, 2135.

(67) Larock, R. C.; Hightower, T. R. *J. Org. Chem.* **1993**, *58*, 5298.

(68) Steinhoff, B. A.; Fix, S. R.; Stahl, S. S. *J. Am. Chem. Soc.* **2002**, *124*, 766.

(69) Peterson, K. P.; Larock, R. C. *J. Org. Chem* **1998**, *63*, 3185.

(70) Wories, H. J.; Koek, J. H.; Lodder, G.; Lugtenburg, J.; Fokkens, R.; Driessen, O.; Mohn, G. R. *Recl. Trav. Chim. Pays-Bas* **1985**, *104*, 288.

(71) Klonis, N.; Sawyer, W. H. *J. Fluoresc.* **1996**, *6*, 147.

(72) Bandichhor, R.; Thivierge, C.; Burgess, K. *ChemTracts* **2006**, *19*, 11.

(73) Godula, K.; Sames, D. *Science* **2006**, *312*, 67.

(74) Bergman, R. G. *Nature* **2007**, *446*, 391.

(75) Ishiyama, T.; Nobuta, Y.; Hartwig, J. F.; Miyaura, N. *Chemical Communications* **2003**, 2924.

(76) Ishiyama, T.; Miyaura, N. *Journal of Organometallic Chemistry* **2003**, *680*, 3.

(77) Miyaura, N.; Suzuki, A. *Chem. Rev.* **1995**, *95*, 2457.

(78) Chen, J.; Mizumura, M.; Shinokubo, H.; Osuka, A. *Chem.--Eur. J.* **2009**, *15*, 5942.

(79) Murphy, J. M.; Tzschucke, C. C.; Hartwig, J. F. *Organic Letters* **2007**, *9*, 757.

(80) Jiao, L.; Yu, C.; Li, J.; Wang, Z.; Wu, M.; Hao, E. *The Journal of Organic Chemistry* **2009**, *74*, 7525.

(81) Boyer, J. H.; Morgan, L. R. Application: EP, 1990; Vol. US Patent 361936, p 41 pp.

(82) Boyer, J. H.; Morgan, L. R. US, 1993; Vol. US Patent 5189029, p 10 pp.

(83) Morgan, L. R.; Boyer, J. H. US, 1994; Vol. WO Patent 9419355, p 78 pp.

(84) Urano, T.; Nagasaka, H.; Tsuchiyama, M.; Ide, H. EP, 1994; Vol. US Patent 5498641, p 20 pp.

(85) Morgan, L. R.; Boyer, J. H. US, 1995; Vol. US Patent 5,189,029, p 26 pp Cont

(86) Li, L.; Han, J.; Nguyen, B.; Burgess, K. *J. Org. Chem.* **2008**, *73*, 1963.

(87) Li, L.; Nguyen, B.; Burgess, K. *Bioorganic & Medicinal Chemistry Letters* **2008**, *18*, 3112.

(88) Niu, S. L.; Ulrich, G.; Ziessel, R.; Kiss, A.; Renard, P.-Y.; Romieu, A. *Org. Lett.* **2009**, *11*, 2049.

(89) McIntosh, T. J.; Simon, S. A. *The Journal of General Physiology* **2007**, *130*, 225.

(90) Silva, A. P. D.; Gunaratne, H. G. N.; Gunnlaugsson, T.; Huxley, A. J. M.; McCoy, C. P.; Rademacher, J. T.; Rice, T. E. *Chem. Rev.* **1997**, *97*, 1515.

(91) Callan, J. F.; de Silva, A. P.; Magri, D. C. *Tetrahedron* **2005**, *61*, 8551.

(92) Que, E. L.; Domaille, D. W.; Chang, C. J. *Chem. Rev.* **2008**, *108*, 1517.

(93) Thomas, J. A.; Buchsbaum, R. N.; Zimniak, A.; Racker, E. *Biochem.* **1979**, *18*, 2210.

(94) Briggs, M. S.; Burns, D. D.; Cooper, M. E.; Gregory, S. J. *Chem. Commun.* **2000**, 2323.

(95) Galindo, F.; Burguete, M. I.; Vigara, L.; Luis, S. V.; Kabir, N.; Gavrilovic, J.; Russell, D. A. *Angew. Chem. Int. Ed.* **2005**, *44*, 6504.

(96) Bizzarri, R.; Arcangeli, C.; Arosio, D.; Ricci, F.; Faraci, P.; Cardarelli, F.; Beltram, F. *Biophys. J.* **2006**, *90*, 330.

(97) Tang, B.; Liu, X.; Xu, K.; Huang, H.; Yang, G.; An, L. *Chem. Commun.* **2007**, *36*, 3726.

(98) Pal, R.; Parker, D. *Chem. Commun.* **2007**, *5*, 474.

(99) Liu, Y.-S.; Sun, Y.; Vernier, P. T.; Liang, C.-H.; Chong, S. Y. C.; Gundersen, M. A. *J. Phys. Chem. C* **2007**, *111*, 2872.

(100) Balut, C.; vande Ven, M.; Despa, S.; Lambrichts, I.; Ameloot, M.; Steels, P.; Smets, I. *Kidney Int.* **2008**, *73*, 226.

(101) Bradley, M.; Alexander, L.; Duncan, K.; Chennaoui, M.; Jones, A. C.; Sanchez-Martin, R. M. *Bioorg. Med. Chem. Lett.* **2008**, *18*, 313.

(102) Diehl, H.; Horchak-Morris, N. *Talanta* **1987**, *34*, 739.

(103) Koo, M. K.; Oh, C. H.; Holme, A. L.; Pervaiz, S. *Cytometry, Part A* **2007**, *71A*, 87.

(104) Geisow, M. J.; Evans, W. H. *Exp. Cell. Res.* **1984**, *150*, 36.

(105) Morris, M. C.; Depollier, J.; Mery, J.; Heitz, F.; Divita, G. *Nature Biotech.* **2001**, *19*, 1173.

(106) Loudet, A.; Han, J.; Barhoumi, R.; Pellois, J.-P.; Burghardt, R. C.; Burgess, K. *Org. Biomol. Chem.* **2008**, *6*, 4516.

(107) Thivierge, C.; Han, J.; Jenkins, R. M.; Burgess, K. *J. Org. Chem.* **2011**, submitted.

(108) Sunahara, H.; Urano, Y.; Kojima, H.; Nagano, T. *J. Am. Chem. Soc.* **2007**, *129*, 5597.

(109) Ziessel, R.; Goze, C.; Ulrich, G. *Synthesis* **2007**, *6*, 936.

(110) Loudet, A.; Burgess, K. In *Handbook of Porphyrin Science: With Applications to Chemistry, Physics, Materials Science, Engineering, Biology and Medicine*;

Kadish, K., Smith, K., Guilard, R., Eds.; World Scientific: Singapore, 2010, p 203.

(111) Li, Z.; Mintzer, E.; Bittman, R. *J. Org. Chem.* **2006**, *71*, 1718.

(112) Sonogashira, K.; Tohda, Y.; Hagihara, N. *Tetrahedron Lett.* **1975**, *16*, 4467.

(113) Burgess, K.; Castro, J. C.; Malakhov, A. *Synthesis* **2008**, *7* 1224.

(114) Shi, J.; Zhang, X.; Neckers, D. C. *J. Org. Chem.* **1992**, *57*, 4418.

(115) Weber, G.; Teale, F. W. J. *Trans. Faraday Soc.* **1957**, *53*, 646.

(116) Thompson, B. C.; Kim, Y.-G.; McCarley, T. D.; Reynolds, J. R. *J. Am. Chem. Soc.* **2006**, *128*, 12714.

(117) Connelly, N. G.; Geiger, W. E. *Chem. Rev.* **1996**, *96*, 877.

(118) Hansen, W. N.; Hansen, G. J. *Phys. Rev. A: At., Mol., Opt. Phys.* **1987**, *36*, 1396.

(119) Burgess, K.; Gibbs, R. In *U.S. Patent 6340750 B1*; (The Texas A&M University System, USA): U.S., 2002; Vol. U.S. Patent 6340750 B1.

(120) Burgess, K. In *US Patent No. US2005/0032120 A1*; (The Texas A&M University System, USA). US, 2005; Vol. U.S. Patent 2005/0032120 A1, p 7.

(121) Azov, V. A.; Diederich, F.; Lill, Y.; Hecht, B. *Helvetica Chimica Acta* **2003**, *86*, 2149.

(122) Scholes, G. D.; Ghiggino, K. P.; Oliver, A. M.; Paddon-Row, M. N. *J. Am. Chem. Soc.* **1993**, *115*, 4345.

(123) Scholes, G. D.; Clayton, A. H. A.; Ghiggino, K. P. *J. Chem. Phys.* **1992**, *97*, 7405.

(124) Scholes, G. D.; Ghiggino, K. P. *Journal of Photochemistry and Photobiology, A: Chemistry* **1994**, *80*, 355.

(125) Scholes, G. D.; Ghiggino, K. P. *J. Phys. Chem.* **1994**, *98*, 4580.

(126) Scholes, G. D.; Ghiggino, K. P. *J. Chem. Phys.* **1994**, *101*, 1251.

(127) Harcourt, R. D.; Scholes, G. D.; Ghiggino, K. P. *J. Chem. Phys.* **1994**, *101*, 10521.

(128) Scholes, G. D.; Harcourt, R. D.; Ghiggino, K. P. *J. Chem. Phys.* **1995**, *102*, 9574.

(129) Scholes, G. D.; Ghiggino, K. P. *J. Chem. Phys.* **1995**, *103*, 8873.

(130) Scholes, G. D.; Harcourt, R. D. *J. Chem. Phys.* **1996**, *104*, 5054.

(131) Ghiggino, K. P.; Yeow, E. K. L.; Haines, D. J.; Scholes, G. D.; Smith, T. A. *Journal of Photochemistry and Photobiology, A: Chemistry* **1996**, *102*, 81.

(132) Vollmer, M. S.; Würthner, F.; Effenberger, F.; Emele, P.; Meyer, D. U.; Stümpfig, T.; Port, H.; Wolf, H. C. *Chem. Eur. J.* **1998**, *4*, 260.

(133) Coskun, A.; Baytekin, B. T.; Akkaya, E. U. *Tetrahedron Lett.* **2003**, *44*, 5649.

(134) Han, J.; Loudet, A.; Barhoumi, R.; Burghardt, R. C.; Burgess, K. *J. Am. Chem. Soc.* **2009**, *131*, 1642.

(135) Thivierge, C.; Loudet, A.; Burgess, K. *Macromolecules* **2011**, submitted.

(136) Donuru, V. R.; Vegesna, G. K.; Velayudham, S.; Meng, G.; Liu, H. *J. Polym. Sci., Part A: Polym. Chem.* **2009**, *47*, 5354.

(137) Kim, B.-S.; Ma, B.; Donuru, V. R.; Liu, H.; Frechet, J. M. J. *Chem. Commun.* **2010**, *46*, 4148.

(138) Zhu, M.; Jiang, L.; Yuan, M.; Liu, X.; Ouyang, C.; Zheng, H.; Yin, X.; Zuo, Z.; Liu, H.; Li, Y. *J. Polym. Sci., Part A: Polym. Chem.* **2008**, *46*, 7401.

(139) Alemdaroglu, F. E.; Alexander, S. C.; Ji, D.; Prusty, D. K.; Borsch, M.; Herrmann, A. *Macromolecules* **2009**, *42*, 6529.

(140) Cakmak, Y.; Akkaya, E. U. *Org. Lett.* **2009**, *11*, 85.

(141) Nagai, A.; Chujo, Y. *Macromolecules* **2010**, *43*, 193.

(142) Cihaner, A.; Algi, F. *Reactive & Functional Polymers* **2009**, *69*, 62.

(143) Cihaner, A.; Algi, F. *Electrochimica Acta* **2008**, *54*, 786.

(144) Algi, F.; Cihaner, A. *Organic Electronics* **2009**, *10*, 453.

(145) Nagai, A.; Miyake, J.; Kokado, K.; Nagata, Y.; Chujo, Y. *J. Am. Chem. Soc.* **2008**, *130*, 15276.

(146) Meng, G.; Velayudham, S.; Smith, A.; Luck, R.; Liu, H. *Macromolecules* **2009**, *42*, 1995.

(147) Scherf, U.; Neher, D. *Polyfluorenes*; Springer: Berlin, 2008; Vol. 212.

(148) Najechalski, P.; Morel, Y.; Stephan, O.; Baldeck, P. L. *Chemical Physics Letters* **2001**, *343*, 44.

(149) Leclerc, M. *J. Polym. Sci., Part A: Polym. Chem.* **2001**, *39*, 2867.

(150) Loudet, A.; Bandichhor, R.; Wu, L.; Burgess, K. *Tetrahedron* **2008**, *64*, 3642.

(151) Berlman, I. B. *Handbook of Fluorescence Spectra of Aromatic Molecules*; 2nd ed.; Academic Press: New York, 1971.

(152) Kubin, R. F.; Fletcher, A. N. *J. Luminescence* **1982**, *27*, 455.

(153) Seybold, P. G.; Gouterman, M.; Callis, J. *Journal of Photochemistry and Photobiology, A: Chemistry* **1969**, *9*, 229.

(154) Kurokawa, N.; Yoshikawa, H.; Hirota, N.; Hyodo, K.; Masuhara, H. *ChemPhysChem* **2004**, *5*, 1609.

(155) McNeill, J. D.; Christensen, K.; Bull, B.; Wu, C. In *Angew. Chem. Int. Ed.* 2009; Vol. 48, p 1.

(156) McNeill, J. D.; Wu, C. *PMSE Prepr.* **2008**, *99*, 770.

(157) Szymanski, C.; Wu, C.; Hooper, J.; Salazar, M. A.; Perdomo, A.; Dukes, A.; McNeill, J. *J. Phys. Chem. B* **2005**, *109*, 8543.

(158) Wu, C.; Bull, B.; Christensen, K.; McNeill, J. *Angew. Chem. Int. Ed.* **2009**, 1.

(159) Wu, C.; Bull, B.; Szymanski, C.; Christensen, K.; McNeill, J. *ACS Nano* **2008**, *2*, 2415.

(160) Wu, C.; McNeill, J. *Langmuir* **2008**, *24*, 5855.

(161) Wu, C.; Peng, H.; Jiang, Y.; McNeill, J. *J. Phys. Chem. B* **2006**, *110*, 14148.

(162) Wu, C.; Szymanski, C.; Cain, Z.; McNeill, J. *J. Am. Chem. Soc.* **2007**, *129*, 12904.

(163) Wu, C.; Szymanski, C.; McNeill, J. *Langmuir* **2006**, *22*, 2956.

(164) Wu, C.; Zheng, Y.; Szymanski, C.; McNeill, J. *J. Phys. Chem. C* **2008**, *112*, 1772.

(165) Bura, T.; Ziessel, R. *Tetrahedron Lett.* **2010**, *51*, 2875.

(166) Bazan, G. C.; Wang, S. In *Organic Semiconductors in Sensor Applications*; Bernards, D. A., Malliaras, G. G., Owens, R. M., Eds.; Springer Berlin Heidelberg: 2008; Vol. 107, p 1.

(167) Wang, H.; Lu, P.; Wang, B.; Qiu, S.; Liu, M.; Hanif, M.; Cheng, G.; Liu, S.; Ma, Y. *Macromol. Rapid Commun.* **2007**, *28*, 1645.

(168) Zhang, Y.; Liu, B.; Cao, Y. *Chemistry--An Asian Journal* **2008**, *3*, 739.

(169) Huang, F.; Wang, X.; Wang, D.; Yang, W.; Cao, Y. *Polymer* **2005**, *46*, 12010.

(170) Qin, C.; Cheng, Y.; Wang, L.; Jing, X.; Wang, F. *Macromolecules* **2008**, *41*, 7798.

(171) Qin, C.; Wu, X.; Gao, B.; Tong, H.; Wang, L. *Macromolecules* **2009**, *42*, 5427.

(172) Yu, M.; He, F.; Tang, Y.; Wang, S.; Li, Y.; Zhu, D. *Macromolecular Rapid Communications* **2007**, *28*, 1333.

(173) Chen, Q.; Cheng, Q.-Y.; Zhao, Y.-C.; Han, B.-H. *Macromolecular Rapid Communications* **2009**, *30*, 1651.

(174) *In Cancer Fact and Figures 2010; American Chemical Society: Atlanta, 2010, http://www.cancer.org/research/cancerfactsfigures/cancerfactsfigures/cancer-facts-and-figures-2010.*

(175) Dolmans, D. E. J. G. J.; Fukumura, D.; Jain, R. K. *Nat Rev Cancer* **2003**, *3*, 380.

(176) Ryter, S. W.; Tyrrell, R. M. *Free Radical Biology and Medicine* **1998**, *24*, 1520.

(177) Allison, R. R.; Downie, G. H.; Cuenca, R.; Hu, X.-H.; Childs, C. J. H.; Sibata, C. H. *Photodiagnosis and Photodynamic Therapy* **2004**, *1*, 27.

(178) Byrne, C. J.; Marshallsay, L. V.; Ward, A. D. *Journal of Photochemistry and Photobiology B: Biology* **1990**, *6*, 13.

(179) Atilgan, S.; Ekmekci, Z.; Dogan, A. L.; Guc, D.; Akkaya, E. U. *Chemical Communications* **2006**, 4398.

(180) Lim, S. H.; Thivierge, C.; Nowak-Sliwinska, P.; Han, J.; Van den Bergh, H.; Wagnieres, G.; Burgess, K.; Lee, H. B. *J. Med. Chem.* **2010**, *53*, 2865.

(181) Byrne, A. T.; O'Connor, A. E.; Hall, M.; Murtagh, J.; O'Neill, K.; Curran, K. M.; Mongrain, K.; Rousseau, J. A.; Lecomte, R.; McGee, S.; Callanan, J. J.; O'Shea, D. F.; Gallagher, W. M. *Br J Cancer* **2009**, *101*, 1565.

(182) Kochevar, I. E.; Redmond, R. W. In *Methods in Enzymology*; Lester Packer, H. S., Ed.; Academic Press: 2000; Vol. Volume 319, p 20.

(183) McBride, H. M.; Neuspiel, M.; Wasiak, S. *Current biology : CB* **2006**, *16*, R551.

(184) Morgan, J.; Oseroff, A. R. *Advanced Drug Delivery Reviews* **2001**, *49*, 71.

(185) Lee, H.; Ho, A.; Teo, S. *Cancer Chemotherapy and Pharmacology* **2006**, *58*, 91.

(186) Vantieghem, A.; Xu, Y.; Assefa, Z.; Piette, J.; Vandenheede, J. R.; Merlevede, W.; de Witte, P. A. M.; Agostinis, P. *Journal of Biological Chemistry* **2002**, *277*, 37718.

(187) Chen, B.; Pogue, B. W.; Hoopes, P. J.; Hasan, T. *Crit. Rev. Eukaryotic Gene Expression* **2006**, *16*, 279.

(188) Lange, N.; Ballini, J.-P.; Wagnieres, G.; van den Bergh, H. *Investigative Ophthalmology & Visual Science* **2001**, *42*, 38.

(189) Vargas, A.; Zeisser-LabouËbe, M.; Lange, N.; Gurny, R.; Delie, F. *Advanced Drug Delivery Reviews* **2007**, *59*, 1162.

(190) Hammer-Wilson, M. J.; Cao, D.; Kimel, S.; Berns, M. W. *Photochemical & Photobiological Sciences* **2002**, *1*, 721.

(191) Ruck, A.; Bohmler, A.; Steiner, R. *Photodiagnosis and Photodynamic Therapy* **2005**, *2*, 79.

(192) Ichikawa, K.; Takeuchi, Y.; Yonezawa, S.; Hikita, T.; Kurohane, K.; Namba, Y.; Oku, N. *Cancer Letters* **2004**, *205*, 39.

(193) Kurohane, K.; Tominaga, A.; Sato, K.; North, J. R.; Namba, Y.; Oku, N. *Cancer Letters* **2001**, *167*, 49.

(194) Maeda, H.; Wu, J.; Sawa, T.; Matsumura, Y.; Hori, K. *Journal of Controlled Release* **2000**, *65*, 271.

(195) Li, C. *Advanced Drug Delivery Reviews* **2002**, *54*, 695.

(196) Kiew, L.-V.; Cheong, S.-K.; Sidik, K.; Chung, L.-Y. *International Journal of Pharmaceutics* **2010**, *391*, 212.

(197) Grosjean, P.; Wagnieres, G.; Fontolliet, C.; van den Bergh, H.; Monnier, P. *Br J Cancer* **1998**, *77*, 1989.

(198) Fischer, G. M.; Ehlers, A. P.; Zumbusch, A.; Daltrozzo, E. *Angewandte Chemie* **2007**, *119*, 3824.

(199) Berezin, M. Y.; Akers, W. J.; Guo, K.; Fischer, G. M.; Daltrozzo, E.; Zumbusch, A.; Achilefu, S. *Biophysical Journal* **2009**, *97*, L22.

(200) Fischer, G. M.; Isomäki-Krondahl, M.; Göttker-Schnetmann, I.; Daltrozzo, E.; Zumbusch, A. *Chemistry – A European Journal* **2009**, *15*, 4857.

(201) Fischer, G. M.; Jungst, C.; Isomaki-Krondahl, M.; Gauss, D.; Moller, H. M.; Daltrozzo, E.; Zumbusch, A. *Chemical Communications* **2010**, *46*, 5289.

(202) Fischer, G. M.; Daltrozzo, E.; Zumbusch, A. *Angew. Chem. Int. Ed.* **2011**, ASAP.

(203) Hao, Z.; Iqbal, A. *Chemical Society Reviews* **1997**, *26*, 203.

(204) Han, J.; Gonzalez, O.; Aguilar-Aguilar, A.; Pena-Cabrera, E.; Burgess, K. *Org. Biomol. Chem.* **2009**, *7*, 34.

(205) Wu, L.; Loudet, A.; Barhoumi, R.; Burghardt, R. C.; Burgess, K. *J. Am. Chem. Soc.* **2009**, *131*, 9156.

(206) Jose, J.; Ueno, Y.; Castro, J. C.; Li, L.; Burgess, K. *Tetrahedron Lett.* **2009**, *50*, 6442.

(207) Ueno, Y.; Jose, J.; Loudet, A.; Perez-Bolivar, C.; Anzenbacher Jr., P.; Burgess, K. *J. Am. Chem. Soc.* **2010**, *133*, 51.

(208) Lin, W.; Yuan, L.; Cao, Z.; Feng, Y.; Song, J. *Angew. Chem. Int. Ed.* **2010**, *49*, 375.

(209) Nierth, A.; Kobitski, A. Y.; Nienhaus, G. U.; Jaschke, A. *J. Am. Chem. Soc.* **2010**, *132*, 2646.

(210) Saki, N.; Dinc, T.; Akkaya, E. U. *Tetrahedron* **2006**, *62*, 2721.

(211) Boldyrev, I. A.; Molotkovsky, J. G. *Russian J. Bioorg. Chem.* **2006**, *32*, 78.

(212) Kim, H.; Burghart, A.; Welch, M. B.; Reibenspies, J.; Burgess, K. *Chem. Commun.* **1999**, 1889.

(213) Chen, J.; Burghart, A.; Derecskei-Kovacs, A.; Burgess, K. *J. Org. Chem.* **2000**, *65*, 2900.

(214) Tahtaoui, C.; Thomas, C.; Rohmer, F.; Klotz, P.; Duportail, G.; Bonnet, D.; Hibert, M. *The Journal of Organic Chemistry* **2006**, *72*, 269.

APPENDIX A

SUPPLEMENTARY DATA FOR REFERENCE 29

This data is supplementary to the data found in reference [29]. In short, Table 2 and Figure 4 do not match. Luckily the raw data was still available within the group and is presented here for clarity.

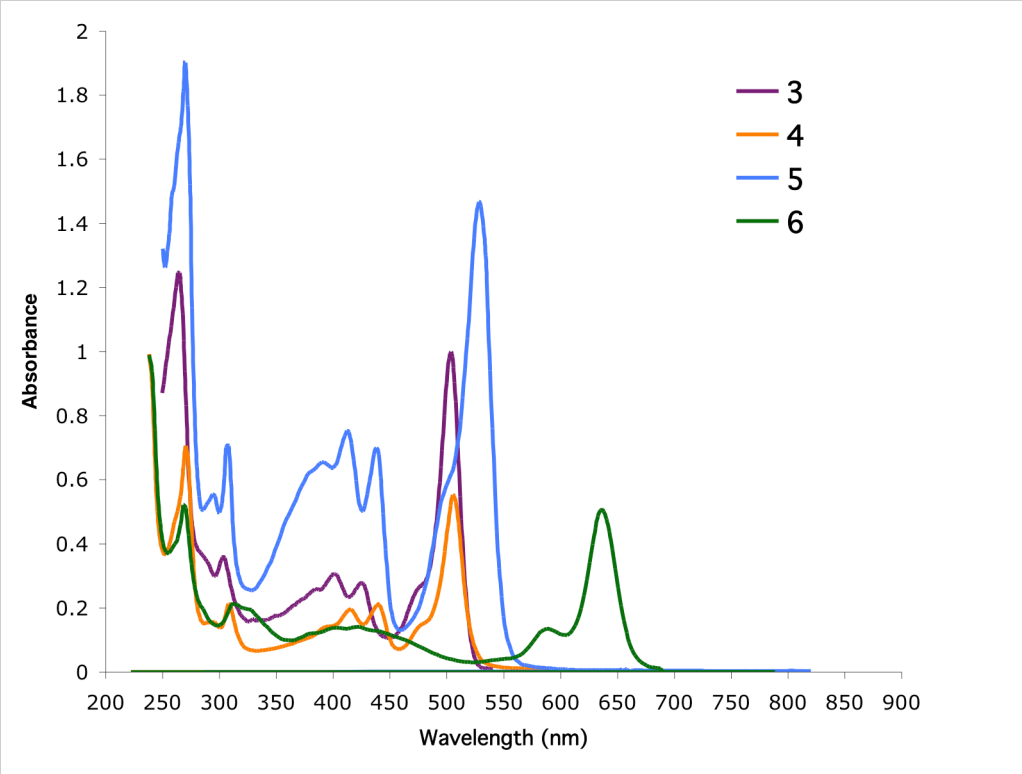

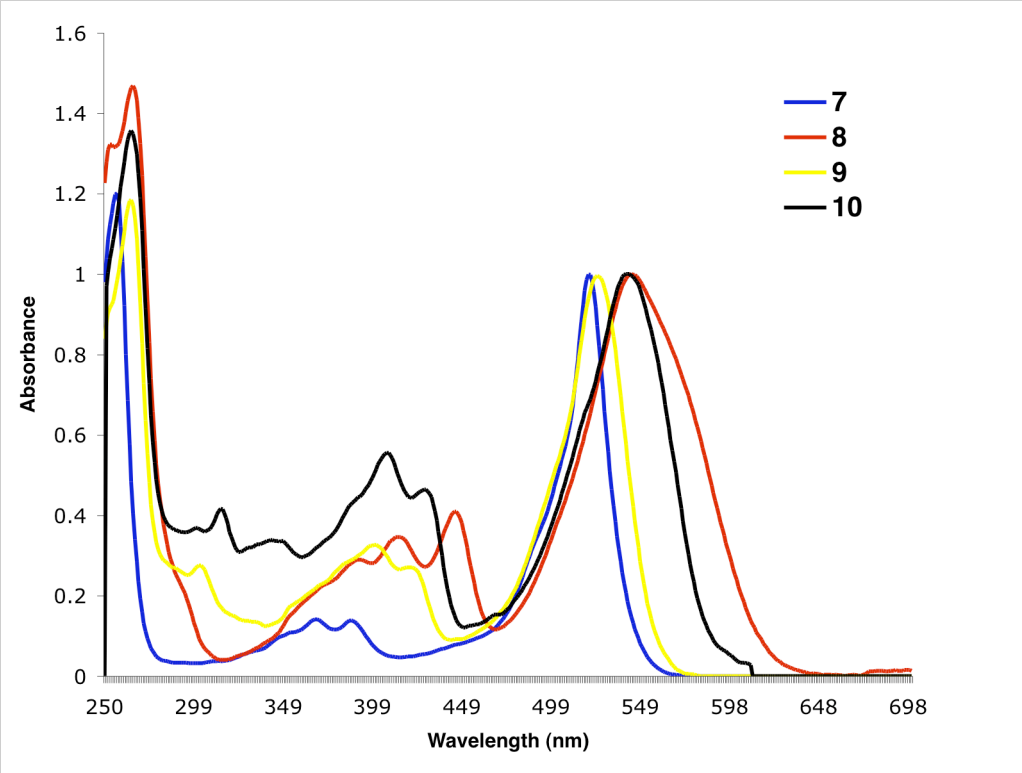
1.6
1.4
1.2
1
0.8
0.6
0.4
0.2
0
Absorbance
250
299
349
399
449
499
549
598
648
698
Wavelength (nm)
7
8
9
10

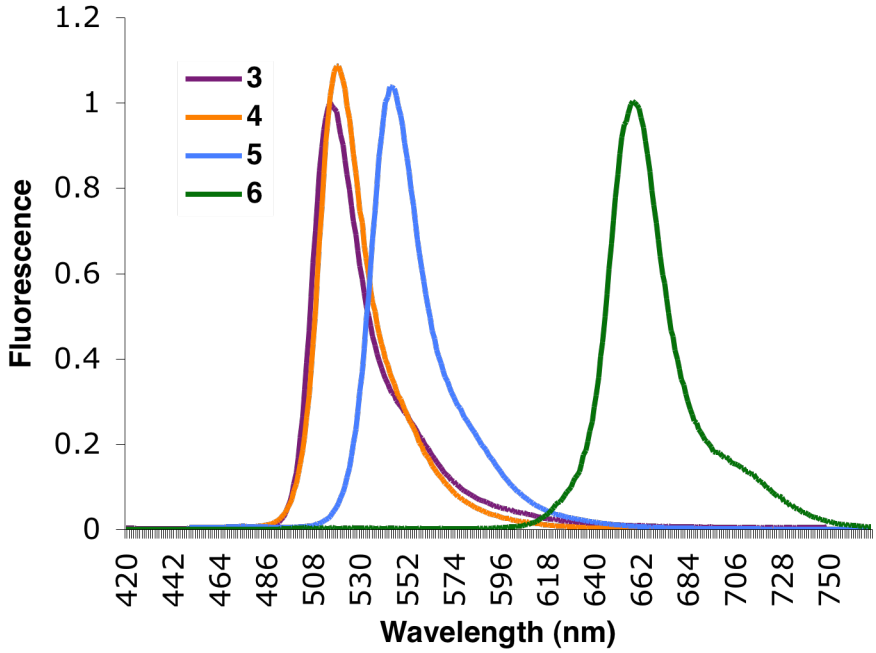
1.2
1
0.8
0.6
0.4
0.2
0
Fluorescence
420
442
464
486
508
530
552
574
596
618
640
662
684
706
728
750
Wavelength (nm)
3
4
5
6

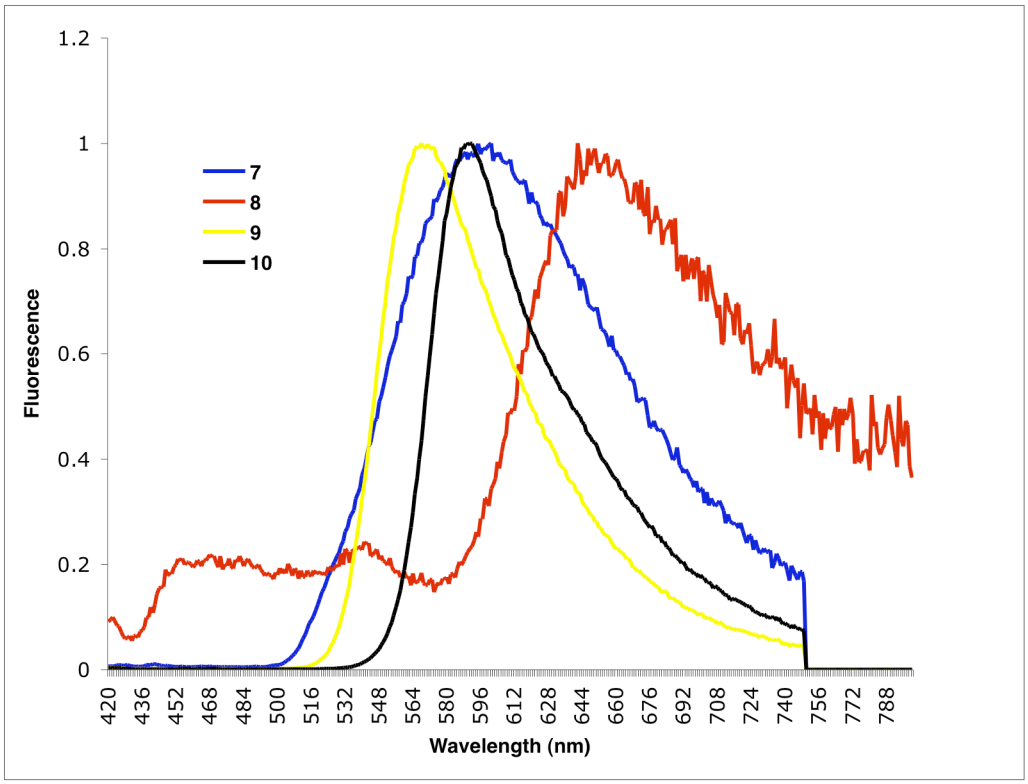
1.2
1
0.8
0.6
0.4
0.2
0
Fluorescence
7
8
9
10
420
436
452
468
484
500
516
532
548
564
580
596
612
628
644
660
676
692
708
724
740
756
772
788
Wavelength (nm)

APPENDIX B

GENERAL EXPERIMENTAL PROCEDURES

All reactions were carried out under an inert nitrogen or argon atmosphere unless specified otherwise. All reaction solvents were either dried on activated alumina or distilled prior to use. All reagents were used as received without further purification.

NMR spectra were recorded on a VXP-300 MHz and Inova-500 MHz spectrometers (^{1}H at 300 MHz or 500 MHz and ^{13}C at 75 or 126 MHz) at room temperature unless otherwise mentioned. Chemical shifts of 1H NMR spectra were recorded and reported in ppm from the solvent resonance ($CDCl_3$ 7.26 ppm, CD_3OD 3.31 ppm). Data are reportedas follows: chemical shift, multiplicity (s = singlet, bs = broad singlet, d = doublet, t = triplet, q = quartet, dd = doublet of doublets, dt = doublet of triplets, br = broad, m = multiplet), coupling constants, and number of protons. Proton decoupled ^{13}C NMR spectra were also recorded in ppm from solvent resonance ($CDCl_3$ 77.16, CD_3OD 49.0 ppm). Analytical thin layer chromatography (TLC) was performed on EM Reagents 0.25 mm silica-gel 60-F plates, and visualized with UV light. Flash chromatography was performed using silica gel (230–600 mesh). MS were measured under ESI, MALDI or APCI conditions. All solvents and reagents were used as received unless noted otherwise.

Determination of Quantum Yields and Molar absorptivities

UV/Vis absorbance spectra were recorded on a Cary 100 Bio spectrophotometer. Steady-state fluorescence spectroscopic studies were performed on a Cary Eclipse

fluorometer. The slit width was 5 nm for both excitation and emission. Fluorescence spectra were corrected. The relative quantum yields of the samples were obtained by comparing the area under the corrected emission spectrum of the test sample with that of a solution of standard. The quantum efficiencies of fluorescence were obtained from three measurements with the following equation:

$$\Phi_x = \Phi_{st} (I_x/I_{st}) (A_{st}/A_x) (\eta_x^2/\eta_{st}^2)$$

Where Φ_{st} is the reported quantum yield of the standard, **I** is the area under the emission spectra, **A** is the absorbance at the excitation wavelength and η is the refractive index of the solvent used, measured on a pocket refractometer from ATAGO. **X** subscript denotes unknown, and **st** denotes standard.

Energy transfer percentage (ET %) were measured a ratio of the integral of fluorescence area corresponding to the acceptor to the total integral of fluorescence area. The energy transfer efficiencies (ETE %) were measured as a relative ratio of the integral of fluorescence area corresponding to the acceptor when exciting the donor to the integral of fluorescence area when exciting the acceptor directly. The molar absorptivities at both excitation wavelengths were used as correction factors.

APPENDIX C

EXPERIMENTAL DATA FOR CHAPTER II

Phenylacetylene-BODIPY Derivatives

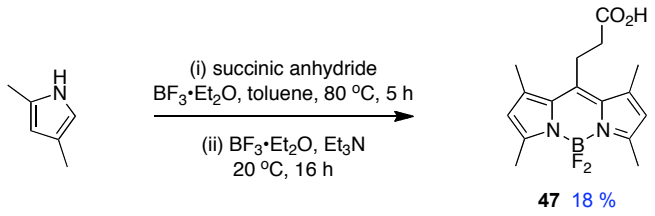

47 18 %

47; A solution of 2,4-dimethylpyrrole (1.0 mL, 10 mmol), succinic anhydride (400 mg, 4.0 mmol), and BF_3•Et_2O (0.50 mL, 4.0 mmol) in 30 mL toluene was heated to 80 °C under N_2 for 5 h. The mixture was cooled to 25 ºC and BF_3•Et_2O (5.0 mL, 40 mmol) and Et_3N (10 mL, 80 mmol) were then added. After stirring for 16 h at 20 ºC under N_2 the reaction was quenched with 60 mL of 0.1 M HCl aqueous solution. Extraction was performed and the organic fractions were combined and dried over magnesium sulfate. The organic solvent was removed under reduced pressure and the product was purified via flash silica column with 85 % ethyl acetate:hexane to afford the desired product as an orange solid (203 mg, 18 %). ^{1}H NMR (300 MHz, $CDCl_3$) δ (ppm) 6.07 (s, 2H), 3.29-3.35 (m, 2H), 2.62-2.68(m, 2H), 2.52 (s, 6H), 2.44 (s, 6H), ^{13}C NMR (75 MHz, $CDCl_3$), δ (ppm), 176.6 154.8, 142.8, 140.3, 131.2, 122.0, 35.1, 23.4, 16.4, 14.5. MS (ESI) calcd for $C_{16}H_{18}BF_2N_2O_2$ $\{M-H\}^-$ 319.15, found 319.15. TLC (50 % EtOAc:Hexane) R_f = 0.50.

^{1}H NMR of 47 ($CDCl_3$)

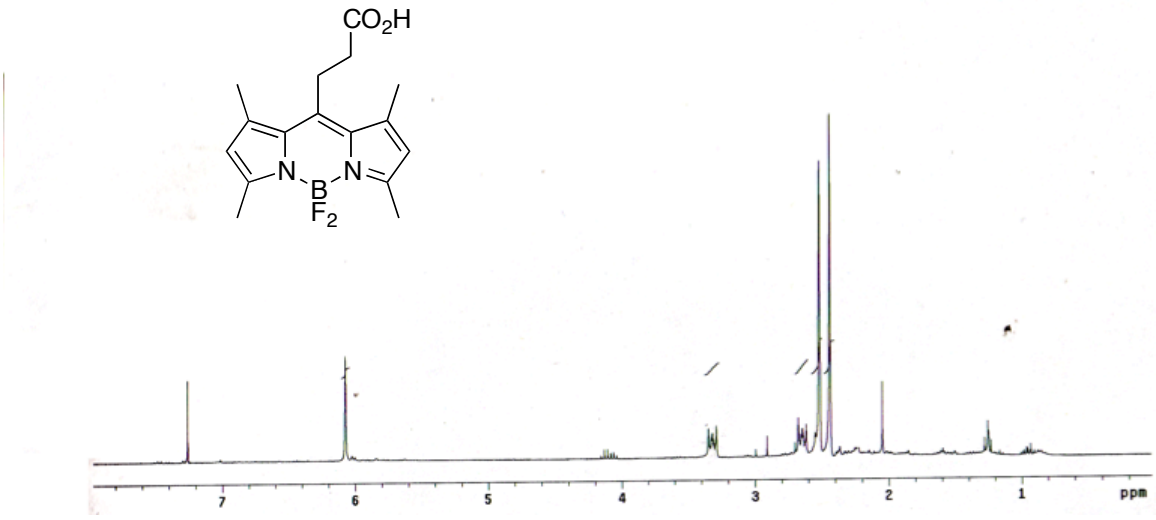

^{13}C NMR of 47 ($CDCl_3$)

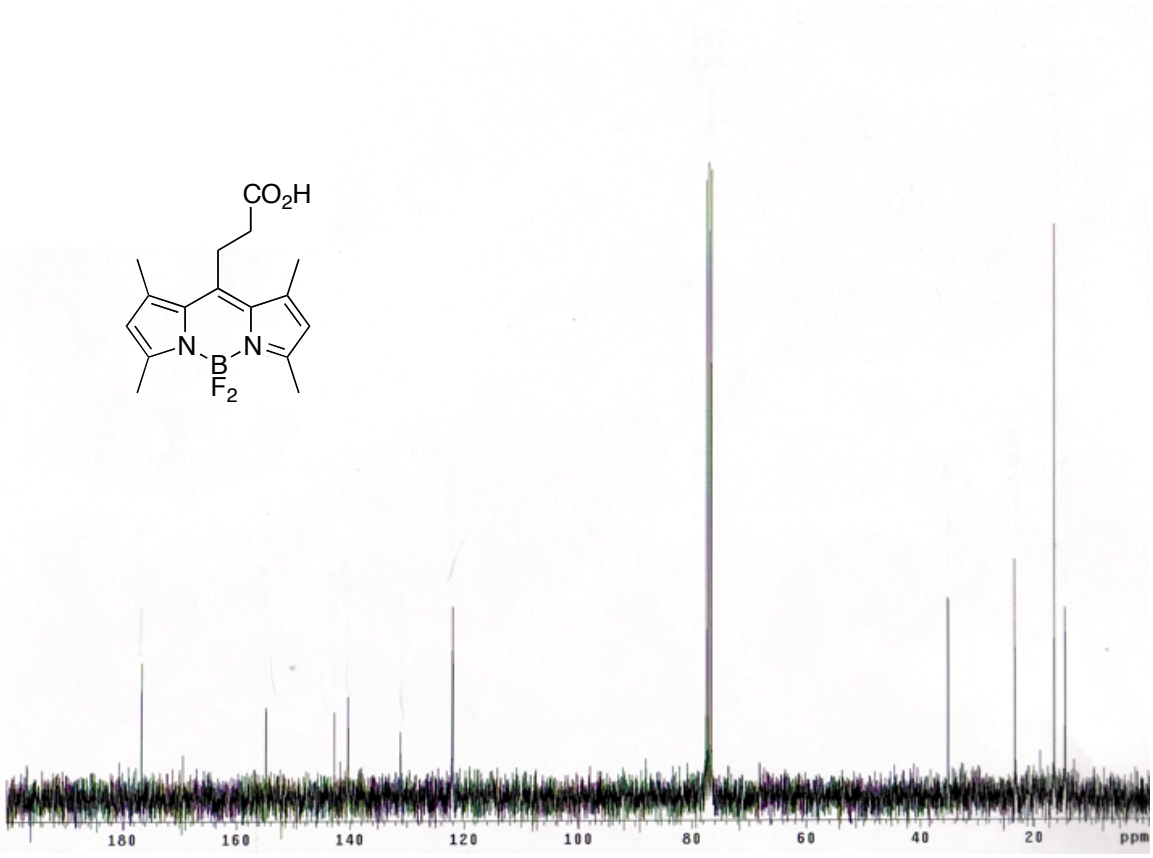

47 **48** 54 %

48; Tetramethyl-BODIPY acid **47** (600 mg, 1.87 mmol) was suspended in 200 mL of MeOH. I_2 (1.24 g, 4.87 mmol) was added followed by iodic acid (660 mg, 3.75 mmol) in ~3 mL water was added over 5 min. The mixture was stirred for 30 min at 25 ºC. The MeOH was then removed under reduced pressure and the crude product was purified via flash silica column with 50 % ethyl acetate:hexane to afford the desired product as a red solid (574 mg, 54 %). ^{1}H NMR (300 MHz, $CDCl_3$) δ (ppm) 3.28-3.32 (m, 2H), 2.45-2.52 (m, 2H), 2.50 (s, 6H), 2.43 (s, 6H), ^{13}C NMR (75 MHz, $CDCl_3$), δ (ppm), 175.1 156.3, 142.5, 142.3, 131.1, 87.0, 34.9, 24.2, 19.3, 16.5. ESI HRMS calcd for $C_{16}H_{16}BF_2I_2N_2O_2\{M\text{-}H\}^-$ 570.9362, found 570.9340. TLC (50 % EtOAc:Hexane) R_f = 0.55.

^{1}H NMR of 48 ($CDCl_3$)

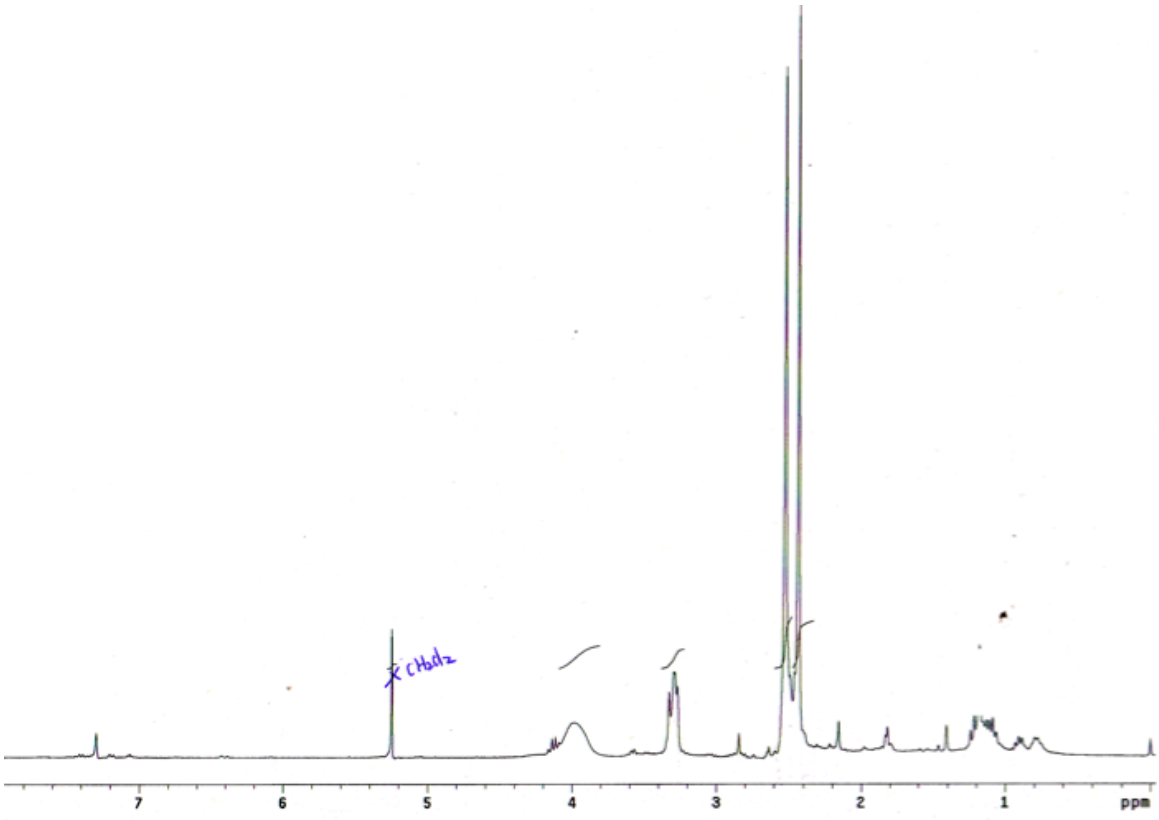

^{13}C NMR of 48 ($CDCl_3$)

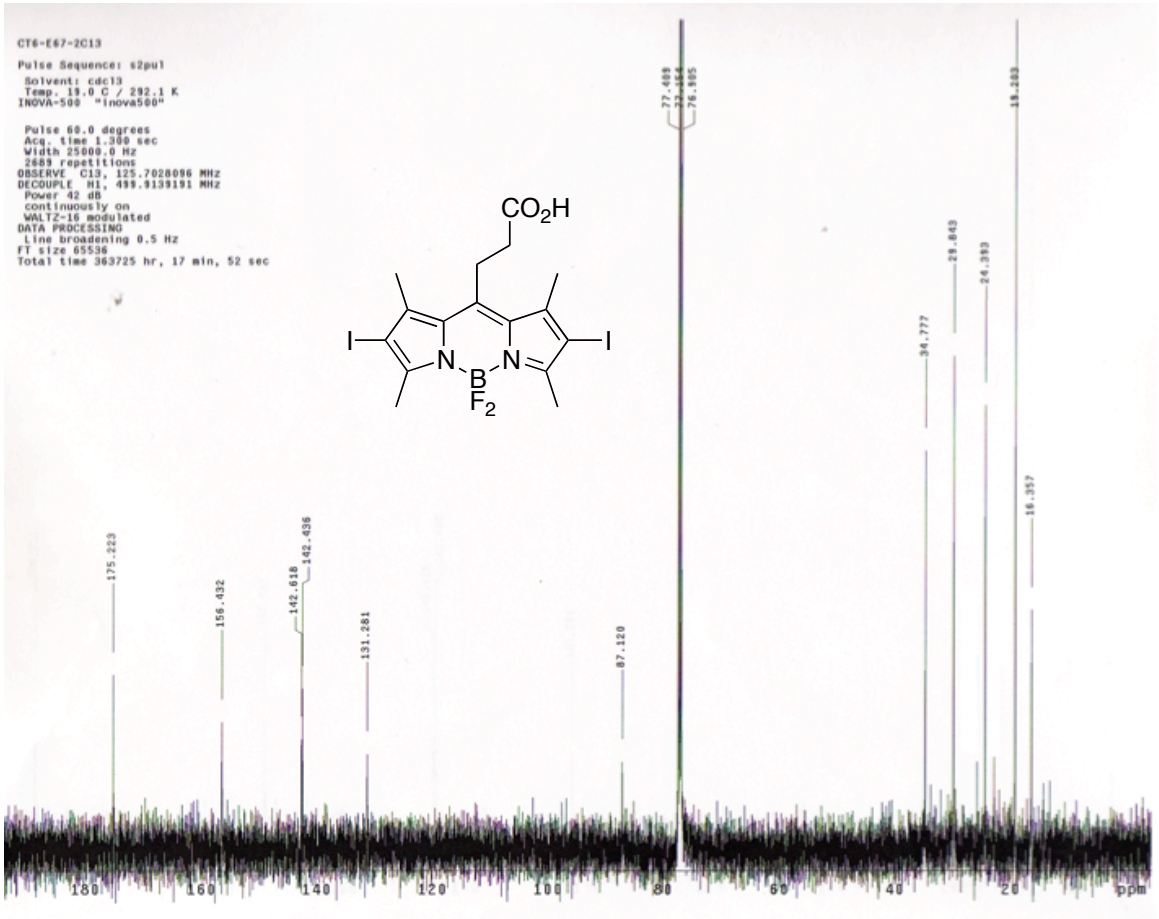

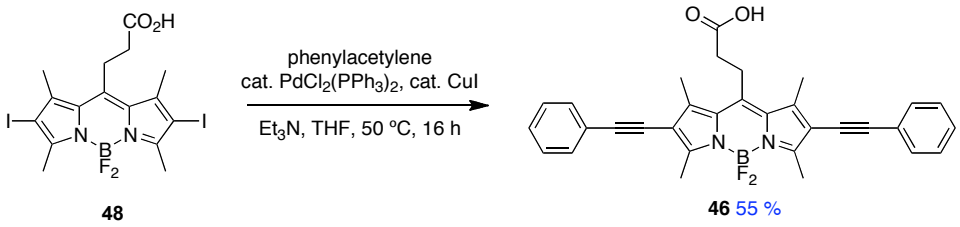

46; A mixture of **48** (34 mg, 0.11 mmol), phenylacetylene (47 μL, 0.43mmol), Et_3N (0.15 mL, 1.1 mmol), $PdCl_2(PPh_3)_2$ (8 mg, 0.01 mmol), and CuI (4 mg, 0.02 mmol) were dissolved in 2 mL THF under N_2. The solution was degassed three times via the freeze-thaw method and then heated to 50 °C for 16 h under N_2. The solvent was removed under reduced pressure and the crude product was purified via flash silica column eluting with 20% methanol:CH_2Cl_2 to give the desired product as a red solid (17 mg, 55 %). ^{1}H NMR (500 MHz, $CDCl_3$), δ 7.44-7.46 (m, 4H), 7.27-7.31 (m, 6H), 3.32-3.36 (m, 2H), 2.62 (s, 6H), 2.56 (s, 6H), 2.53-2.57 (m, 2H), ^{13}C NMR (125 MHz, 3:1 $CDCl_3$:CD_3OD), δ 174.0, 157.5, 144.9, 141.4, 131.4, 131.2, 128.4, 128.3, 123.2, 116.7, 96.7, 81.4, 24.2, 15.1, 15.1, 13.6. MALDI MS calcd for $C_{32}H_{27}BF_2N_2O_2$ $(M-H)^-$ 519.21, found 519.21. TLC (50 % EtOAc:Hexane) $R_f = 0.20$.

^{1}H NMR of 46 (1:2 $CDCl_3/CD_3OD$)

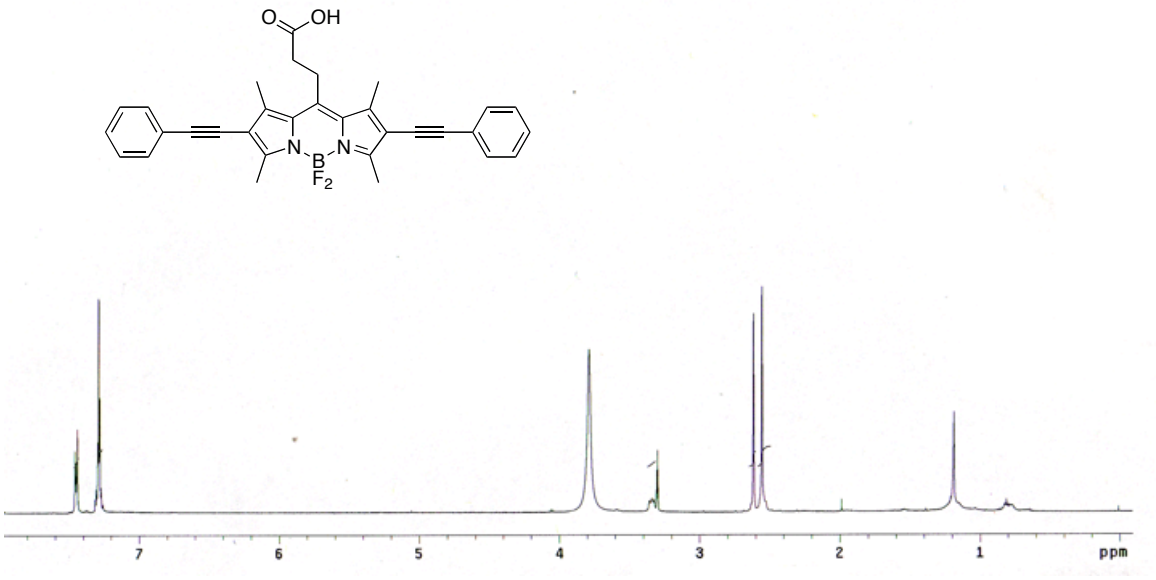

^{13}C NMR of 46 (1:2 $CDCl_3/CD_3OD$)

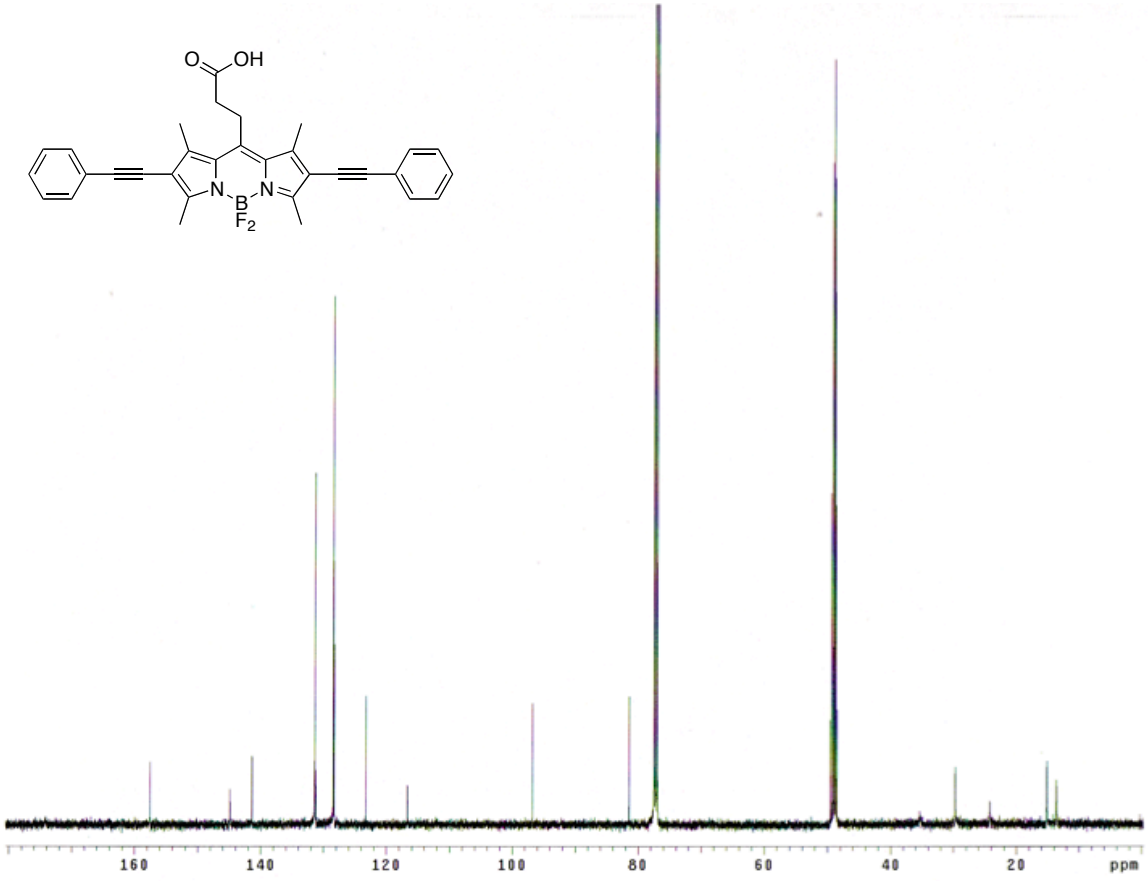

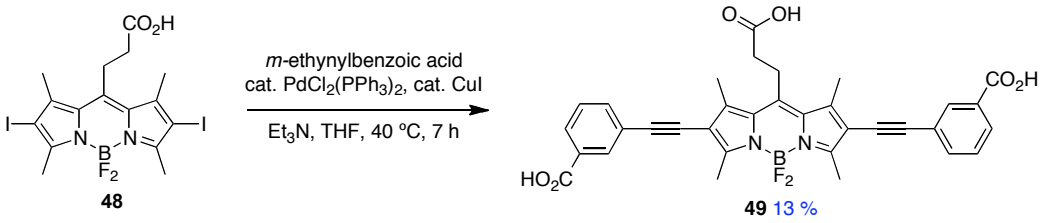

49; A mixture of **48** (30 mg, 0.05 mmol), *m*-ethynylbenzoic acid (23 mg, 0.16 mmol), Et_3N (0.30 mL, 2.1 mmol), $PdCl_2(PPh_3)_2$ (5 mg, 0.01 mmol), and CuI (2 mg, 0.01 mmol) were dissolved in 1 mL DMF under N_2. The solution was degassed three times via the freeze-thaw method and then heated to 40 °C for 7 h under N_2. The solvent was removed under reduced pressure and the crude product was extracted from ether (20 mL) using 10 % MeOH in 0.1 M $NaHCO_3$ aqueous solution (3 x 20 mL). The aqueous layers are combined and brought to pH ~ 3 using 1 M HCl to yield purple precipitate. The precipitate is filtered and further purified via C-18 preparative HPLC eluting with a 75 – 95 % MeOH and 0.1 % TFA/water linear gradient over 25 min gave the desired product with a retention time of 11 min as a purple solid (4 mg, 13 %). ^{1}H NMR (500 MHz, CD_3OD), δ 8.11 (s, 2H), 8.00 (d, J = 7.5 Hz, 2H), 7.72 (d, J = 7.5 Hz, 2H), 7.50 (t, J = 7.5 Hz, 2H), 3.65 (bs, 2H), 2.66 (s, 14H). ^{13}C NMR could not be obtained due to poor solubility in organic solvents. ESI MS calcd for $C_{34}H_{27}BF_2N_2O_6$ $(M\text{-}H)^-$ 607.19, found 607.19. TLC (5 % MeOH:CH_2Cl_2) R_f = 0.10.

^{1}H NMR of 49 (CD_3OD)

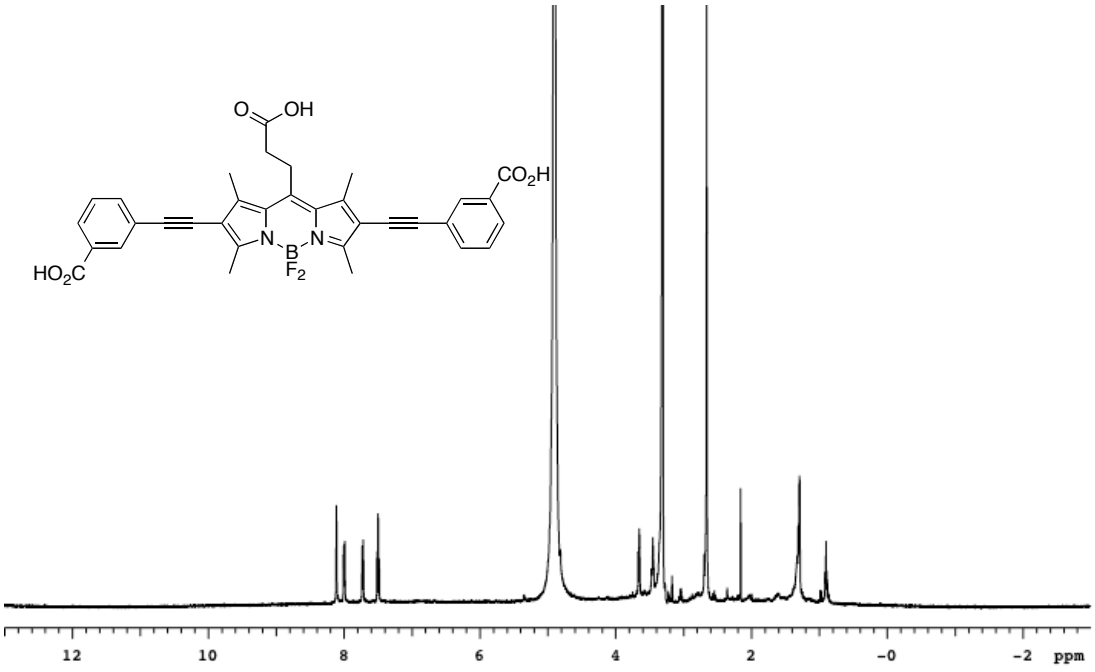

C-H Functionalization on BODIPYs

Method A

Solid $Pd(OAc)_2$ (0.2 equiv) was added to a solution of 4,4-difluoro-1,3,5,7-tetramethyl-4-bora-3a,4a-diaza-s-indacene (0.2 mmol, 50 mg), alkyl acrylate (5.0 equiv.), and *tert*-butylperbenzoate (2.0 equiv.) in 3:9:1 (AcOH:Dioxane:DMSO) (1.5 mL). After stirring for 5 d at 35 °C, the reaction mixture was diluted with water (15 mL) and diethyl ether (15 mL). The resulting solution was filtered through short pad of celite. The filtrate was washed with saturated solution of sodium bicarbonate (3 X 10 mL), organic layers were dried over anhydrous $MgSO_4$, filtered and concentrated under vacuum.

Method B

Solid $Pd(OAc)_2$ (0.2 equiv.) was added to a solution of 4,4-difluoro-1,3,5,7-tetramethyl-4-bora-3a,4a-diaza-s-indacene (0.4 mmol, 100 mg), vinylsulfonic acid sodium salt (3 equiv.) and $Cu(OAc)_2$ (4.0 equiv.) in 10:1 (DMF:DMSO) (8.2 mL). The reaction mixture was irradiated with microwave radiation (200 W) at 80 ºC for 30 min with constant N_2 cooling flow. The resulting suspension was concentrated under vacuum.

Method C

Solid $Pd(OAc)_2$ (0.2 equiv.) was added to a solution of 4,4-difluoro-1,3,5,7-tetramethyl-4-bora-3a,4a-diaza-s-indacene (0.4 mmol, 100 mg), methyl-1-cyclohexene-1-carboxylate (4.0 equiv.) and $Cu(OAc)_2$ (3.6 equiv.) in 10:1 (DMF:DMSO) (1.0 mL). After stirring for 5 days at 70 °C, the reaction mixture was diluted with water (15 mL) and extracted into diethyl ether (2 x 15 mL). The resulting solution was dried with $MgSO_4$ and filtered through short pad of celite and concentrated under vacuum.

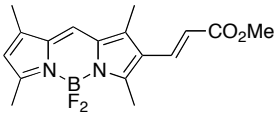

50a

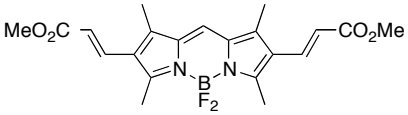

51a

Method A was followed. Crude mixture was subjected to flash column chromatography that provided **50a** (75% hexanes in ethyl acetate) in 61% (37 mg) and **51a** (60% hexanes in ethyl acetate) in 30% (20 mg) yields as orange solids: **50a**; R_f = 0.30 (60% hexanes/EtOAc); ^{1}H NMR (300 MHz, $CDCl_3$) δ 7.66 (d, 1H, J = 16 Hz), 7.07 (s, 1H), 6.14 (d, 1H, J = 16 Hz), 6.14 (s, 1H), 3.80 (s, 3H), 2.65 (s, 3H), 2.56 (s, 3H), 2.37 (s, 3H), 2.28 (s, 3H); ^{13}C NMR (75 MHz, $CDCl_3$) δ 168.2, 160.2, 154.9, 143.8, 138.1, 136.2, 135.6, 132.1, 123.9, 120.8 (2C), 116.5, 51.8, 15.2 (2C), 13.7, 11.6; MS (ESI) calcd for $C_{17}H_{19}BF_2N_2O_2$ 332.15 found 333.15 ($M+H^+$).

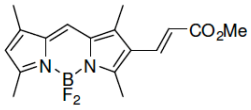
CO2Me
N
B
F2
N

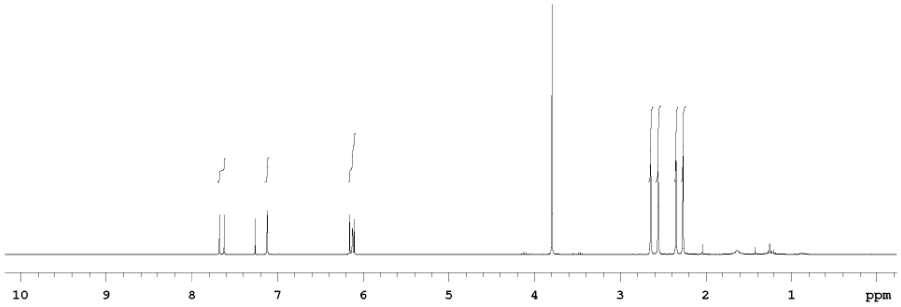
10
9
8
7
6
5
4
3
2
1
ppm

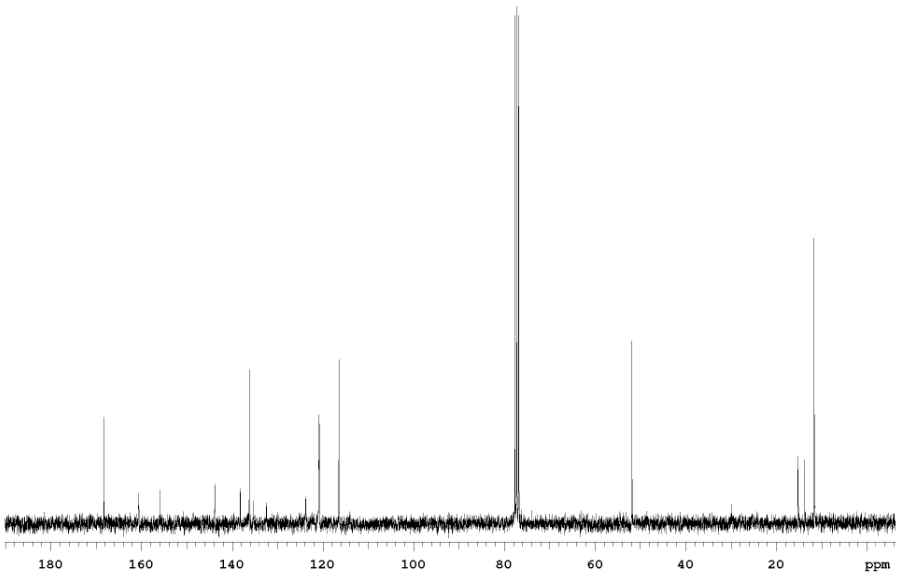
180
160
140
120
100
80
60
40
20
ppm

51a; R_f = 0.20 (60% hexanes/EtOAc); ^{1}H NMR (300 MHz, $CDCl_3$) δ 7.64 (d, 2H, J = 10 Hz), 7.25 (s, 1H), 6.18 (d, 2H, J = 10 Hz), 3.80 (s, 6H), 2.68 (s, 6H), 2.40 (s, 6H); ^{13}C NMR (125 MHz, $CDCl_3$) δ 167.9, 159.0, 140.4, 135.4, 133.8, 125.2, 121.6, 118.0, 52.0, 14.1, 11.7; MS (APCI) calcd for $C_{21}H_{23}BF_2N_2O_4$ 416.17 found 417.20 ($M+H^+$).

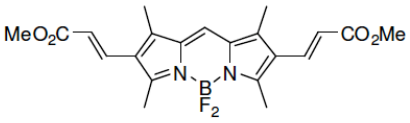
MeO2C
CO2Me
N
B
N
F2

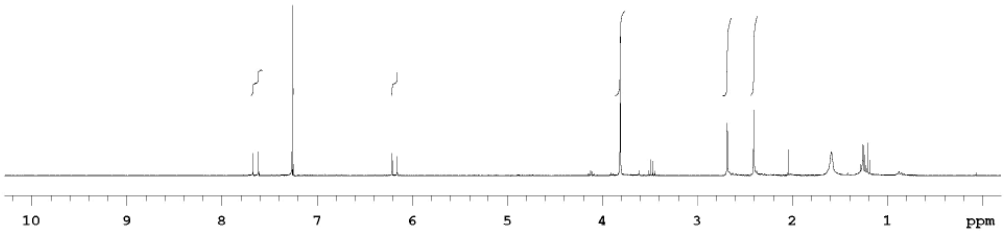
10
9
8
7
6
5
4
3
2
1
ppm

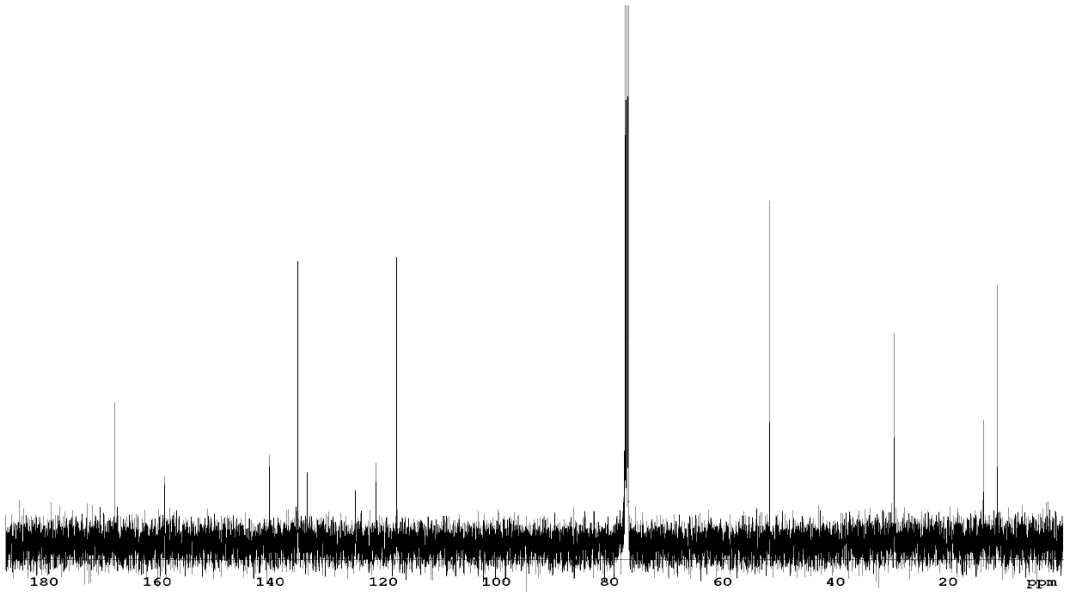
180
160
140
120
100
80
60
40
20
ppm

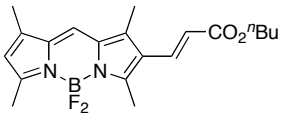

50b

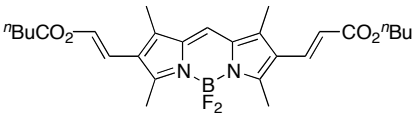

51b

Method A was followed. Reaction was carried out at 0.4 mmol scale. Crude mixture was subjected to flash column chromatography that provided **50b** (90% hexanes in ethyl acetate) in 61% (72 mg) and **51b** (75% hexanes in ethyl acetate) in 30% (56 mg) yields as orange solids: **50b**; R_f = 0.40 (60% hexanes/EtOAc); ^{1}H NMR (300 MHz, $CDCl_3$) δ 7.66 (d, 1H, *J* = 16 Hz), 7.14 (s, 1H), 6.13 (d, 1H, *J* = 16 Hz), 6.14 (s, 1H), 4.20 (t, 2H, *J* = 7 Hz), 2.65 (s, 3H), 2.56 (s, 3H), 2.37 (s, 3H), 2.28 (s, 3H), 1.63-1.71 (m, 2H), 1.39-1.48 (m, 2H), 0.97 (t, 3H, *J* = 7 Hz); ^{13}C NMR (75 MHz, $CDCl_3$) δ 167.7, 160.2, 155.8, 143.5, 138.0, 135.7, 135.0, 132.1, 123.6, 120.6, 120.5, 116.7, 64.5, 30.8, 29.7, 19.2, 14.9, 13.9, 13.7, 11.4; MS (ESI) calcd for $C_{20}H_{25}BF_2N_2O_2$ 374.20 found 381.21 ($M+Li^+$).

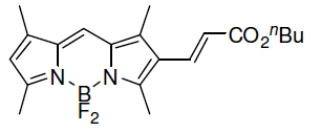
CO2nBu
N
B
F2
N

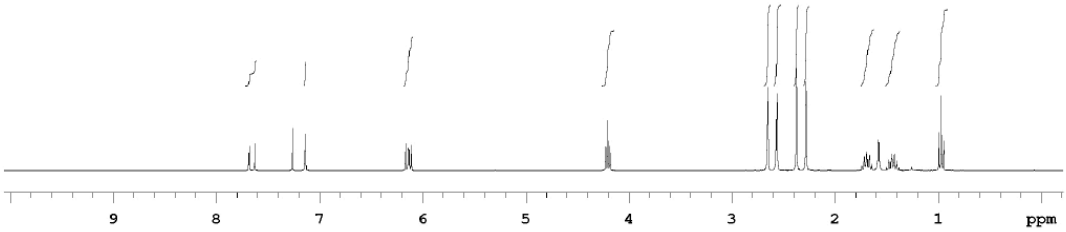
9
8
7
6
5
4
3
2
1
ppm

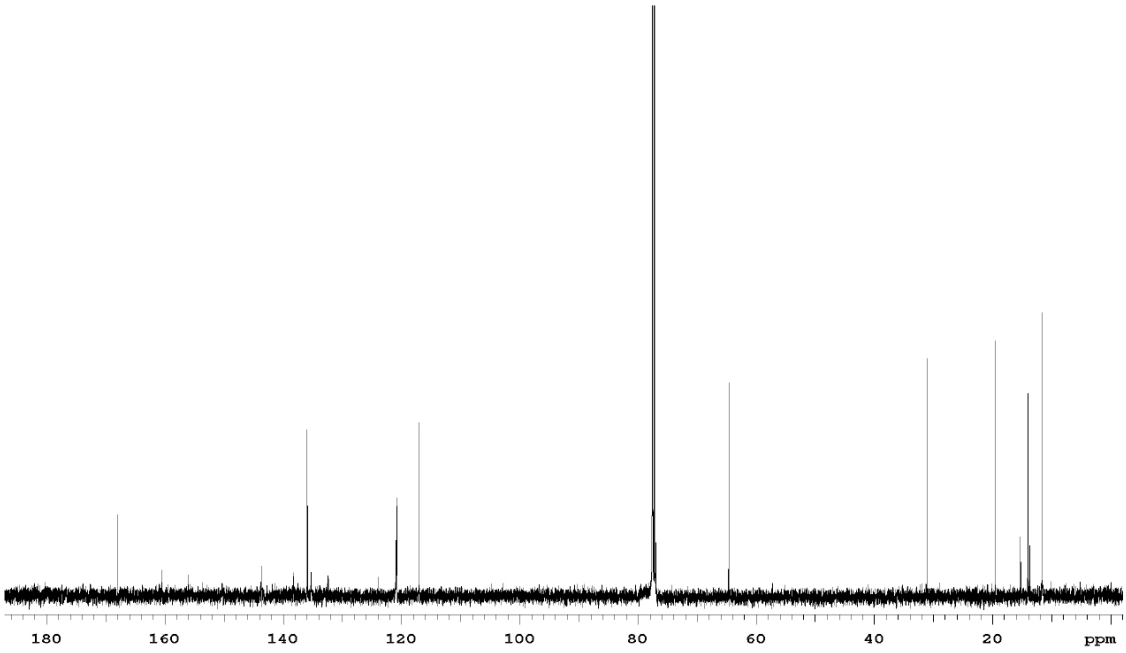
180
160
140
120
100
80
60
40
20
ppm

51b; R_f = 0.35 (75% hexanes/EtOAc); ^{1}H NMR (300 MHz, $CDCl_3$) δ 7.64 (d, 2H, J = 16 Hz), 7.26 (s, 1H), 6.18 (d, 2H, J = 16 Hz), 4.24 (t, 4H, J = 6.6 Hz), 2.69 (s, 6H), 2.40 (s, 6H), 1.63-1.78 (m, 4H), 1.39-1.48 (m, 4H), 0.97 (t, 6H, J = 7.5 Hz); ^{13}C NMR (125 MHz, $CDCl_3$) δ 167.4, 158.7, 140.1, 134.9, 133.5, 125.0, 121.3, 118.2, 64.50, 30.8, 19.2, 13.9, 13.8, 11.4; MS (APCI) calcd for $C_{15}H_{17}BF_2N_2O_3S$ 354.1 found 501.10 ($M\text{-}H^+$).

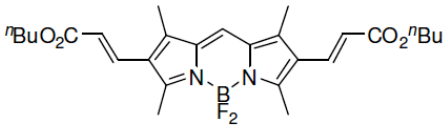
nBuO2C
CO2nBu
N
B
N
F2

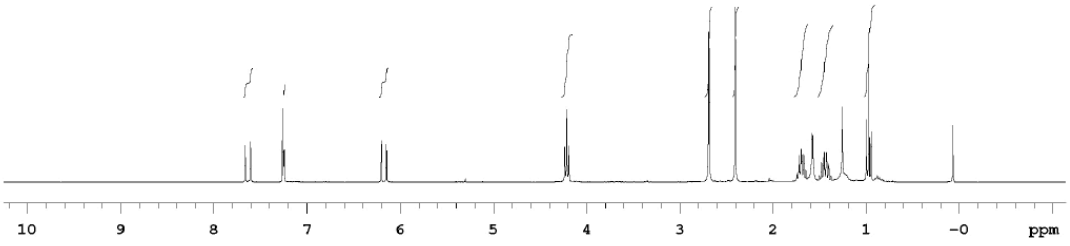
10
9
8
7
6
5
4
3
2
1
−0
ppm

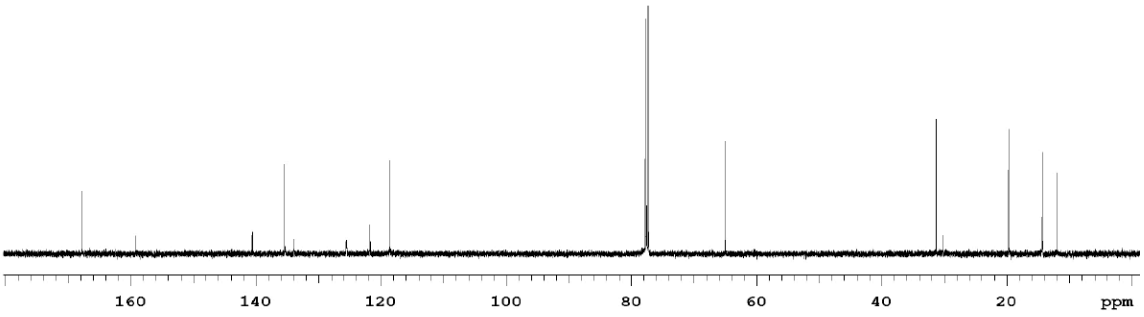
160
140
120
100
80
60
40
20
ppm

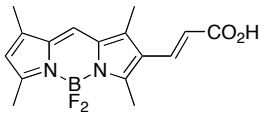

50c

Method A was followed. Reaction was carried out at 0.2 mmol scale. Crude mixture was subjected to flash column chromatography that provided **50c** (50% hexanes in ethyl acetate) in 29% (19 mg) as an orange solid: **50c**; R_f = 0.30 (50% hexanes/EtOAc); ^{1}H NMR (300 MHz, CD_3OD) δ 7.47 (d, 1H, J = 16.2 Hz), 7.27 (s, 1H), 6.20 (d, 1H, J = 16.2 Hz), 6.13 (s, 1H), 2.60 (s, 3H), 2.50 (s, 3H), 2.37 (s, 3H), 2.28 (s, 3H); ^{13}C NMR (75 MHz, CD_3OD) δ 172.7, 168.9, 158.5, 155.2, 143.0, 137.9, 134.3, 132.3, 124.1, 122.0, 120.6, 120.0, 13.7, 12.1, 10.2 (2C); MS (ESI) calcd for $C_{16}H_{17}BF_2N_2O_2$ 318.13 found 317.14 (M^+-H).

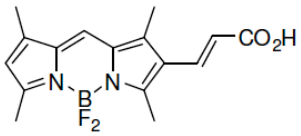
CO2H
N
B
F2
N

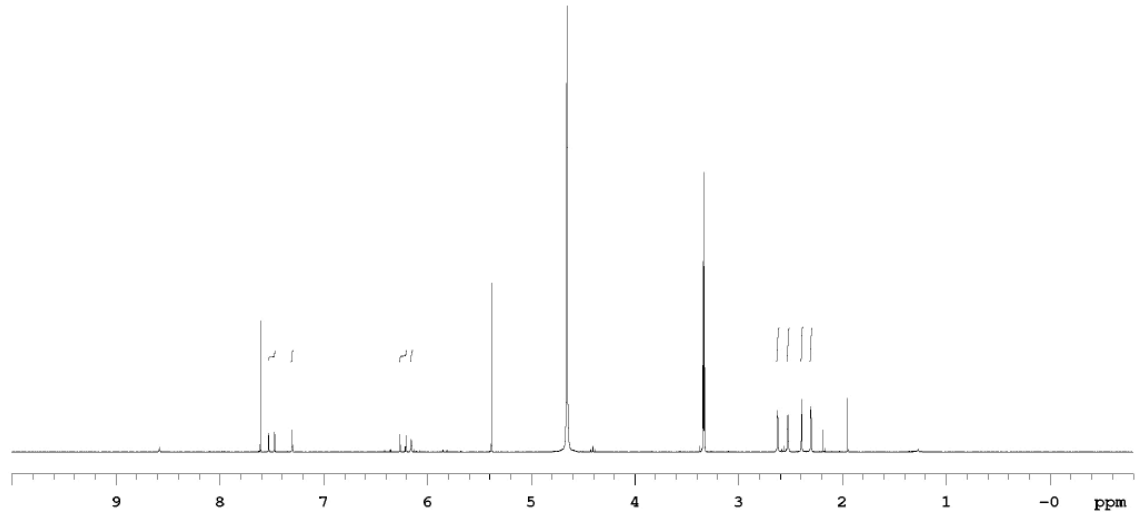
9
8
7
6
5
4
3
2
1
−0
ppm

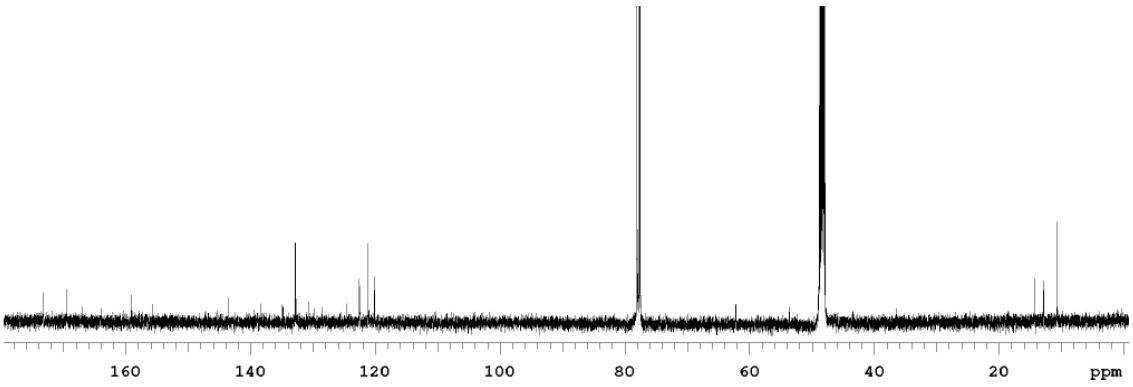
160
140
120
100
80
60
40
20
ppm

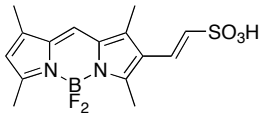

50d

Method B was followed. Crude mixture was subjected to flash column chromatography that provided **50d** (4% methanol in dichloromethane) in 2% (4 mg) an orange solid; ^{1}H NMR (300 MHz, CD_3OD_3) δ 7.52 (s, 1H), 7.23 (d, 1H, *J* = 18 Hz), 6.66 (d, 1H, *J* = 18 Hz), 6.21 (s, 1H), 2.57 (s, 3H), 2.55 (s, 3H), 2.40 (s, 3H), 2.32 (s, 3H); MS (ESI) calcd for $C_{15}H_{17}BF_2N_2O_3S$ 354.10 found 353.11 ($M\text{-}H^+$). ^{13}C could not be obtained due to small isolated quantity.

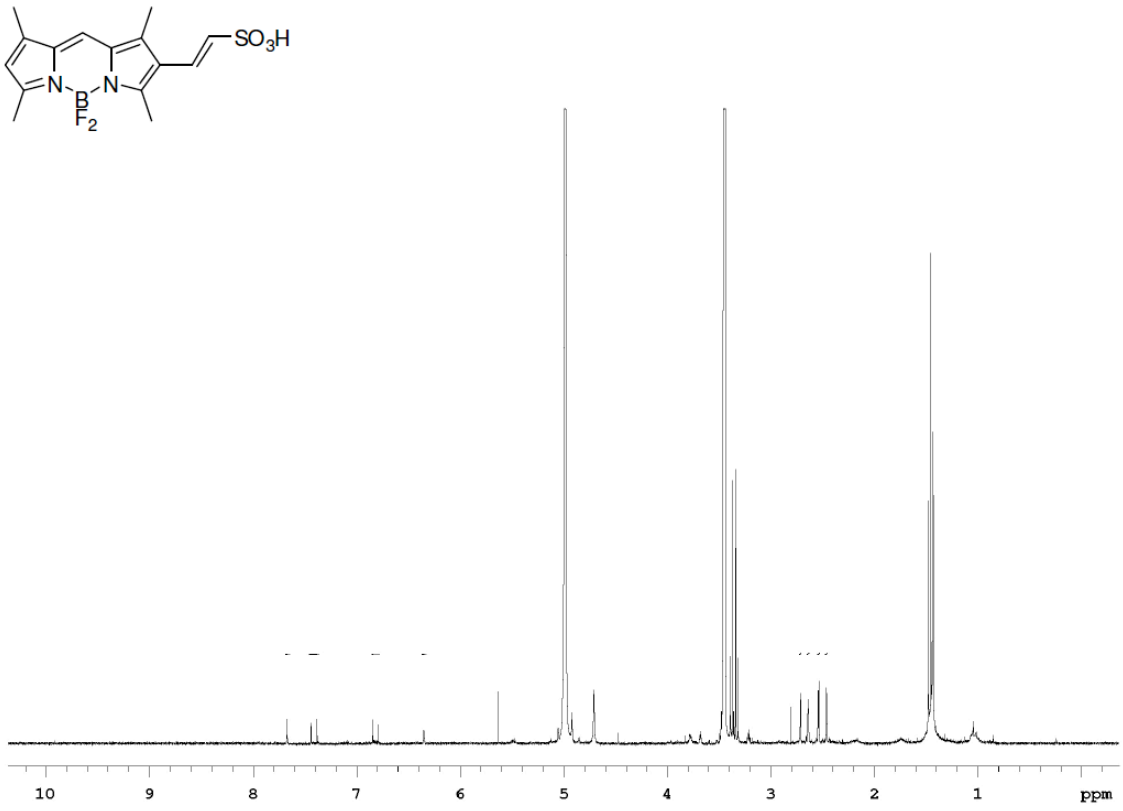
SO3H
N
B
F2
N
10
9
8
7
6
5
4
3
2
1
ppm

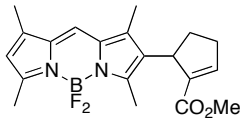

52e

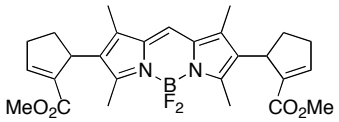

53e

Method A was followed. Reaction was carried out at 0.4 mmol scale. Crude mixture was subjected to flash column chromatography that provided **52e** (75% hexanes in ethyl acetate) in 7.3% (11 mg) and **53e** (75% hexanes in ethyl acetate) in 63% (126 mg) yields as orange solids: **52e**; R_f = 0.30 (75% hexanes/EtOAc); ^{1}H NMR (300 MHz, $CDCl_3$) δ 6.99 (s, 1H), 6.88 (s, 1H), 6.00 (s, 1H), 4.18-4.21 (m, 1H), 3.63 (s, 3H), 2.45-2.78 (m, 9H), 2.23 (s, 3H), 2.16 (s, 3H), 1.86-195 (m, 1H); ^{13}C NMR (125 MHz, $CDCl_3$) δ 165.2, 156.5, 155.6, 144.2, 140.3, 137.6, 133.1, 132.0, 127.9, 119.5, 118.6, (2C), 51.6, 40.6, 32.8, 30.7, 29.9, 14.7, 11.4, 9.8; MS (APCI) calcd for $C_{20}H_{23}BF_2N_2O_4$ 372.18 found 373.04 ($M+H^+$).

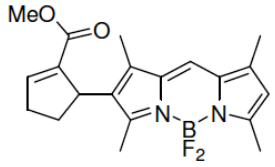
MeO
O
N
B
N
F2

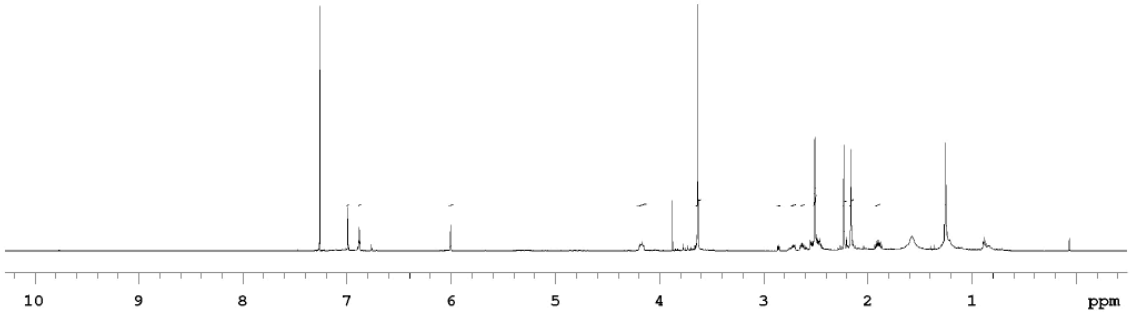
10
9
8
7
6
5
4
3
2
1
ppm

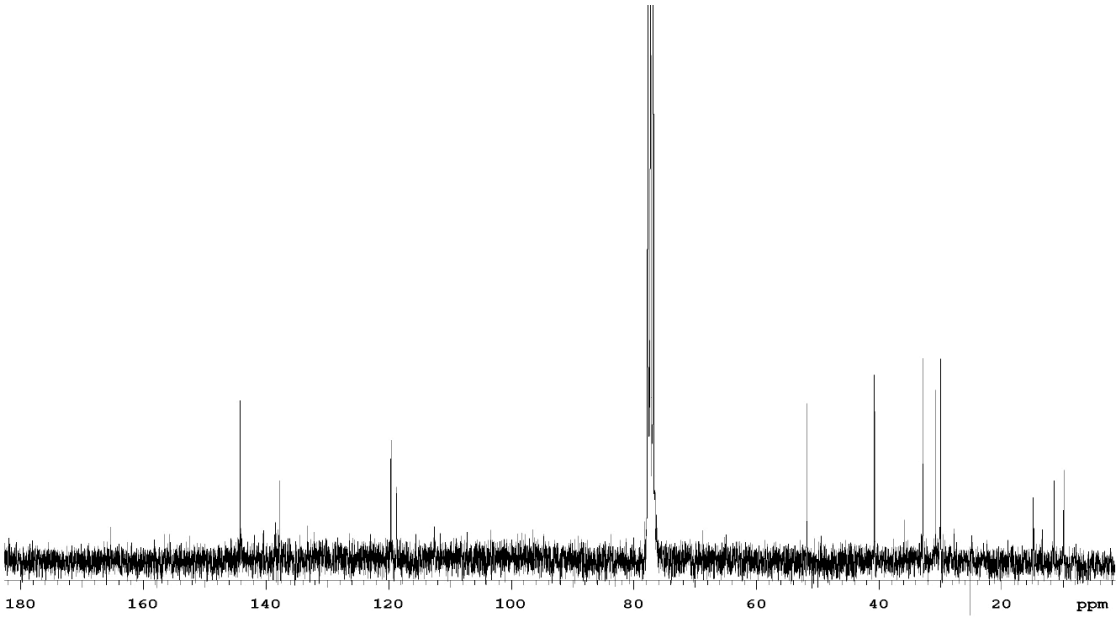
180
160
140
120
100
80
60
40
20
ppm

53e; R_f = 0.20 (75% hexanes/EtOAc); ^{1}H NMR (300 MHz, $CDCl_3$) δ 6.93 (s, 1H), 6.86 (dd, 2H, *J* = 2.4, 4.5Hz), 4.12-4.18 (m, 2H), 3.60 (s, 6H), 2.42-2.80 (m, 12H), 2.13 (s, 6H), 1.82-1.98 (m, 2H); ^{13}C NMR (125 MHz, $CDCl_3$) δ 165.3, 155.2, 144.1, 137.8, 137.2, 132.8, 131.5, 119.0, 51.6, 40.6, 32.8, 30.8, 13.2, 9.8; MS (APCI) calcd for $C_{27}H_{31}BF_2N_2O_4$ 496.23 found 497.98 ($M+H^+$).

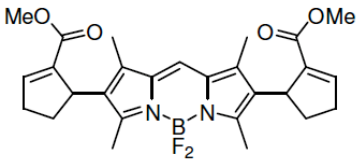
MeO
O
O
OMe
N
B
N
F2

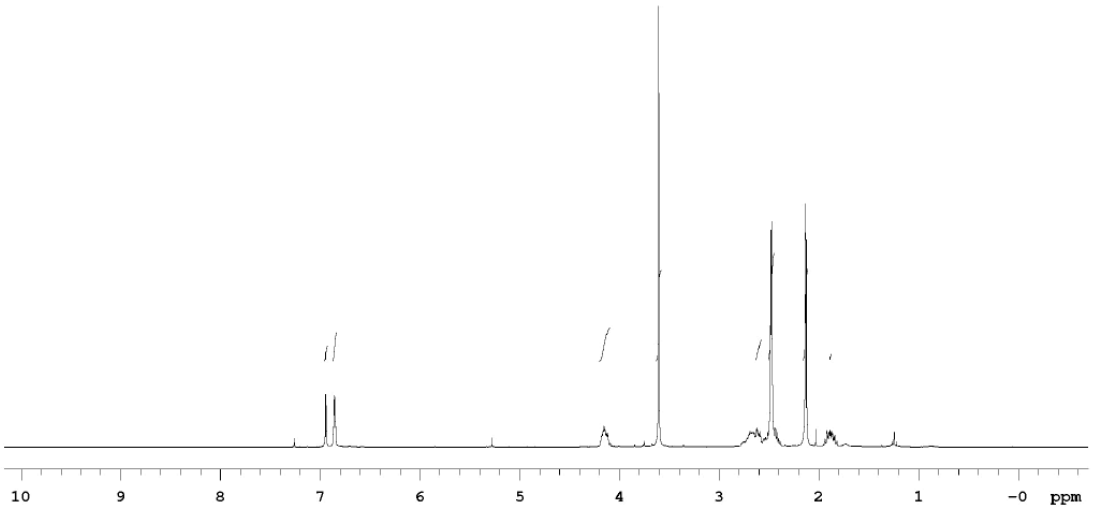
10
9
8
7
6
5
4
3
2
1
-0
ppm

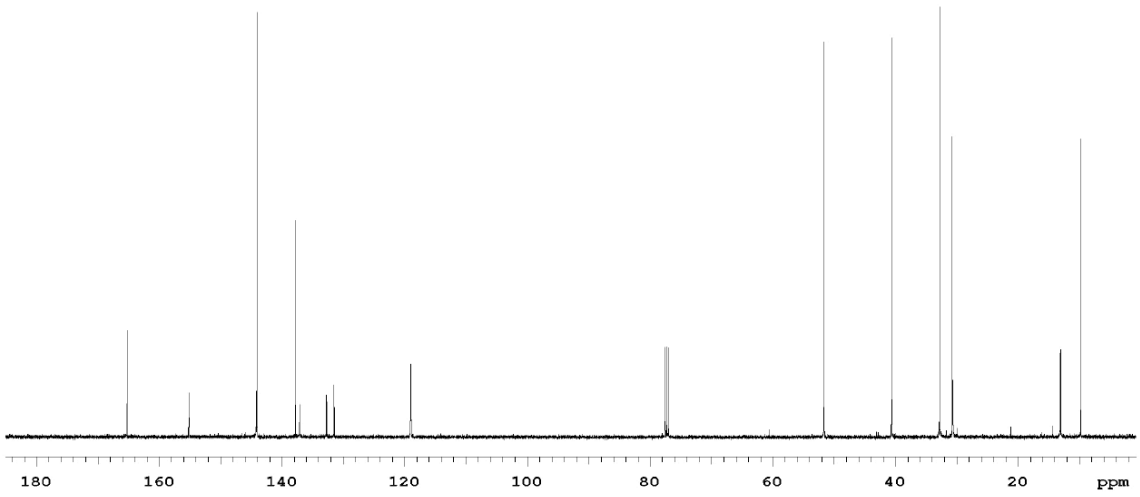
180
160
140
120
100
80
60
40
20
ppm

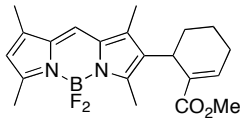

52f

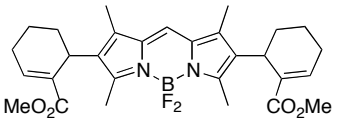

53f

Method C was followed. Crude mixture was subjected to flash column chromatography that provided **52f** (75% hexanes in ethyl acetate) in 35 % (54 mg) and **53f** (75% hexanes in ethyl acetate) in 21% (45 mg) yields as orange solids: **52f**; $R_f = 0.30$ (75% hexanes/EtOAc); ^{1}H NMR (300 MHz, $CDCl_3$) δ 7.06-7.08 (m, 1H), 6.97 (s, 1H), 6.00 (s, 1H), 3.75-3.83 (m, 1H), 3.60 (s, 3H), 2.51 (s, 6H), 2.29-2.30 (m, 2H), 2.21 (s, 3H), 2.15 (s, 3H), 1.82-1.91 (m, 2H), 1.60-1.79 (m, 2H); ^{13}C NMR (125 MHz, $CDCl_3$) δ 167.8, 156.6, 155.5, 140.4, 140.2, 137.8, 133.2, 133.0, 132.5, 132.2, 119.4, 118.5, 51.7, 32.1, 29.8, 25.9, 20.5, 14.7, 13.2, 11.4, 10.0; MS (APCI) calcd for $C_{21}H_{25}BF_2N_2O_4$ 386.20 found 387.01 ($M+H^+$).

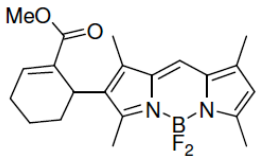
MeO
O
N
B
N
F2

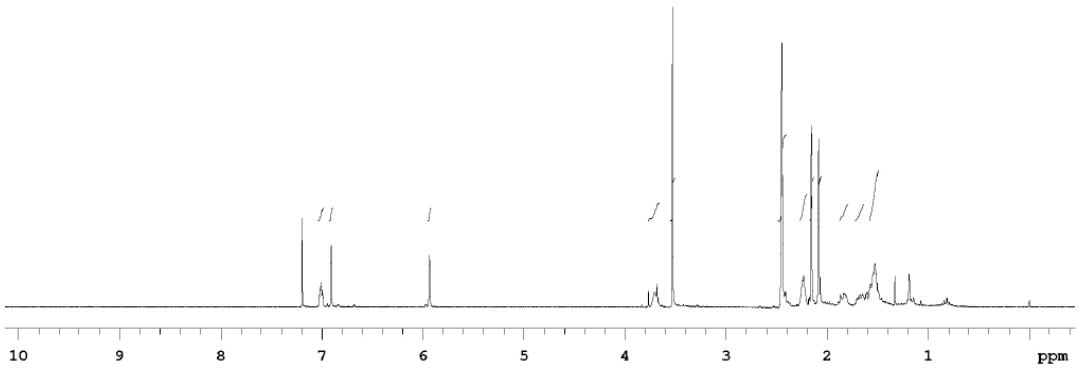
10
9
8
7
6
5
4
3
2
1
ppm

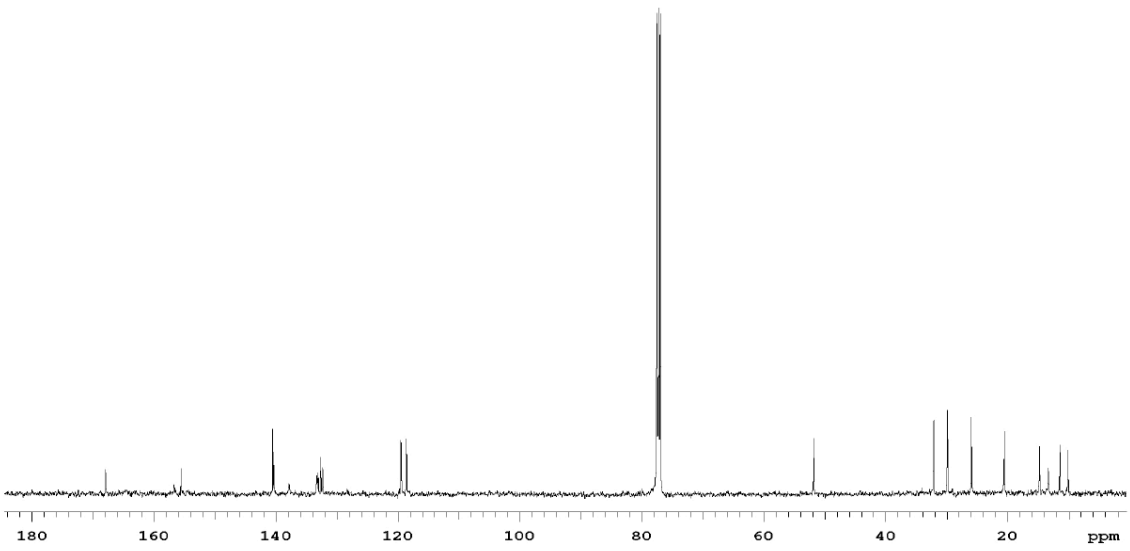
180
160
140
120
100
80
60
40
20
ppm

53f; R_f = 0.25 (75% hexanes/EtOAc); ^{1}H NMR (300 MHz, $CDCl_3$) δ 7.03-7.07 (m, 2H), 6.91 (s, 1H), 3.74-3.78 (m, 2H), 3.58 (s, 6H), 2.49 (s, 6H), 2.28-2.29 (m, 4H), 2.12 (s, 6H), 1.55-1.92 (m, 8H); ^{13}C NMR (125 MHz, $CDCl_3$) δ 167.9, 140.5, 140.2, 133.0, 132.5, 132.2, 119.5, 118.6, 51.8, 36.9, 32.2, 26.0, 20.6, 14.7, 11.5; MS (ESI) calcd for $C_{29}H_{35}BF_2N_2O_4$ 524.27 found 531.27 ($M+Li^+$).

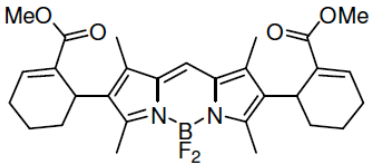
MeO
O
O
OMe
N
B
N
F2

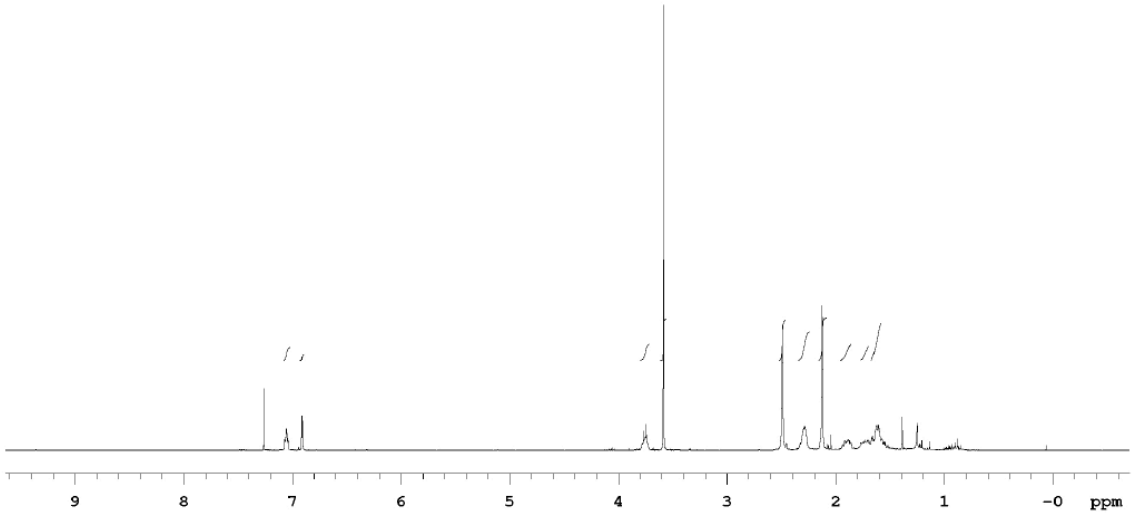
9
8
7
6
5
4
3
2
1
−0
ppm

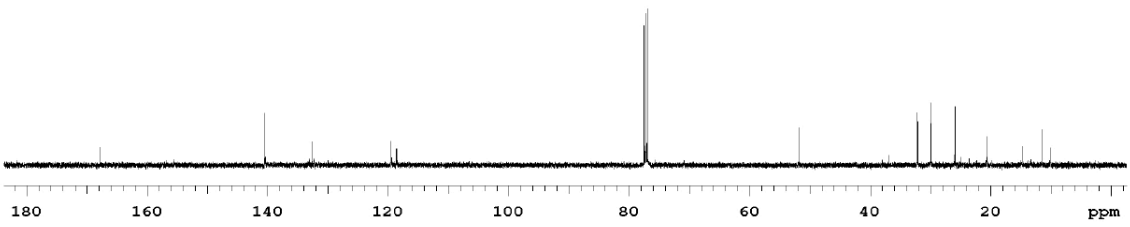
180
160
140
120
100
80
60
40
20
ppm

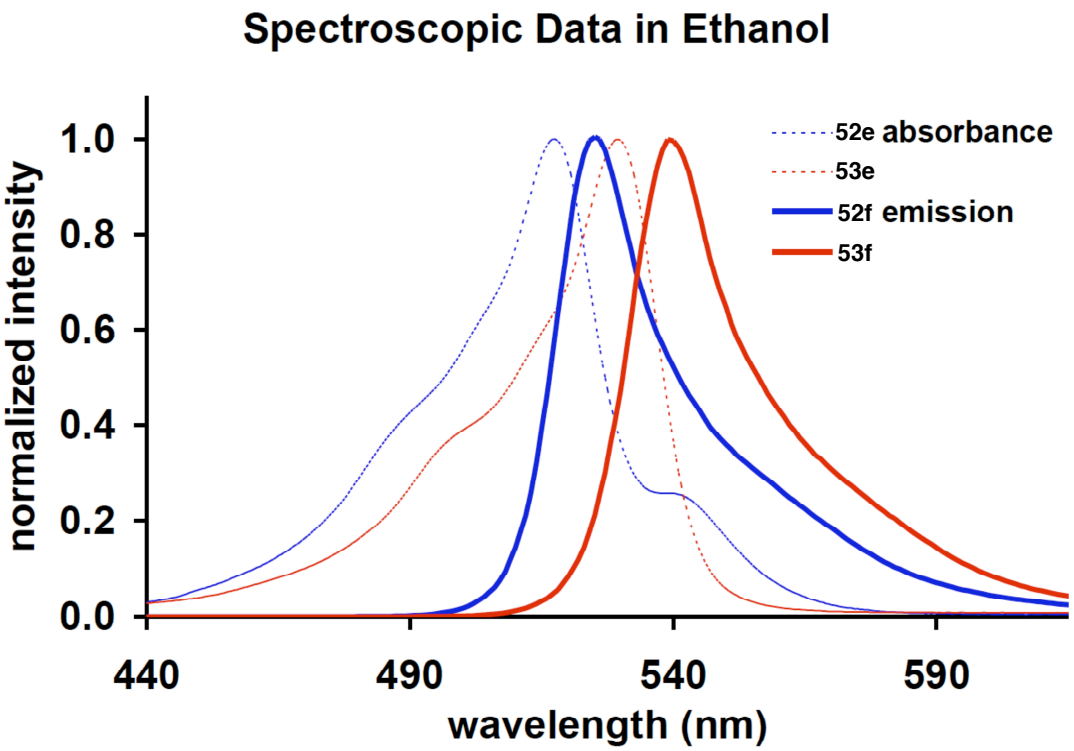
Spectroscopic Data in Ethanol
normalized intensity
1.0
0.8
0.6
0.4
0.2
0.0
440
490
540
590
wavelength (nm)
52e absorbance
53e
52f emission
53f

APPENDIX D

EXPERIMENTAL DATA FOR CHAPTER III

Scheme for Synthesis of Cassette 60

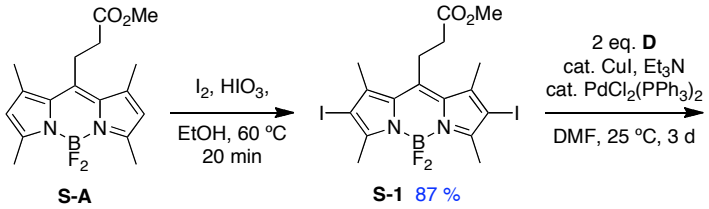

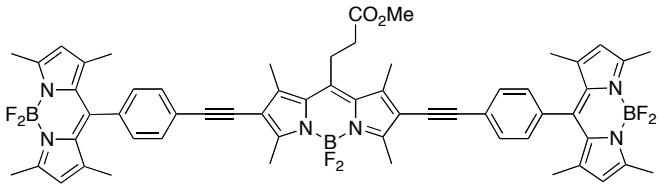

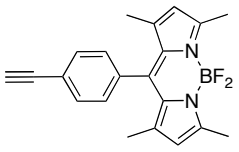

Synthesis and Characterization

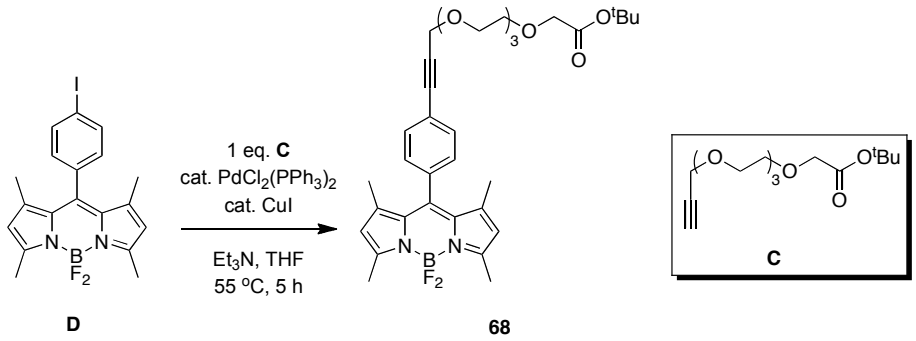

68; Iodophenyl BODIPY (**D**) (142 mg, 0.316 mmol), propargyltriethyleneglycylester **C** (100 mg, 0.331 mmol), $PdCl_2(PPh_3)_2$ (24 mg, 0.032 mmol), CuI (12 mg, 0.064 mmol), Et_3N (0.44 ml, 3.16 mmol) and 5 ml THF were added into a 50 mL round bottom flask. The solvent was degassed three times via the freeze-thaw method to remove oxygen, and then the reaction was heated to 55 ºC for 5 h under nitrogen. The reaction solvent was removed under reduced pressure. The crude product was purified by flash column chromatography eluting with 30 % hexane/ethyl acetate to give the desired product as an orange solid (151 mg, 77 %). ^{1}H NMR (300 MHz, $CDCl_3$), δ7.53 (d, J = 8.1, 2H), 7.20 (d, J = 8.1 Hz, 2H), 5.95 (s, 2H), 4.42 (s, 2H), 3.98 (s, 2H), 3.72-3.78 (m, 2H), 3.63-3.69 (m, 10H), 2.51 (s, 6H), 1.45 (s, 9H), 1.36 (s, 6 H) ^{13}C NMR (125 MHz, $CDCl_3$), δ169.5, 155.6, 142.8, 140.6, 135.0, 132.3, 131.0, 128.0, 123.4, 121.2, 86.5, 85.4, 81.4, 70.6, 70.5, 70.4, 70.3, 69.2, 68.9,59.0, 27.9, 14.4. MS (ESI) calcd for $C_{34}H_{43}BF_2N_2O_6$ $(M+H)^+$, 624.32, found 624.13. TLC (1:1 EtOAc/Hexane), R_f = 0.42.

^{1}H NMR of compound **68** ($CDCl_3$, 300 MHz)

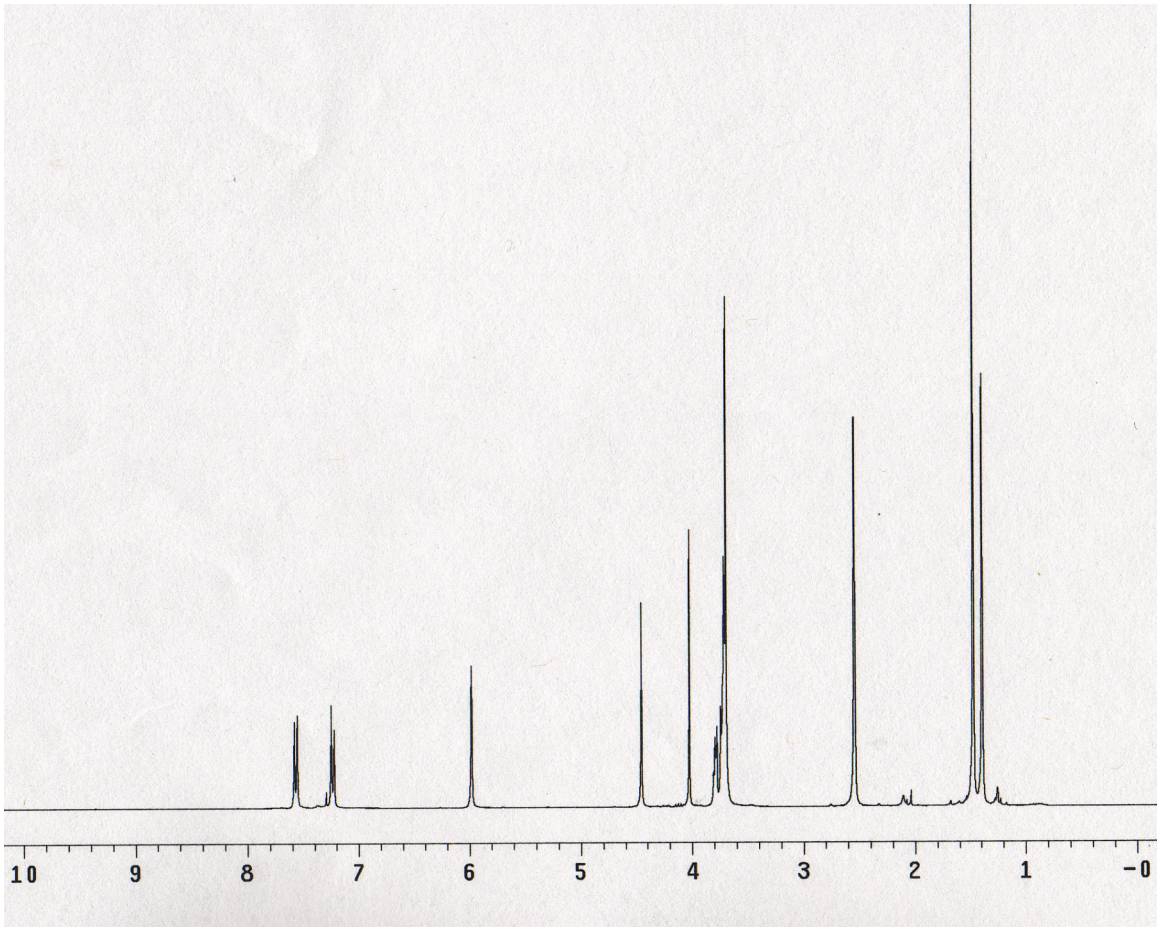

^{13}C NMR of compound **68** ($CDCl_3$, 125 MHz)

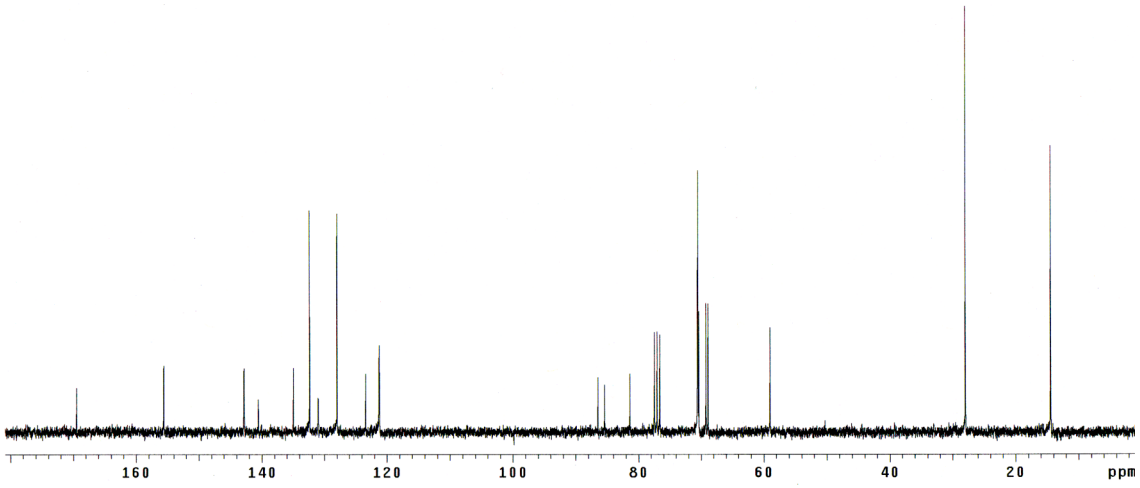

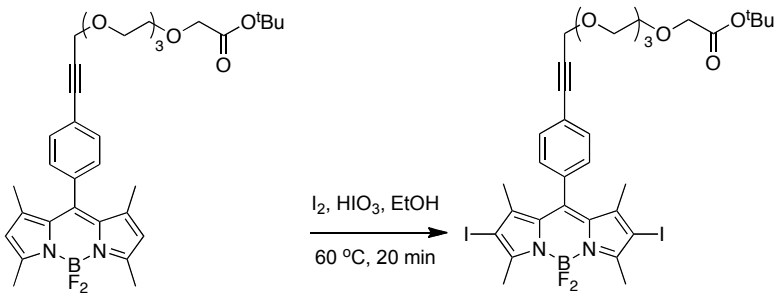

68 **69**

69; A mixture of **68** (104 mg, 0.165 mmol), I_2 (100 mg, 0.412 mmol), HIO_3 (58 mg, 0.33 mol) and 10 mL EtOH in a 50 mL flask were warmed up to 60 ºC for 20 min, and then it was cooled to 25 ºC. The reaction was quenched by addition of Na_2SO_3 (2 mL 1M). Water (20 mL) was added to the reaction mixture, and the product was extracted from water with CH_2Cl_2 (25 mL x 3). The combined organics were concentrated under reduced pressure, and the resulting crude product was purified by flash chromatography eluting with hexane and ethyl acetate (1:1) to give **69** (145 mg, 99%) as a red solid. ^{1}H NMR (300 MHz, $CDCl_3$), δ 7.60 (d, *J* = 8.4 Hz, 2H), 7.21 (d, *J* = 8.4 Hz, 2H), 4.47 (s, 2H), 4.02 (s, 2H), 3.78-3.81 (m, 2H), 3.70-3.75 (m, 10H), 2.64 (s, 6H), 1.47 (s, 9H), 1.40 (s, 6 H). ^{13}C NMR (125 MHz, $CDCl_3$), δ 169.9, 157.3, 145.4, 140.6, 135.0, 133.0, 131.3, 128.2, 124.4, 87.3, 86.1, 85.5, 81.8, 71.0, 70.9, 70.9, 70.8, 70.7, 69.7, 69.3, 59.4, 28.4, 17.4, 14.4. MS (MALDI) calcd for $C_{34}H_{41}BF_2N_2NaO_6^+$ $(M+Na)^+$, 899.10, found 898.91. TLC (1:1 EtOAc/Hexane), R_f = 0.45.

^{1}H NMR of compound **69** ($CDCl_3$, 300 MHz)

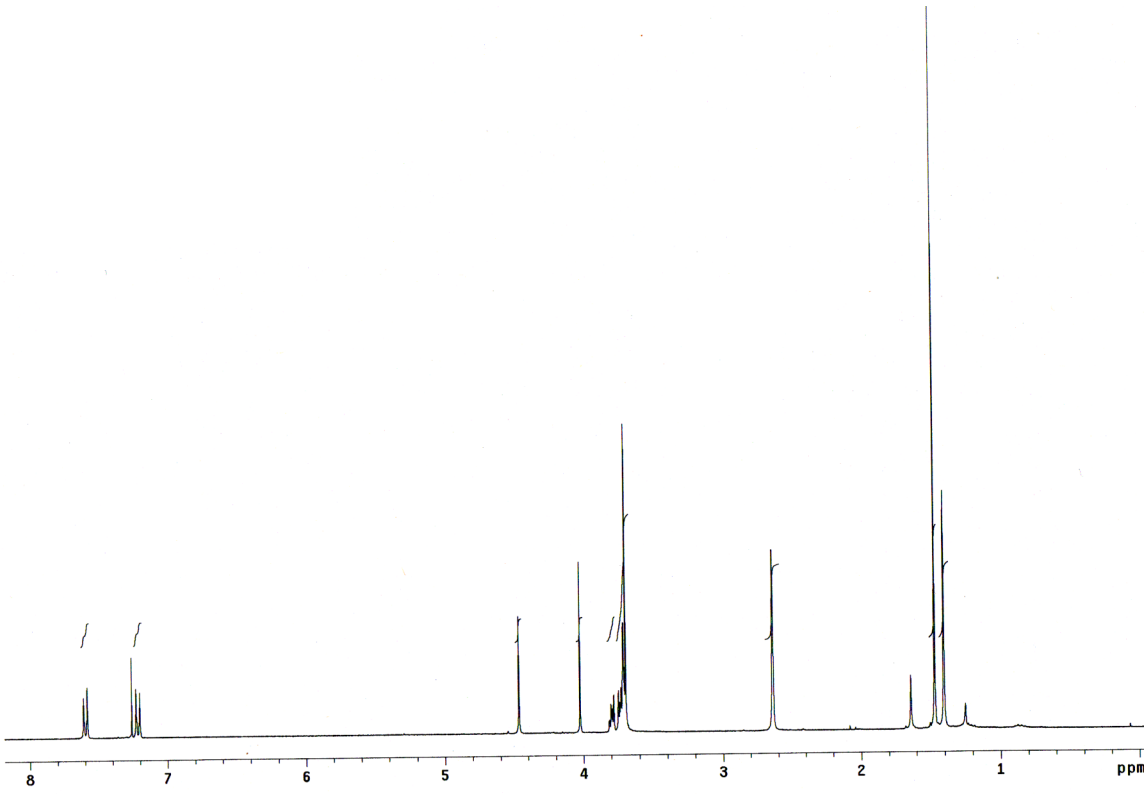

^{13}C NMR of compound **69** ($CDCl_3$, 125 MHz)

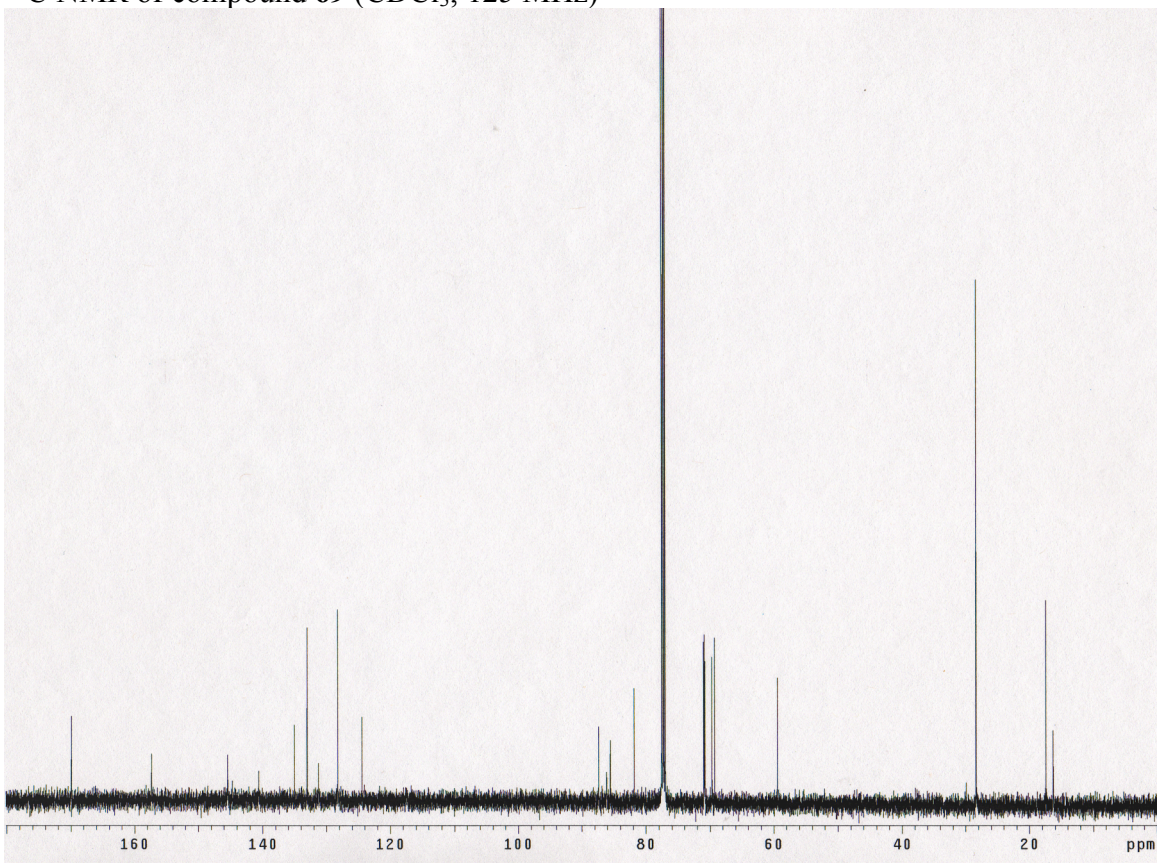

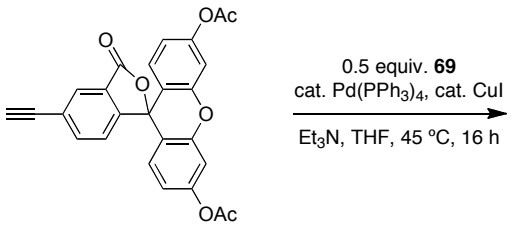

E

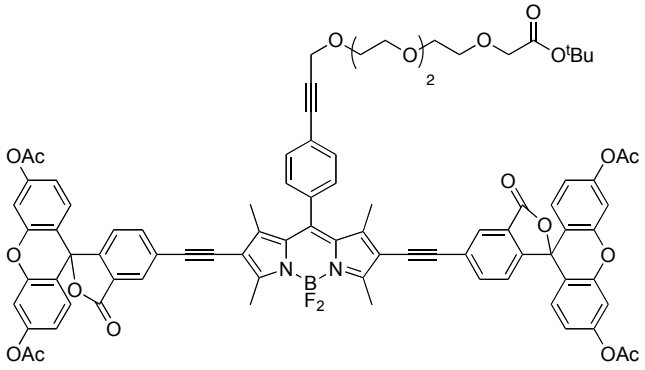

70

70; A mixture of **69** (65 mg, 0.074 mmol), diacetylfluorescein alkyne **E** [21] (82 mg, 0.186mmol), Et_3N (0.11 mL, 0.74 mmol), $Pd(PPh_3)_4$ (8 mg, 0.007 mmol), CuI (3 mg, 0.014 mmol) were dissolved in THF (2 mL). After the solution was degassed three times via the freeze-thawed method, the mixture was heated up to 45 ºC for 16 h. The reaction solvent was removed under reduced pressure and the crude product was purified by flash column eluting with 50% hexane:ethyl acetate to give the desired product as a light yellow solid (80 mg, 72%). ^{1}H NMR (500 MHz, $CDCl_3$), δ 8.08 (m, 2H), 7.73 (dd, J =8.0, 1.5 Hz, 2H), 7.65(d, *J* = 8.0 Hz, 2H), 7.29 (d, *J* = 8.5 Hz, 2H), 7.15 (d, J = 8.2 Hz, 2H), 7.10 (d, *J* = 2.0 Hz, 4H), 6.83 (bs, 4H), 6.83 (d, *J* = 2.0 Hz, 4H), 4.48 (s, 2H), 4.02 (s, 2H), 3.80-3.82 (m, 2H), 3.70-3.75 (m, 10H), 2.75 (s, 6H), 2.32 (s, 12H), 1.58 (s, 6H), 1.47(s, 9H). ^{13}C NMR (125 MHz, $CDCl_3$), δ 169.6, 168.8, 168.2, 159.1, 152.1,

151.8, 151.5, 144.6, 142.1, 137.9, 134.1, 132.8, 131.1, 128.9, 127.9, 127.7, 126.6, 125.8, 124.3, 124.2, 117.8, 116.0, 115.6, 110.5, 94.7, 87.2, 85.3, 84.1, 81.8, 81.5, 70.7, 70.6 (2 C), 70.5, 69.5, 69.0, 59.2, 28.1, 21.1, 13.8, 13.7 MALDI MS calcd for $C_{86}H_{71}BF_2N_2NaO_{20}^+$ $(M+Na)^+$ 1523.46, found 1523.26. TLC (1:1 EtOAc/Hexane), R_f = 0.20.

^{1}H NMR of compound **70** ($CDCl_3$, 500 MHz)

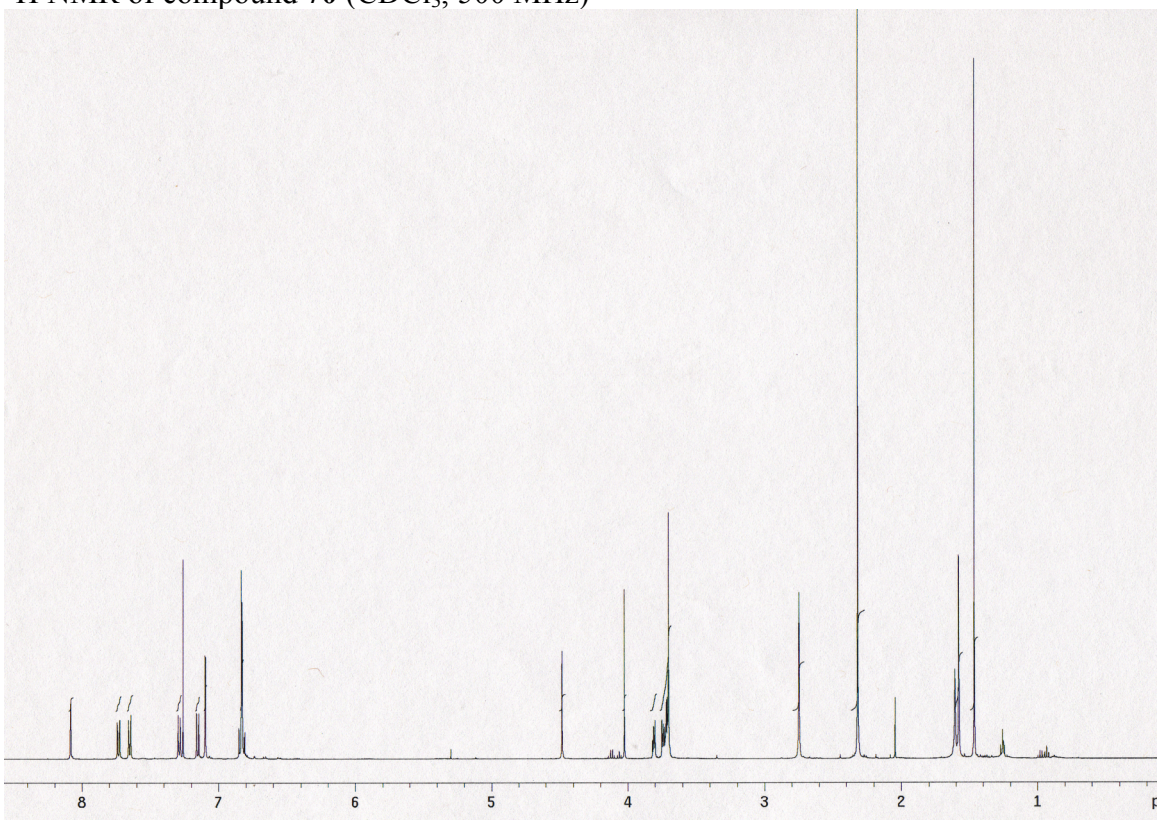

^{13}C NMR of compound **70** ($CDCl_3$, 125 MHz)

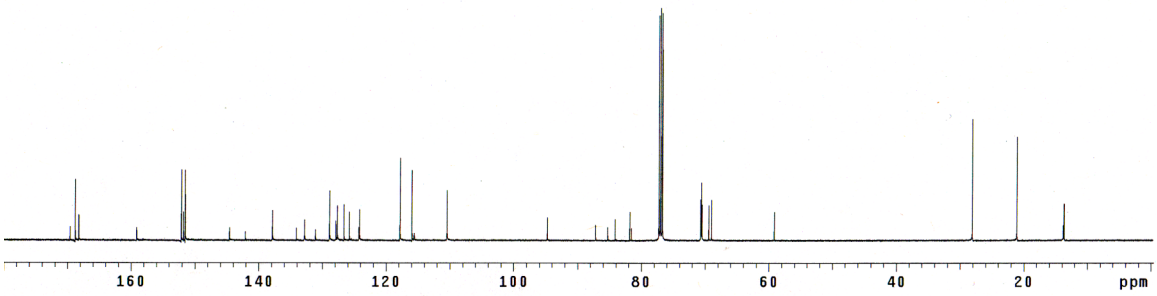

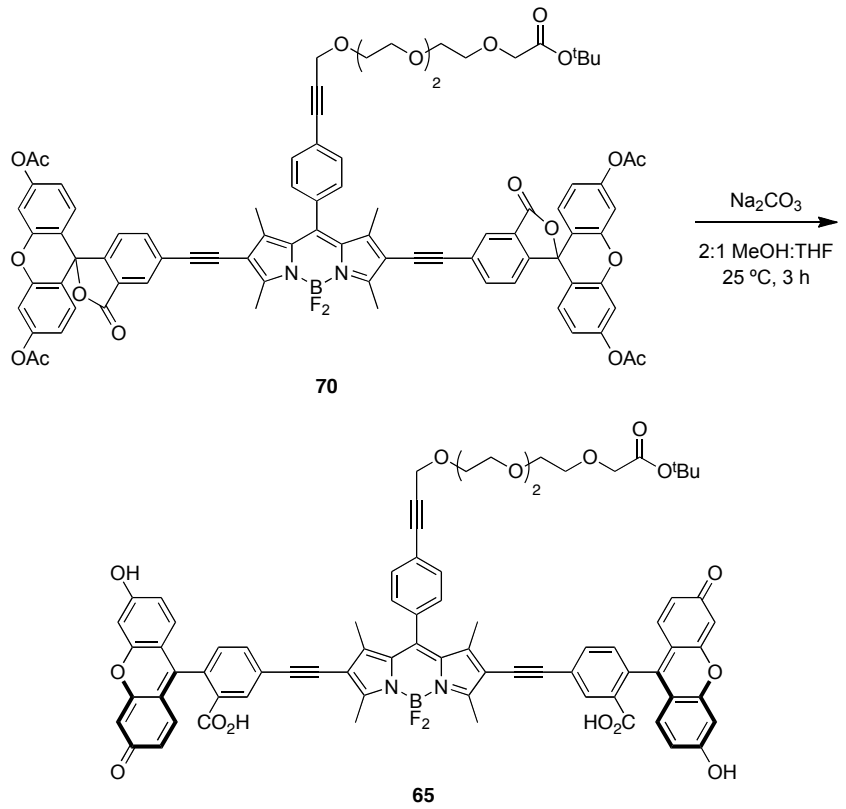

65; To **70** (12 mg, 0.01 mmol) in 5 mL 2:1 methanol/THF in was added Na_2CO_3 (3.5 mg, 0.03 mmol). The mixture was stirred for 3 h at 25 ºC under N_2. The reaction was quenched by adding aqueous HCl (0.1M, 10 mL) and the product was extracted out of the solution with 75% CH_2Cl_2:^{i}PrOH (5 mL x 3). The organic layers were washed with brine solution (10 mL) and dried with magnesium sulfate. The desired product was isolated as a purple solid (10 mg, 99 %). ^{1}H NMR (500 MHz, 75% CD_3OD:$CDCl_3$), δ 8.00 (s, 2H), 7.74 (dd, *J* = 8.0 Hz, 1.5 Hz, 2H), 7.65 (d, *J* = 7.5Hz, 2H), 7.33 (d, *J* = 8.5 Hz, 2H), 7.15 (d, *J* = 8.0 Hz, 2H), 6.67 (d, *J* = 2.5 Hz 4H), 6.59 (d, *J* = 8.0 Hz, 4H), 6.51 (dd, *J* = 9.0 Hz, 2.5 Hz, 4H), 4.47 (s, 2H), 4.00 (s, 2H), 3.79-3.81 (m, 2H), 3.71-3.73 (m,

2H), 3.66-3.69 (m, 8H), 2.71 (s, 6H), 1.58 (s, 6H), 1.44 (s, 9H), ^{13}C NMR (125 MHz, 75% CD_3OD:CDCl3), δ 170.9, 170.1, 169.8, 159.5, 153.5, 145.2, 142.9, 138.3, 134.8, 133.4, 131.7, 131.2, 129.6, 128.7, 128.5, 128.0, 126.1, 125.9, 124.9, 116.3, 110.3, 108.2, 103.3, 95.6, 87.4, 86.0, 84.1, 82.7, 71.0, 70.9 (2 C), 70.8 (2 C), 69.7, 69.3, 59.5, 30.2, 28.3, 14.0. MS (MALDI) calcd for $C_{78}H_{63}BF2N_2O_{16}^+$ $(M+H)^+$ 1333.42, found 1333.44.

^{1}H NMR of 65 (1:2 $CDCl_3/CD_3OD$)

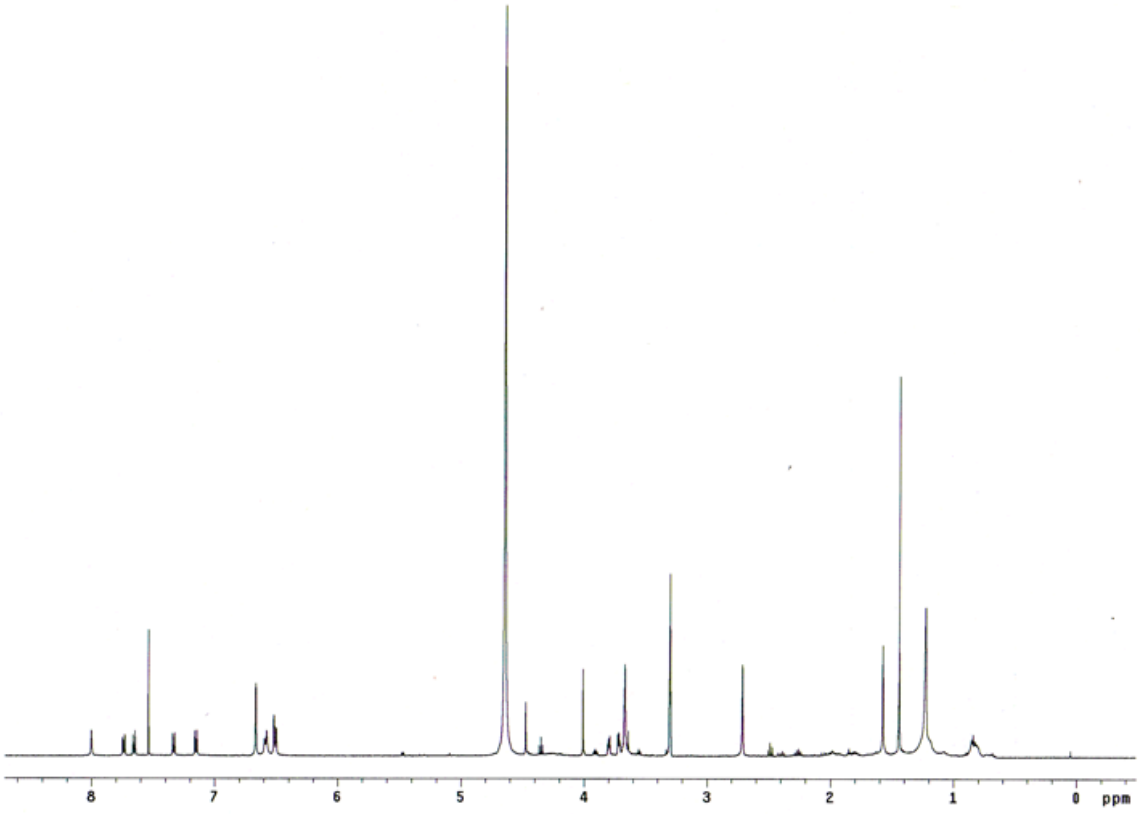

^{13}C NMR of 65 (1:2 $CDCl_3/CD_3OD$)

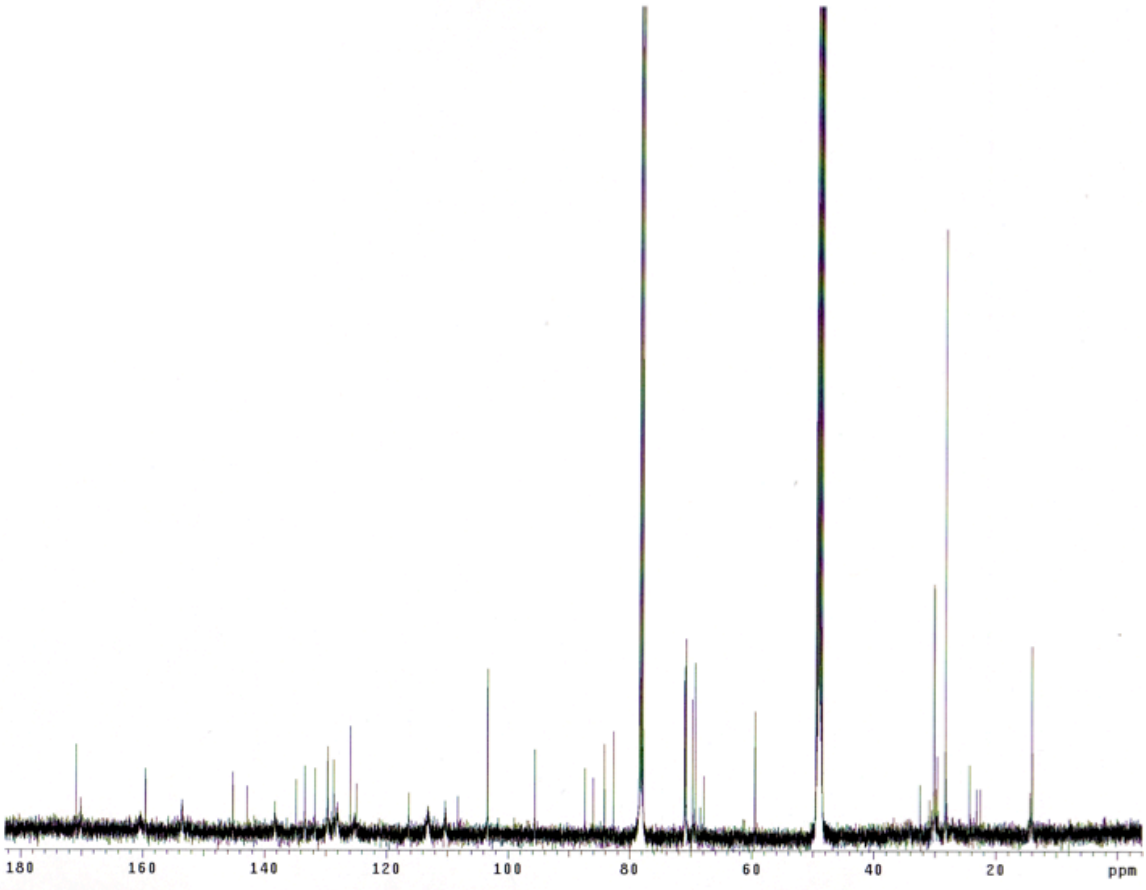

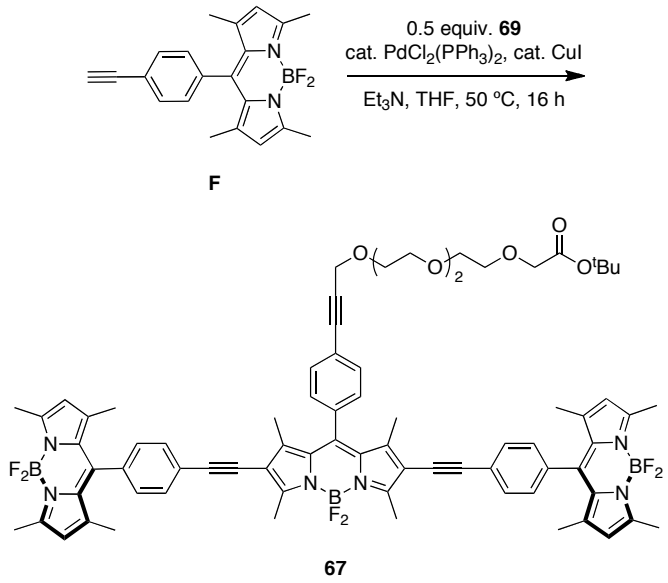

67; A mixture of **69** (80 mg, 0.09 mmol), **F**[29] (69 mg, 0.20 mmol), Et_3N (0.13 mL, 0.91 mmol), $PdCl_2(PPh_3)_2$ (6 mg, 0.01 mmol), CuI (4 mg, 0.01 mmol) were dissolved in 3.0 mL THF. The solution was degassed three times via the freeze-thaw method and the mixture was heated to 50 °C for 16 h under N_2. The reaction solvent was removed under reduced pressure and the crude product was purified via flash silica column eluting with 67% hexane:ethyl acetate to give the desired product as a purple solid (89 mg, 74 %). ^{1}H NMR (500 MHz, $CDCl_3$), δ 7.64 (d, *J* = 8.0 Hz, 2H), 7.59 (d, J =8.0 Hz, 4H), 7.29 (d, *J* = 8.5 Hz, 2H), 7.27 (d, *J* = 8.0 Hz, 4H), 5.99 (s, 4H), 4.48 (s, 2H), 4.02 (s, 2H), 3.80-3.82 (m, 2H), 3.70-3.75 (m, 10H), 2.76 (s, 6H), 2.55 (s, 12H), 1.58 (s, 6H), 1.47(s, 9H), 1.43 (s, 12H), ^{13}C NMR (125 MHz, $CDCl_3$), δ 169.6, 158.9, 155.7, 144.1, 143.0, 141.7, 140.7, 134.8, 134.3, 132.8, 131.9, 131.2, 128.2 (2 C), 128.0, 124.1 (2 C), 121.3, 116.0, 96.0, 87.1, 85.3, 82.9, 81.6, 70.7, 70.6 (3 C), 70.5, 69.5, 69.0, 59.2, 28.1, 14.6 (2 C),

14.6, 13.7. MALDI HRMS calcd for $C_{76}H_{77}B_3F_6N_6O_6^+$ ($M^{\bullet+}$) 1316.6113, found 1316.6172.

^{1}H NMR of 67 ($CDCl_3$)

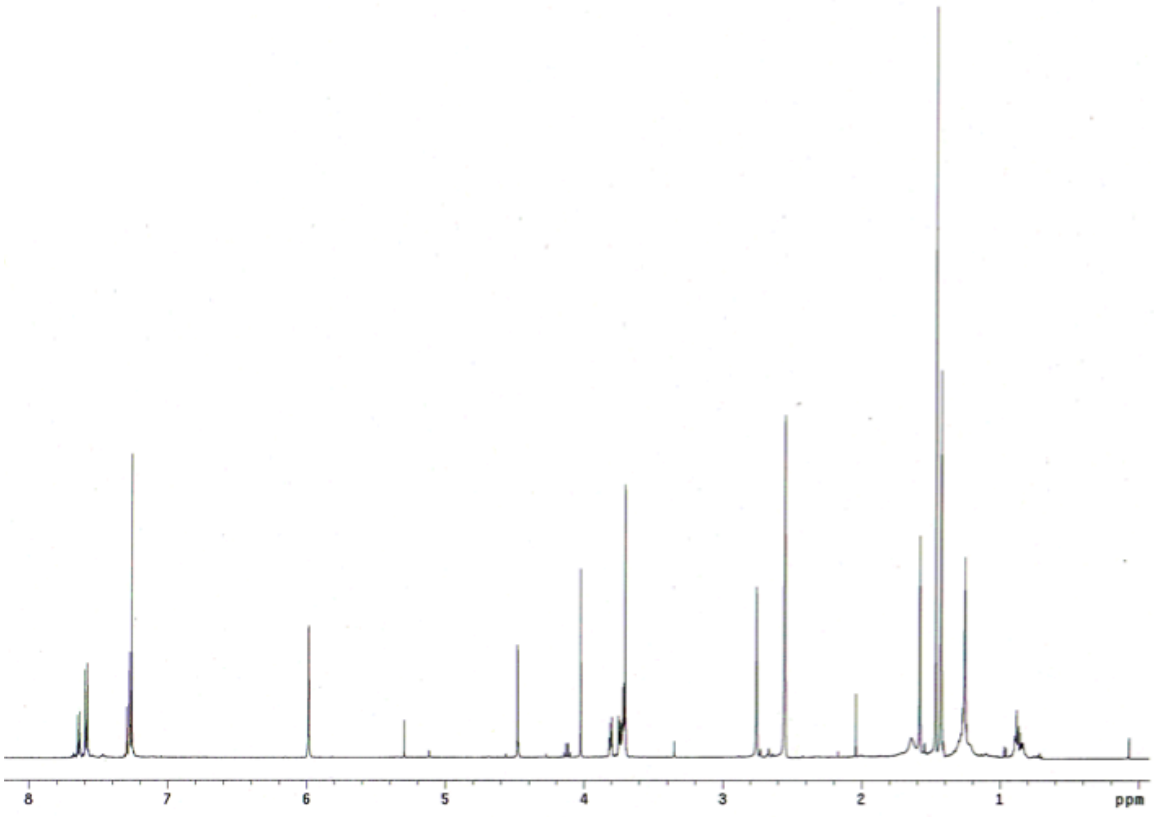

^{13}C NMR of 67 ($CDCl_3$)

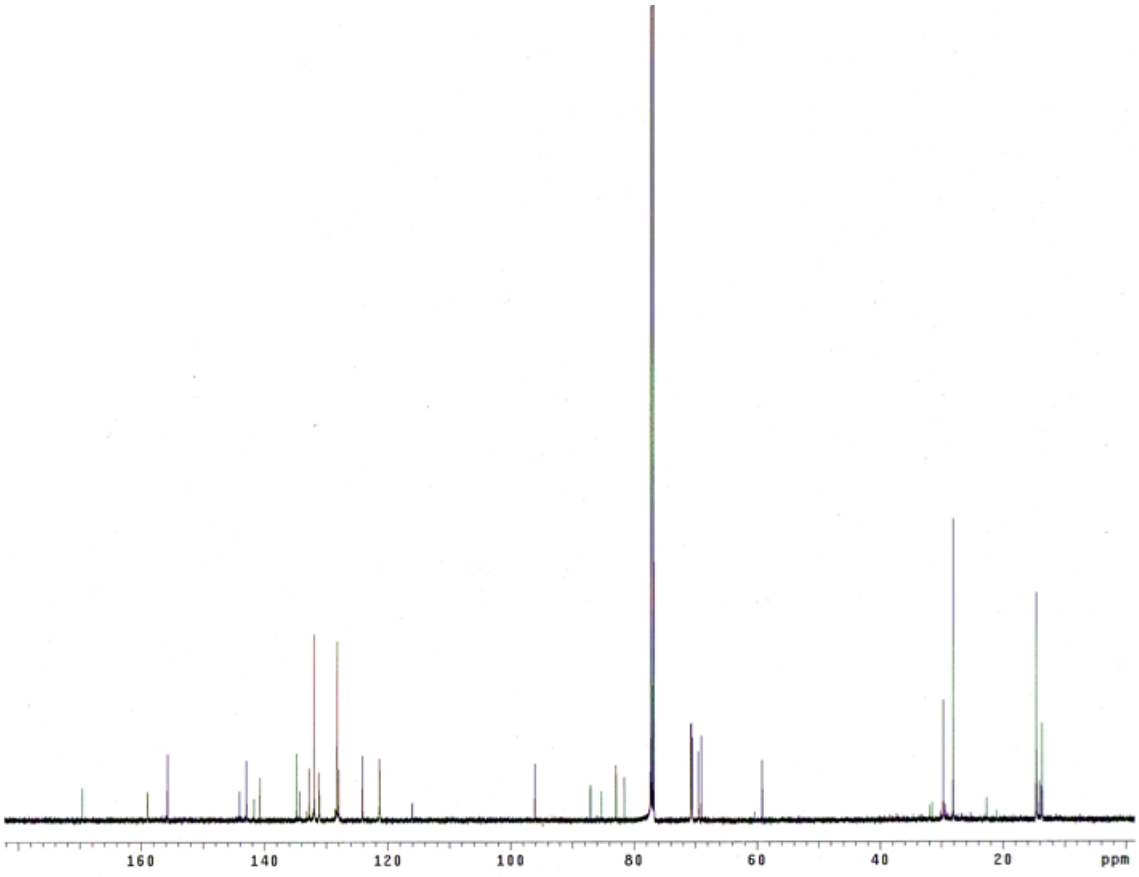

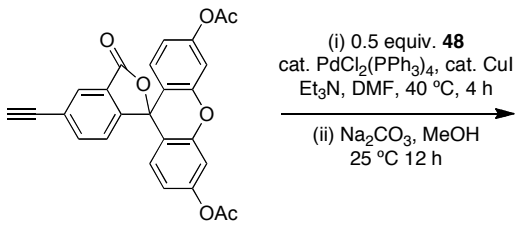

E

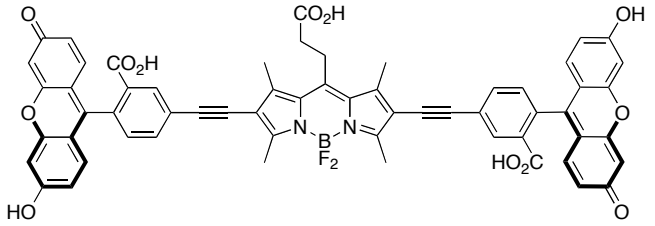

66

66; A mixture of **48** (30 mg, 0.05 mmol), **E**[21] (55 mg, 0.13 mmol), Et_3N (0.30 mL, 2.1 mmol), $PdCl_2(PPh_3)_2$ (5 mg, 0.01 mmol), and CuI (2 mg, 0.01 mmol) were dissolved in 1.0 mL DMF under N_2. The solution was degassed three times via the freeze-thaw method and then stirred at 40 ºC for 4 h and then at 25 ºC for 12 h under N_2. The solvent was removed under reduced pressure and the crude product partially purified via flash silica column eluting with 7 % methanol:CH_2Cl_2 to give the acetate protected form of **66** as a purple solid (15 mg).

The product from above (15 mg) was treated with sodium carbonate (6 mg, .05 mmol) in 5.0 mL of methanol. The mixture was stirred at 25 ºC for 3 h. The solvent was removed under reduced pressure and extraction was performed using CH_2Cl_2 and 0.1 M HCl aqueous solution. The aqueous layer was washed with CH_2Cl_2 (2 x 5 mL) and the organic fractions were combined and dried over magnesium sulfate. The solvent was then removed under reduced pressure and purified via C-18 preparative HPLC eluting with a 50 – 95 % MeOH and 0.1 % TFA/water linear gradient over 25 min to give the

desired product with a retention time of 18 min as a purple solid (2 mg, 4 %). ^{1}H NMR (500 MHz, CD_3OD), δ 8.08 (s, 2H), 7.87 (d, J = 8.0 Hz, 2H), 7.23 (d, J = 8.0 Hz, 2H), 6.70 (s, 4H), 6.67 (d, J = 8.5 Hz, 4H), 6.58 (d, J = 7.5 Hz, 4H), 3.45 (m, 2H), 3.12 (m, 2H), 2.70 (s, 6H), 2.68 (s, 6H) MALDI HRMS calcd for $C_{60}H_{37}BF_2N_2O_{12}$ $(M\text{-}2H/2)^{-2}$ 513.6243, found 513.6244 TLC (5 % MeOH :CH_2Cl_2) R_f = 0.20.

^{1}H NMR of 66 (CD_3OD)

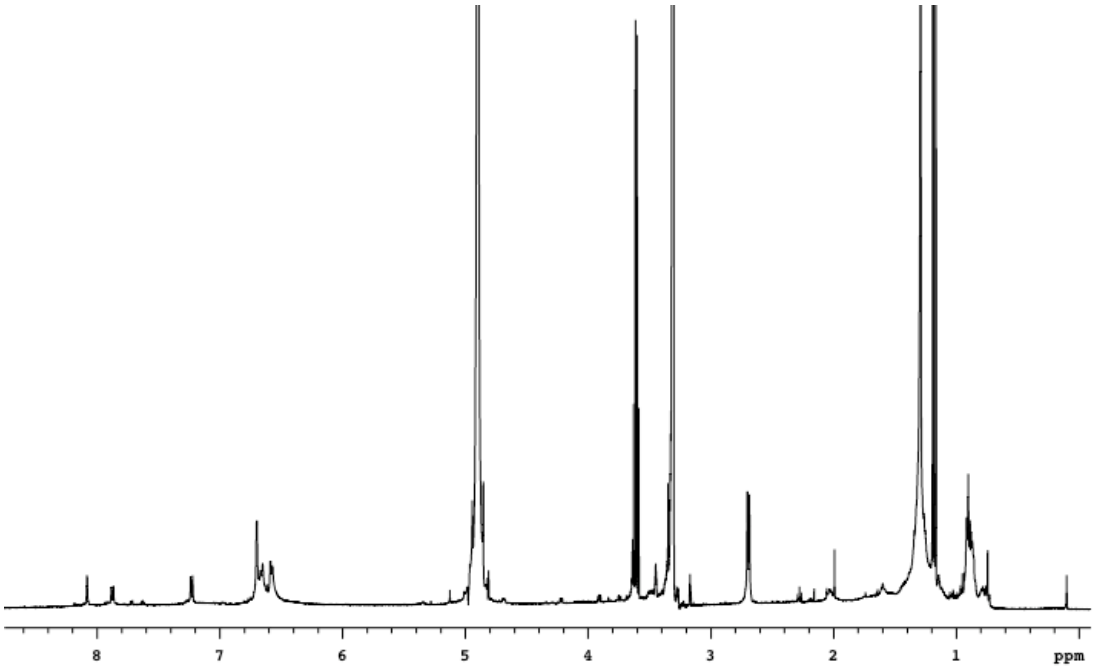

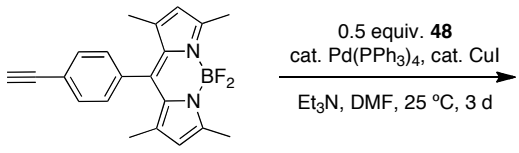

F

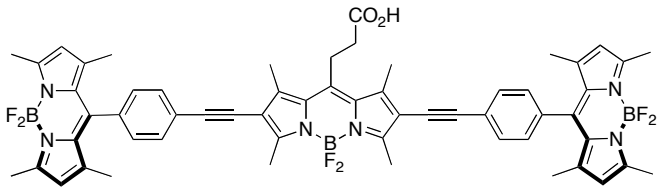

64

64; A mixture of **48** (30 mg, 0.05 mmol), **F**[29] (47 mg, 0.14 mmol), Et_3N (0.29 mL, 2.1 mmol), $Pd(PPh_3)_4$ (8 mg, 0.01 mmol), and CuI (2 mg, 0.01 mmol) were dissolved in 1.5 mL DMF under N_2. The solution was degassed three times via the freeze-thaw method and then stirred for 3 d at 25 ºC under N_2. The solvent was removed under reduced pressure and the crude product was purified via flash silica column eluting with 3 % methanol:CH_2Cl_2 followed by recrystalization from methanol to give the desired product as a purple solid (28 mg, 53%). ^{1}H NMR (300 MHz, $CDCl_3$), δ 7.65 (d, J = 8.5 Hz, 4H), 7.30 (d, J = 8.0 Hz, 4H), 6.00 (s, 4H), 3.78 (bs, 1H), 3.46 (m, 2H), 2.73 (s, 6H), 2.70 (m, 2H), 2.66 (s, 6H), 2.56 (s, 12H), 1.45 (s, 12H), ^{13}C NMR (125 MHz, $CDCl_3$), δ 158.2, 155.9, 143.1, 141.5, 140.9, 135.1 (2 C), 132.1, 131.3, 128.4, 124.2, 121.5, 116.6, 96.4, 83.1, 29.8, 15.5 (2 C), 14.8 (2 C), 13.9. MALDI HRMS calcd for $C_{58}H_{53}B_3F_6N_6O_2$ ($M^{\bullet-}$) 1012.4434, found 1012.4472. TLC (1:1 EtOAc:Hexane) R_f = 0.30.

^{1}H NMR of 64 ($CDCl_3$)

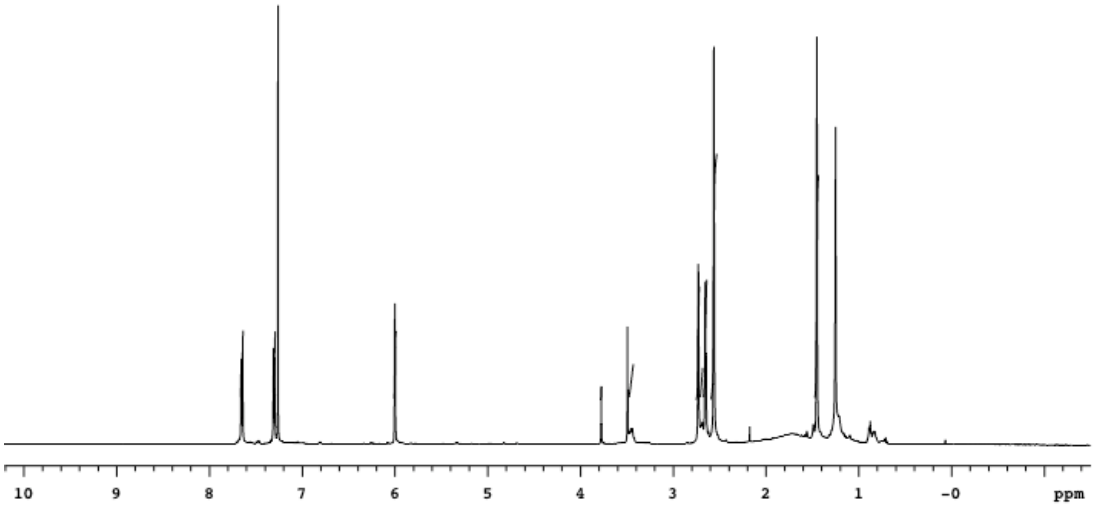

^{13}C NMR of 64 ($CDCl_3$)

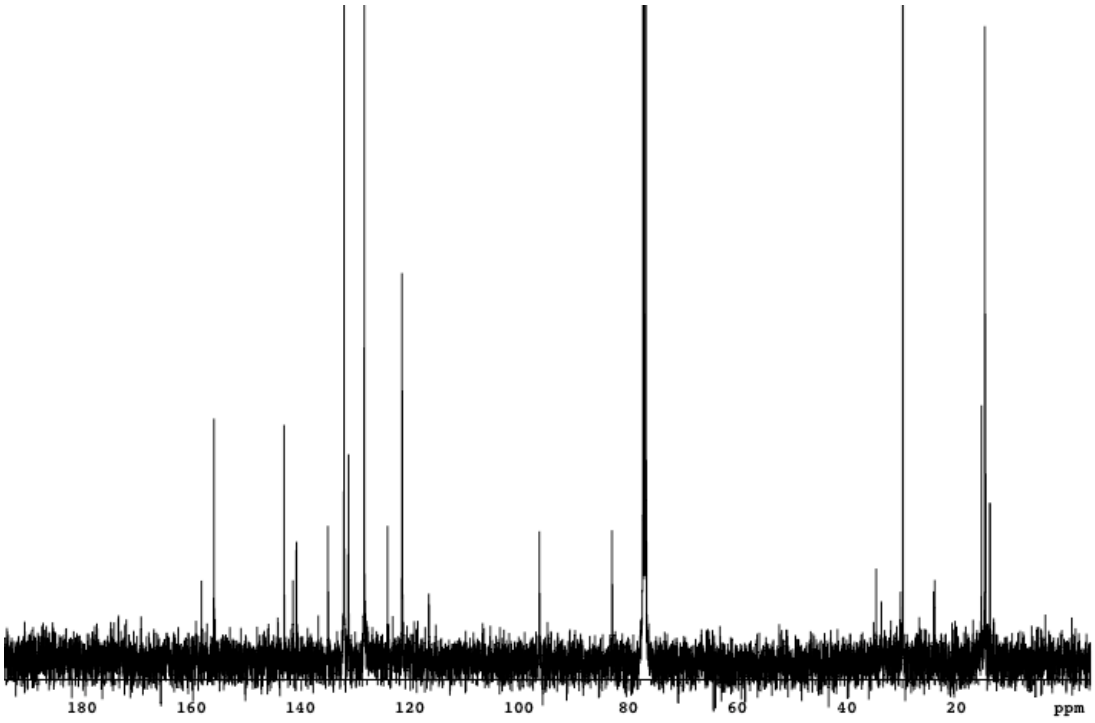

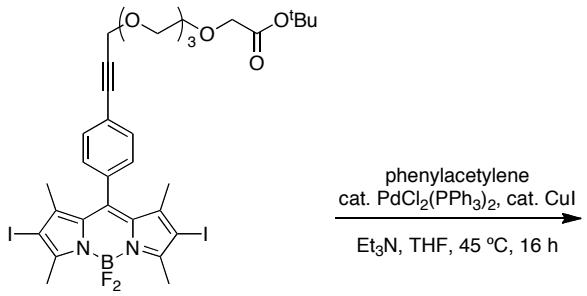

69

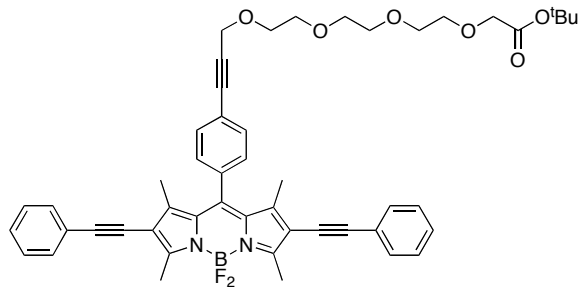

108

108; A mixture of **69** (66 mg, 0.08 mmol), phenylacetylene (42 μL, 0.38 mmol), Et_3N (0.10 mL, 0.75 mmol), $PdCl_2(PPh_3)_2$ (6 mg, 0.01 mmol), and CuI (3 mg, 0.01 mmol) were dissolved in 5.0 mL THF. The solution was degassed three times via the freeze-thaw method and then heated to 45 °C for 16 h under N_2. The reaction solvent was removed under reduced pressure and the crude product was purified via flash silica column eluting with 50% hexane:ethyl acetate to give the desired product as a purple solid (52 mg, 79%). ^{1}H NMR (500 MHz, $CDCl_3$), δ 7.62 (d, *J* = 8.0 Hz, 2H), 7.45-7.47 (m, 4H), 7.31-7.34 (m, 6H), 7.27 (d, *J* = 8.5 Hz, 2H), 4.47 (s, 2H), 4.02 (s, 2H), 3.80-3.81 (m, 2H), 3.69-3.75 (m, 10H), 2.72 (s, 6H), 1.54 (s, 6H), 1.47(s, 9H), ^{13}C NMR (125 MHz, $CDCl_3$), δ 169.6, 158.7, 143.7, 141.4, 134.5, 132.7, 131.3, 130.9, 128.3, 128.1, 128.0, 124.0, 123.2, 116.3, 96.6, 86.9, 85.4, 81.5, 81.4, 70.7, 70.6 (2 C), 70.5, 69.4, 69.0,

59.1, 28.1, 13.7, 13.6. MALDI MS calcd for $C_{50}H_{51}BF_2N_2NaO_6^+$ $(M+Na)^+$ 847.37, found 847.12.

^{1}H NMR of 108 ($CDCl_3$)

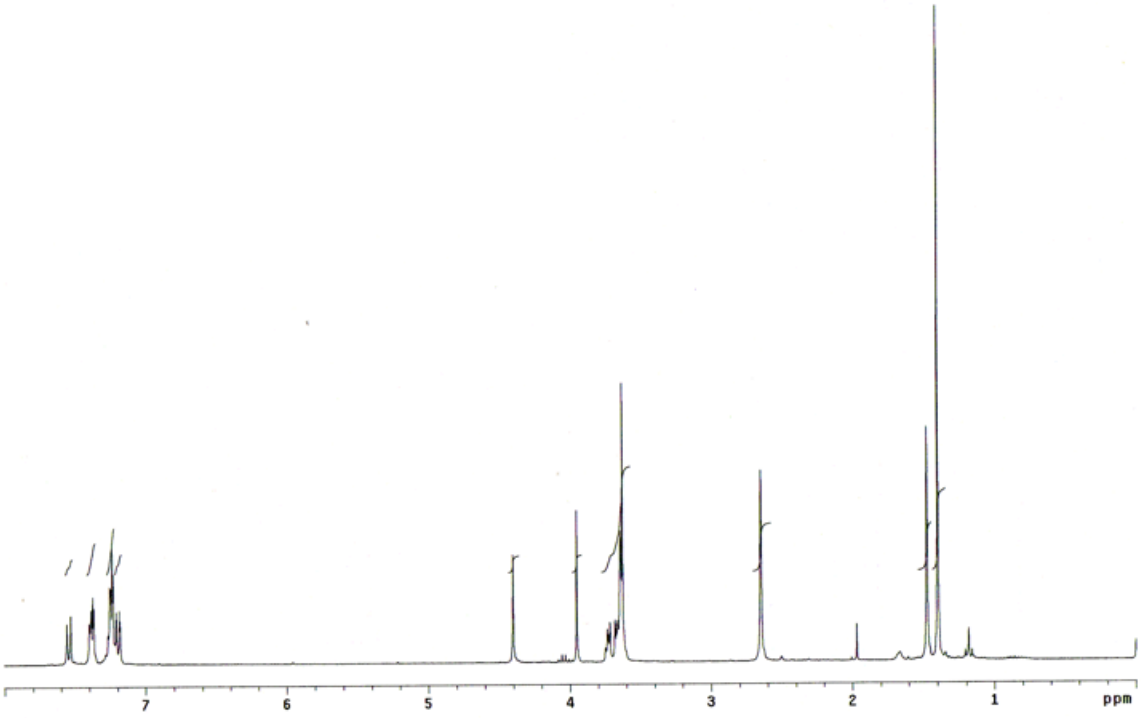

^{13}C NMR of 108 ($CDCl_3$)

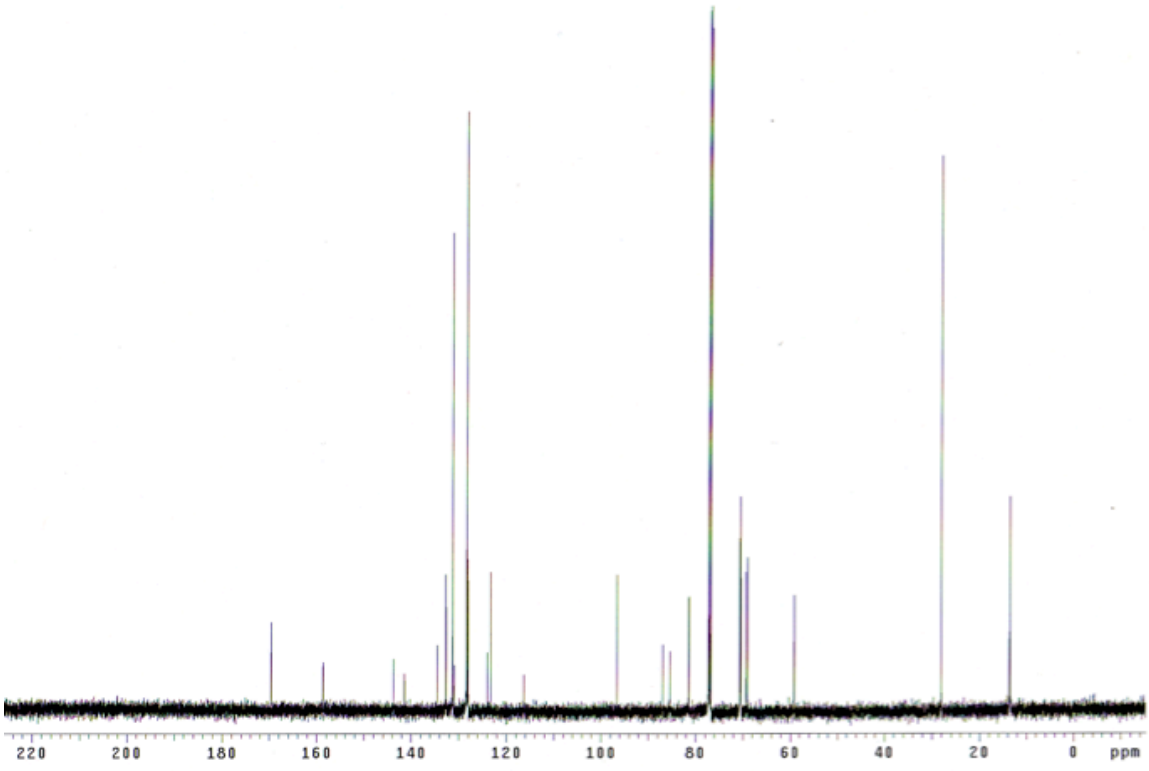

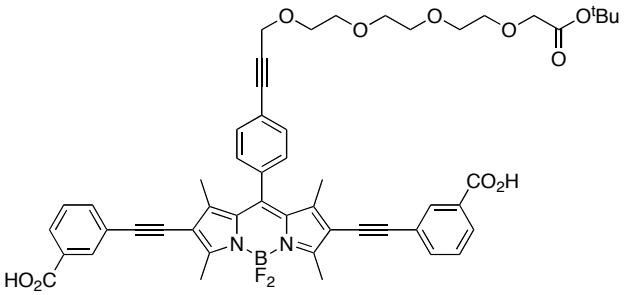

109

109; A mixture of **69** (58 mg, 0.066 mmol), *m*-ethynylbenzoic acid (30 mg, 0.20 mmol), Et_3N (0.10 mL, 0.75 mmol), $PdCl_2(PPh_3)_2$ (5 mg, 0.003 mmol), and CuI (3 mg, 0.01 mmol) were dissolved in 5.0 mL THF. The solution was degassed three times via the freeze-thaw method and heated to 45 °C for 16 h under N_2. The reaction solvent was removed under reduced pressure and the crude product was purified by flash silica column eluting with 80% CH_2Cl_2:MeOH to give the desired product as a purple solid (35 mg, 58%). ^{1}H NMR (500 MHz, CD_3OD), δ 8.12 (s, 2H), 8.01 (d, J = 8.0 Hz, 2H), 7.75-7.78 (m, 4H), 7.53-7.58 (m, 6H), 4.49 (s, 2H), 4.00 (s, 2H), 3.76-3.77 (m, 2H), 3.66-3.69 (m, 4H), 3.61-3.64 (m, 6H), 2.71 (s, 6H), 1.60 (s, 6H), 1.44 (s, 9H), ^{13}C NMR (125 MHz, CD_3OD), δ 166.9, 159.2, 144.9, 141.4, 136.0, 135.0, 133.5, 132.8, 132.0, 131.8, 130.2, 129.7, 129.3, 125.1, 124.4, 116.5, 108.8, 96.6, 88.5, 85.6, 82.8, 81.2, 71.2, 71.1, 70.0, 69.3, 59.2, 32.6, 30.5, 28.2, 23.3, 14.3, 13.8. MALDI HRMS calcd for $C_{52}H_{51}BF_2N_2KO_{10}^+$ $(M+K)^+$ 951.3245, found 951.3284.

^{1}H NMR of 109 (CD_3OD)

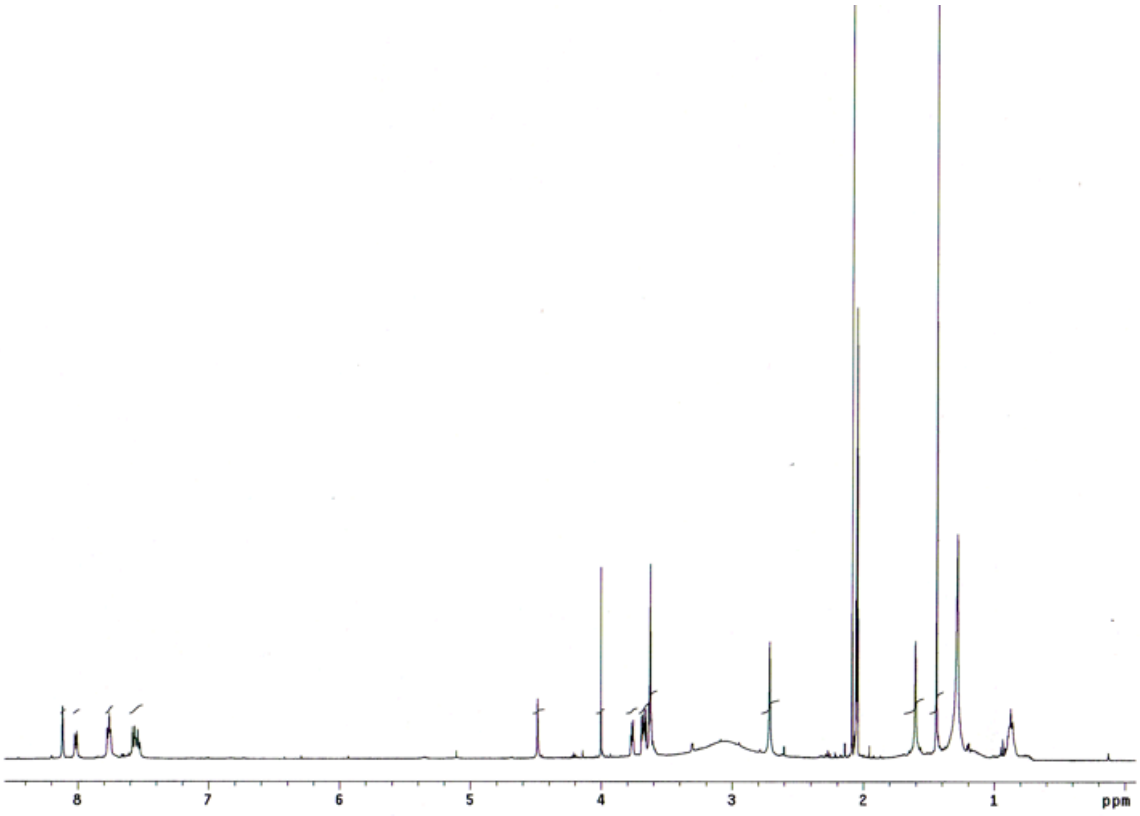

^{13}C NMR of 109 (CD_3OD)

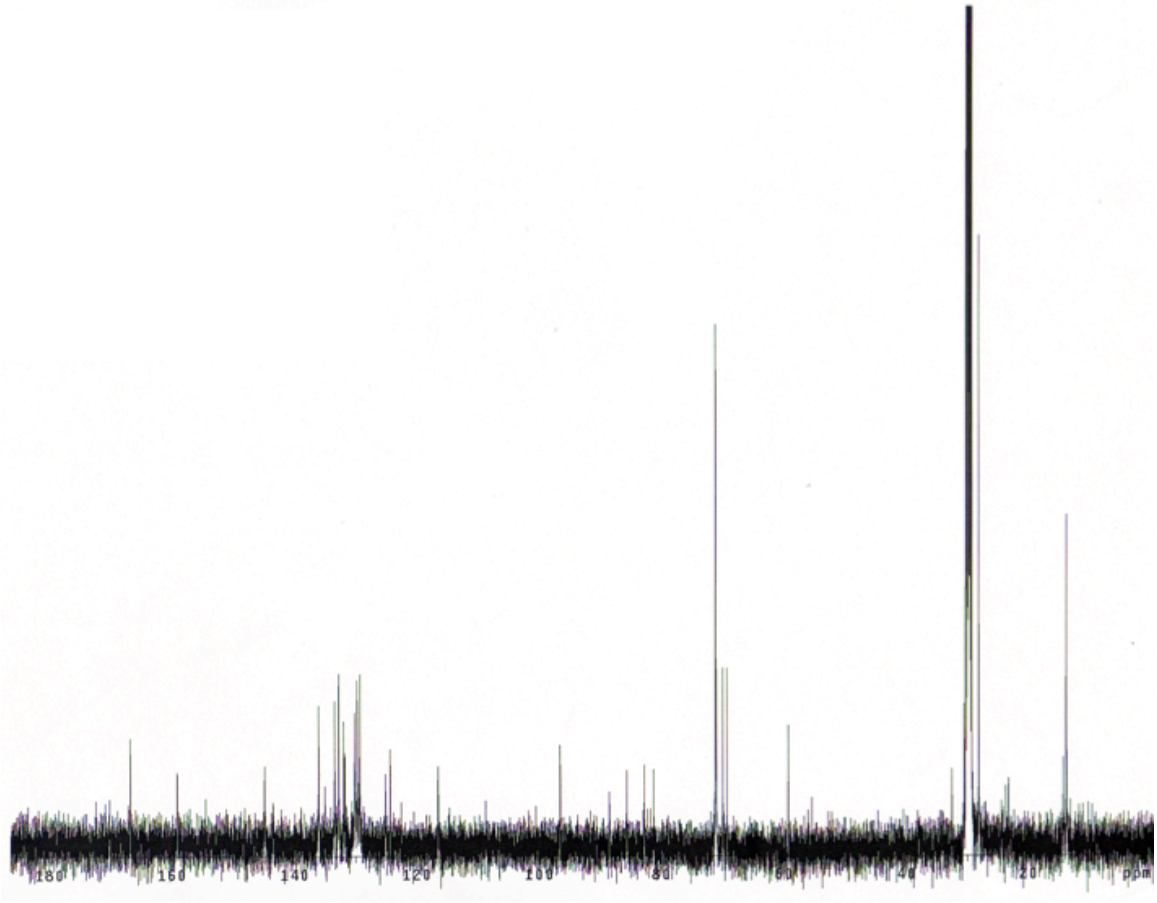

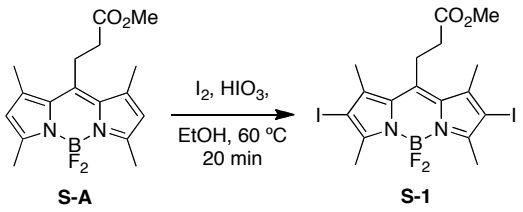

S-A **S-1**

S-1; Tetramethyl-BODIPY ester **S-A**[211] (150 mg, 1.1 mmol) was suspended in 15 mL of EtOH. I_2 (290 mg, 1.1 mmol) was added and iodic acid (170 mg, 0.95 mmol) in ~0.7 mL water was added over 20 min. The mixture was stirred for 20 min at 60 ºC and then at 25 ºC for 30 min. Formed precipitate was filtered to afford the desired product as a red solid (230 mg, 86 %) in adequate purity. ^{1}H NMR (300 MHz, $CDCl_3$) δ (ppm) 3.75 (s, 3H), 3.38 (t, J = 9Hz, 2H), 2.62 (s, 6H), 2.50 (m, 8H). Compound solubility to poor for carbon NMR. MALDI HRMS calcd for $C_{16}H_{18}BF_2I_2N_2O_2\{M\text{-}H\}^-$ 584.9519, found 584.9532. TLC (4:1 Hexane:EtOAc) R_f = 0.45.

^{1}H NMR of S-1 ($CDCl_3$)

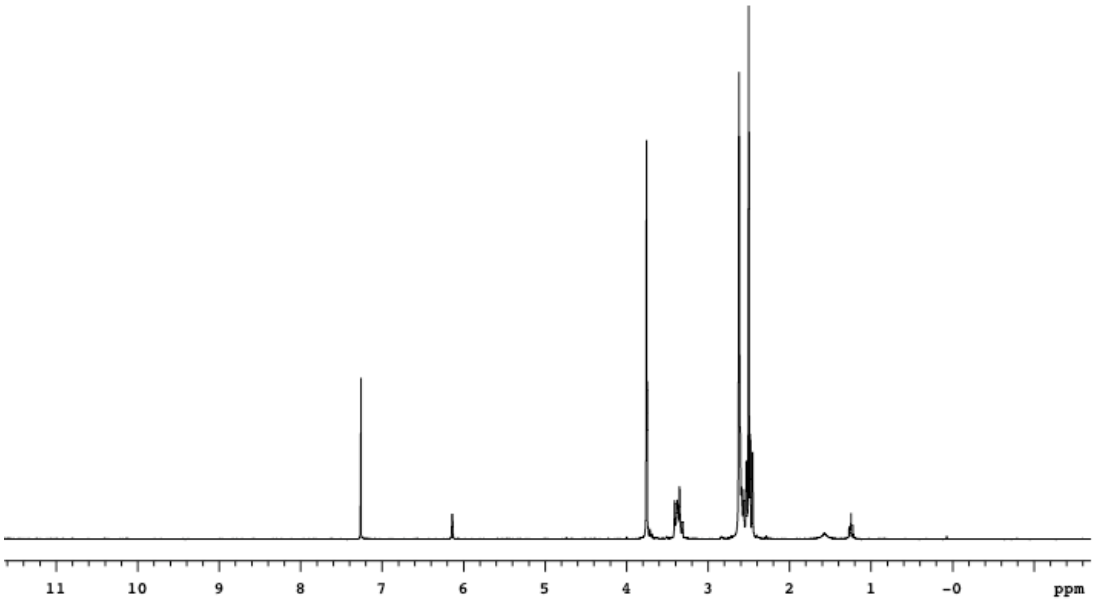

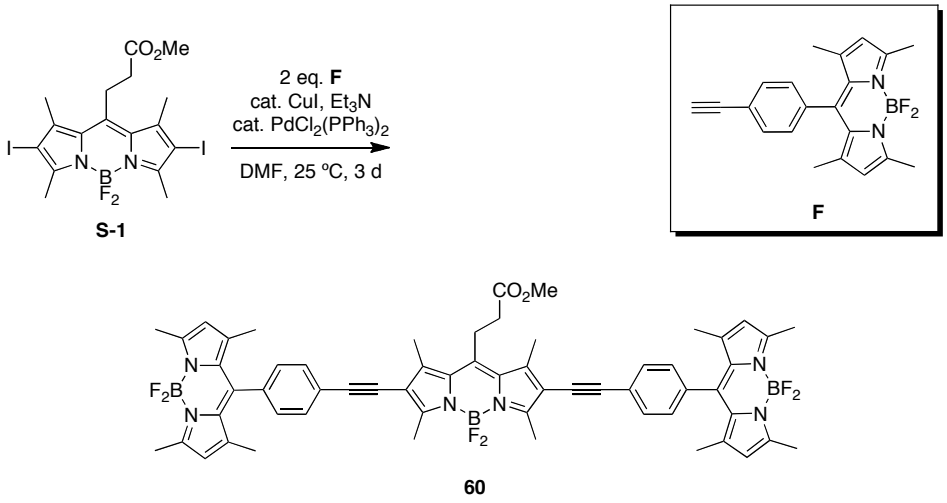

60; A mixture of **S-1** (20 mg, 0.03 mmol), **F** (24 mg, 0.07 mmol), Et_3N (0.19 mL, 1.4 mmol), $PdCl_2(PPh_3)_2$ (4 mg, 0.01 mmol), and CuI (2 mg, 0.01 mmol) were dissolved in 1.0 mL DMF under N_2. The solution was degassed three times via the freeze-thaw method and then stirred for 3 d at 25 ºC under N_2. The solvent was removed under reduced pressure and the crude product was purified via flash silica column eluting with 3:1 Hexane:EtOAc followed by recrystalization from CH_2Cl_2/hexanes to give the desired product as a purple solid (10 mg, 28%). ^{1}H NMR (300 MHz, $CDCl_3$), δ 7.64 (d, J = 8.4 Hz, 4H), 7.30 (d, J = 8.1 Hz, 4H), 6.00 (s, 4H), 3.78 (s, 3H), 3.43 (b, 2H), 2.73 (s, 6H), 2.65 (s, 8H), 2.56 (s, 12H), 1.45 (s, 12H), ^{13}C NMR (125 MHz, $CDCl_3$), δ 172.0, 158.2, 156.0, 144.6, 143.1, 141.6, 140.9, 135.1, 132.2, 131.4, 128.5, 124.2, 121.5, 96.3, 83.1, 52.4, 35.2, 15.5, 14.8 (2 C), 13.9. X-Ray obtained for this compound (see text) MALDI HRMS calcd for $C_{59}H_{55}B_3F_6N_6O_2$ ($M^{\bullet+}$) 1026.4591, found 1026.4607. TLC (4:1 EtOAc:Hexane) R_f = 0.20.

^{1}H NMR of 60 ($CDCl_3$)

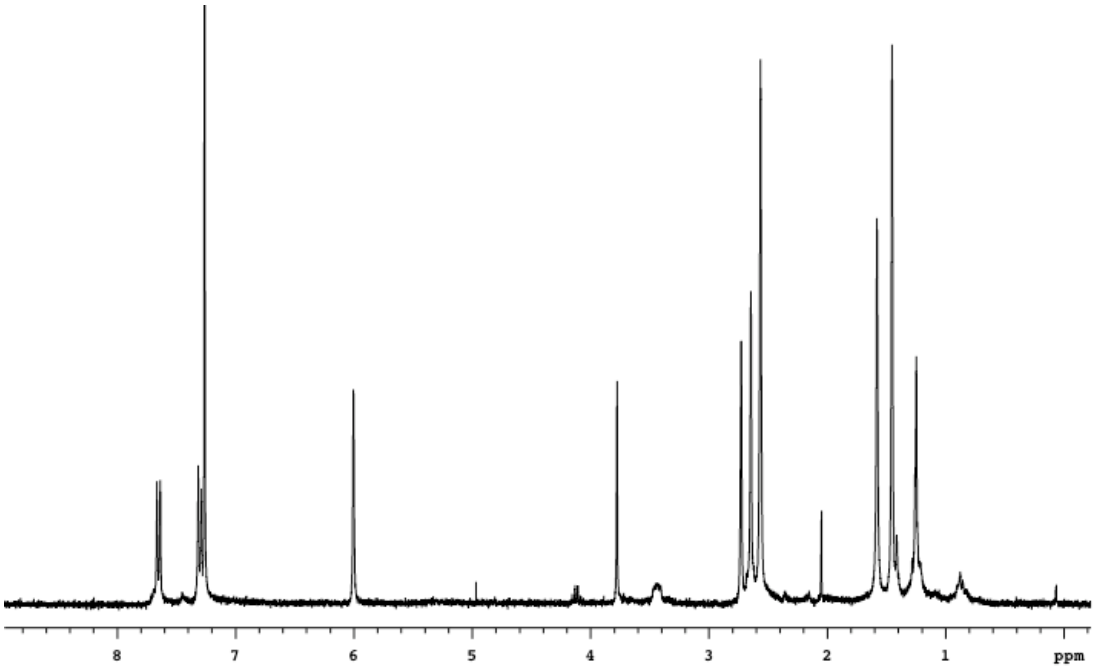

^{13}C NMR of 60 ($CDCl_3$)

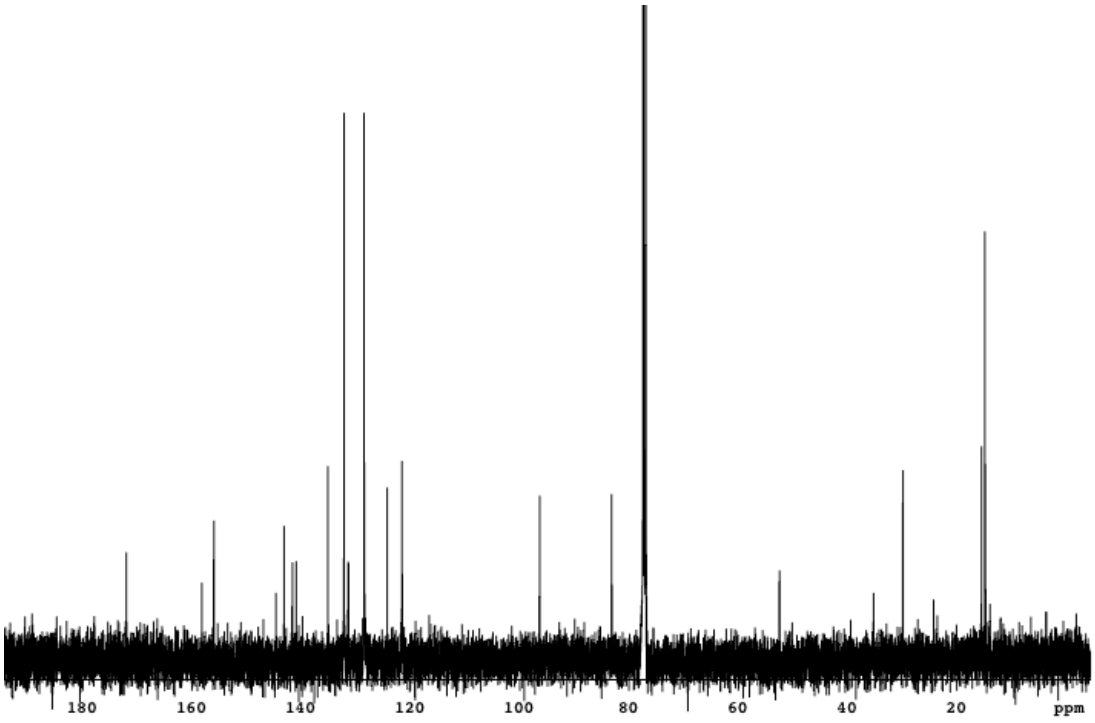

Complete Electrochemical Data

	Cyclic Voltammetry (CV)					Differential Pulse Voltammetry (DPV)[e]				
cmpd	$E_{onset,ox}$ (V)	HOMO (eV)	$E_{onset,red}$ (V)	LUMO (eV)	E_g (eV)	$E_{onset,ox}$ (V)	HOMO (eV)	$E_{onset,red}$ (V)	LUMO (eV)	E_g (eV)
G[a]	+0.68	5.84	-1.32	3.84	2.00	+0.70	5.86	-1.19	3.97	1.89
H[b]	+0.33	5.48	-1.03	4.12	1.36	+0.07	5.79	-0.92	4.23	1.56
$\mathbf{H}_{Na}$[b, d]	+0.04	5.19	-1.67	3.48	1.71	-0.25	4.85	-1.49	3.61	1.24
46[a]	+0.87	6.03	-0.88	4.28	1.75	-	-	-	-	-
49[b]	+0.40	5.55	-1.00	4.16	1.39	+0.55	5.70	-0.83	4.32	1.38
108[a]	+0.99	6.15	-0.91	4.28	1.87	+0.98	6.14	-0.75	4.41	1.73
109[b]	+0.49	5.64	-0.93	4.22	1.42	+0.47	5.62	-0.85	4.30	1.32
109[c]	+0.49	5.64	-0.92	4.23	1.41	-	-	-	-	-

Electrochemical data for **G**, **H**, **46**, **49**, **108**, and **109**. All experiments were recorded using a glassy carbon working electrode (A = 0.071 cm^2) referenced to Fc/Fc^+ and a Pt counter electrode at a scan rate of 200 mV/s. All potentials are reported vs. Fc/Fc^+ and all HOMO and LUMO energies are derived form electrochemical results based on Fc/Fc^+ = 5.1 eV vs vacuum. All solvents were dearated using $Ar_{(g)}$. a. CH_2Cl_2 solution b. DMF solution. c. DMF solution (0.1 M pyridine). d. xanthene was first reacted with NaOH to obtain the sodium salt. e. Compounds **46** and **109** (base) decomposed during DPV scan.

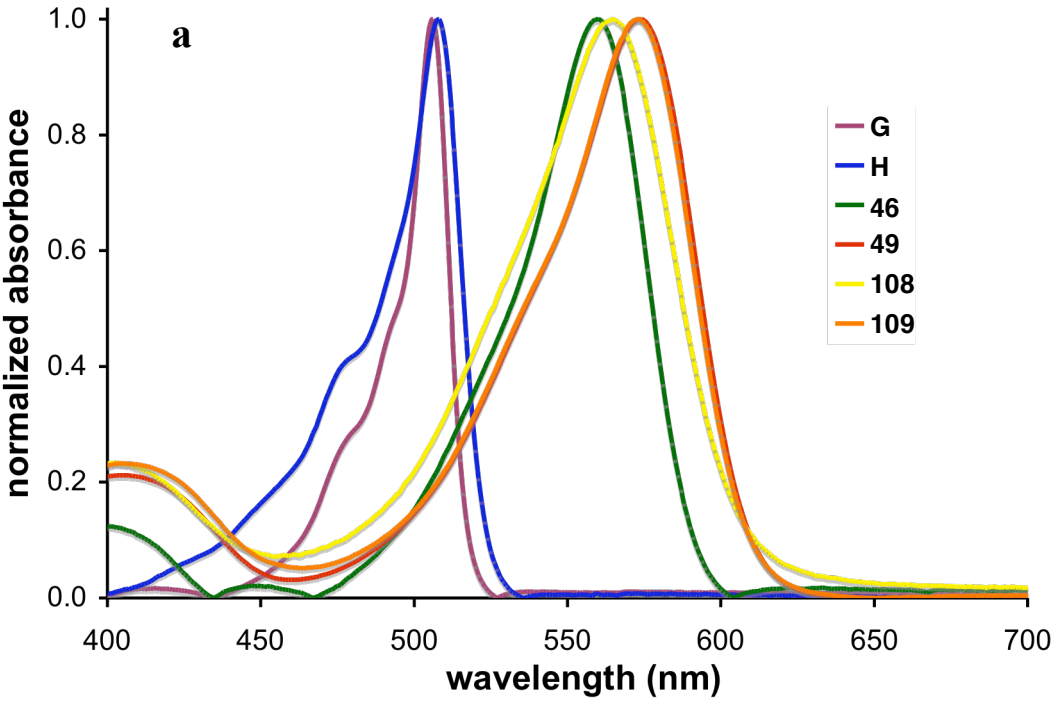
a
normalized absorbance
1.0
0.8
0.6
0.4
0.2
0.0
400
450
500
550
600
650
700
wavelength (nm)
G
H
46
49
108
109

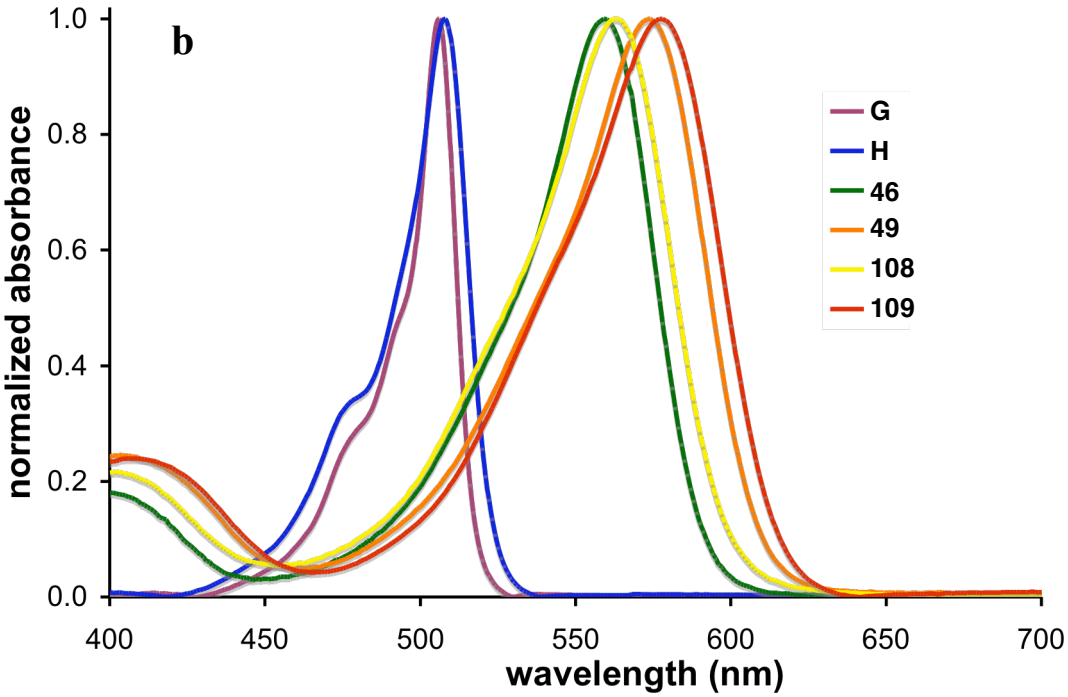
b
normalized absorbance
1.0
0.8
0.6
0.4
0.2
0.0
400
450
500
550
600
650
700
wavelength (nm)
G
H
46
49
108
109

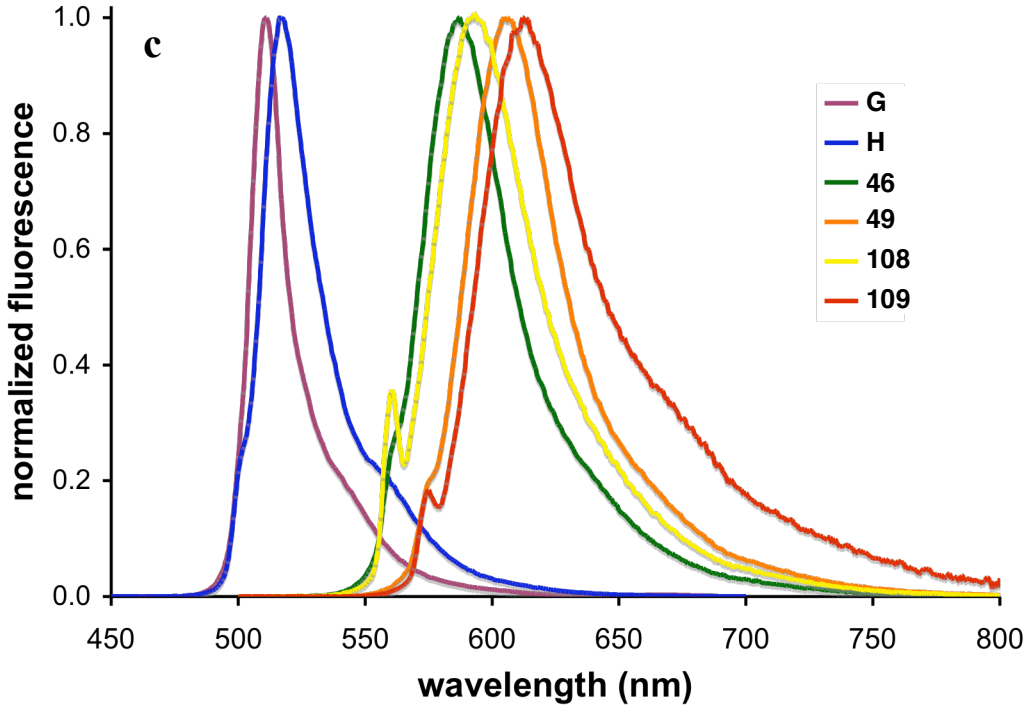
c
normalized fluorescence
1.0
0.8
0.6
0.4
0.2
0.0
450
500
550
600
650
700
750
800
wavelength (nm)
G
H
46
49
108
109

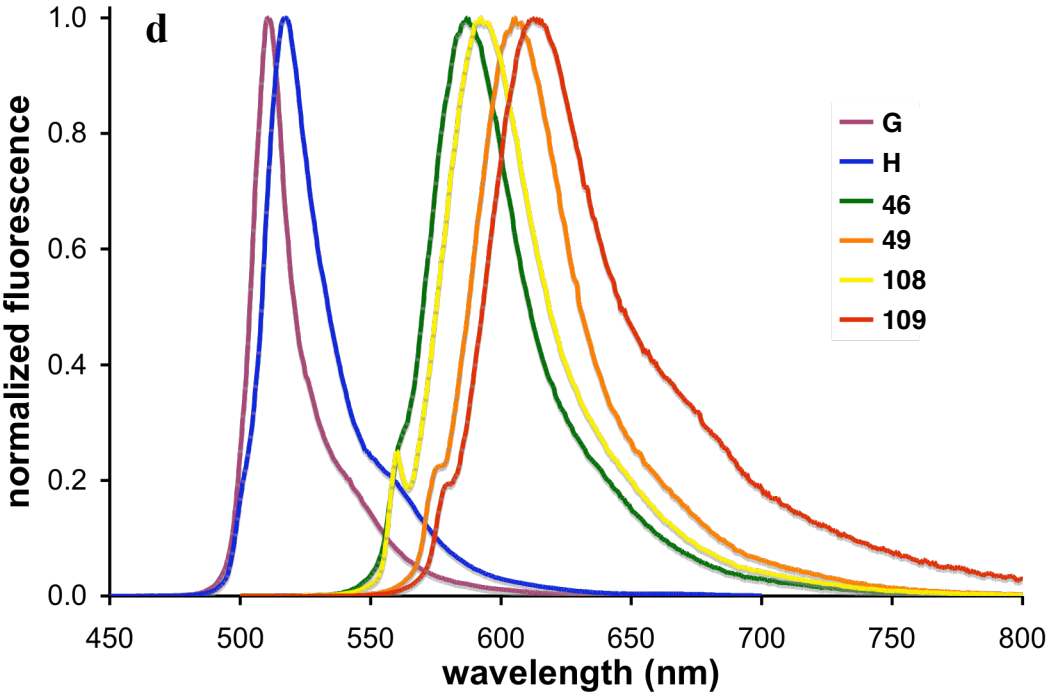
d
normalized fluorescence
1.0
0.8
0.6
0.4
0.2
0.0
450
500
550
600
650
700
750
800
wavelength (nm)
G
H
46
49
108
109

Figure 2. Spectra of compounds **G**, **H**, **46**, **49**, **108**, and **109** in 1:1 ethanol/CH_2Cl_2 $1x10^{-6}$ M: **a** absorbance; **b** absorbance with $8x10^{-5}$ M Bu_4NOH; **c** emission; **d** emission with $8x10^{-5}$ M Bu_4NOH.

Electrochemistry Spectra

Electrochemistry of **67**

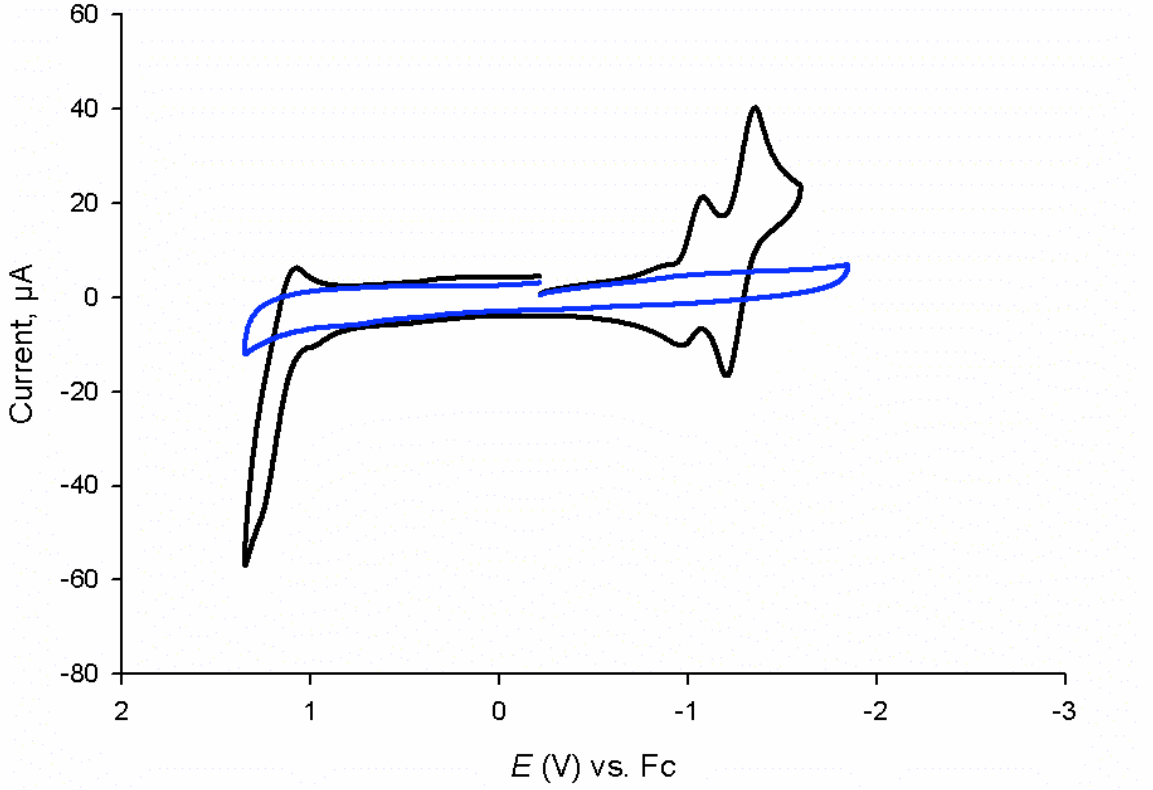

Electrochemistry of **46**

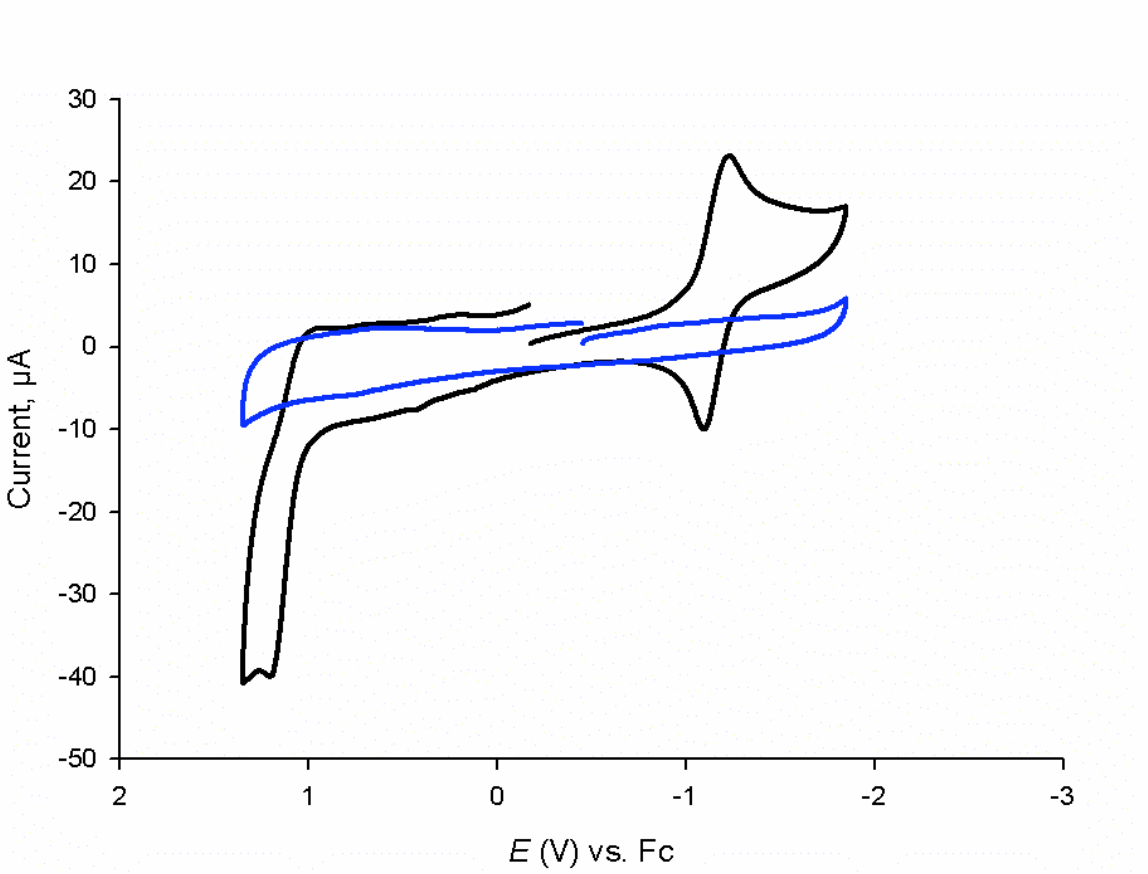

Electrochemistry of **49**

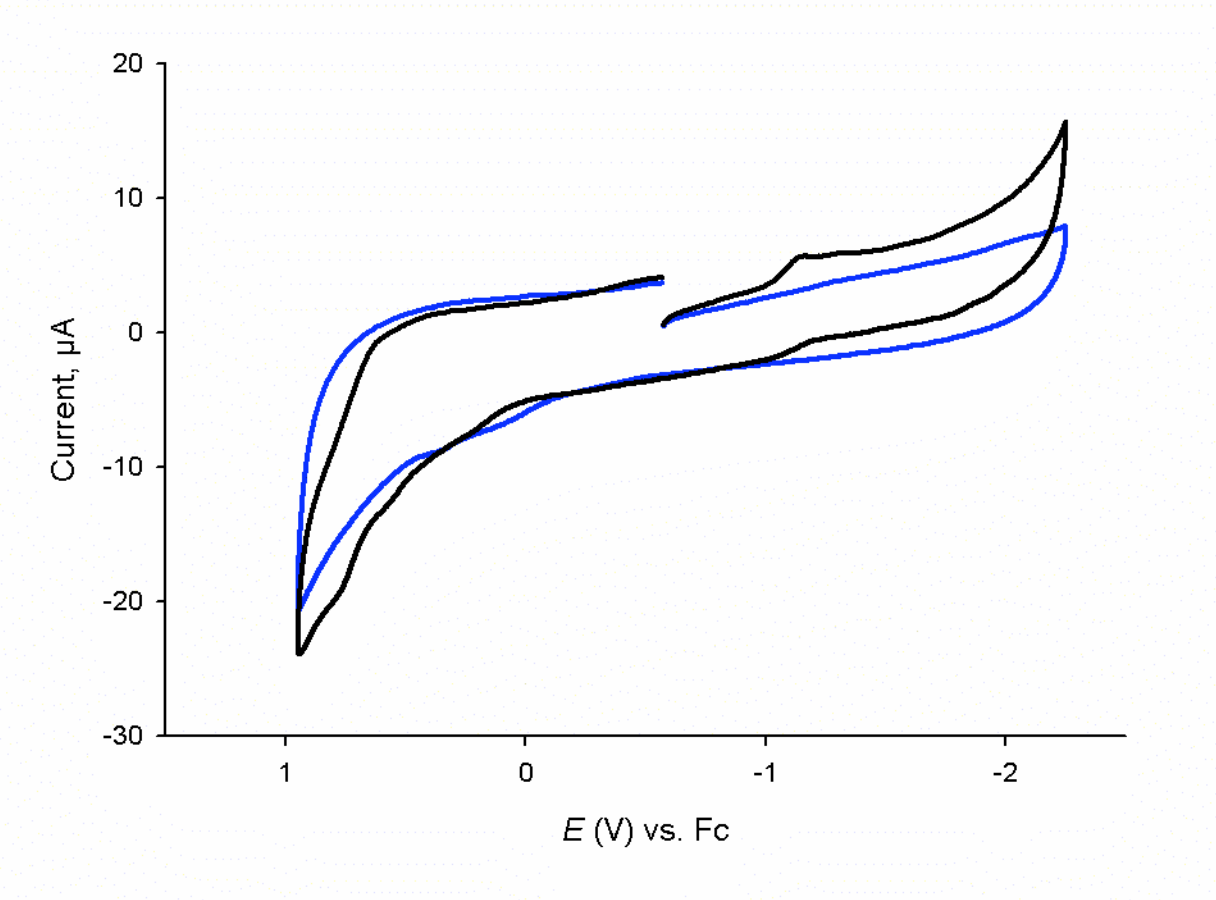

DPV - reduction

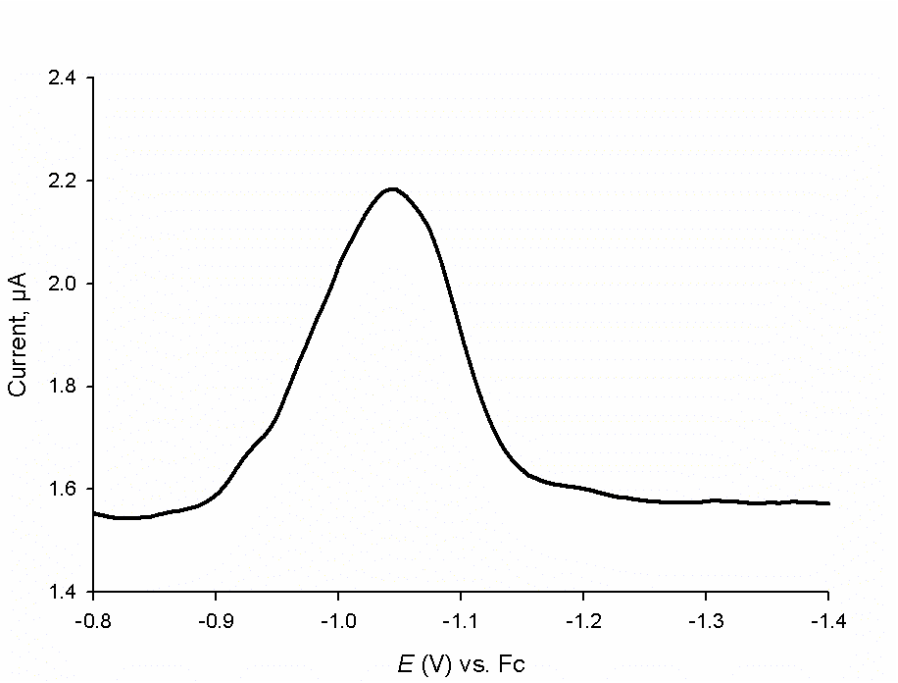

DPV - oxidation

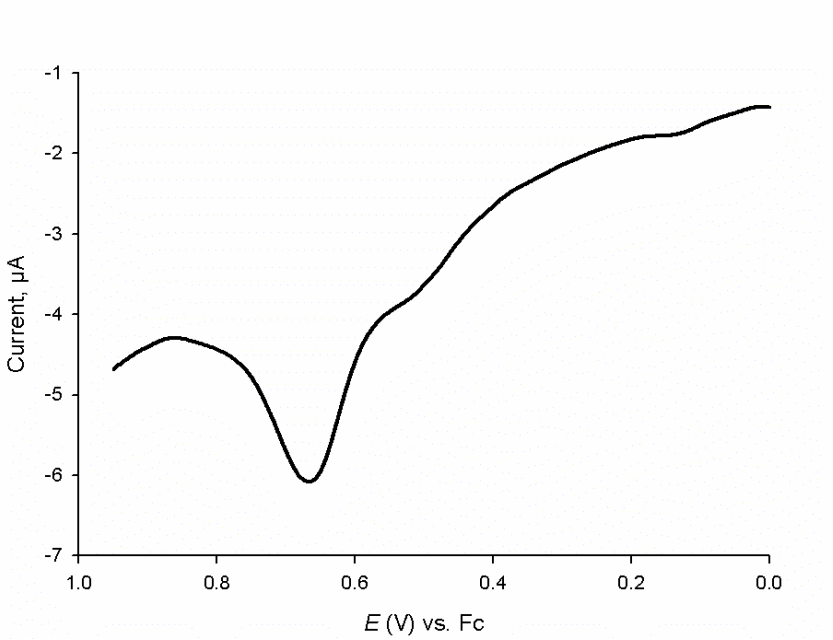

Electrochemistry of **108**

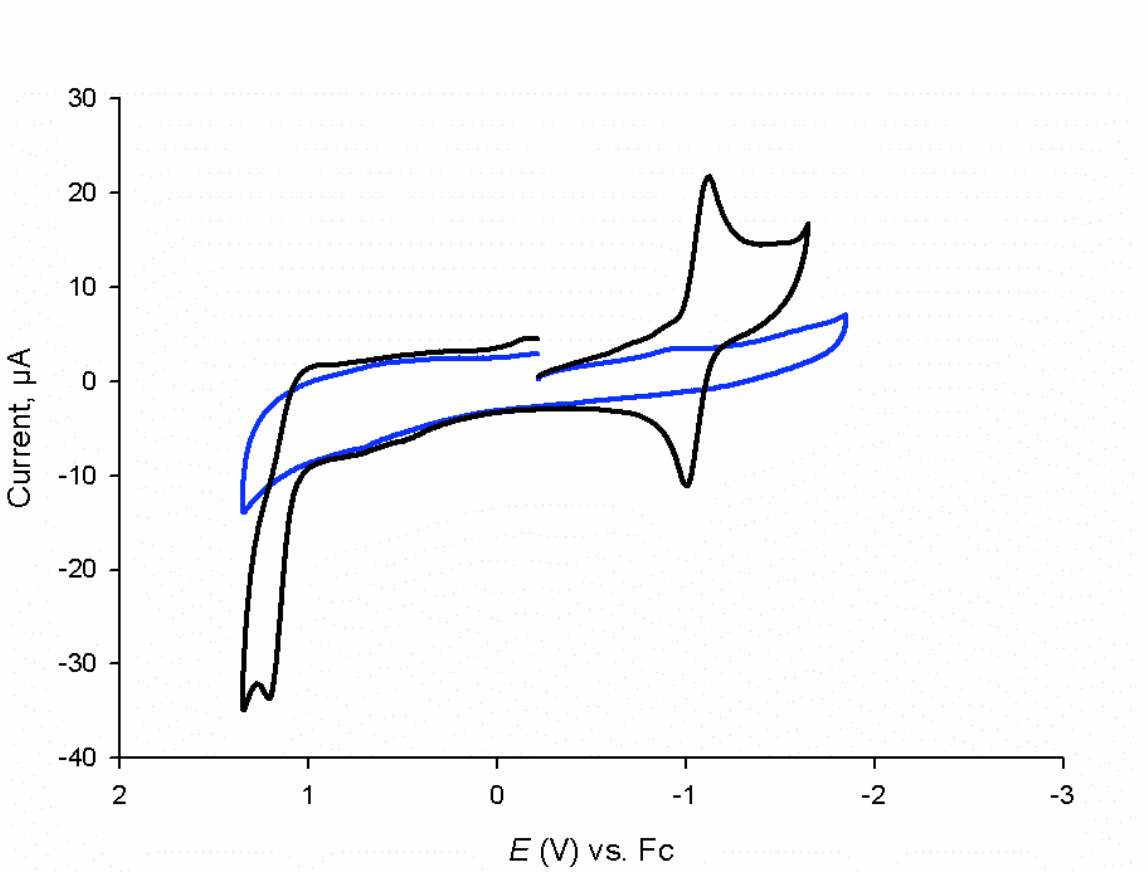

DPV - reduction

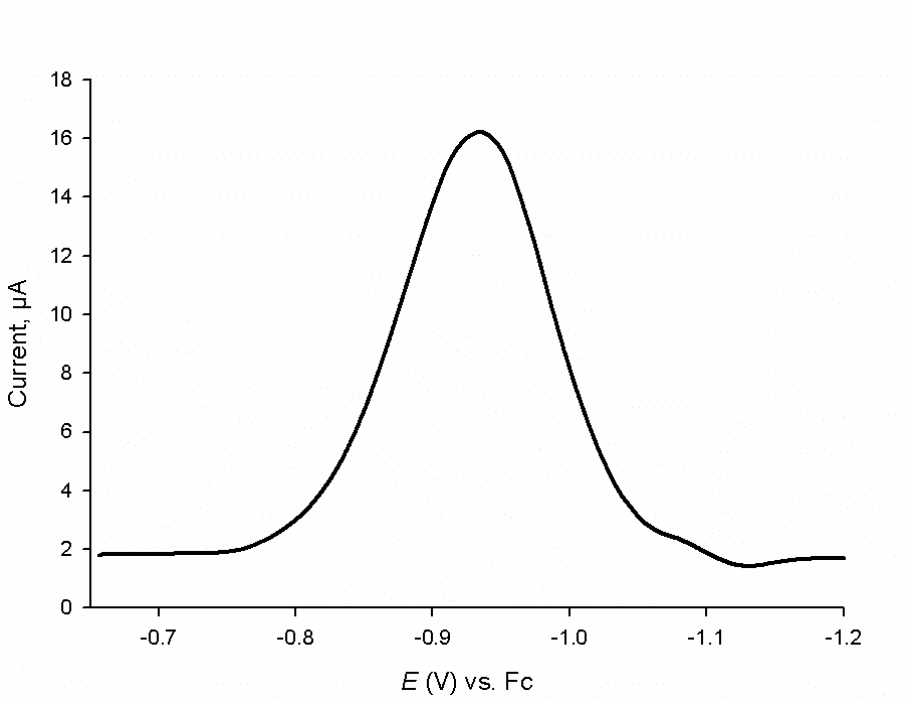

DPV - oxidation

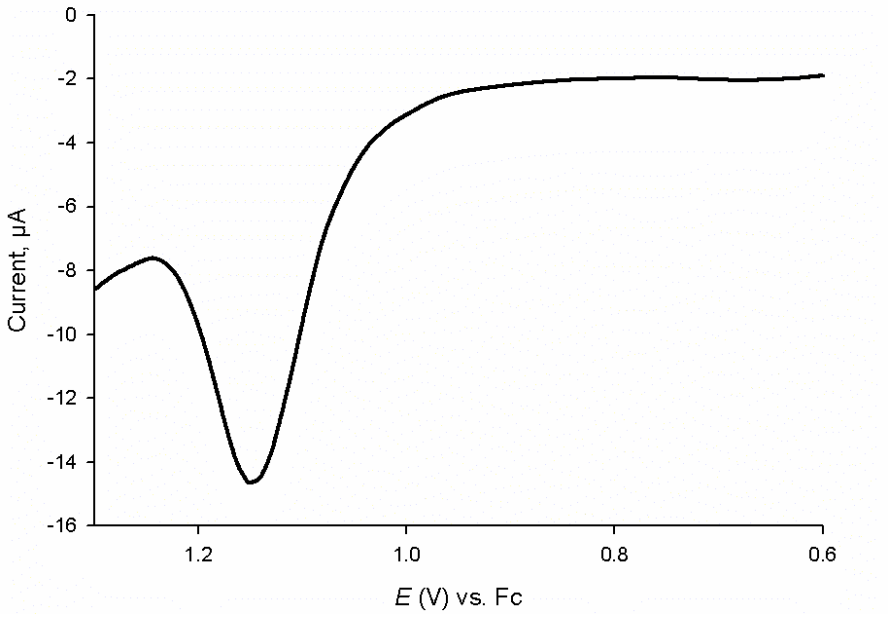

Electrochemistry of **109**

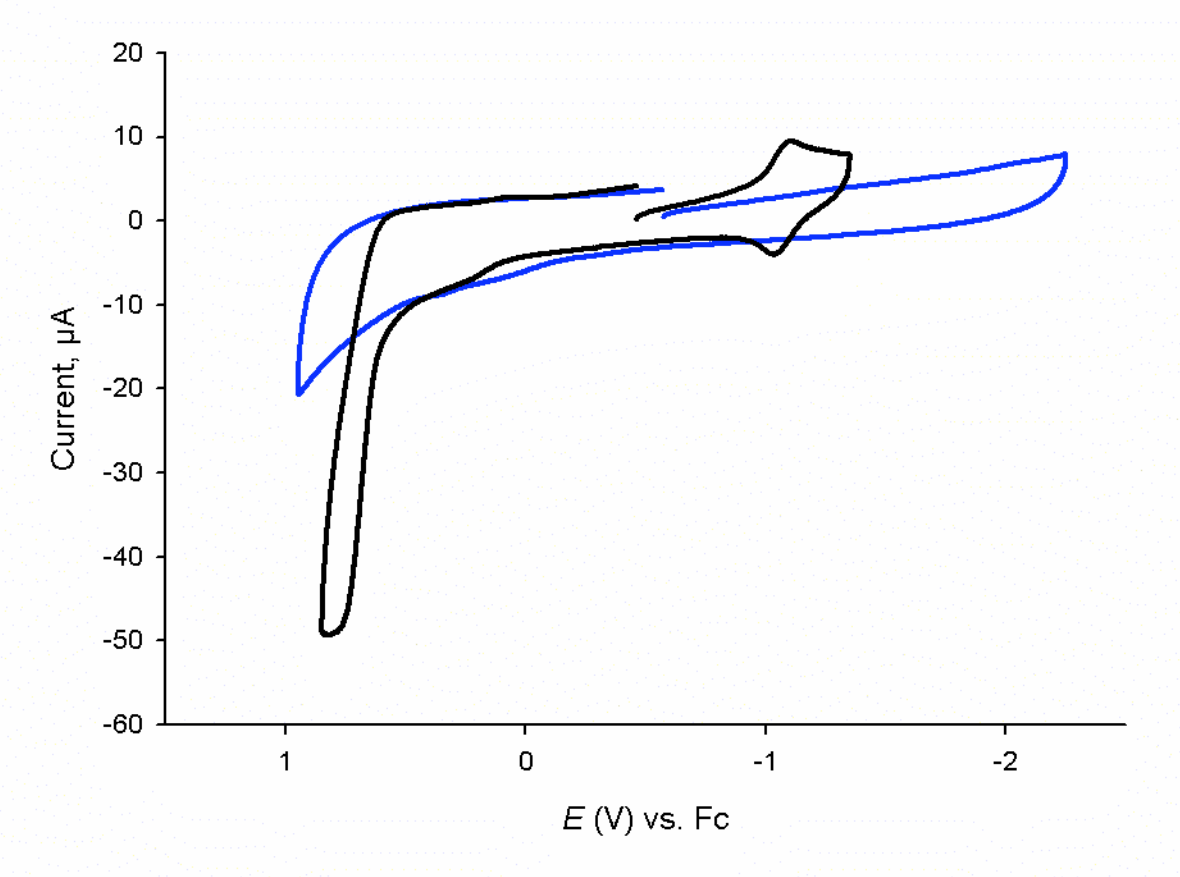

DPV - reduction

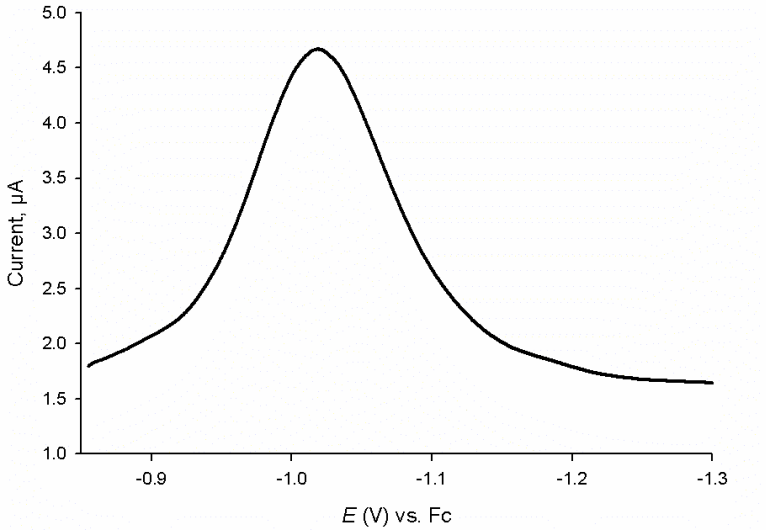

DPV - oxidation

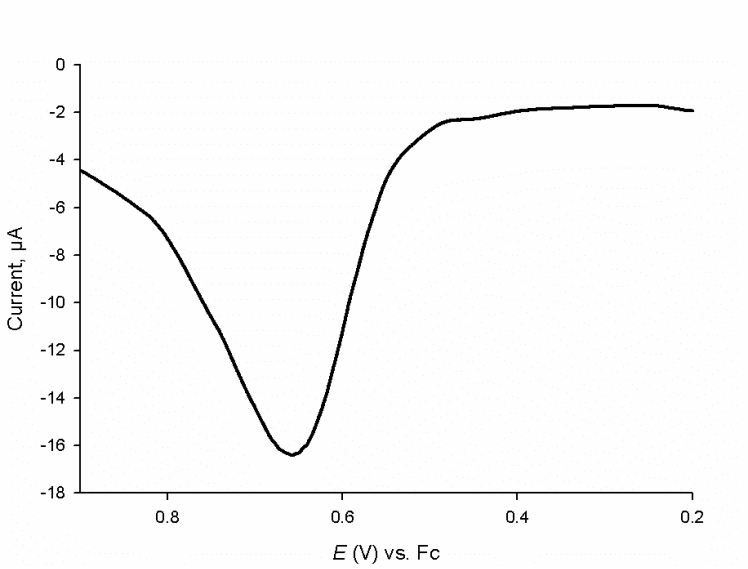

109 with pyridine

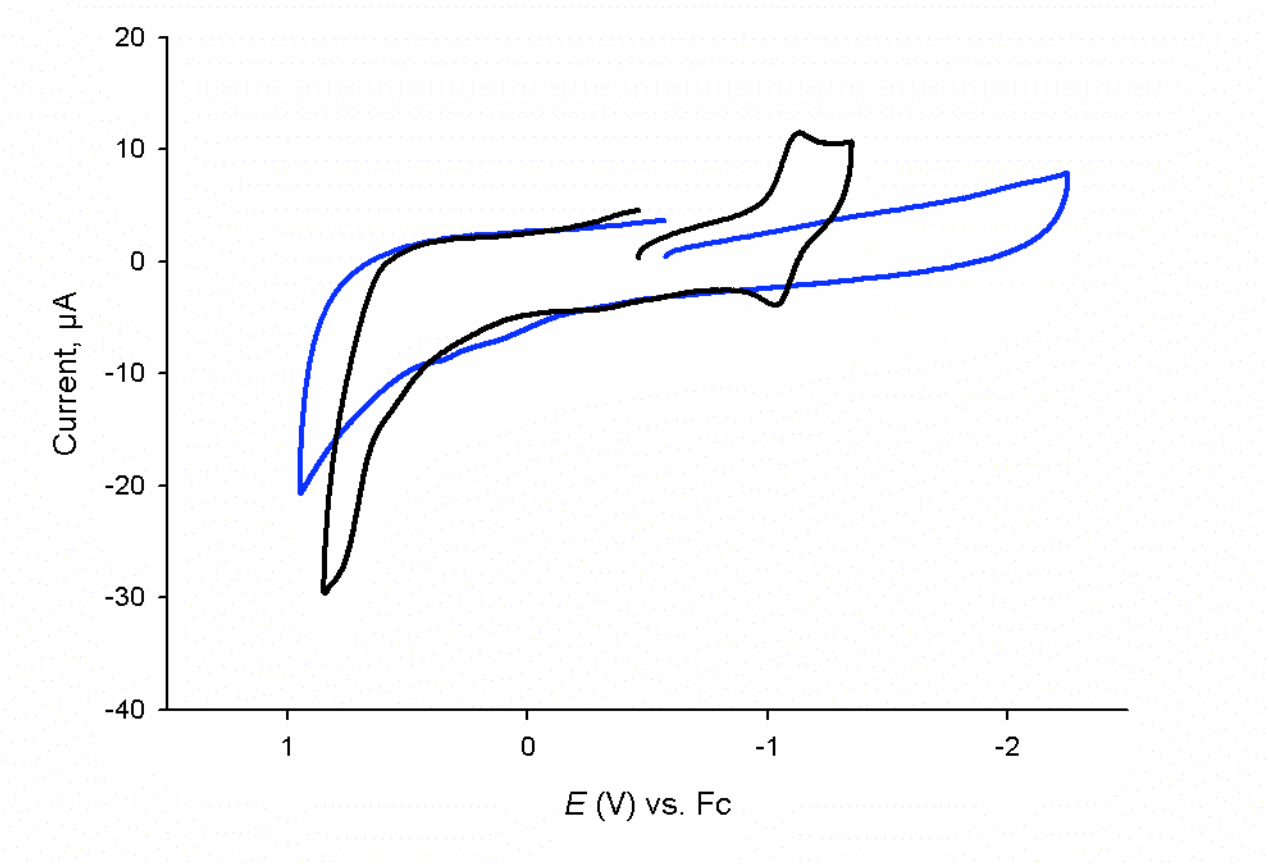

Electrochemistry of **G**

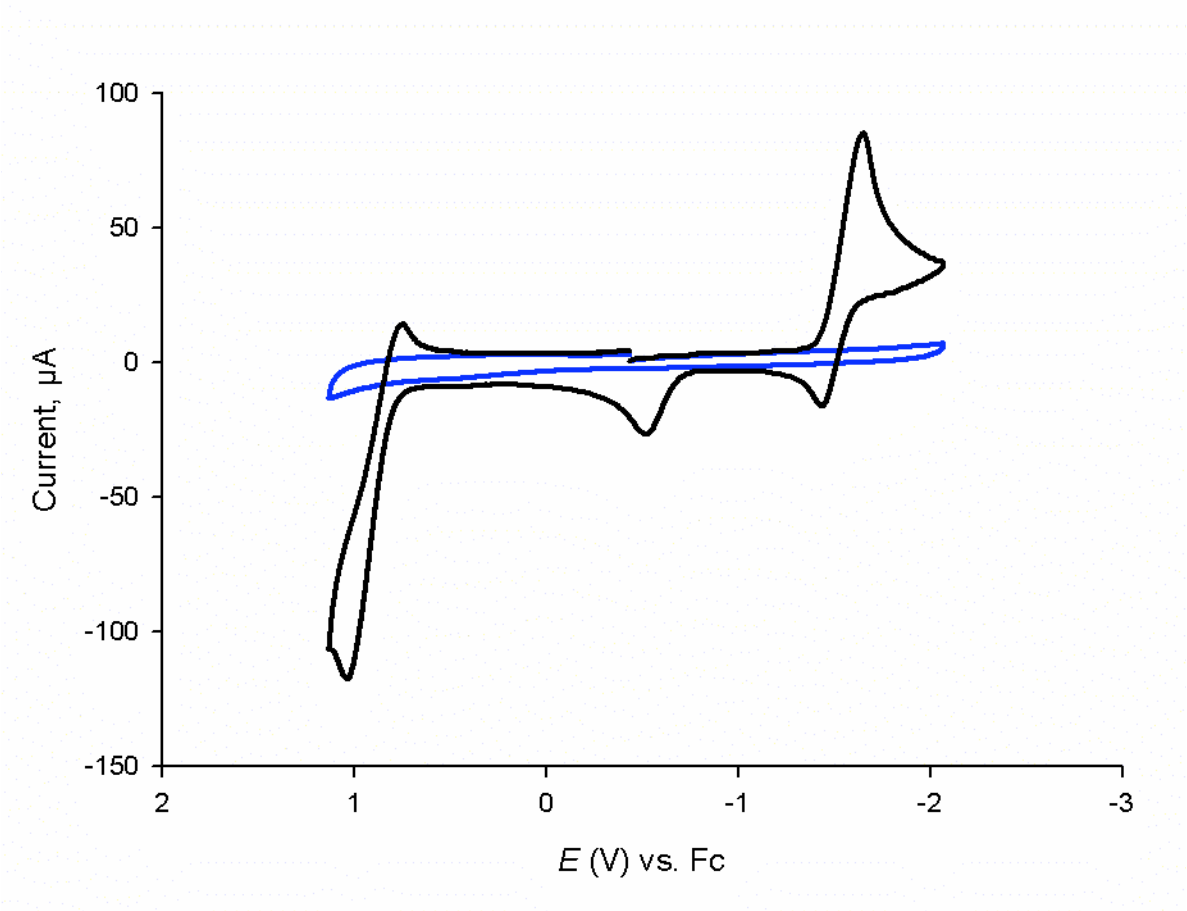

DPV - Reduction

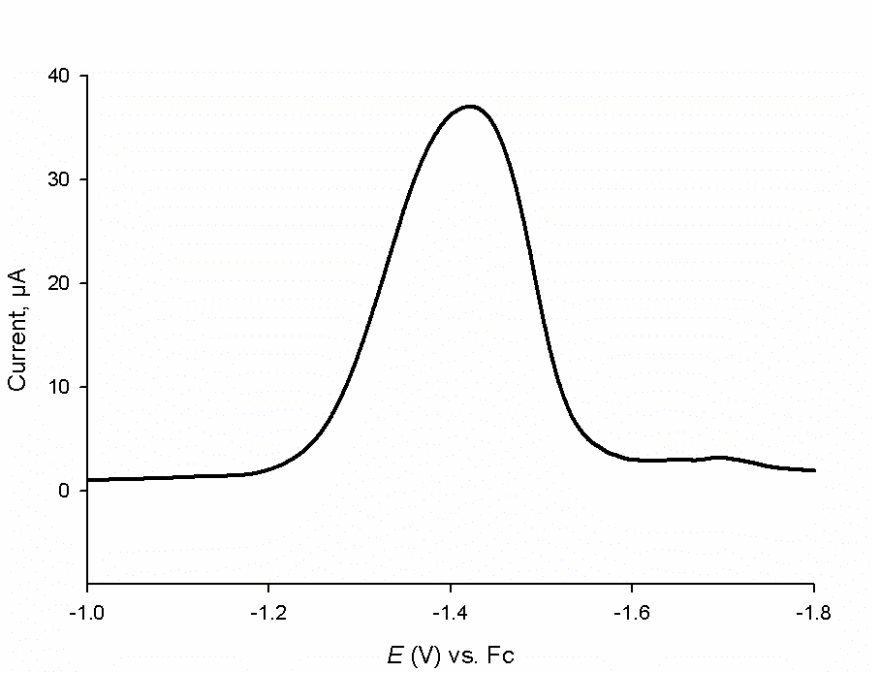

DPV - oxidation

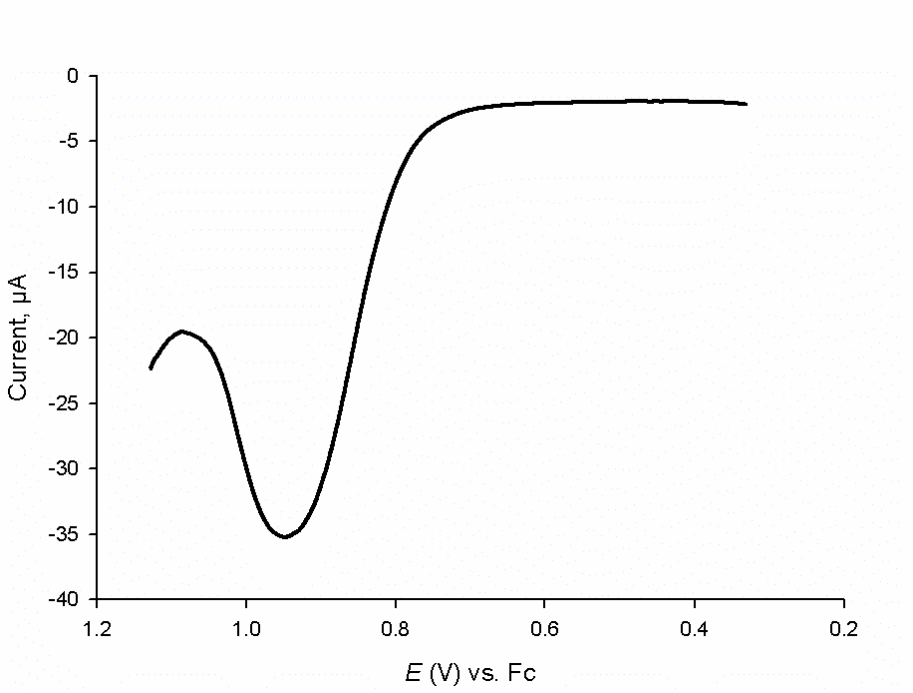

Electrochemistry of **H**

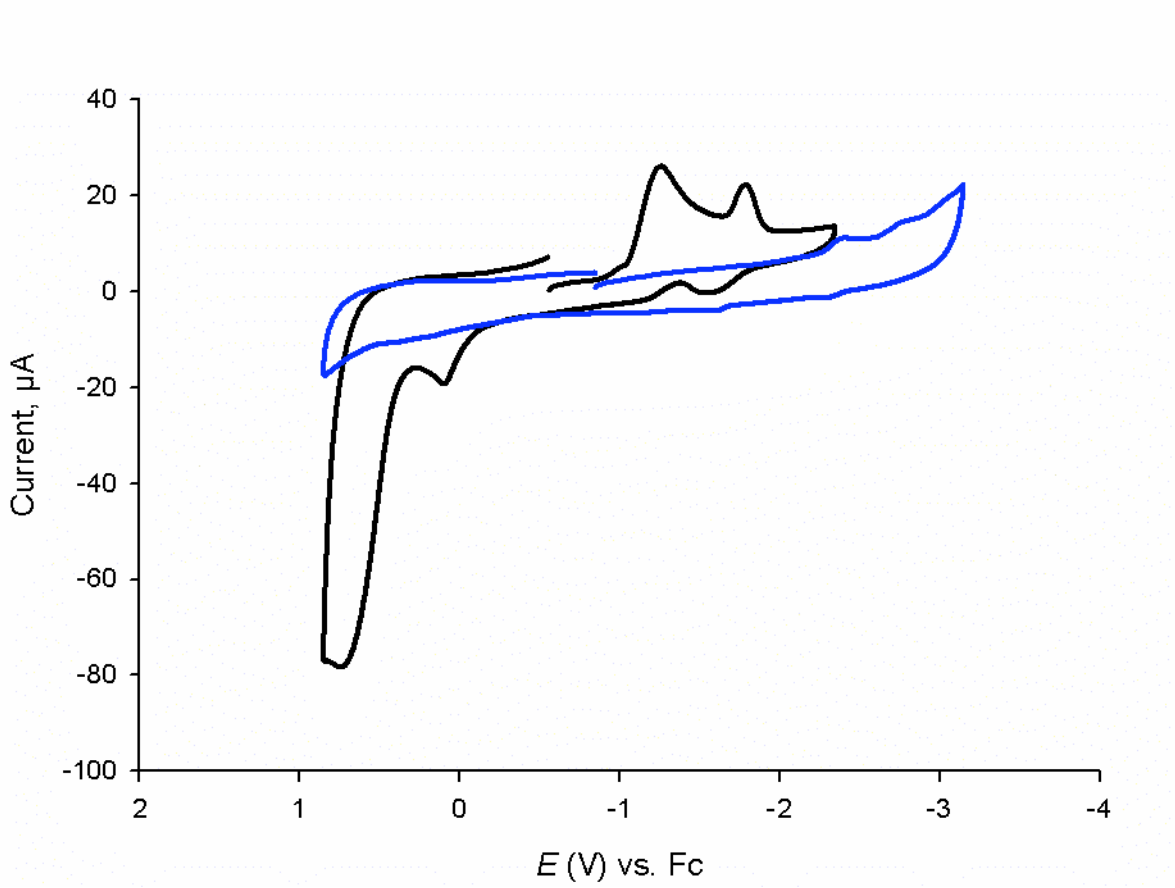

DPV - reduction

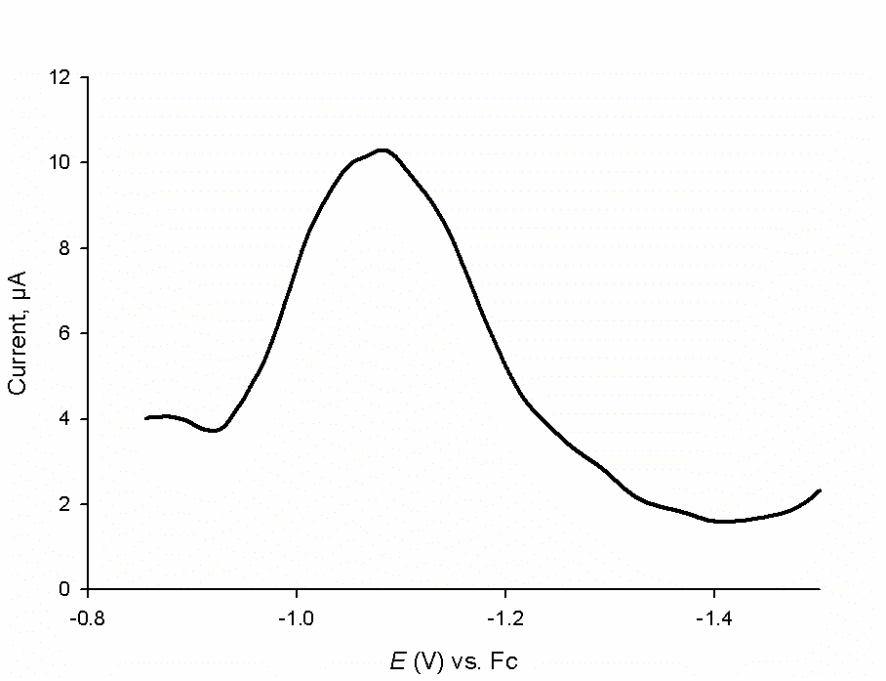

DPV - oxidation

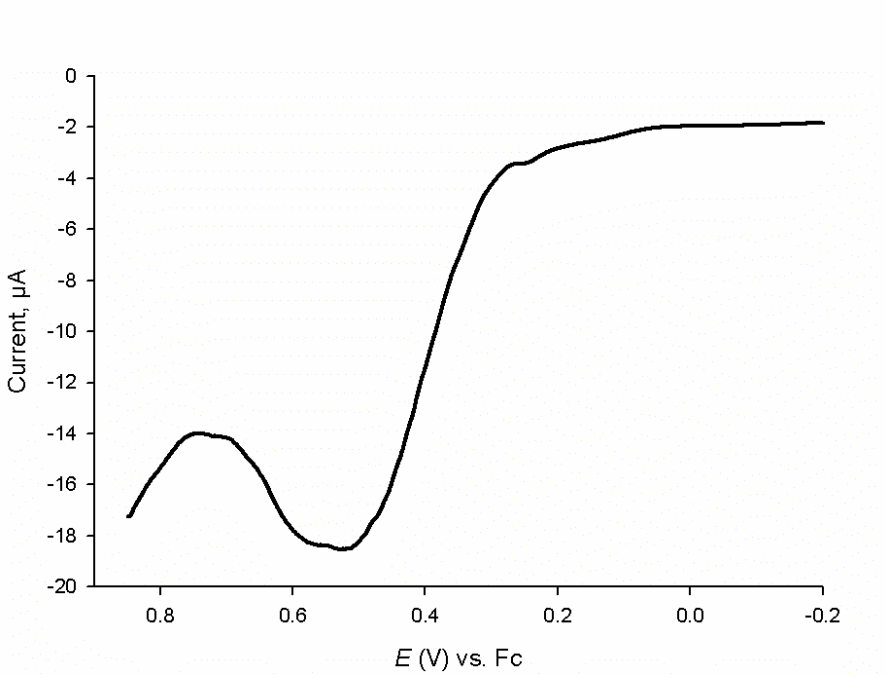

Electrochemistry of **H-Na**

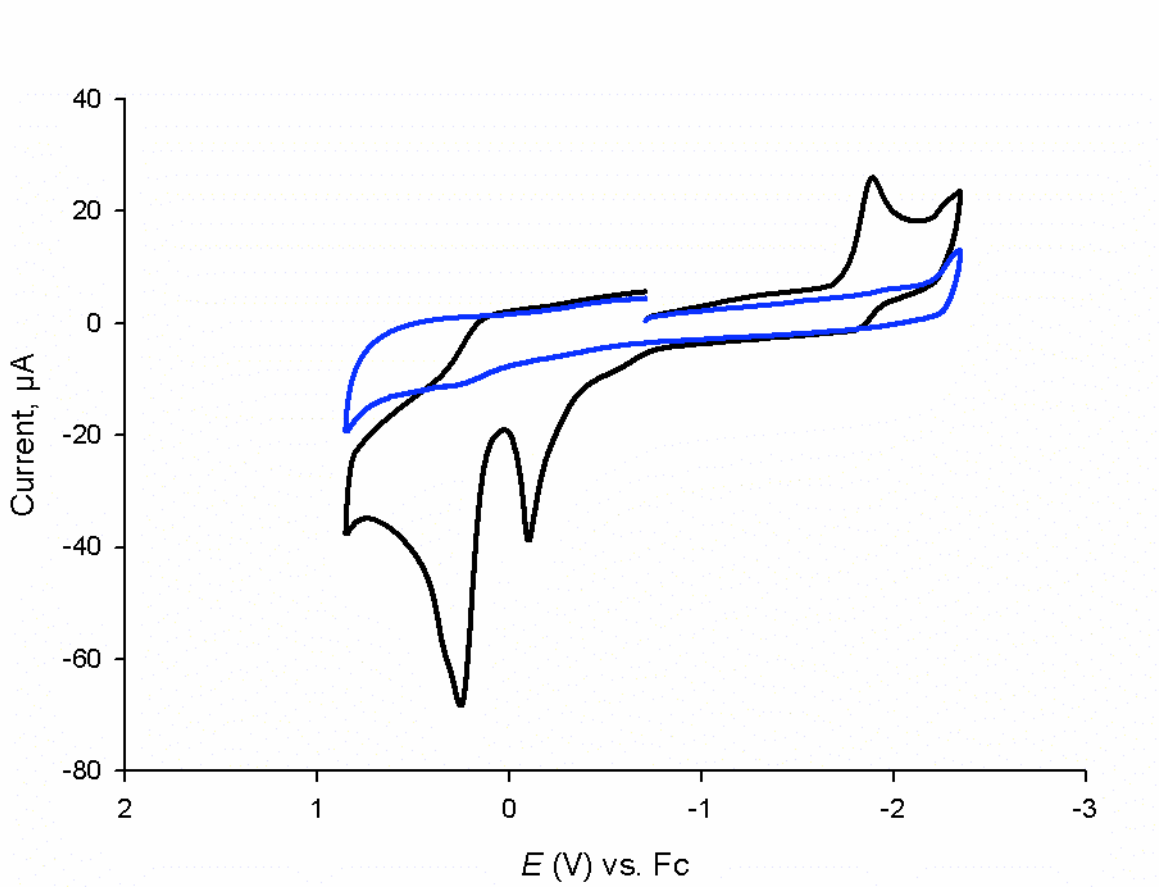

DPV - reduction

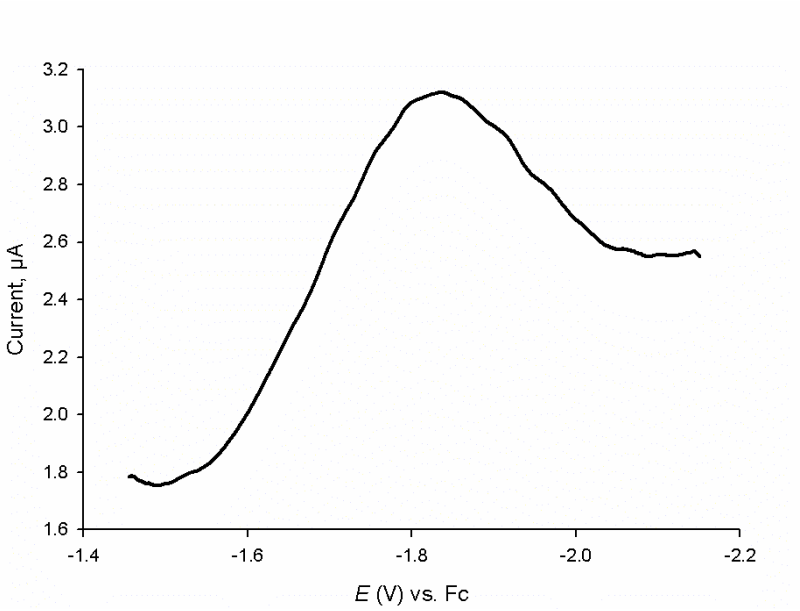

DPV - oxidation

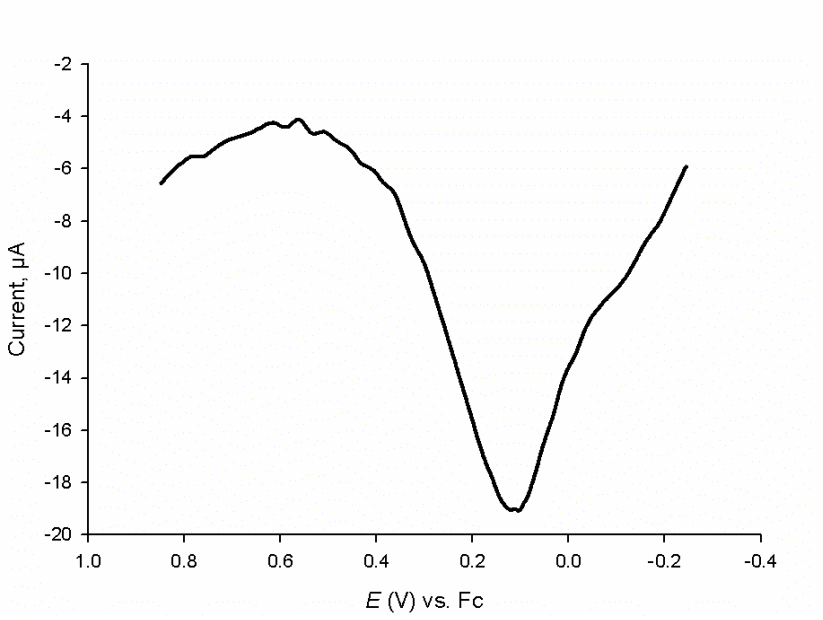

APPENDIX E

EXPERIMENTAL DATA FOR CHAPTER IV

Synthesis and Characterization

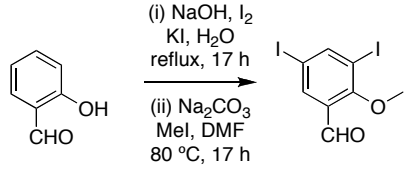

3,5-diiodo-2-methoxybenzaldehyde; Salicylaldehyde (10.0 g, 81.9 mmol) was dissolved in 83 mL of 1 M NaOH. Na_2CO_3 (23.3 g, 220 mmol) was then added followed by 100 mL of Lugol's solution.* The reaction was heated to reflux for 17 h and then cooled to room temperature. The precipitate was filtered, washed with an ice/water mixture and then dissolved in near boiling water. The undissolved parts were removed by filtration and the filtrate was cooled in an ice bath. Sodium 2-formyl-4,6-diiodophenolate was isolated after filtration as green crystals (12.0 g, 37 %).

Sodium 2-formyl-4,6-diiodophenolate (5.00 g, 12.6 mmol) was added to 50 mL of DMF. Na_2CO_3 (4.02 g, 37.9 mmol) was added along with MeI (3.93 mL, 63.2 mmol). The suspension was stirred at 80 ºC for 24 h. The reaction was then cooled to room temperature and 25 mL of 0.2 M Na_2CO_3 was added. The product was extracted with 50 mL EtOAc (x 2) and the combined organic layers were washed with 25 mL 0.2 M Na_2CO_3 (x 2) and 25 mL of brine. The organic layer was dried over $MgSO_4$ and filtered. The filtrate was evaporated under reduced pressure to yield 3,5-diiodo-2-

methoxybenzaldehyde as a white powder (3.9 g, 80 %) ^{1}H NMR (300 MHz, $CDCl_3$), δ 10.18 (s, 1H), 8.31 (d, *J* = 2.4 Hz, 1 H), 8.07 (d, *J* = 2.4 Hz, 1H), 3.92 (s, 3H). ^{13}C NMR (75 MHz, $CDCl_3$), δ 188.0, 162.6, 152.7, 138.0, 131.4, 94.6, 89.5, 64.2.

*Lugol's solution was prepared by addition of I_2 (43.3 g, 170.6 mmol) to KI (66.7 g, 401.6 mmol) in ~100 mL H_2O.

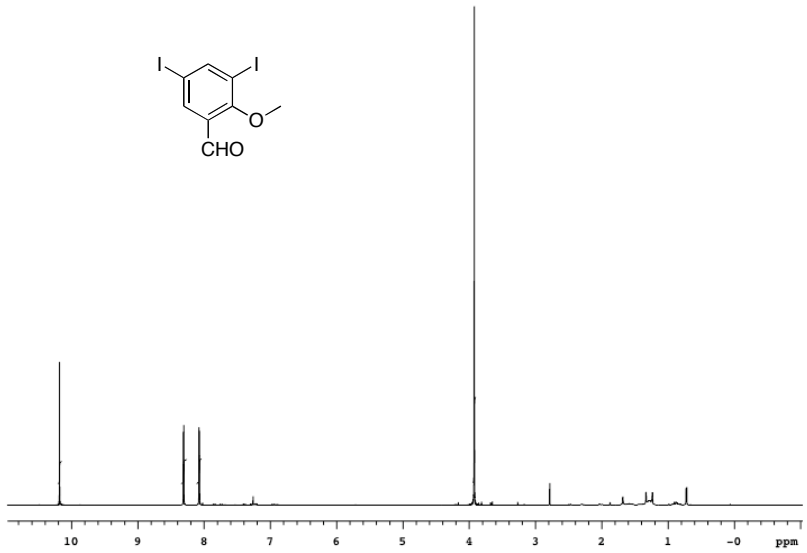
I
I
O
CHO
10
9
8
7
6
5
4
3
2
1
-0
ppm

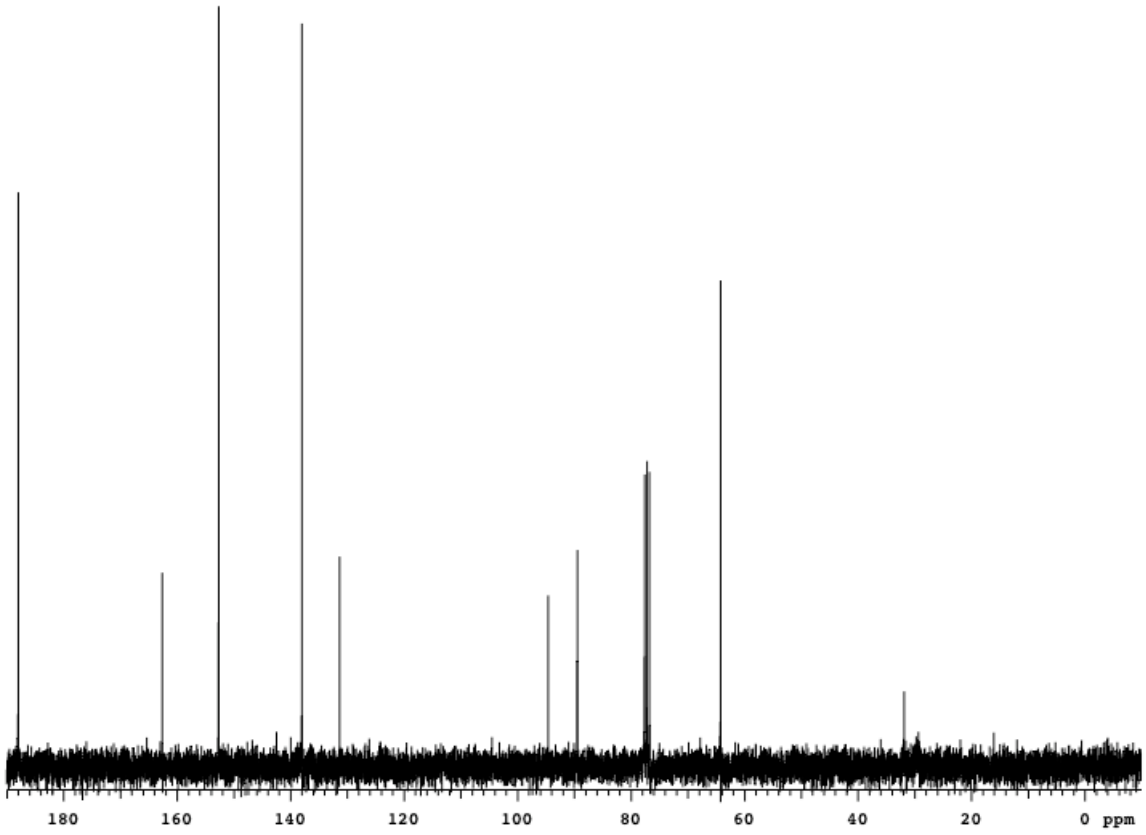
180
160
140
120
100
80
60
40
20
0 ppm

Representative procedure for preparation of all BODIPYs

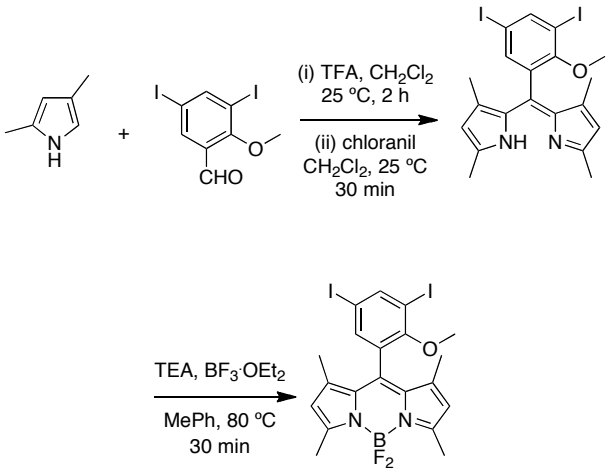

71a; A solution of 2,4-dimethylpyrrole (0.88 mL, 8.51 mmol), 3,5-diiodo-2-methoxybenzaldehyde (1.5 g, 3.87 mmol), and 5 drops of TFA (catalytic amt.) in 40 mL CH_2Cl_2 were stirred at 25 ºC for 2 h. *p*-chloranil (1.00 g, 4.25 mmol) was added and the reaction was stirred at 25 ºC for 30 min. The crude solution was transferred directly unto a basic aluminum column eluting with CH_2Cl_2. Collected fractions containing the dipyrromethene intermediate were combined and evaporated under reduced pressure. The dipyrromethene was dissolved in 80 mL of toluene and triethylamine (1.60 mL, 11.6 mmol) was added. The mixture was stirred at 25 ºC for 15 min and BF_3•OEt_2 (2.40 mL, 19.3 mmol) was added. The reaction was stirred at 80 ºC for 30 min and then cooled to room temperature. The reaction was quenched with 40 mL of H_2O and stirred for 3 h. The mixture was extracted with 40 mL EtOAc (x 2). The combined organic layers were washed with 40 mL H_2O (x 2) and 40 mL of brine. The organic layer was dried over $MgSO_4$ and then filtered. The filtrate was evaporated under reduced pressure and the

residue was purified via flash silica column eluting with 2:1 to 1:1 hexanes/CH_2Cl_2 to yield 576 mg (25 %) of **71a** as an orange powder. ^{1}H NMR (300 MHz, $CDCl_3$), δ 8.22 (d, *J* = 2.0 Hz, 1 H), 7.51 (d, *J* = 2.0 Hz, 1H), 6.01 (s, 2H), 3.67 (s, 3H), 2.55 (s, 6H), 1.54 (s, 6H). ^{13}C NMR (126 MHz, $CDCl_3$), δ 156.5, 156.4, 148.3, 142.4, 139.0, 134.9, 131.1, 130.9, 121.8, 94.2, 88.2, 60.9, 14.8, 14.3. HRMS (MALDI) calc for $C_{20}H_{18}BF_2I_2N_2O^{\bullet}$ 605.9648, found 605.9631.

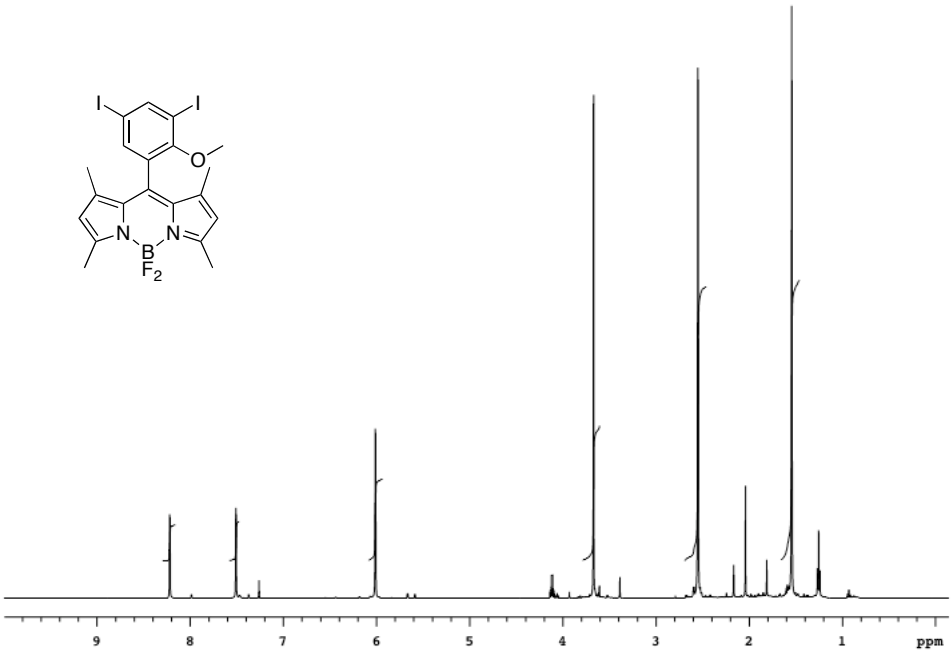
I
I
O
N
B
F2
N
9
8
7
6
5
4
3
2
1
ppm

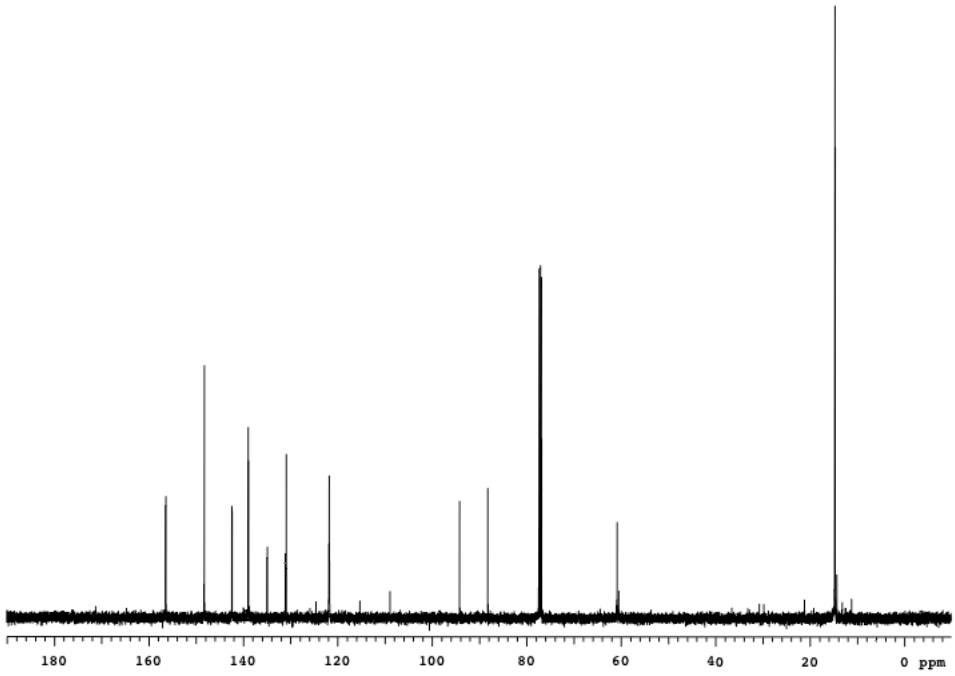

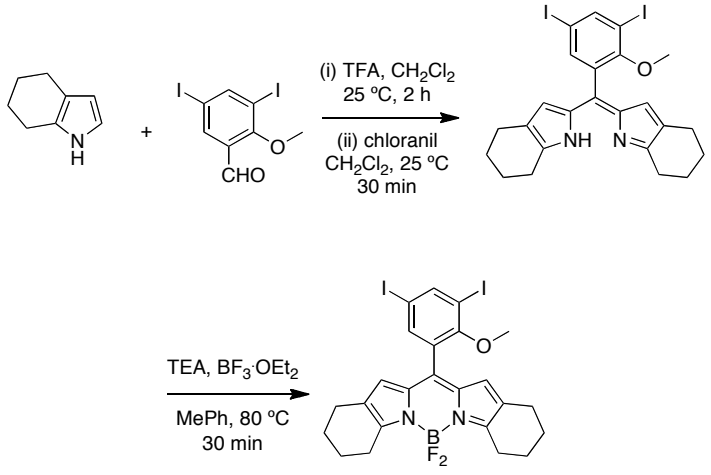

71b; Representative procedure was followed. The residue obtained after extraction was purified via flash silica column eluting with 5:2 hexanes/CH_2Cl_2 to yield 1.5 g (66 %) of **71b** as a red powder. ^{1}H NMR (500 MHz, $CDCl_3$), δ 8.19 (d, J = 2.0 Hz, 1 H),

7.55 (d, *J* = 2.0 Hz, 1H), 6.31 (s, 2H), 3.61 (s, 3H), 3.07 (t, *J* = 6.0 Hz, 4H), 2.49 (t, *J* = 6.0 Hz, 4H), 1.85 (m, 4H), 1.73 (m, 4H). ^{13}C NMR (126 MHz, $CDCl_3$), δ 158.7, 157.7, 148.0, 140.7, 133.9, 133.7, 130.0, 129.9, 125.8, 93.8, 87.3, 62.0, 24.9, 23.3, 22.9, 22.4. HRMS (MALDI) calc for $C_{24}H_{23}BF_2I_2N_2O^{\bullet}$ 657.9961, found 657.9974.

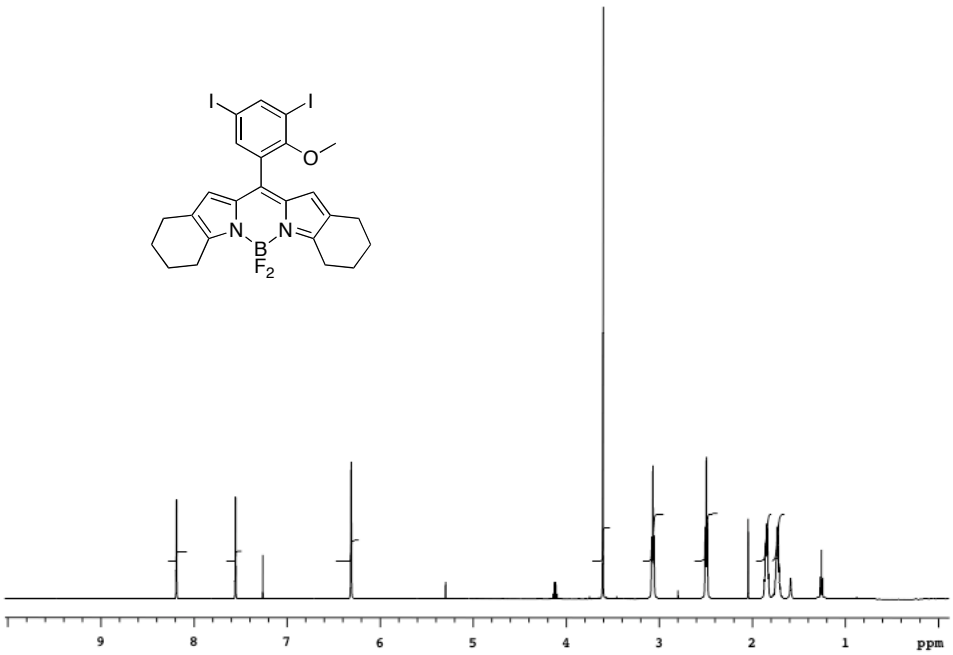
I
I
O
N
B
F2
N
9
8
7
6
5
4
3
2
1
ppm

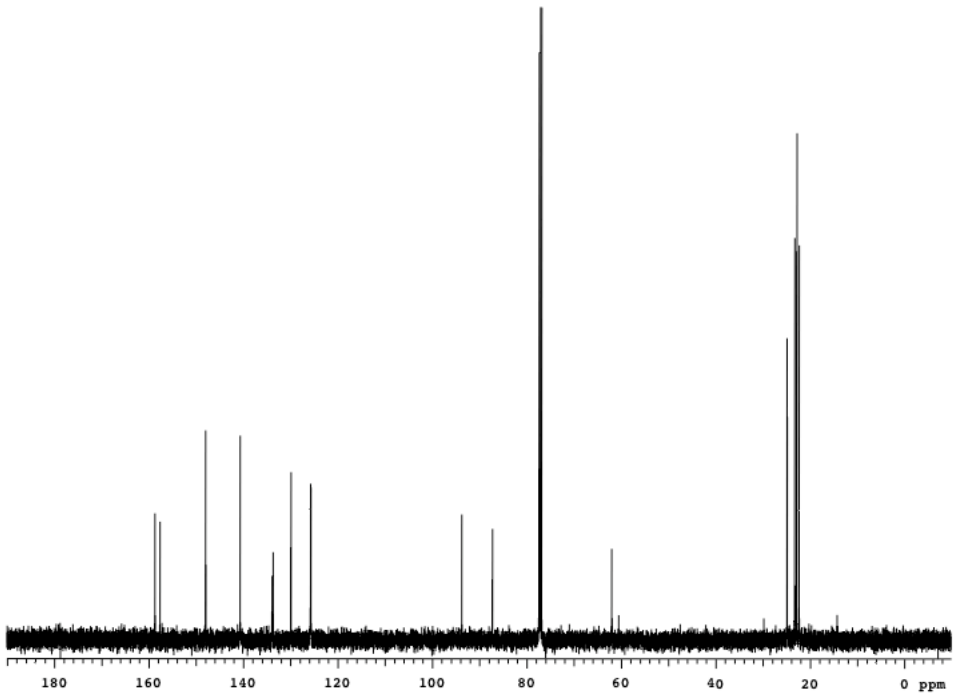

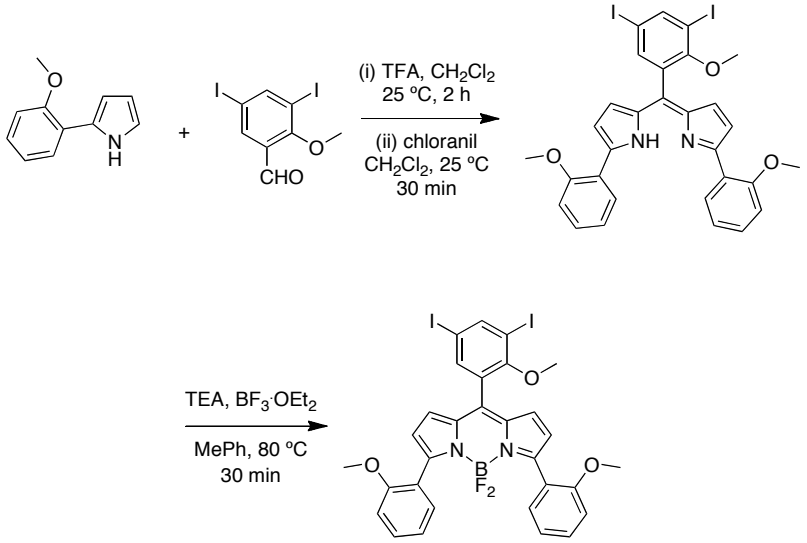

71c; Representative procedure was followed. 2-(2-methoxyphenyl)-1H-pyrrole was synthesized according to literature procedure.[212] The residue obtained after extraction

was purified via flash silica column eluting with 1:1 to 1:2 hexanes/CH_2Cl_2 to yield 2.6 g (75 %) of **71c** as a red powder. ^{1}H NMR (500 MHz, $CDCl_3$), δ 8.27 (d, *J* = 2.0 Hz, 1 H), 7.78 (dd, *J* = 7.5, 1.5 Hz, 2H), 7.73 (d, *J* = 2.0 Hz, 1H), 7.35 (dt, *J* = 8.5, 7.5, 0.5 Hz, 2H), 7.01 (dt, *J* = 7.5, 7.5, 0.5 Hz, 2H), 6.92 (d, *J* = 8.5 Hz, 2H), 6.77 (d, *J* = 4.5 Hz, 2H), 6.62 (d, *J* = 4.5 Hz, 2H), 3.79 (s, 6H), 3.73 (s, 3H). ^{13}C NMR (126 MHz, $CDCl_3$), δ 157.8, 157.6, 156.3, 148.3, 140.8, 136.0, 135.3, 131.9 (t, *J* = 4.5 Hz), 130.9, 129.8, 128.8, 122.9, 121.7, 120.3, 110.9, 93.8, 87.3, 66.3, 55.7 HRMS (MALDI) calc for $C_{30}H_{23}BF_2I_2N_2O_3^{\bullet}$ 761.9859, found 761.9849.

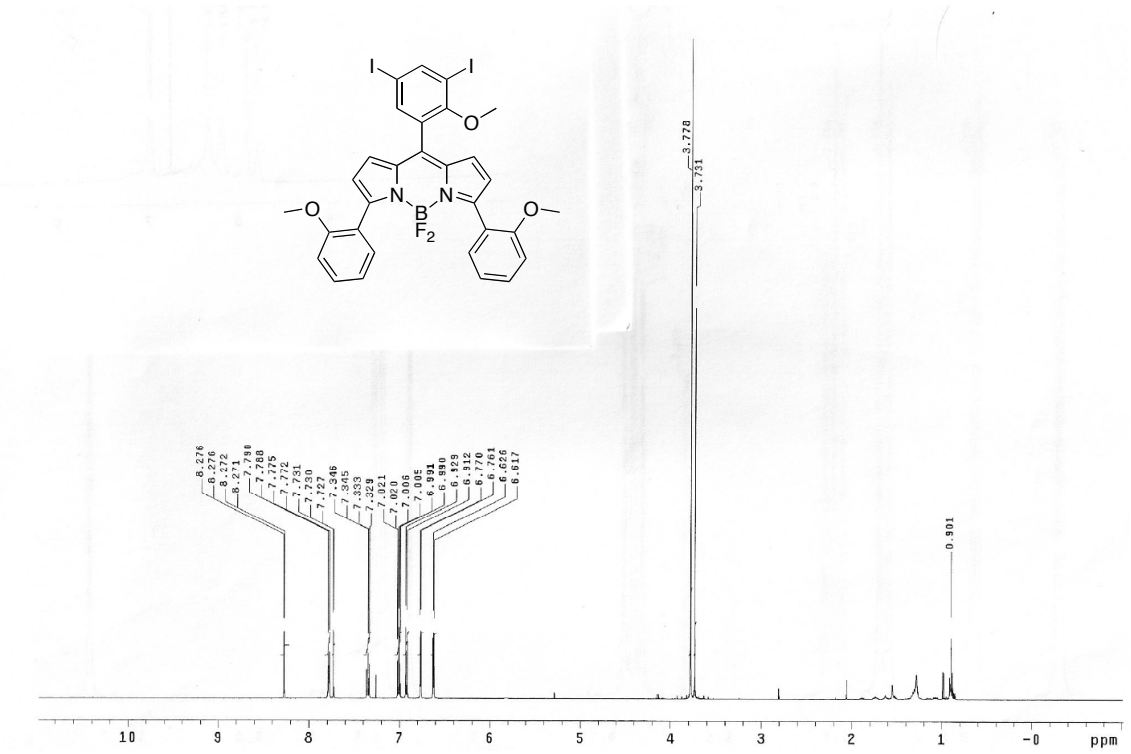
I
I
O
O
N
B
N
O
F2
3.778
3.751
8.276
8.270
8.272
7.798
7.788
7.775
7.772
7.751
7.750
7.727
7.346
7.345
7.333
7.329
7.021
7.020
7.006
7.005
6.991
6.990
6.129
6.112
6.770
6.761
6.626
6.617
0.901
10
9
8
7
6
5
4
3
2
1
-0
ppm

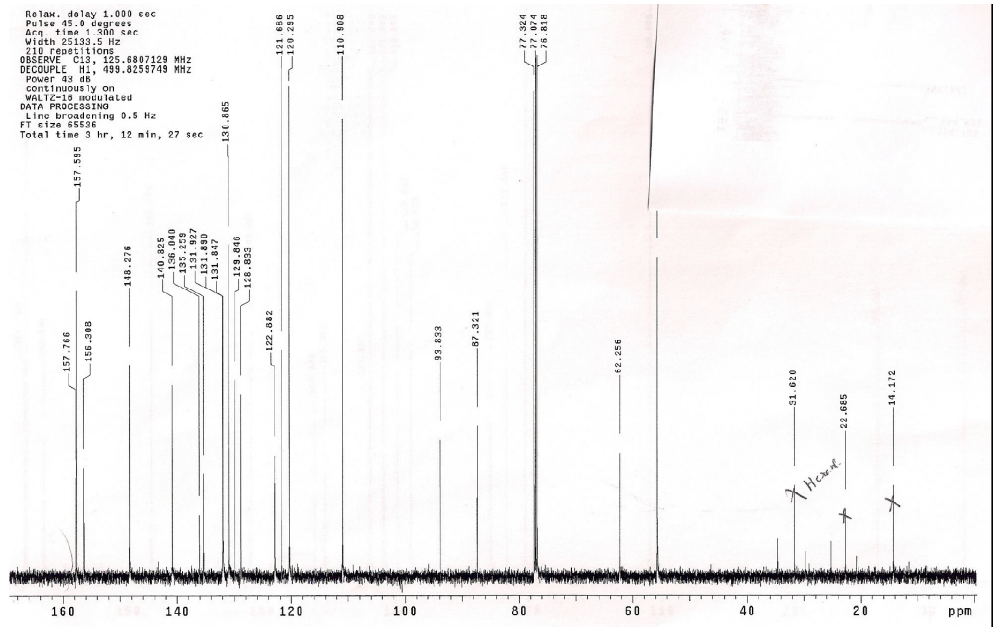
Relax. delay 1.000 sec
Pulse 45.0 degrees
Acq. time 1.300 sec
Width 25133.5 Hz
210 repetitions
OBSERVE C13, 125.6807129 MHz
DECOUPLE H1, 499.8255749 MHz
Power 49 dB
continuously on
WALTZ-16 modulated
DATA PROCESSING
Line broadening 0.5 Hz
FT size 65536
Total time 3 hr, 12 min, 27 sec
157.595
157.766
156.308
140.825
136.040
135.259
133.877
131.839
131.847
131.665
128.846
126.882
122.682
121.656
120.255
110.968
93.833
87.321
77.324
77.074
76.818
62.256
51.620
22.665
14.172
Heart
160
140
120
100
80
60
40
20
ppm

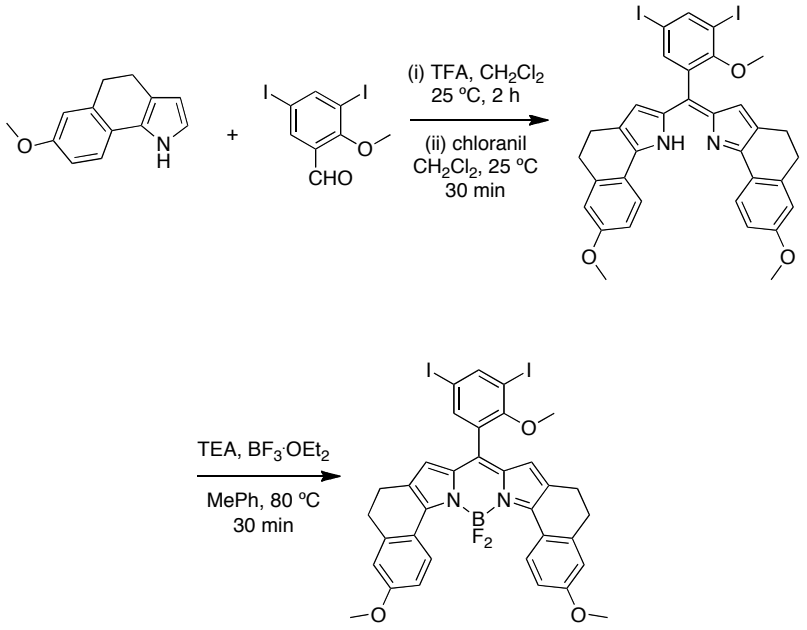

71d; Representative procedure was followed. 7-methoxy-4,5-dihydro-1H-benzo{*g*}indole was synthesized according to literature procedure.[213] The residue obtained after extraction was purified via flash silica column eluting with 3:1 to 2:1 hexanes/CH_2Cl_2 to yield **71d** (35 %) as a green powder. ^{1}H NMR (500 MHz, $CDCl_3$), δ 8.76 (d, *J* = 9.0 Hz, 2 H), 8.22 (d, *J* = 2.5 Hz, 1H), 7.64 (d, *J* = 2.0 Hz, 1H), 6.99 (dd, *J* = 9.0, 3.0 Hz, 2H), 6.80 (d, *J* = 2.5 Hz, 2H), 6.40 (s, 2H), 3.88 (s, 6H), 3.67 (s, 3H), 2.88 (t, *J* = 7.0 Hz, 4H), 2.67 (t, *J* = 7.0 Hz, 4H). ^{13}C NMR (126 MHz, $CDCl_3$), δ 160.9, 157.9, 152.4, 147.9, 143.1, 141.1, 135.6, 132.6, 130.9, 130.3 {m, (triplet overlapping with another peak, 2C}, 123.9, 121.5, 114.4, 112.6, 93.8, 87.4, 62.0, 55.4, 31.0, 22.5 HRMS (MALDI) calc for $C_{34}H_{27}BF_2I_2N_2O_3^{\bullet}$ 814.0172, found 814.0185.

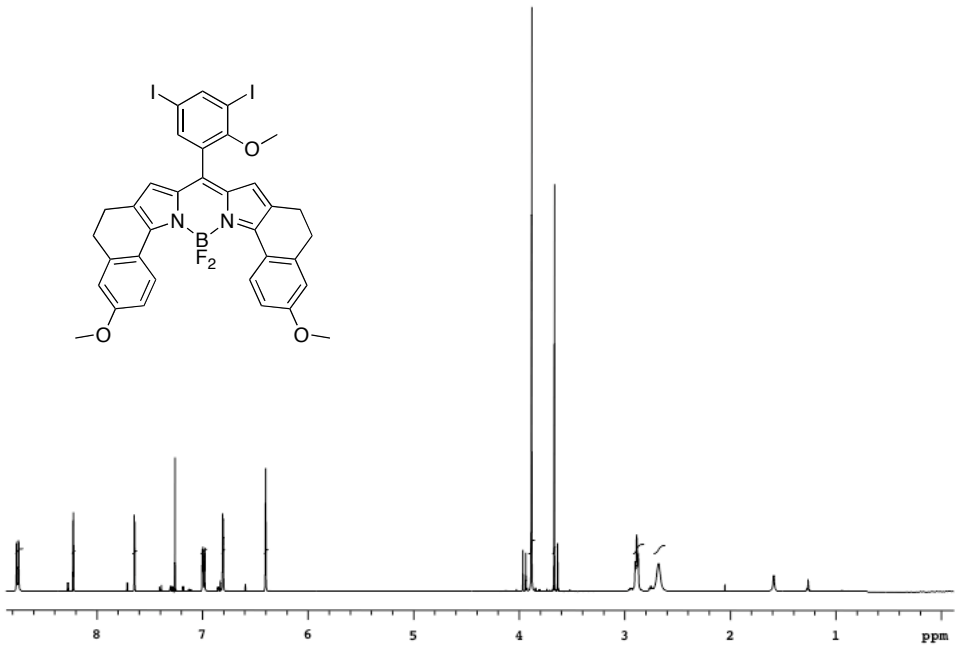
I
I
O
N
B
F2
N
O
O
8
7
6
5
4
3
2
1
ppm

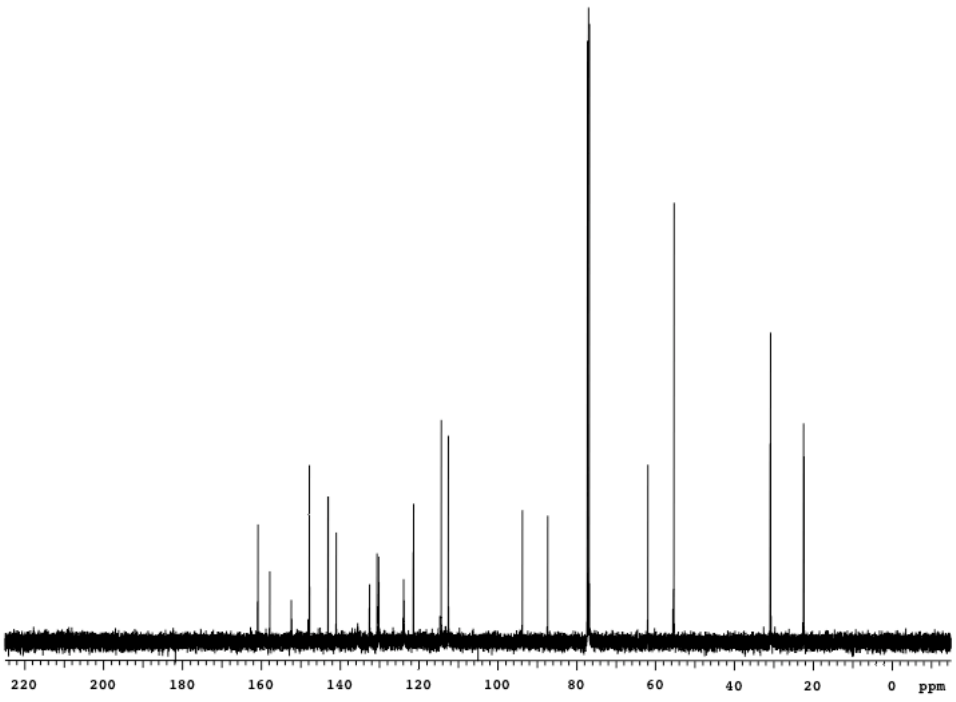

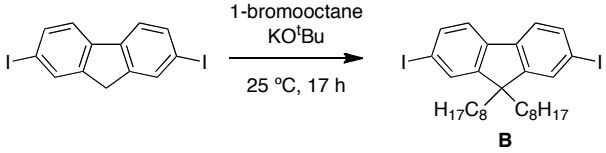

B

B; 2,7-diiodo-9*H*-fluorene[Raymond, 2008 #15498] (10 g, 24 mmol) and 1-bromooctane (10 mL, 57 mmol) were suspended in THF (60 mL). Mixture was cooled to 0 ºC and KO^{t}Bu (8.1 g, 72 mmol) was added. The reaction was warmed to 25 ºC and stirred for 17 h. The reaction was then quenched with 4 N HCl until a color change from purple to tan was obtained at 0 ºC. The product was then extracted with ether. The combined ether fractions were washed with 0.2 N HCl, dried over $MgSO_4$ and filtered. The solvent from the filtrate was removed under reduced pressure. The crude mixture was purified by flash silica chromatography eluting with 100:0 to 99:1 hexanes/CH_2Cl_2.

The product was obtained as a colorless powder (11 g, 73 %). ^{1}H NMR (300 MHz, $CDCl_3$), δ 7.70 (s, 2 H), 7.66 (d, *J* = 7.8 Hz, 2H), 7.40 (d, *J* = 7.8 Hz, 2H), 1.94 (t, *J* = 8.1, 4H), 1.30-1.08 (m, 24H), 0.86 (t, *J* = 7.1 Hz, 6H. ^{13}C NMR (75 MHz, $CDCl_3$), δ 152.5, 139.7, 136.1, 132.0, 121.5, 93.4, 55.6, 40.2, 31.8, 29.9, 29.3, 29.2, 23.7, 22.7, 14.3.

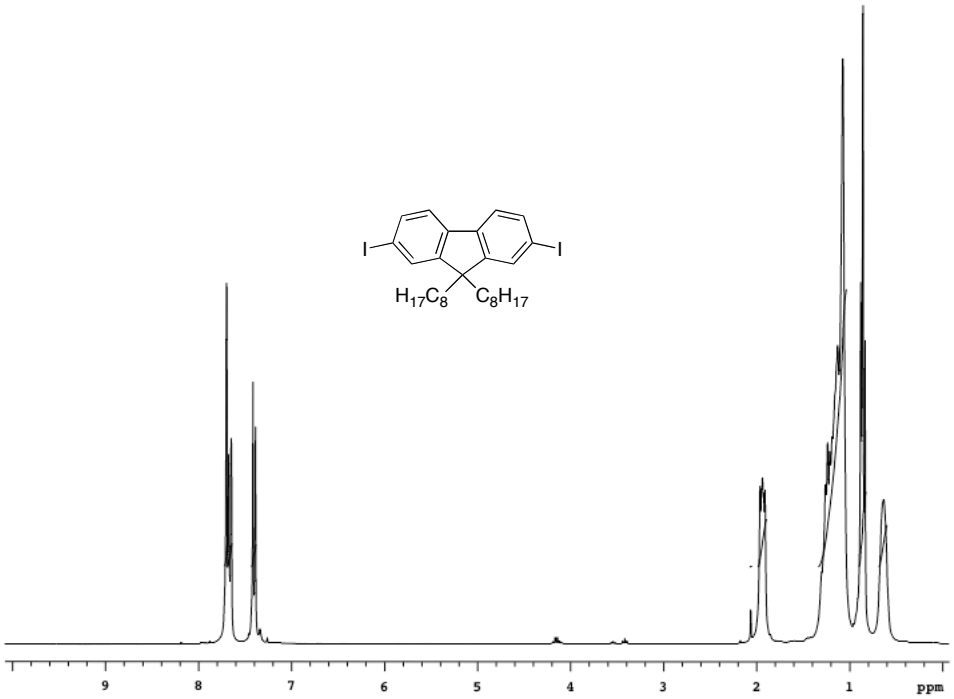
I
I
H17C8
C8H17
9
8
7
6
5
4
3
2
1
ppm

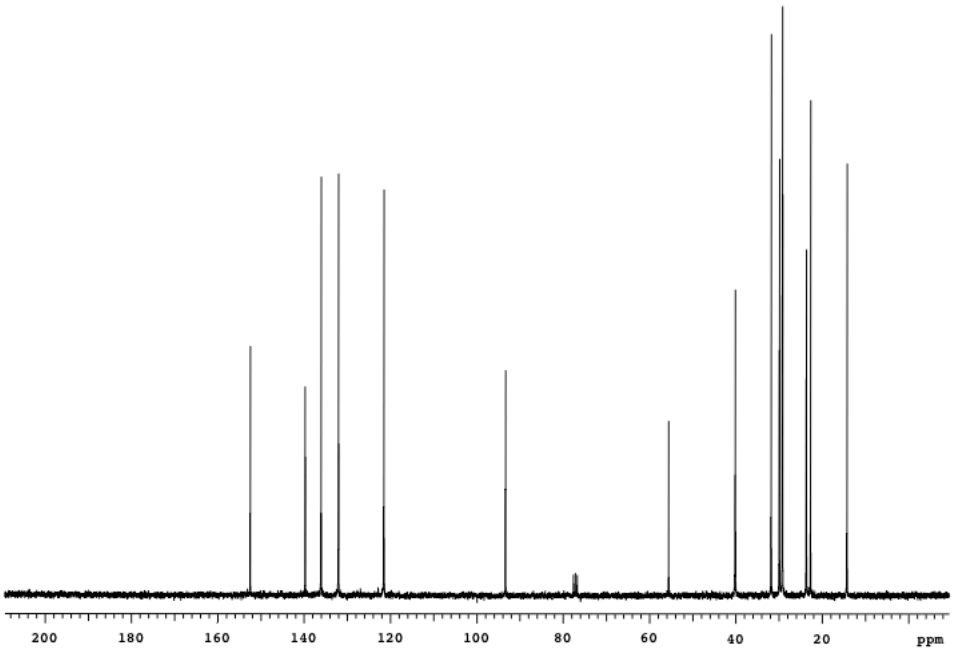

Representative procedure for preparation of polymers

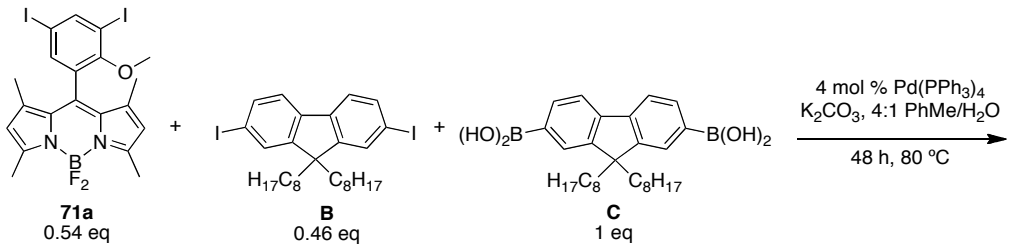

71a
0.54 eq

B
0.46 eq

C
1 eq

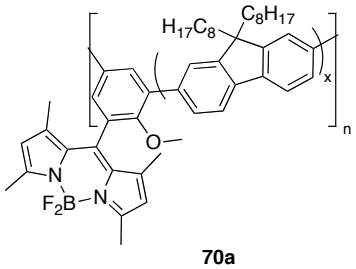

70a

70a; 2,7-diiodo-9,9-dioctyl-9*H*-fluorene (**B**) (31 mg, 0.048 mmol), 9,9-dioctyl-9*H*-fluorene-2,7-diboronic acid (**C**) (50 mg, 0.10 mmol), **71a** (34 mg, 0.056 mmol), and K_2CO_3 (55 mg, 0.40 mmol) were placed in a schlenk tube. The tube was evacuated and refilled with $N_{2(g)}$ three times and $Pd(PPh_3)_4$ (5 mg, 0.004 mmol) was added. The tube was then charged with 4:1 toluene/H_2O (10 mL and further degassed three times using the freeze/thaw method. Reaction was heated to 80 ºC and stirred under $N_{2(g)}$. After 60 h 2 drops of iodobenzene were added and the reaction was stirred for an additional 1 h at 80 ºC. The mixture is then precipitated by addition to ~150 mL of vortexing MeOH, filtered, and thoroughly washed with MeOH. The precipitate was transferred to a vial equipped with a stir bar and was stirred in 5mL of acetone at 25 ºC under $Ar_{(g)}$. After 24 h, the acetone was decanted off and the solid was stirred into an additional 5 mL of acetone. This was repeated for a total of 3 times (72 h). **70a** was obtained as a red powder (15 mg). Note: all polymers were made in parallel using a heating block to simultaneously heat all six mixtures with different acceptors. ^{1}H NMR (500 MHz, $CDCl_3$), δ 7.83 (bs), 7.66 – 7.35 (b), 6.07 (bs, 2H), 3.35 (bs), 2.61 (bs), 2.05 (bs, 26H), 1.77 (bs), 1.08 (bs), 0.78 (bs).

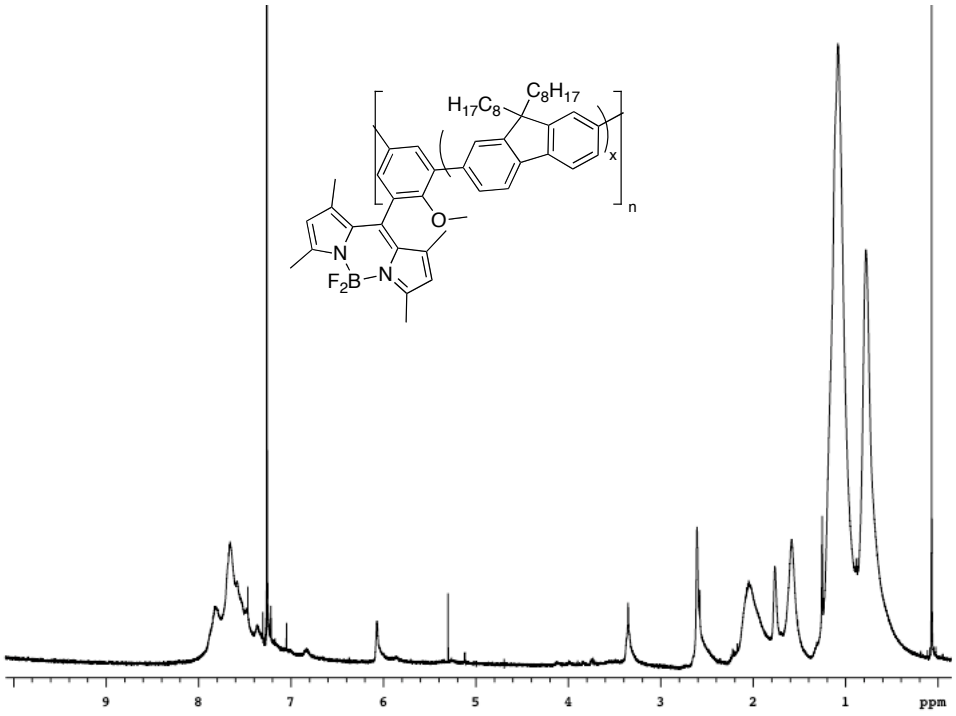
H17C8
C8H17
x
n
O
N
F2B
N
9
8
7
6
5
4
3
2
1
ppm

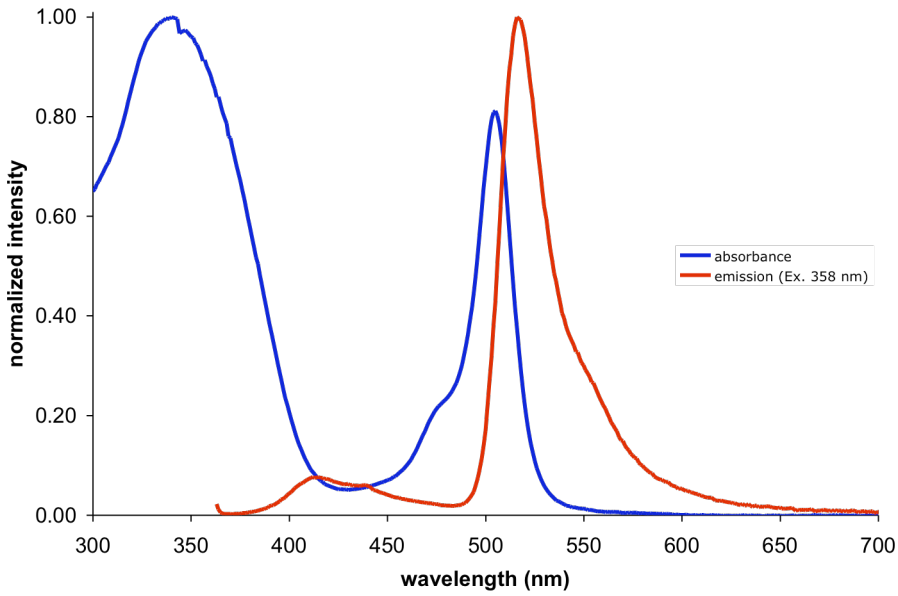
1.00
0.80
0.60
0.40
0.20
0.00
normalized intensity
300
350
400
450
500
550
600
650
700
wavelength (nm)
absorbance
emission (Ex. 358 nm)

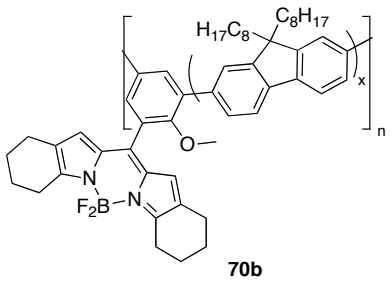

70b

70b; Representative polymer synthesis was followed. **70b** was obtained as an orange powder (26 mg, 0.10 mmol scale). ^{1}H NMR (500 MHz, $CDCl_3$), δ 7.83 (bs), 7.67 (bs), 7.58 (bs), 7.48 (bs), 7.35 (bs), 6.54 (bs, 2H), 3.36 (bs), 3.12 (bs), 2.54 (bs), 2.04 (bs, 11H), 1.87 (bs), 1.76 (bs), 1.08 (bs), 0.77 (bs).

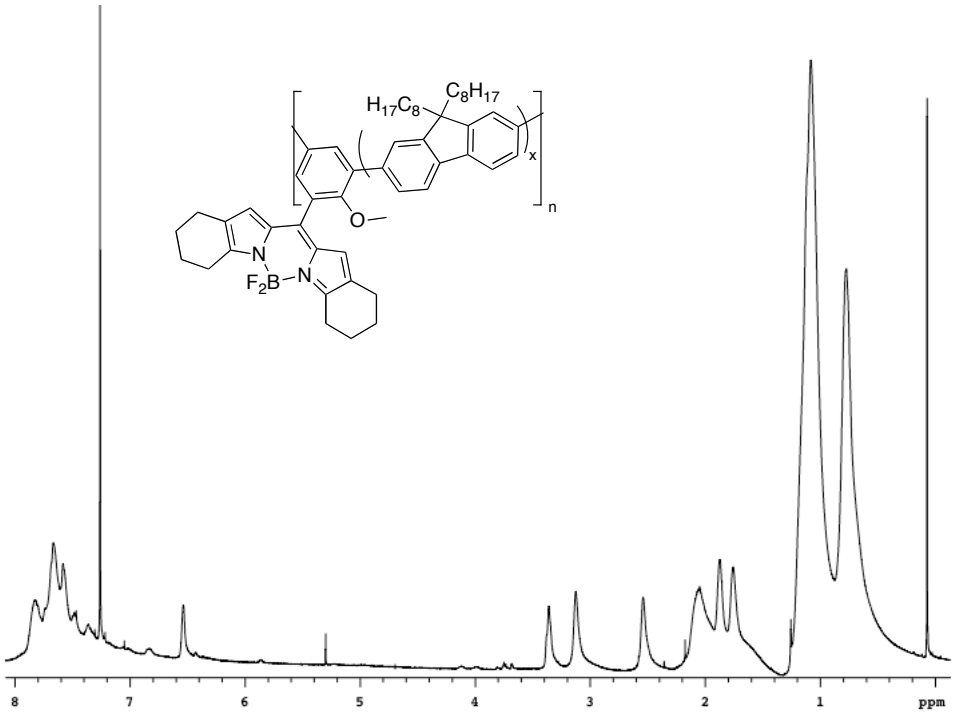
H17C8
C8H17
x
n
O
N
F2B
N
8
7
6
5
4
3
2
1
ppm

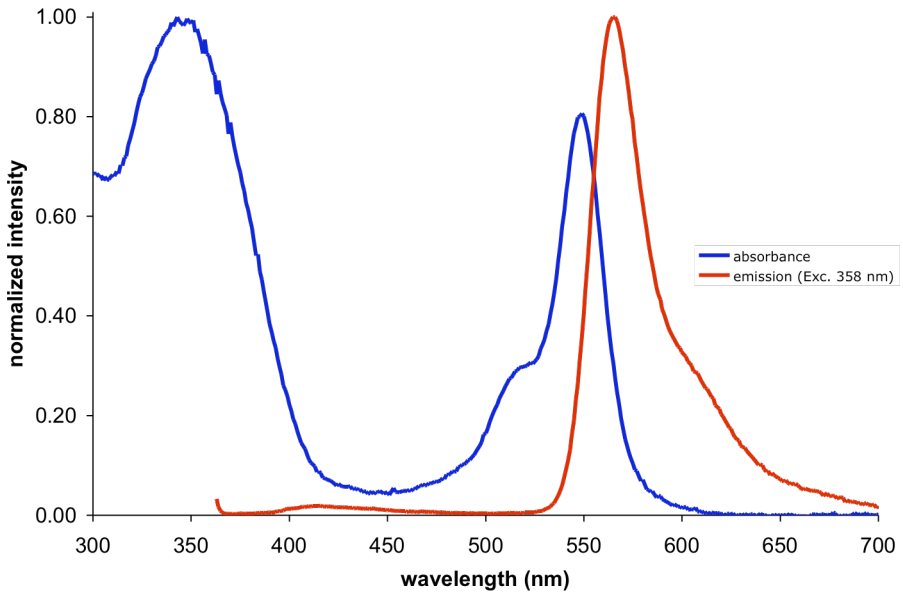
1.00
0.80
0.60
0.40
0.20
0.00
normalized intensity
300
350
400
450
500
550
600
650
700
wavelength (nm)
absorbance
emission (Exc. 358 nm)

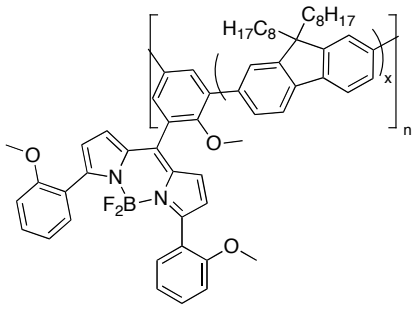

70c

70c; Representative polymer synthesis was followed. **70c** was obtained as an orange powder (5 mg, 0.046 mmol scale). ^{1}H NMR (500 MHz, $CDCl_3$), δ 7.81 (bs), 7.66 (bs), 7.47 (bs), 7.35 (bs), 6.99 (b), 6.93 (bs), 6.64 (bs), 3.80 (bs, 6H), 3.44 (bs), 2.10 (bs, 15H), 1.09 (bs), 0.78 (bs).

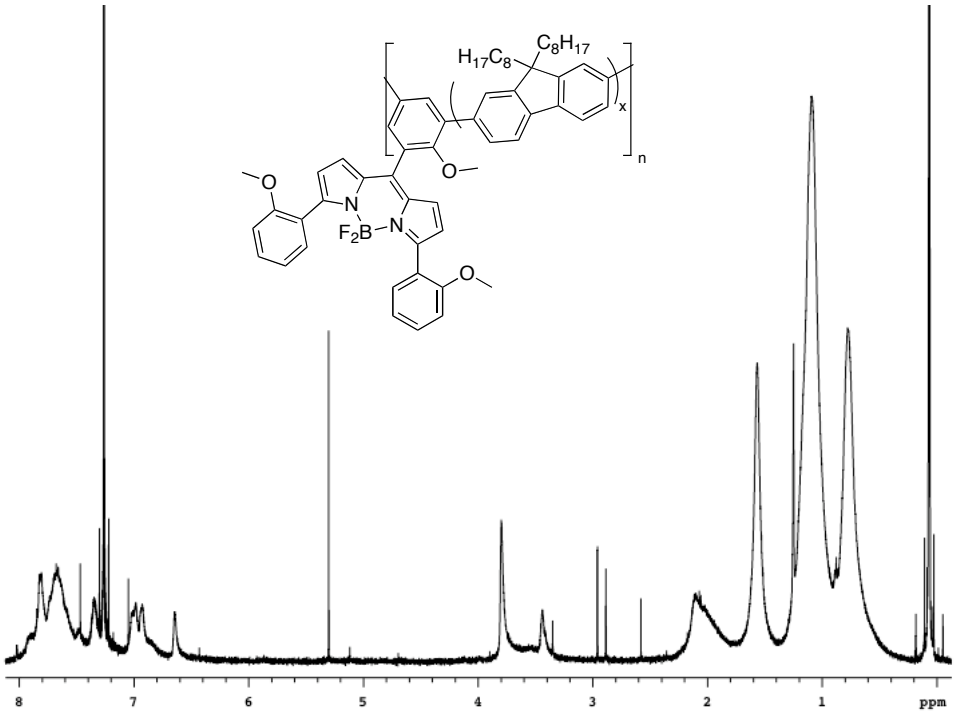
H17C8
C8H17
x
n
O
N
F2B
N
O
O
8
7
6
5
4
3
2
1
ppm

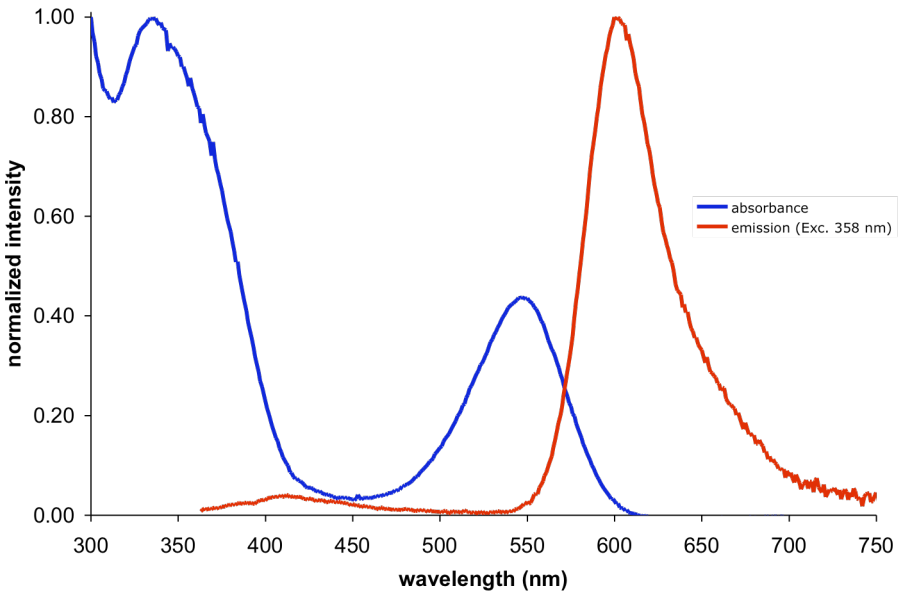
1.00
0.80
0.60
0.40
0.20
0.00
normalized intensity
300
350
400
450
500
550
600
650
700
750
wavelength (nm)
absorbance
emission (Exc. 358 nm)

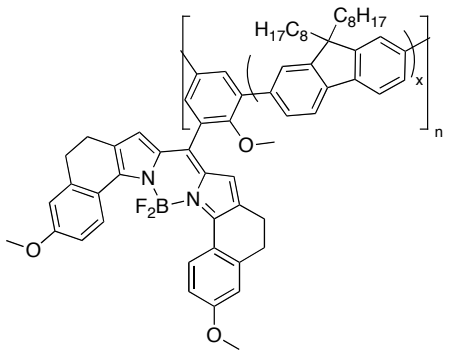

70d

70d; Representative polymer synthesis was followed. **70d** was obtained as a green powder (23 mg, 0.10 mmol scale). ^{1}H NMR (500 MHz, $CDCl_3$), δ 8.79 (bs), 7.82 (b), 7.67 (bs), 7.00 (bs), 6.82 (bs), 6.63 (bb), 3.89 (bs, 6H), 3.41 (bs), 2.91 (bs), 2.71 (bs), 2.06 (bs, 12H), 1.08 (bs), 0.77 (bs).

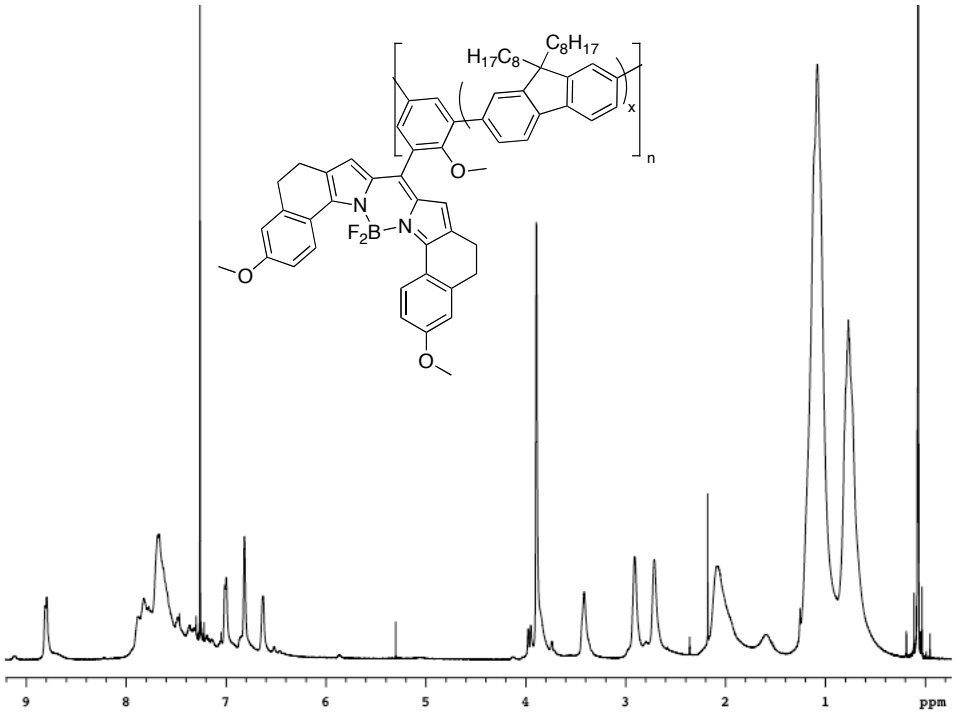
H17C8
C8H17
x
n
O
N
F2B
N
O
O
9
8
7
6
5
4
3
2
1
ppm

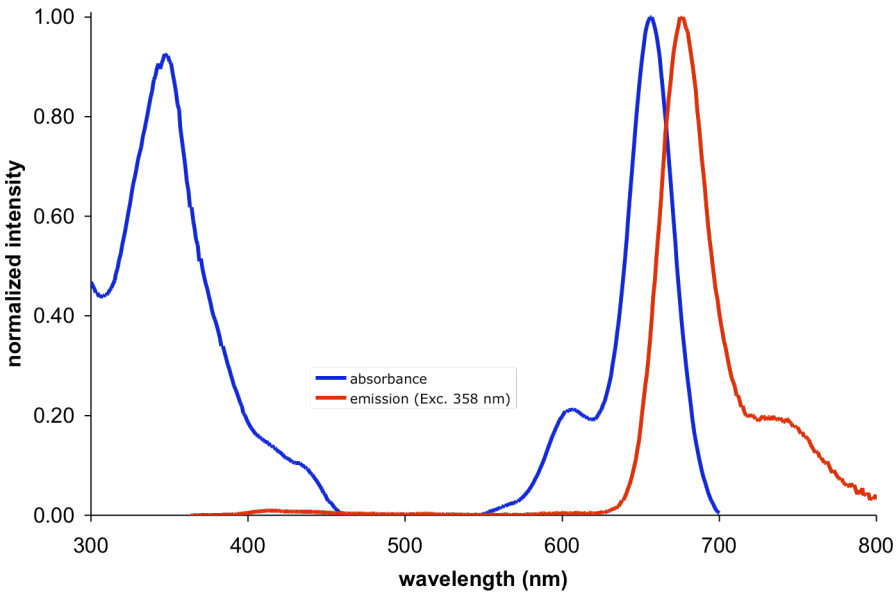
1.00
0.80
0.60
0.40
0.20
0.00
normalized intensity
absorbance
emission (Exc. 358 nm)
300
400
500
600
700
800
wavelength (nm)

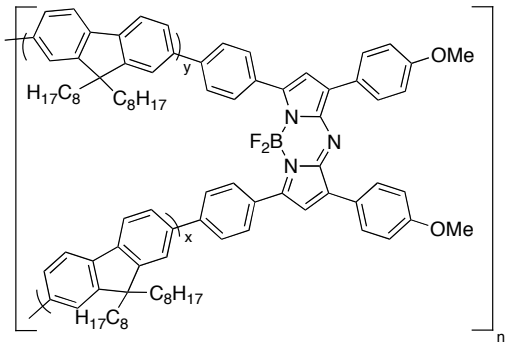

1e

1e. Representative polymer synthesis was followed. **1e** was synthesized according to literature procedure.[150] The polymer was obtained as a blue powder (26 mg, 0.10 mmol scale). ^{1}H NMR (500 MHz, $CDCl_3$), δ 8.22 (bs), 8.10 (bs), 7.82 (bs), 7.66 (bs), 7.03 (bs), 3.92 (bs, 6H), 2.07 (bs, 6H), 1.09 (bs), 0.78 (bs).

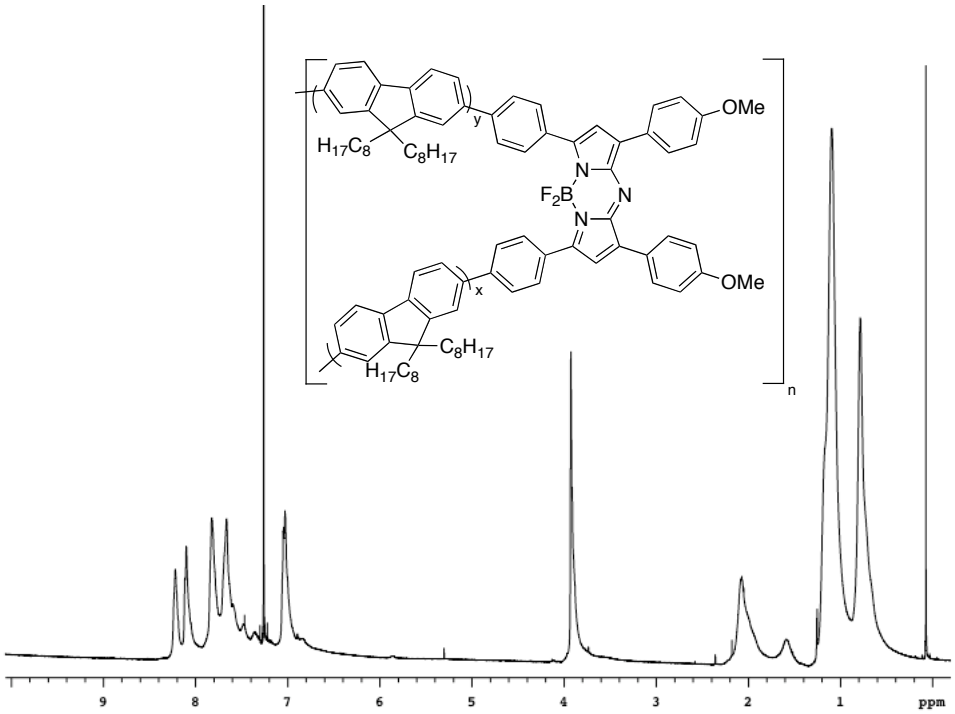
OMe
OMe
N
N
N
F_2B
y
x
n
$H_{17}C_8$
C_8H_{17}
C_8H_{17}
$H_{17}C_8$
9
8
7
6
5
4
3
2
1
ppm

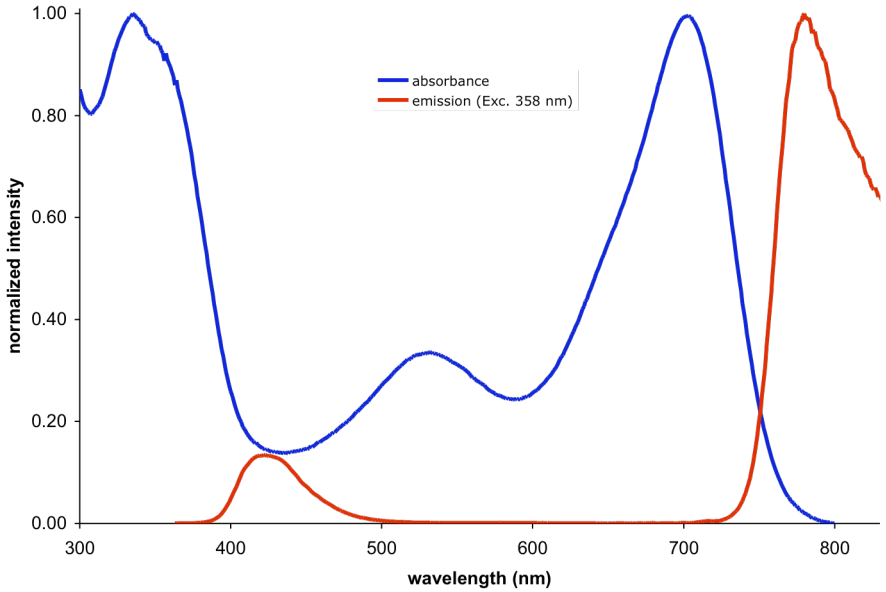
absorbance
emission (Exc. 358 nm)
normalized intensity
1.00
0.80
0.60
0.40
0.20
0.00
300
400
500
600
700
800
wavelength (nm)

Syntheses of Nanoparticles

Polymers were dissolved in THF at 4 ppm and and 2 mL were added to 8 mL of H_2O under probe sonication over 7 min via syringe pump. The mixture was passed through a 0.2 mm filter and rotovaped for 5 min at 30 ºC.

Optimization of brightness as a function of mol % acceptor

Optimization of brightness as a function of mol % acceptor was done by varying the amount of acceptor in the polymerization while at the same time adjusting the amount of diiodofluorene to keep a constant 1:1 ratio of diiodinated to boronic acid monomers. Acceptor **71a** was chosen for this study and was copolymerized in 0.05 - 0.67 equivalents. NMR studies show that BODIPY was incorporated in 6 – 19 mol % in the polymer.

Optimization of reaction time on brightness

The optimization of brightness of polymers **70** as a function of reaction time was studied by quenching the polymerizations at different times. Analysis of crude polymers was performed in order to avoid removal of smaller polymers from shorter reaction times. The maximum absorbance of the polymers in the crude mixture was determined by their excitation spectra. The relative brightness of each polymer was then determined by exciting solutions of equal concentration at the λ_{max} of the polymers and integrating the resulting fluorescence from the acceptors.

DLS and TEM Analysis of Particles

Dynamic light scattering (DLS) measurements were conducted using Delsa Nano C from Beckman Coulter, Inc. (Fullerton, CA) equipped with a laser diode operating at 658 nm. Size measurements were made water (n = 1.3329, η = 0.890 cP at 25 ± 1 °C; n = 1.3293). Scattered light was detected at 15° angle and analyzed using a log correlator over 70 accumulations for a 0.5 mL of sample in a glass size cell (0.9 mL capacity). The photomultiplier aperture and the attenuator were automatically adjusted to obtain a photon counting rate of *ca*. 10 kcps. The calculation of the particle size distribution and distribution averages was performed using CONTIN particle size distribution analysis routines. The peak average of histograms from number distributions out of 70 accumulations was reported as the average diameter of the particles.

TEM showed mostly large aggregates (see **70c**) for all polymers. Smaller, individual particles ranging from 20 to 60 nm were harder to find (**70a**, **70d**). Dynamic light scattering was done to make sure aggregation was not present on solution. DLS showed average particle size of 48.4 ± 13.3 nm.

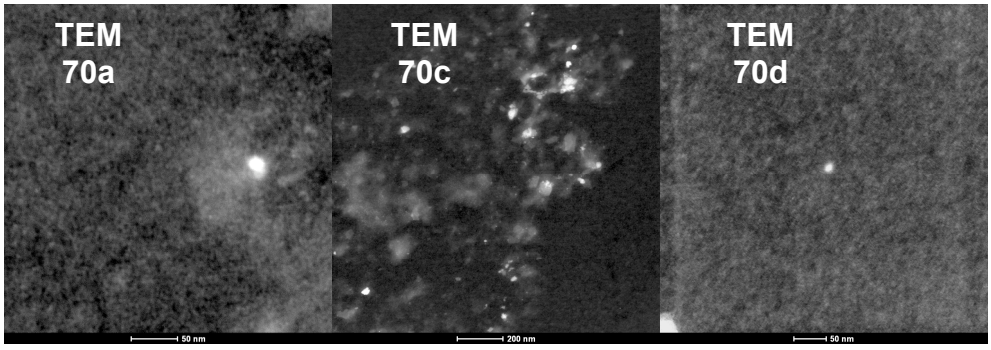

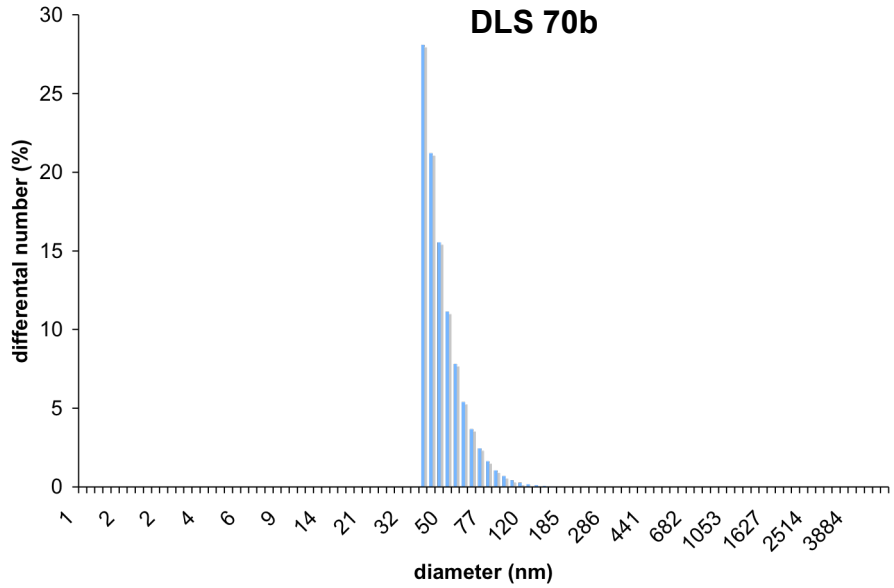

DLS and TEM analysis of particles.

In vitro Cellular Imaging Studies

(a) Cell culture

Clone 9 normal rat liver cells (American Type Culture Collection) were cultured as subconfluent monolayers on 75 cm^2 culture flask with vent caps in Ham's medium supplemented with 10 % fetal bovine serum (FBS) in a humidified incubator at 37 ºC with 5 % CO_2. Cells grown to subconfluence were enzymatically dissociated from the surface with trypsin and plated 2-3 days prior to the experiments in Lab-Tek two well chambered coverglass slides (Nunc).

(b) Fluorescence microscopy

Uptake and subcellular localization of the organic/McNeil nanoparticles were studied on living Clone 9 normal rat liver cells using a Zeiss 510 META NLO Multiphoton Microscope System consisting of an Axiovert 200 MOT microscope. Throughout, digital images were captured with a 40x / 1.3 oil objective with the following filter sets:

- for PFO nanoparticles: Excitation 740 nm; Emission BP 390-465 for the donor part ; Emission BP 565-615 for the acceptor part

- for **70a** nanoparticles: Excitation 740 nm; Emission BP 390-465 and BP 500-550 for the donor part and acceptor part, respectively

- for **70b** nanoparticles: Excitation 740 nm; Emission BP 390-465 and BP 565-615 for the donor part and acceptor part, respectively

- for **70c** nanoparticles: Excitation 740 nm; Emission BP 390-465 and BP 565-615 for the donor part and acceptor part, respectively

- for **70d** nanoparticles: Excitation 740 nm; Emission BP 390-465 and BP 650-710 for the donor part and acceptor part, respectively

Clone 9 cells were incubated for 40 hrs at 37 ºC in Ham's + 5 % FBS culture medium with 60 μL of 4 ppm nanoparticles solution. After the incubation period, the cells were washed with serum free culture medium (ACAS) several times before imaging.

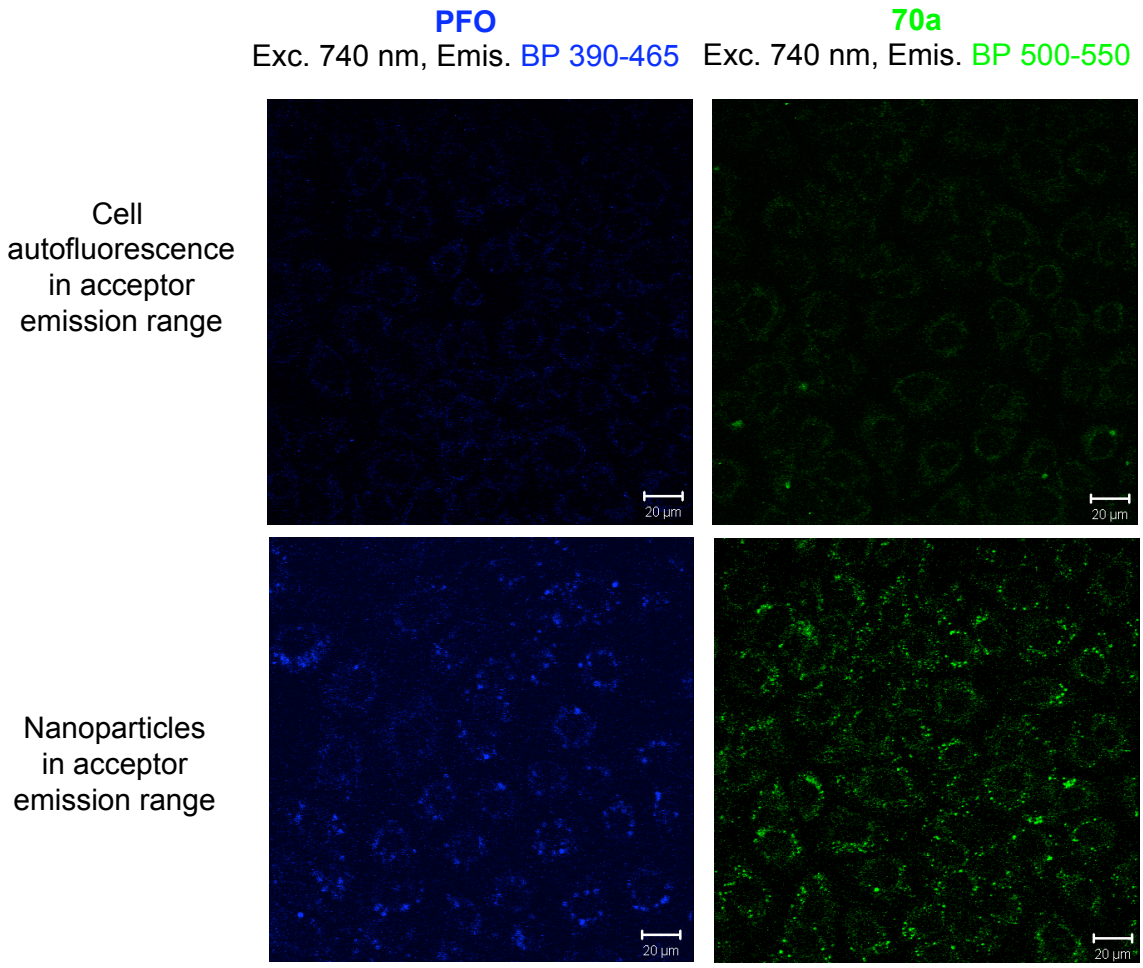
PFO
Exc. 740 nm, Emis. BP 390-465
70a
Exc. 740 nm, Emis. BP 500-550
Cell autofluorescence in acceptor emission range
Nanoparticles in acceptor emission range
20 µm
20 µm
20 µm
20 µm

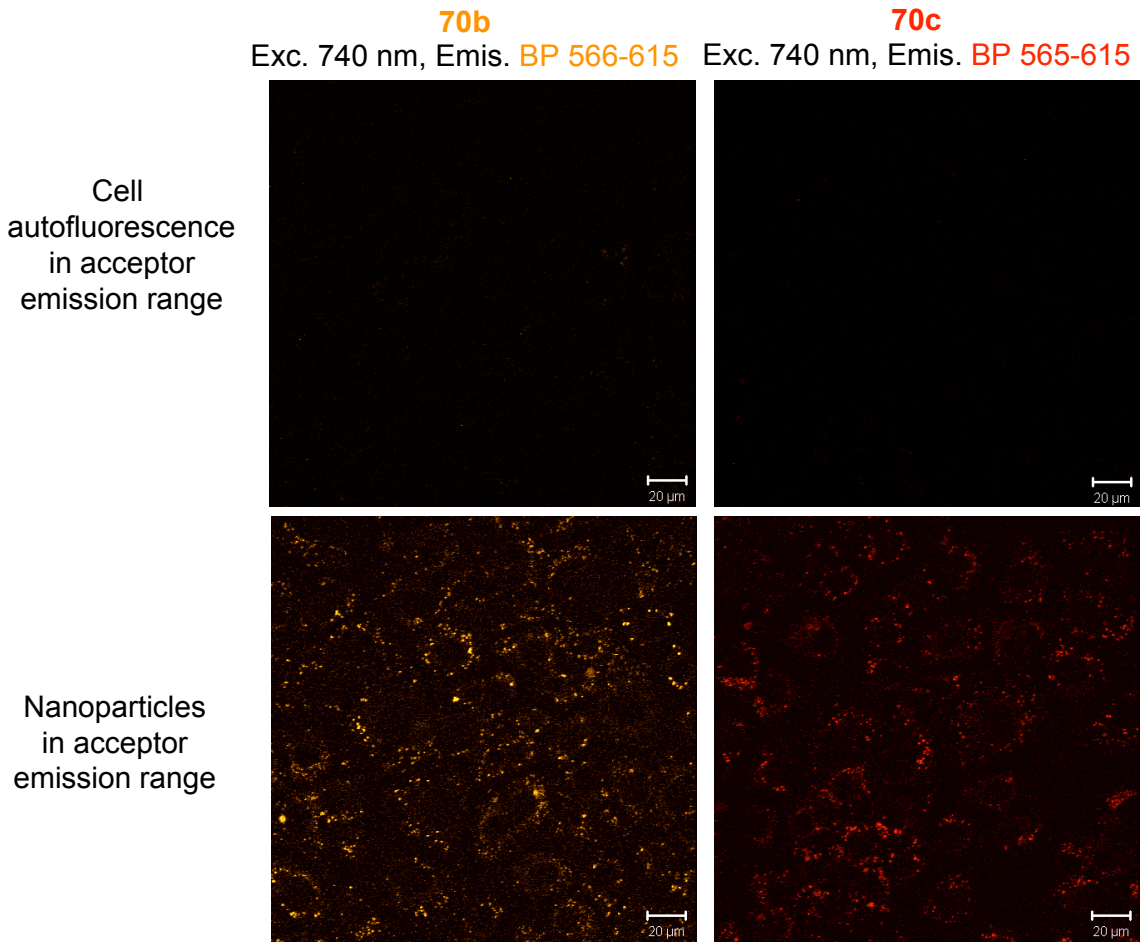
70b
Exc. 740 nm, Emis. BP 566-615
70c
Exc. 740 nm, Emis. BP 565-615
Cell autofluorescence in acceptor emission range
Nanoparticles in acceptor emission range
20 µm
20 µm
20 µm
20 µm

70d

Exc. 740 nm, Emis. BP 650-710

Cell autofluorescence in acceptor emission range

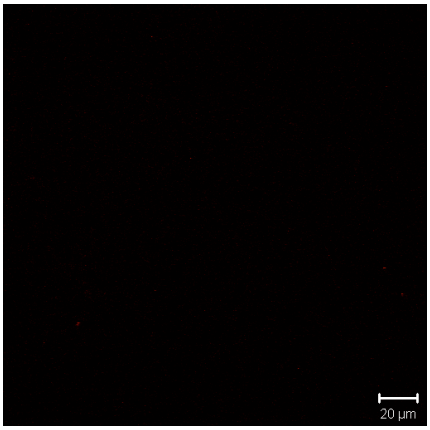

Nanoparticles in acceptor emission range

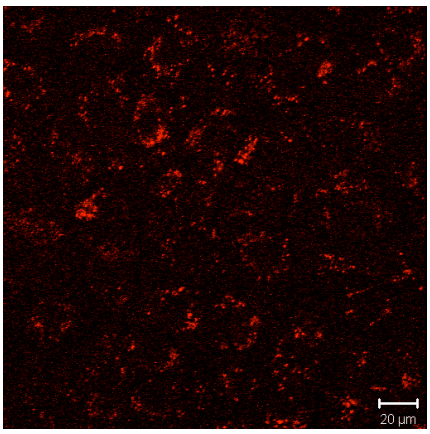

APPENDIX F

EXPERIMENTAL DATA FOR CHAPTER V

Photosensitizers

The synthesis of many of the compounds studied here has already been reported elsewhere. Compound **A** was prepared using a new method whereby 3,5-dimethylpyrrole-2-carbaldehyde was treated with 1.2 equivalents of $POCl_3$ followed by addition of $BF_3.OEt_2$.[45] Compound **B** was prepared from condensation of 2,4-dimethylpyrrole with 4-iodobenzene acid in $POCl_3$, and reaction of the resultant dipyrromethene intermediate with $BF_3.OEt_2$.[214] Compound **C** was prepared from compound **A** by using chlorosulphonic acid.[86]

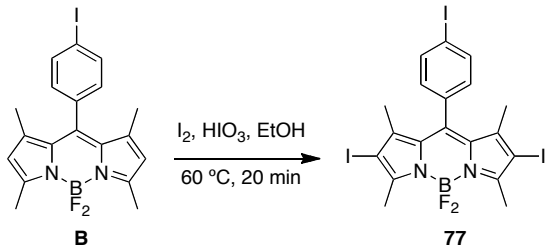

B **77**

A mixture of **B** (107 mg, 0.238 mmol), I_2 (151 mg, 0.476 mmol), HIO_3 (84.0 mg, 0.476 mmol) in 10 mL EtOH was warmed to 60 °C for 20 min. The mixture was then cooled to room temperature. The precipitate was filtered and washed thoroughly with MeOH to yield 135 mg (81 %) of product as an orange powder. ^{1}H NMR (300 MHz, $CDCl_3$) δ 7.88 (d, J = 8.4 Hz, 2H), 7.02 (d, J = 8.4 Hz, 2H), 2.64 (s, 6H), 1.43 (s, 6H). ^{13}C could not be obtained due to the tendency of the compound to crash out of solution during analysis. MS (APCI) calcd for $C_{19}H_{15}BF_2I_3N_2$ $\{M-H\}^-$ 700.84, found 701.38. R_f = 0.29 (49:1 hexanes/EtOAc). Compound is photosensitive and should be stored over extended periods accordingly.

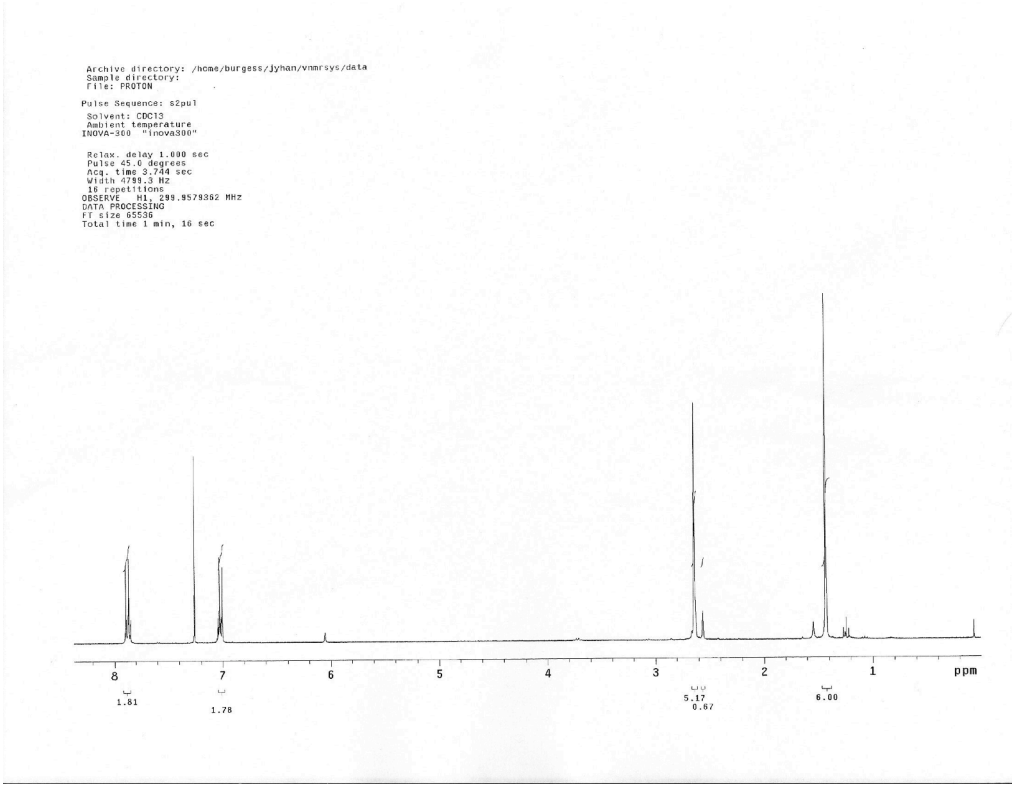
Archive directory: /home/burgess/jyhan/vnmrsys/data
Sample directory:
File: PROTON
Pulse Sequence: s2pul
Solvent: CDCl3
Ambient temperature
INOVA-300 "inova300"
Relax. delay 1.000 sec
Pulse 45.0 degrees
Acq. time 3.744 sec
Width 4789.3 Hz
16 repetitions
OBSERVE H1, 299.9579382 MHz
DATA PROCESSING
FT size 65536
Total time 1 min, 16 sec
8
7
6
5
4
3
2
1
ppm
1.81
1.78
5.17
0.67
6.00

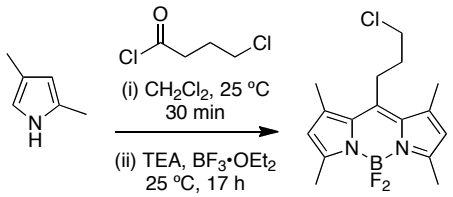

79

To a solution of 4-chlorobutanoyl chloride (0.99 mL, 8.8 mmol) in 20 mL of CH_2Cl_2 was added 2,4-dimethylpyrrole (2.0 mL, 19 mmol) over 10 min at 0 ºC. The reaction was stirred at 0 ºC for 30 min and then heated to 25 ºC and stirred for an additional 30 min. Triethylamine (3.7 mL, 26 mmol) was then added in small portions at 0 ºC and the mixture was stirred at 25 ºC for 10 min. BF_3•OEt_2 (5.5 mL, 44 mmol) was then added in portions and the mixture was stirred at 25 ºC for 17 h. The reaction was quenched with careful addition of 20 mL of H_2O and the system was stirred vigorously for 15 min. The layers were separated and the aqueous layer was extracted three times with 10 mL CH_2Cl_2. The organic layers were combined and washed twice with 10 mL H_2O and 10 mL of brine. The organic layer was dried over $MgSO_4$, filtered, and the solvent was removed under reduced pressure. The brown powder was dissolved in small amount of CH_2Cl_2 and filtered through a short plug of silica. The solvent was removed under reduced pressure and the remaining powder was recrystalized from ethyl acetate to yield 0.90 g (32 %) of **79** as a red needles. ^{1}H NMR (300 MHz, $CDCl_3$) δ 6.06 (s, 2H), 3.70 (t, J = 6.0 Hz, 2H), 3.13 (t, J = 8.4 Hz, 2H), 2.52 (s, 6H), 2.43 (s, 6H), 2.08 (m, 2H). ^{13}C (75 MHz, $CDCl_3$) δ 154.5, 144.6, 140.4, 131.6, 122.0, 44.9, 34.2, 26.1, 16.7, 14.6. MS (ESI) calcd for $C_{16}H_{21}BClF_2N_2$ $\{M+H\}^+$ 325.14, found 325.47.

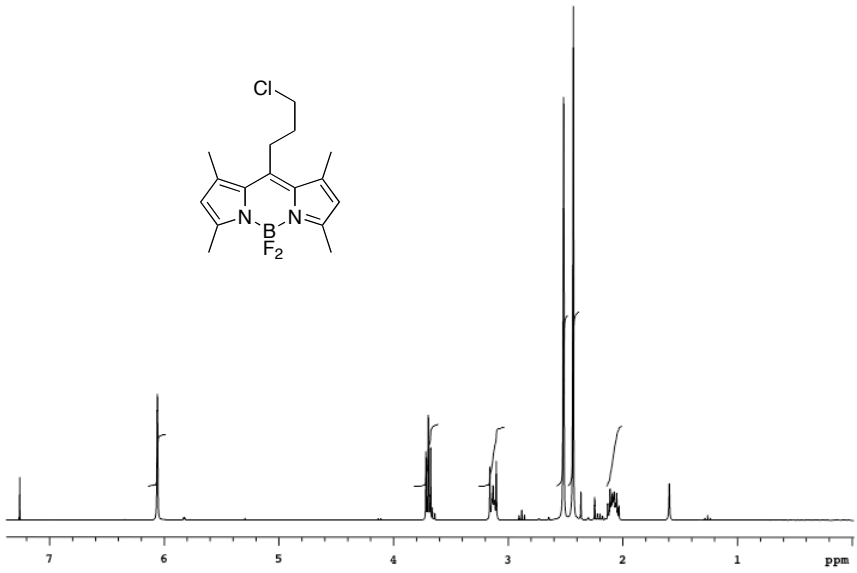
Cl
N
B
F2
N
7
6
5
4
3
2
1
ppm

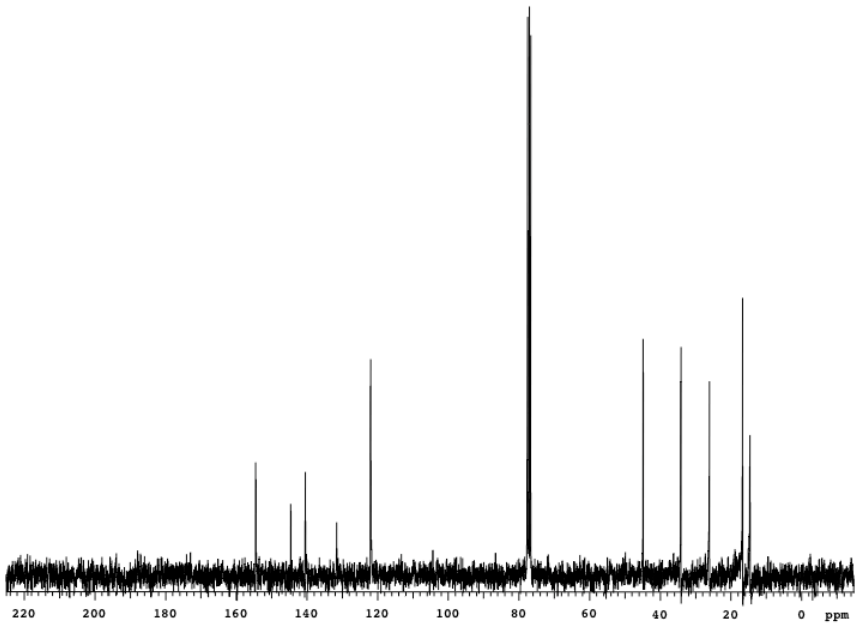
220
200
180
160
140
120
100
80
60
40
20
0
ppm

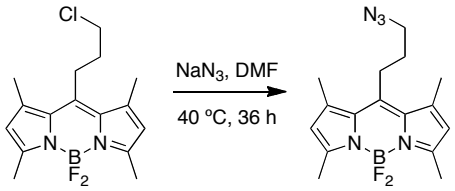

79 **80**

The a solution of **79** (200 mg, 0.62 mmol) in 12 mL of DMF was added sodium azide (80 mg, 1.2 mmol). The mixture was stirred at 40 ºC for 24 h. To the mixture was added 12 mL of water and the suspension was extracted three times with 24 mL of ethyl acetate. The combined organic layers were washed three times with 24 mL H_2O and finally 24 mL of brine. The organic layer was dried over $MgSO_4$, filtered and the solvent was removed under removed pressure to afford 200mg (99 %) of **80** as an orange powder. ^{1}H NMR (300 MHz, $CDCl_3$) δ 6.06 (s, 2H), 3.49 (t, J = 6.0 Hz, 2H), 3.03 (t, J = 8.4 Hz, 2H), 2.51 (s, 6H), 2.42 (s, 6H), 1.86 (m, 2H). ^{13}C (75 MHz, $CDCl_3$) δ 154.4, 144.7, 140.4, 131.4, 122.0, 51.6, 31.2, 25.7, 16.5, 14.6. MS (ESI) calcd for $C_{16}H_{19}BF_2N_5$ $\{M-H\}^-$ 330.17, found 330.28.

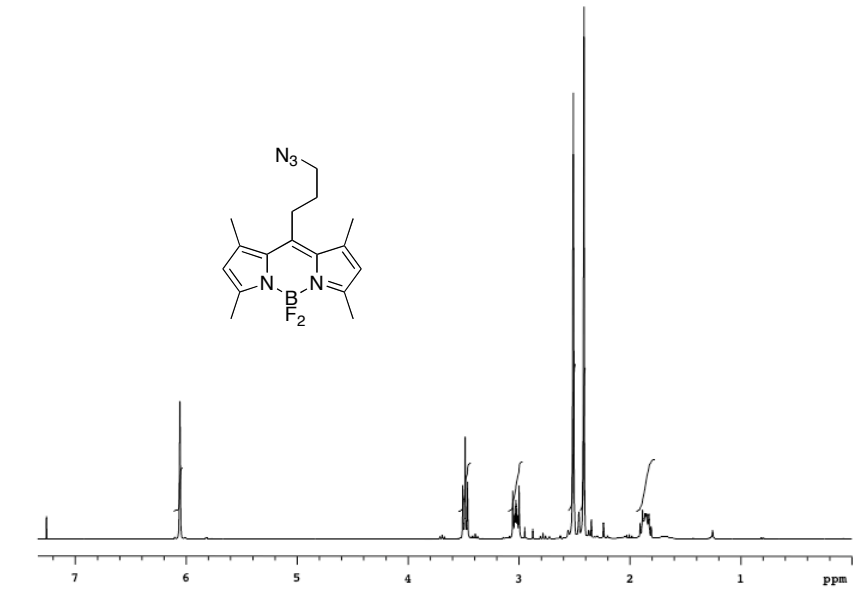
N3
N
B
N
F2
7
6
5
4
3
2
1
ppm

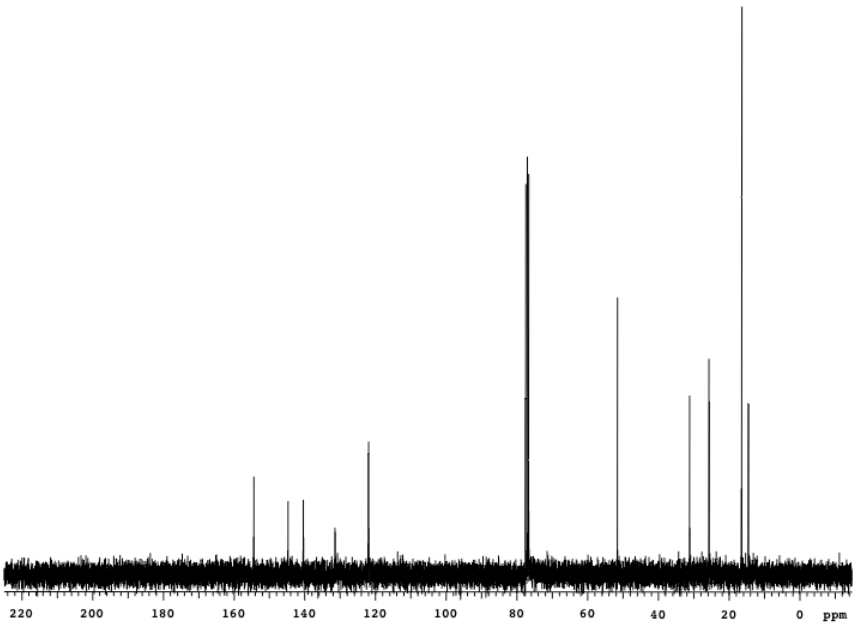
220
200
180
160
140
120
100
80
60
40
20
0
ppm

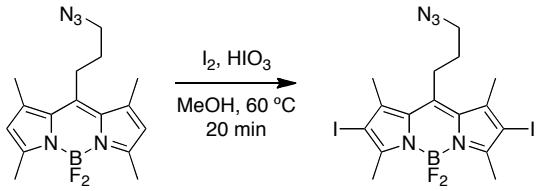

80 **81**

To a suspension of **80** (117 mg, 0.308 mmol) in 6 mL ethanol was added iodine (195 mg, 0.770 mmol) and iodic acid (114 mg, 0.647 mmol). The mixture was stirred at 60 ºC for 30 min. The mixture was cooled to 25 ºC and 12 mL of water was added. The product was extracted three times with 24 mL CH_2Cl_2. The combined organic layers were dried over $MgSO_4$, filtered, and the solvent was removed under reduced pressure. The residue was purified by flash silica chromatography eluting with 3:1 to 2:1 hexanes/CH_2Cl_2. The solvent was removed under reduced pressure to yield 117 mg (65 %) as a red powder. ^{1}H NMR (500 MHz, $CDCl_3$) δ 3.53 (t, J = 6.5 Hz, 2H), 3.11 (t, J = 8.5 Hz, 2H), 2.62 (s, 6H), 2.49 (s, 6H), 1.85 (m, 2H). ^{13}C (126 MHz, $CDCl_3$) δ 156.0, 144.5, 142.3, 131.4, 86.9, 51.5, 31.0, 26.6, 19.2, 16.3. MS (ESI) calcd for $C_{16}H_{17}BF_2I_2N_5$ $\{M\text{-}H\}^-$ 581.96, found 582.09.

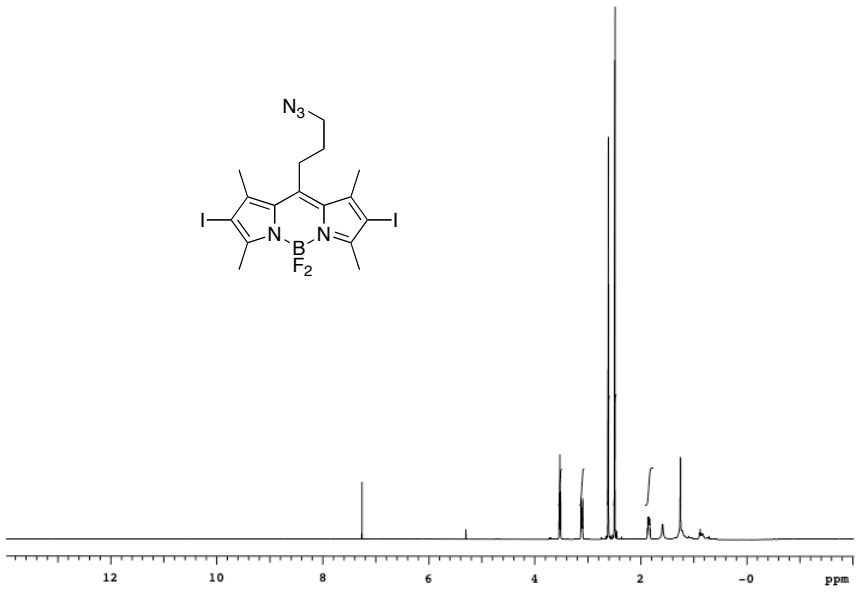
N3
I
I
N
B
F2
12
10
8
6
4
2
-0
ppm

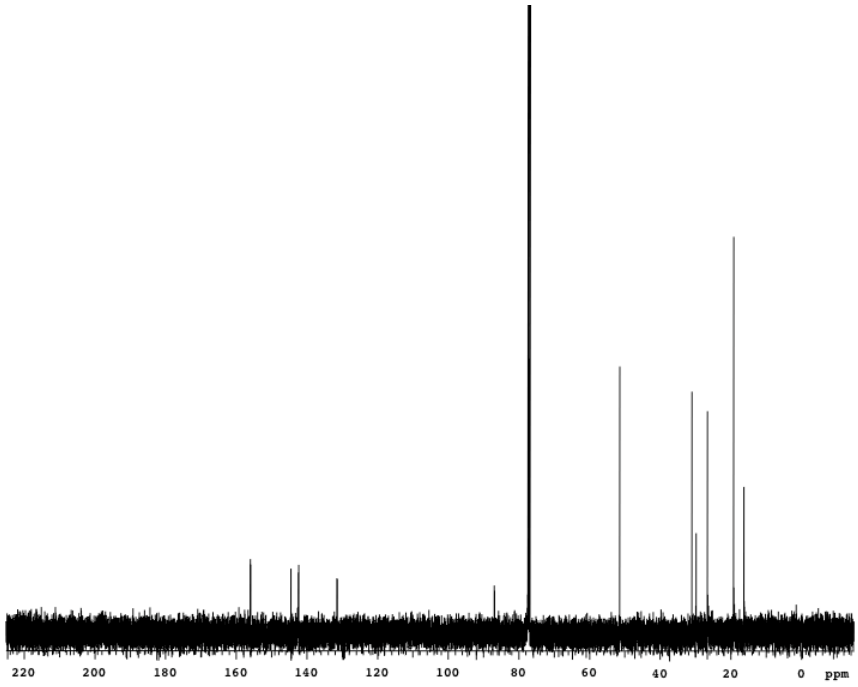
220
200
180
160
140
120
100
80
60
40
20
0
ppm

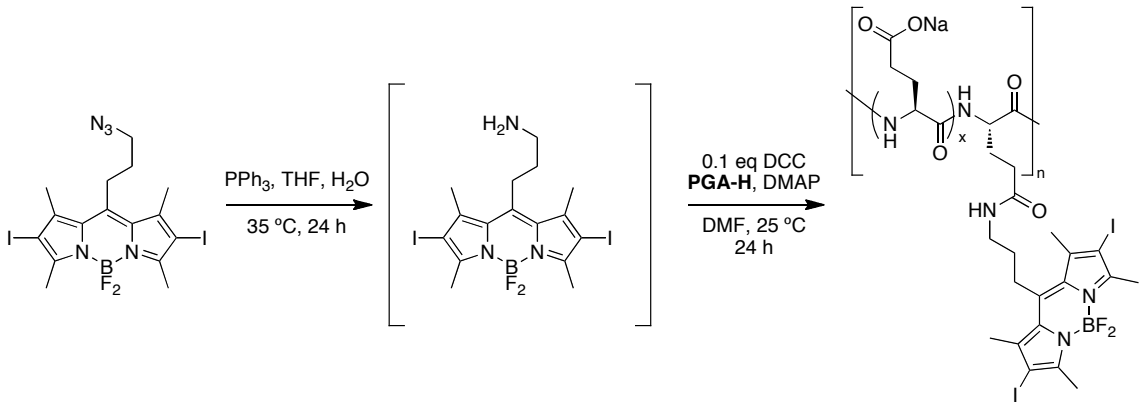

81 **78** **PGA-78**

To BODIPY **81** (100 mg, 0.17 mmol) in 2 mL of 10:1 THF/H_2O was added PPh_3 (49 mg, 0.19 mmol). The reaction was stirred at 25 ºC for 24 h and the solvent was removed under reduced pressure. Residue partially purified by flash silica chromatography eluting with 1 % to 3 % MeOH in CH_2Cl_2. **78.** MS (ESI) calcd for $C_{16}H_{20}BF_2I_2N_3Na$ $\{M+Na\}^+$ 579.97, found 579.53.

In a flame dried flask was added **PGA-H**[196] (33 mg, 0.26 mmol {-COOH}), DCC (11 mg, 0.051 mmol), DMAP (catalytic) in 7 mL of DMF. BODIPY-amine **78** (14 mg, 0.039 mmol) was added and the mixture was stirred at 25 ºC for 24 h. To the mixture was added 6 mL of 0.1 M $NaHCO_3$ and the mixture was stirred for 5 min. To the mixture was added 6 mL of $CHCl_3$. The layers were separated and the *aqueous layer* was washed twice with 6 mL of $CHCl_3$. The *aqueous layer* was dialysed in 5 L of H_2O for 5 h, changing out the water every 1.5 h. The pink solution was then lyophilized to yield 43 mg of **PGA-78** as pink fibers.

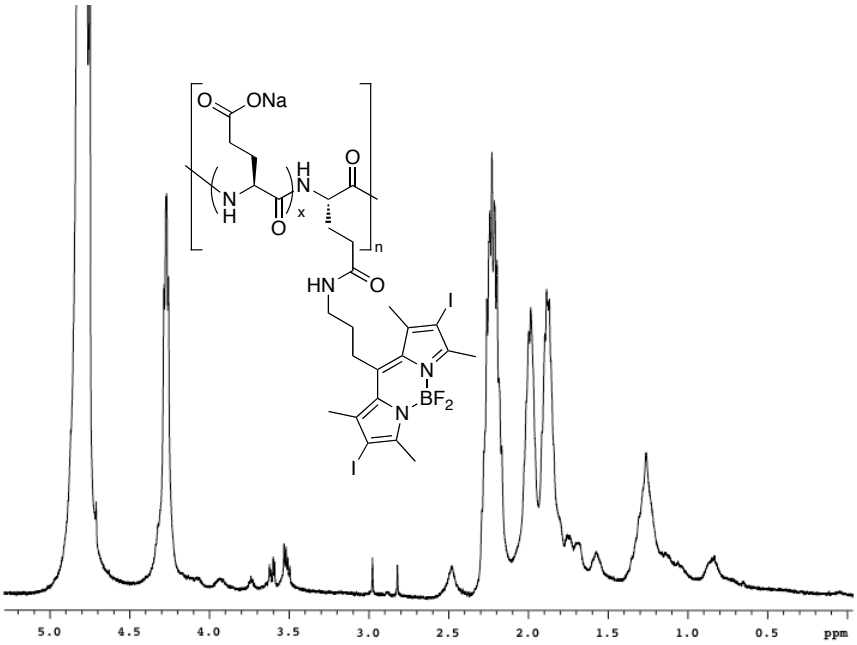
O
ONa
N
H
O
x
H
N
O
n
HN
O
I
N
BF2
N
I
5.0
4.5
4.0
3.5
3.0
2.5
2.0
1.5
1.0
0.5
ppm

Biological Assays

Cells

HL60 human promyelocytic leukemia cells were obtained from American Tissue Culture Collection (Virginia, USA) and maintained in RPMI 1640 medium supplemented with 10% FBS. HSC2 oral cavity human squamous carcinoma cells were obtained from Health Science Research Resources Bank (Japan Health Sciences Foundation, Japan). HK1 nasopharyngeal epithelial carcinoma cell-line is a gift from University of Hong Kong Culture Collection (University of Hong Kong, Hong Kong). Both cells were grown in MEM medium supplemented with 10% FBS.

Photo-induced cytotoxicity assay

Approximately 15 000 HL60 cells/well or 3 000 cells/well for HSC2 and HK1 cells in phenol red-free culture medium containing 10% fetal bovine serum were seeded in 96-well plate. HSC2 and HK1 cells were allowed to adhere overnight before test compounds were introduced. Photosensitisers stock solution (10 mM in DMSO) was diluted with medium, and concentrations varying from 0.001-100.0 μM were tested on the cells. The control wells received 0.01 % of DMSO equivalent to the highest amount of DMSO used as vehicle in the compound-treated wells. Following 2 h of treatment, cells were irradiated with a light dose of 9.6 J/cm^2 from a broad spectrum light source and were further incubated for 24 h before cell viability was assessed using MTT assay. Following incubation, 15 μl of MTT solution (5 mg/ml) was added into each well, and incubated for 4 h at 37 ºC. The medium was then removed and 100 μl of DMSO was

added to dissolve the formazan crystal formed. Absorbance, as a measure of viable cell number was read at 570 nm with OpsysMR microplate spectrometer (ThermoLabsystems, Chantilly, Virginia, USA). The dark toxicity of each photosensitiser was also determined in every experiment.

Comparative singlet-oxygen generation measurements

A 8 ml of aerated isopropanol containing 50 μM of DPBF and photosensitiser (0.5 μM or 5 μM) in a 6-well plate was irradiated at 1.6 mW/cm^2 of filtered light source of > 510 nm wavelength with a Roscolux medium yellow #10 filter (Rosco, New York, USA) at room temperature for 1 h. Aliquots of 200 μl were removed from the mixture at various fixed intervals and the absorbance was measured at 410 nm. The rate of singlet oxygen production was determined from the reduction in intensity of absorbance recorded over time. Irradiation of DPBF-isopropanol solution in the absence of photosensitiser as a negative control and solution containing methylene blue as a comparative control were also carried out. The relative singlet oxygen generation rate for each of the photosensitisers was determined by using methylene blue as a reference.

Cellular localisation

HSC2 cells grown on round glass coverslips in 12-well plate were co-incubated with 100 nM of photosensitiser together with organelle-specific fluorescence probes. The endoplasmic reticulum was labeled with 100 nM of ER-Tracker Blue-White DPX, the lysosomes were stained with 500 nM of LysoTracker Blue DND-22, and the

mitochrondria was tracked with 100 nM of Rh123 respectively for 15-30 min of incubation at room temperature. After incubation, cells were gently rinsed in PBS to remove free dyes, and the stained cells were observed using Olympus DSU spinning disk confocal microscope configured with a PlanApo ×63 oil objective (Olympus Optical Corp. Ltd., Tokyo, Japan) and iXon EM + digital camera (Andor Technology, South Windsor, Connecticut, USA). Fluorescent images of *X-Y* sections at 0.2 μm were collected sequentially using Olympus Cell^R software. Organelle-specific fluorescence probes were respectively excited at 330-385 nm wavelength to illuminate ER-tracker and LysoTracker, at 460-490 nm for Rh123 and at 520-550 nm for photosensitiser.

AnnexinV-FITC apoptosis analysis

HSC2 cells grown in 60-mm dishes at 50% confluency were treated with 0.5 μM of compound **5**. Following 2 h of incubation, cells were irradiated with 9.6 J/cm^2 of broad spectrum light. At various treatment intervals, floating cells in the medium were pooled together with the adherent cells after trypsinisation and were washed twice with cold phosphate buffered saline (PBS). The cells were resuspended with 1× binding buffer at 1×10^6 cells/mL. A 100 μL of cell suspension was transferred to a flow cytometry tube followed by 5 μL of AnnexinV-FITC and 5 μL of 200 μg/mL propidium iodide in PBS. The cells were gently mixed and incubated for 15 min at room temperature in the dark before analysed on a FACSCalibur flow cytometer equipped with 488 nm argon laser. The fluorescence data of 1×10^4 cells were collected with the FL1 detector with 530/30

band pass filter to collect Annexin-FITC fluorescence, and the FL3 detector with a 630 nm long pass filter to collect propidium iodide fluorescence.

Cell cycle analysis

HSC2 cells were treated with 0.25 μM of compound **5** and collected as above. Cells were then fixed in 70% ice-cold ethanol (v/v in PBS) overnight at 4 ºC. Following fixation, the cells were washed twice in cold PBS. The pellet was then resuspended in PBS solution containing 20 μg/ml RNase A and 1 μM SYTOX Green for 30 min. The cells were analysed on a FACSCalibur flow cytometer with 488 nm argon laser. The DNA-SYTOX Green fluorescence of 1×10^4 cells were collected with the FL1 detector with 530/30 band pass filter.

PDT on CAM vasculature

Freshly obtained fertilised chicken eggs were incubated with the narrow apex down in a 90 degree swinging incubator (Savimat MG 200, Chauffry, France) at 37 °C and 65% relative humidity. On embryo development day (EDD) three, an opening on the eggshell, about 4 mm in diameter, was bored at the apex and sealed with adhesive tape to avoid contamination and desiccation of the egg contents. The eggs were further incubated in stationary position with the apex upright until EDD-9.

Microscopic observation of CAM vasculature and the light irradiation during PDT were performed with an epifluorescence Eclipse 600 FN microscope equipped with a CFI Achromat 4×/0.1 objective (Nikon, Japan). Illumination was provided by a 100 W

mercury arc lamp. Light doses were adjusted with neutral density filters and measured with a calibrated Field-Master GS power analyser (Coherent, Santa Clara, USA). For exciting and detecting compound **48**, the microscope was equipped with a G-2A filter set (excitation, 510-560 nm) (Nikon, Japan). For detecting FITC, a B-2E/C filter set (excitation, 465-495 nm) was used (Nikon, Japan). Fluorescence images were acquired with an F-view II 12-bit monochrome Peltier-cooled digital CCD camera driven with analySIS® DOCU software from Soft Imaging System (Münster, Germany).

On EDD-9, the egg opening was extended to ~30 mm in diameter. Embryo was intravenously administered with a single bolus of 3.5 to 7 nmol/embryo of photosensitisers in dosing vehicle (CrEL 5%, EtOH 5% in saline) at the CAM main vasculature. A minute after injection, site with vessels of diameter between 5-100 μm was irradiated at light dose of 20-40 J/cm^2 filtered at 510-560 nm with an irradiation area of 0.02 cm^2 and fluence rate of 40 mW/cm^2. The site was photographed at the beginning and at the end of irradiation. Subsequently, the egg opening was sealed with parafilm and the embryo was further incubated for 24 h before assessing the PDT damage induced.

Fluorescence angiographies were performed in order to assess the PDT-induced vasculature damage. Blood vessels were perfused with 10 μl of 25 mg/ml FITC – dextran followed by injection of Indian ink into the amnion cavity for better viewing contrast. The vasculature network at the site of irradiation was illuminated by exciting the FITC at 465-495 nm on the fluorescence microscope. The vasculature network was

imaged and the damage induced by PDT was scored according to the criteria as defined by Lange et al. At least 10 embryos were assessed for each treatment group.

Design and Synthesis of Near-IR PDT Agents

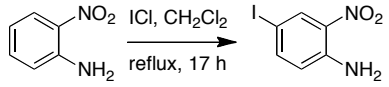

83

To 2-nitroaniline (10.0 g, 72.4 mmol) in 75 mL CH_2Cl_2 was added ICl (12.9 g, 79.6 mmol) in 10 mL CH_2Cl_2 over 30 min at 0 ºC. The reaction was stirred at 25 ºC for 24 h. The reaction was cooled to 0 ºC and *ca* 75 mL of saturated Na_2CO_3 solution was slowly added to obtain a pH of 7.0. The layers were separated and the aqueous layer was extracted three times with CH_2Cl_2. The organic layers were combined and washed twice with 75 mL of saturated Na_2CO_3, twice with 75 mL of 1 M Na_2SO_3, and 75 mL of brine. The organic layer was dried over $MgSO_4$, filtered, and the solvent was removed under reduced pressure. The brown residue was digested in methanol, filtered and washed with warm methanol to yield 8.23 g (43 %) **83** as a dark red powder. ^{1}H NMR (300 MHz, $CDCl_3$) δ 8.41 (d, J = 1.8 Hz, 1H), 7.56 (dd, J = 2.1 Hz, J = 8.7 Hz, 1H), 6.61 (d, J = 8.7 Hz, 1H), 6.12 (bs, 2H). ^{13}C (75 MHz, $CDCl_3$) δ 144.2, 143.8, 134.4, 120.7, 90.1, 76.0. HRMS (ESI) calcd for $C_6H_4IN_2O_2$ $\{M-H\}^-$ 262.9318, found 262.9323.

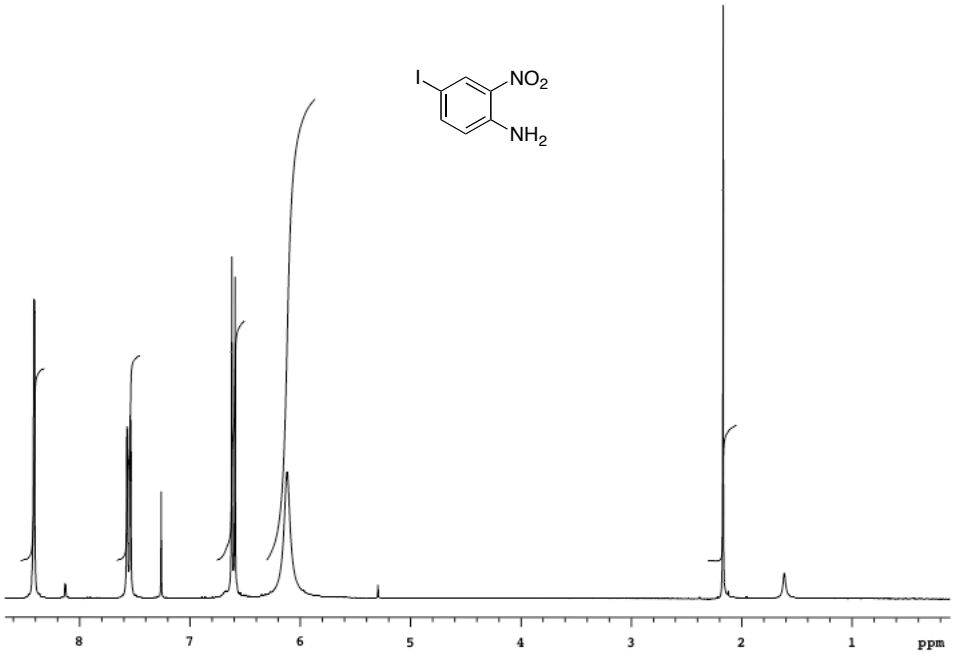
I
NO2
NH2
8
7
6
5
4
3
2
1
ppm

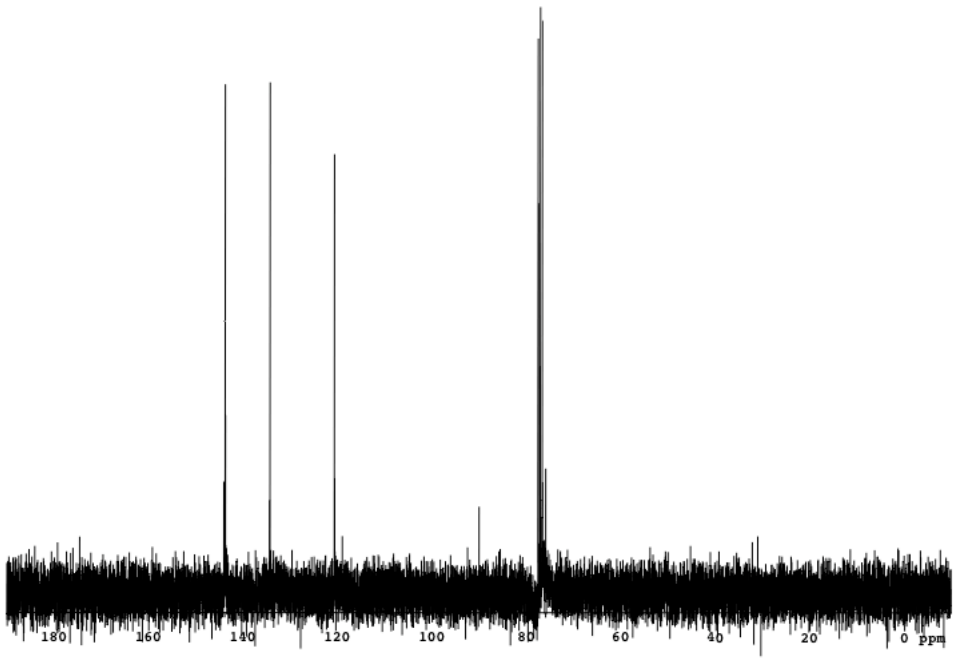
180
160
140
120
100
80
60
40
20
0 ppm

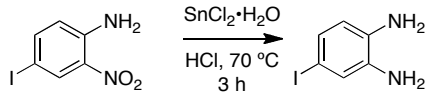

83 **84**

To a slurry of **83** (7.00 g, 26.5 mmol) in 250 mL concentrated HCl was added $SnCl_2 \bullet H_2O$ (30.0 g, 133 mmol). The reaction was stirred at reflux for 3 h. Mixture was cooled to 0 ºC and *slowly* neutralized with Na_2CO_3 (note: this has been done with both solid and concentrated Na_2CO_3 solution, with the later proving more convenient though large volumes were required). Once a basic pH was reached, the product was extracted three times with 250 mL ethyl acetate. The combined organic layers were dried over $MgSO_4$, filtered, and the solvent was removed under reduced pressure. Diamine **84** was obtained as a brown powder in sufficient purity ^{1}H NMR (300 MHz, $CDCl_3$) δ 6.92 (m, 2H), 6.39 (dd, J = 2.1 Hz, J = 7.5 Hz, 1H), 3.67 (bs, 4H). ^{13}C (75 MHz, $CDCl_3$) δ 136.3, 134.2, 128.5, 124.6, 118.3, 81.2. HRMS (ESI) calcd for $C_6H_8IN_2$ $\{M+H\}^+$ 234.9732, found 234.9745.

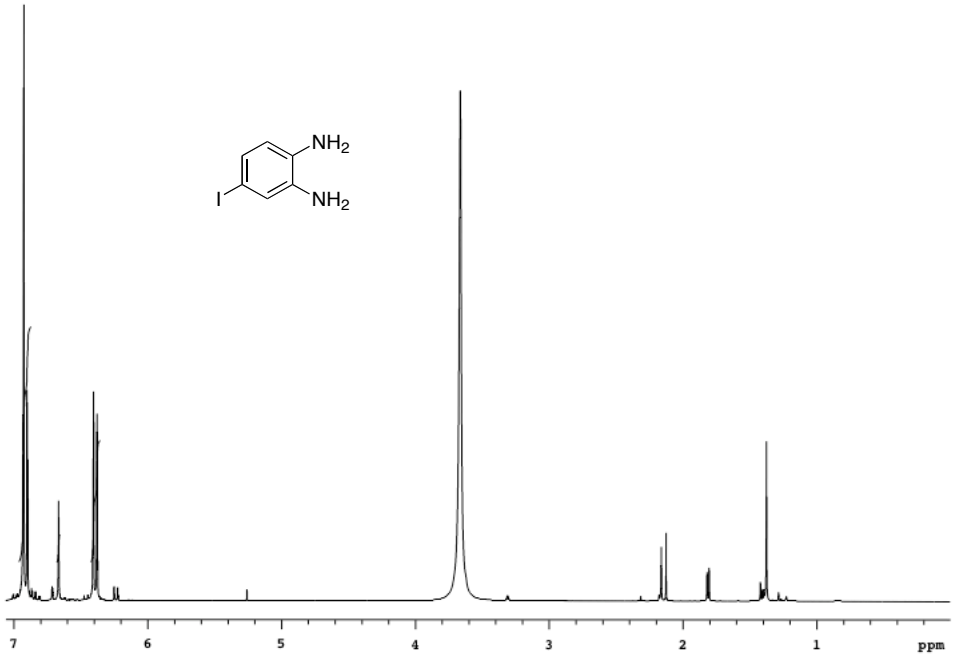
NH2
NH2
I
7
6
5
4
3
2
1
ppm

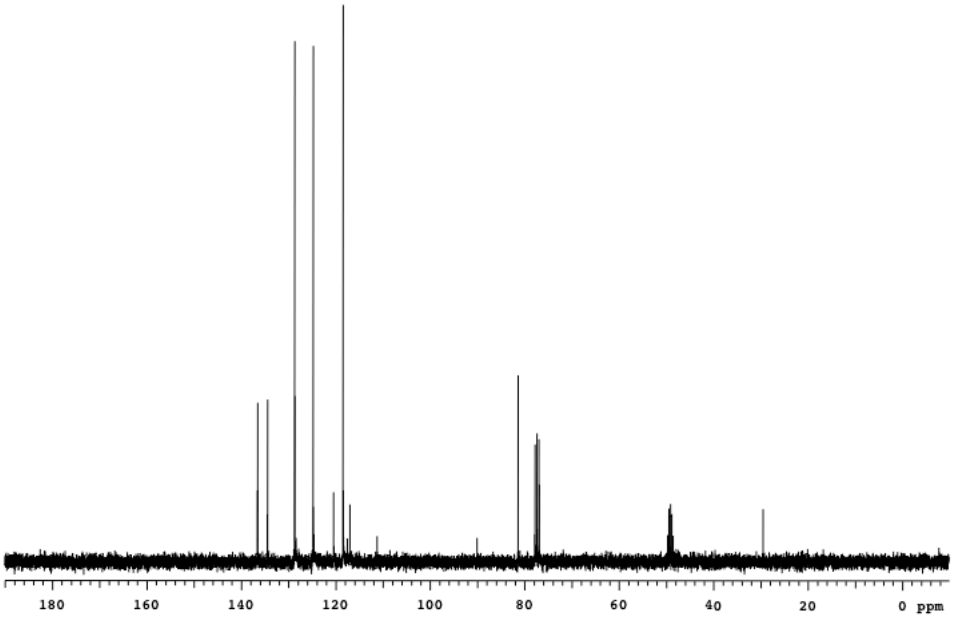
180
160
140
120
100
80
60
40
20
0 ppm

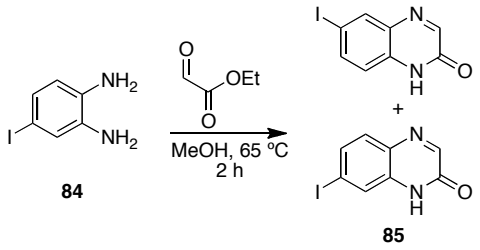

To a solution of **84** (5.92 g, 25.3 mmol) in methanol (60 mL) was added 50 % ethyl glyoxylate in toluene (5.06 mL, 25.6 mmol). The reaction was heated to reflux for 2 h. The reaction was cooled to 25 ºC. The precipitate was filtered and washed with copious amounts of methanol. Product **85** (5.8 g, 86 %) was obtained as a white powder and 1:1 regioisomeric mixture. ^{1}H NMR (300 MHz, DMSO) δ 8.17-8.16 (2 overlapping singlets, 2H), 8.10 (d, *J* = 1.8 Hz, 1H), 7.83 (dd, *J* = 1.8 Hz, *J* = 8.4 Hz, 1H), 7.64 (d, *J* = 1.8 Hz, 1H), 7.60 (dd, *J* = 1.8 Hz, *J* = 8.4 Hz, 1H), 7.52 (d, *J* = 8.4 Hz, 1H), 7.10 (d, *J* = 8.4 Hz, 1H). Compound solubility was unsuitable for routine ^{13}C analysis. HRMS (ESI) calcd for $C_8H_6IN_2O$ $\{M+H\}^+$ 272.9525, found 272.9517.

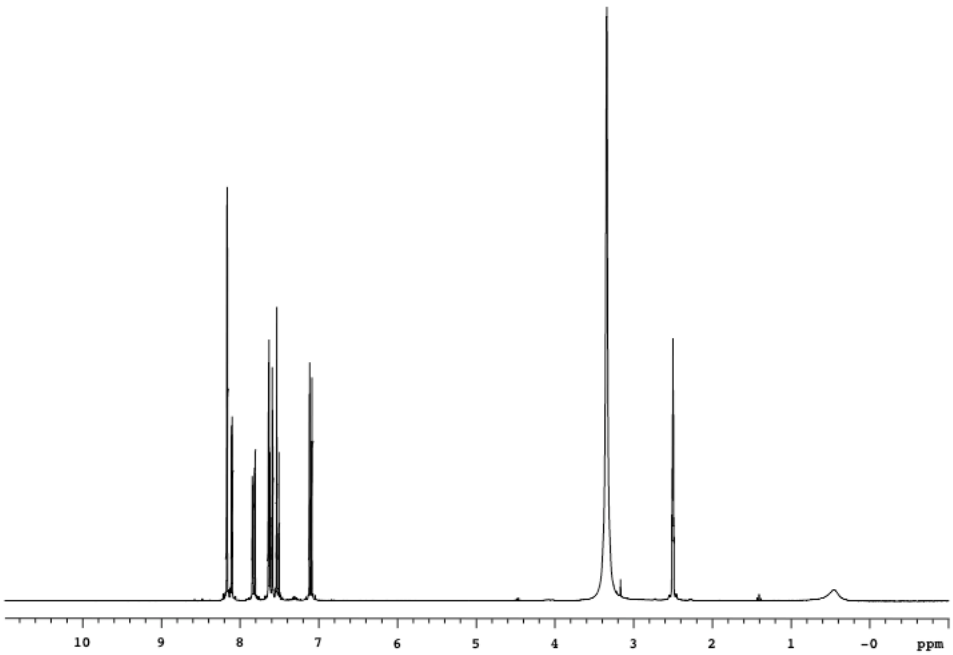
10
9
8
7
6
5
4
3
2
1
-0
ppm

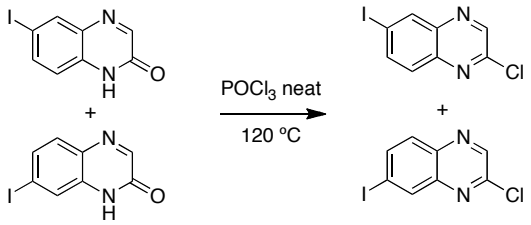

85 **86**

Quinoxalinones **85** (5.00 g, 18.4 mmol) were suspended in $POCl_3$ (75 mL) and brought to reflux. After 3 h the solution was cooled to 25 ºC and the $POCl_3$ was removed under reduced pressure. The precipitate was dissolved in 75 mL ethyl acetate and washed three times with 75 mL of water and once with 75 mL of brine. The organic layer was dried over $MgSO_4$, filtered, and the solvent was removed under reduced pressure to yield isomeric mixture **86** as a white powder (5.1 g, 96 %). (Note: white powder darkens upon standing with no noticeable drop in purity by NMR). ^{1}H NMR (300 MHz, $CDCl_3$) δ 8.78 (s, 1H), 8.75 (s, 1H), 8.49-8.40 (m, 2H), 8.05-8.00 (m, 2H), 7.81 (d, *J* = 10.5 Hz, 1H), 7.73 (d, *J* = 9.0 Hz, 1H). ^{13}C (75 MHz, $CDCl_3$) δ 148.1, 147.9, 145.0, 144.7, 142.7, 141.4, 140.7, 140.5, 139.7, 139.0, 137.7, 137.6, 129.7 (2C), 98.2, 96.6. MS (ESI) calcd for $C_8H_5ClIN_2$ $\{M+H\}^+$ 290.92, found 291.63

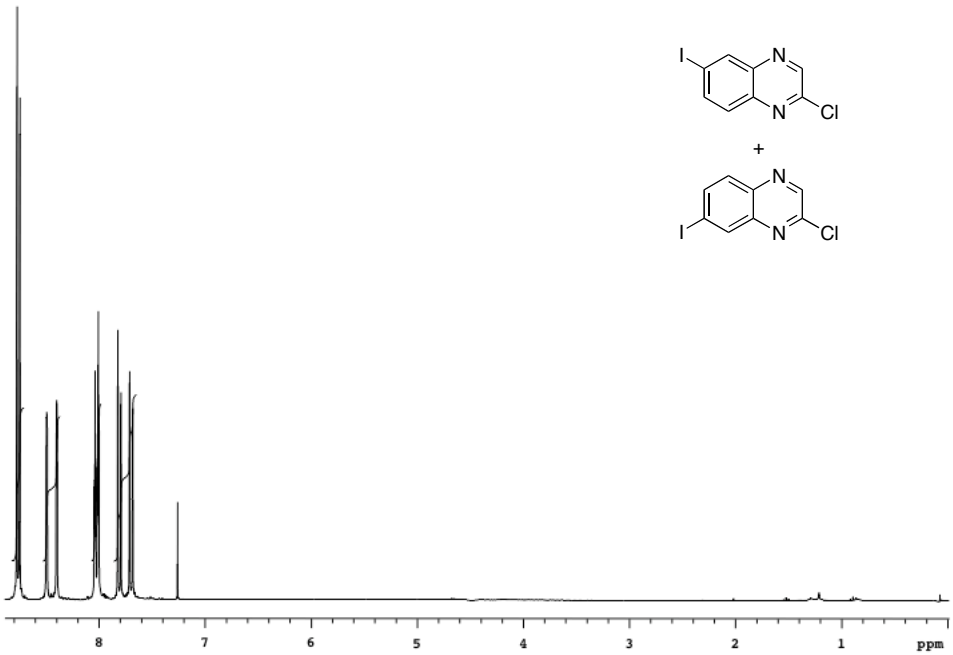
I
N
N
Cl
+
N
I
N
Cl
8
7
6
5
4
3
2
1
ppm

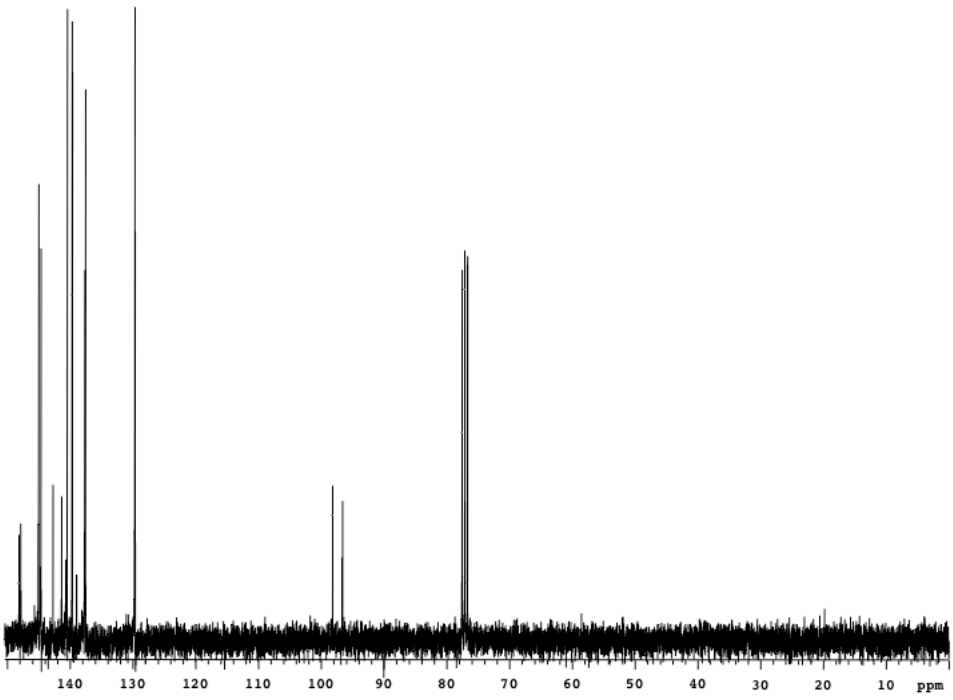
140
130
120
110
100
90
80
70
60
50
40
30
20
10
ppm

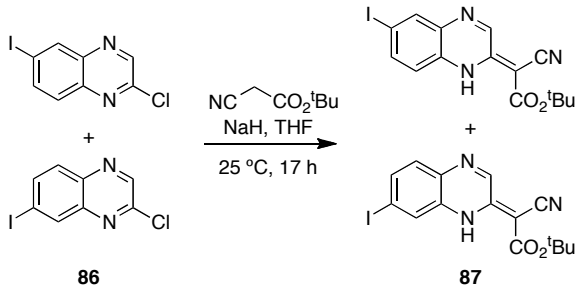

In a flame dried flask was placed sodium hydride (60 % in oil, 1.03 g, 25.8 mmol) in THF at 0 ºC. ^{t}butyl 2-cyanoacetate (2.95 mL, 20.7 mmol) was added over 30 min and stirred at 0 ºC for an additional 15 min. Mixture was warmed to 25 ºC and stirred for 30 min. In a separate flask, quinoxaline **86** (5.00 g, 17.2 mmol) was dissolved in 30 mL of THF and the quinoxaline solution was added to the cyanoacetate mixture over 15 min at 0 ºC. The mixture was warmed to 25 ºC and stirred for 17 h. The reaction was *carefully* quenched with ice water (20 mL) and then glacial acetic acid was added until a suspension formed. The product was extracted three times with 30 mL CH_2Cl_2 and the combined organic layers were washed three times with 40 mL of water and once with brine. The red solution was dried over $MgSO_4$, filtered, and the solvent was removed under reduced pressure. The orange residue was digested in *ca* 100 mL of hexanes for 1 h. The orange precipitate was filtered and washed thoroughly with hexanes to afford **87** as an orange powder (4.9 g, 72 %). ^{1}H NMR (500 MHz, $CDCl_3$) δ 13.03-13.00 (2 overlapping broad singlets, 2H), 8.80-8.79 (m, 2H), 8.21 (d, J = 2 Hz, 1H), 7.82 (dd, J = 2 Hz, J = 8.5 Hz, 1H), 7.71-7.68 (m, 2H), 7.54 (d, J = 8.5 Hz, 1H), 7.07 (d, J = 8.5 Hz, 1H, 1.56 (2 overlapping singlets, 18H). ^{13}C (126 MHz, $CDCl_3$) δ 168.9 (2C), 148.4, 147.9, 146.6, 140.5, 138.6, 136.5, 135.2, 134.9, 131.1, 129.3, 128.1, 125.4, 118.0, 116.4,

116.3, 98.0, 88.8, 83.3 (2C), 71.8 (2C), 28.4, 28.3. (Note: 1 carbon is missing). HRMS (ESI) calcd for $C_{15}H_{15}IN_3O_2$ $\{M+H\}^+$ 396.0209, found 396.0226.

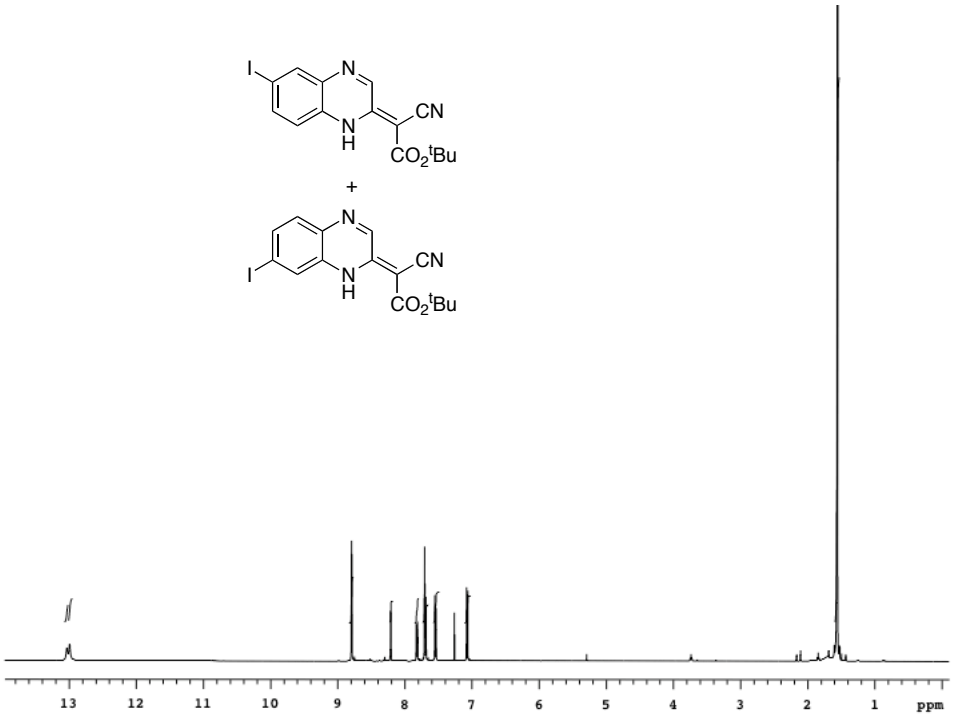
I
N
H
CN
CO2tBu
+
I
N
H
CN
CO2tBu
13
12
11
10
9
8
7
6
5
4
3
2
1
ppm

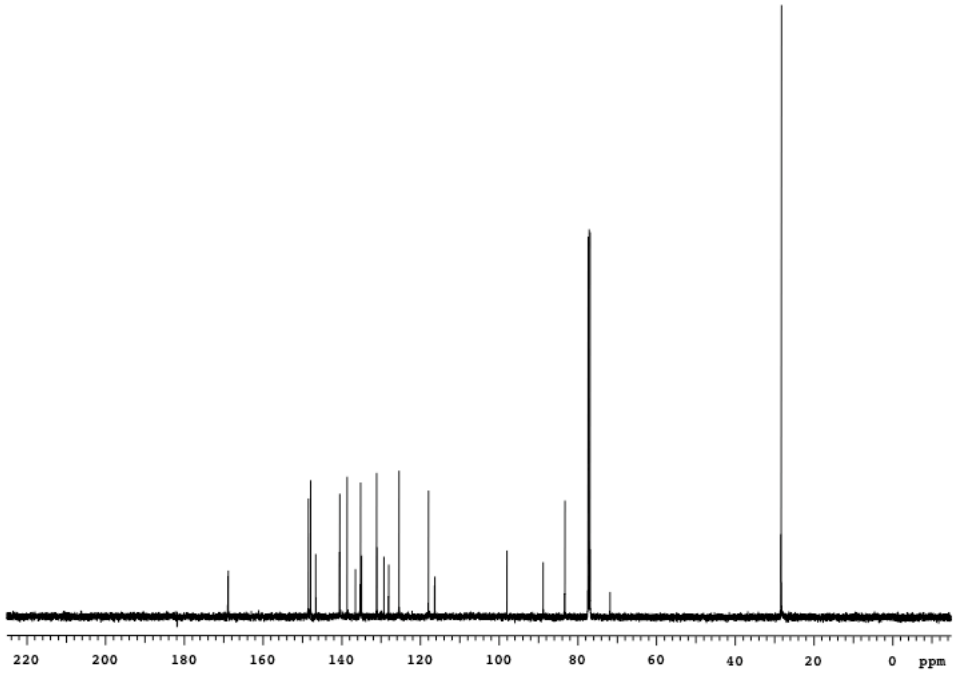

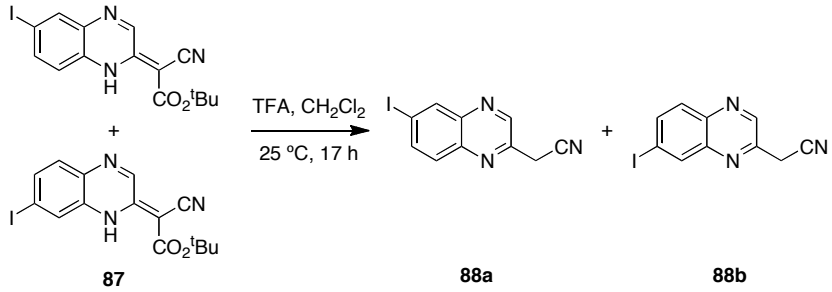

To a solution of **87** in 50 mL of CH_2Cl_2 was added trifluoroacetic acid. The reaction was stirred at 25 ºC for 17 h. The solution was washed three time with 50 mL of saturated Na_2CO_3 and once with 50 mL of brine. The organic layer was dried over $MgSO_4$, filtered, and the solvent was removed under reduced pressure. The residue was purified by flash silica chromatography eluting with 4:1 to 3:1 hexanes/ethyl acetate. The first polar compound to elute was identified as **88a** (692 mg, 21 %) and the second as **88b** (650 mg, 19 %).

88a. ^{1}H NMR (500 MHz, $CDCl_3$) δ 8.91 (s, 1H), 8.57 (d, *J* = 2 Hz, 1H), 8.07 (dd, *J* = 2 Hz, *J* = 9 Hz, 1H), 7.81 (d, *J* = 9 Hz, 1H), 4.15 (s, 2H). HRMS (ESI) calcd for $C_{10}H_7IN_3$ $\{M+H\}^+$ 295.9685, found 295.9677.

88b. ^{1}H NMR (500 MHz, $CDCl_3$) δ 8.93 (s, 1H), 8.53 (d, *J* = 1.5 Hz, 1H), 8.05 (dd, *J* = 2 Hz, *J* = 8.5 Hz, 1H), 7.84 (d, *J* = 8.5 Hz, 1H), 4.16 (s, 2H).

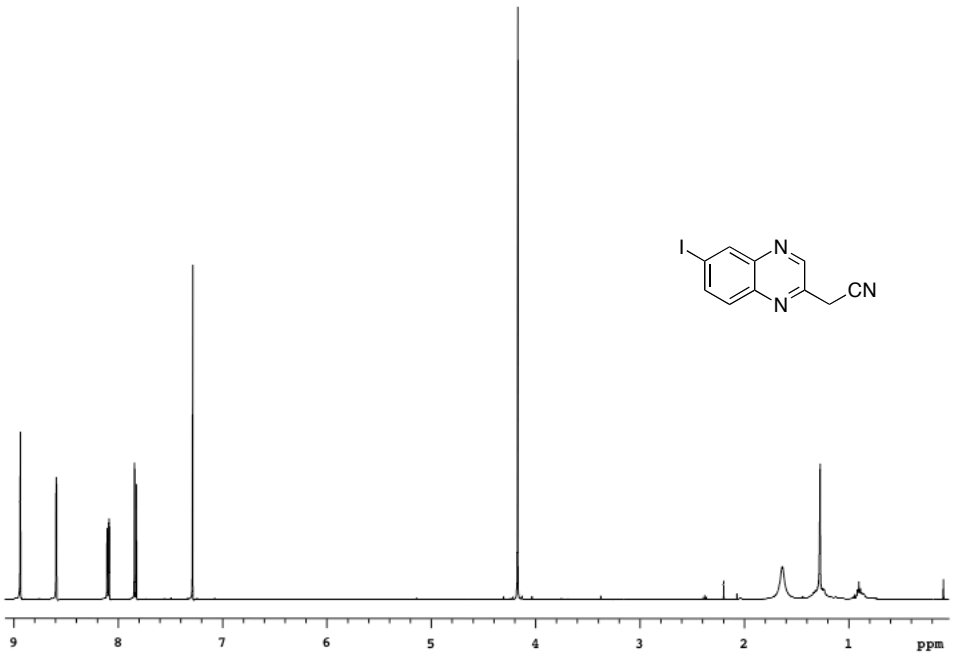

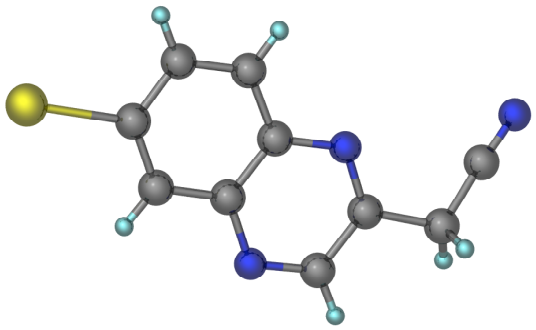

X-ray structure of **88a**.

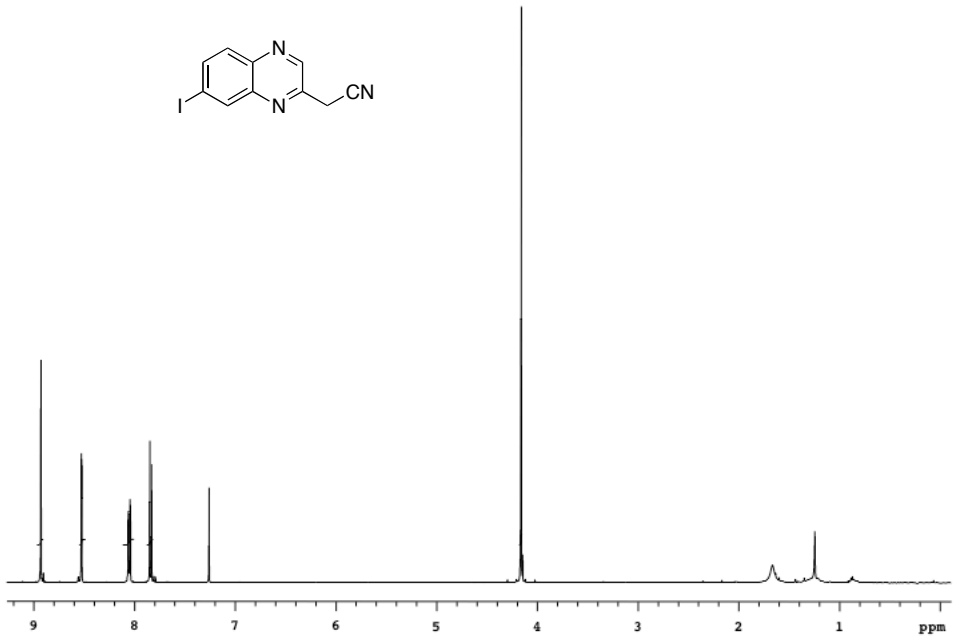
N
N
I
CN
9
8
7
6
5
4
3
2
1
ppm

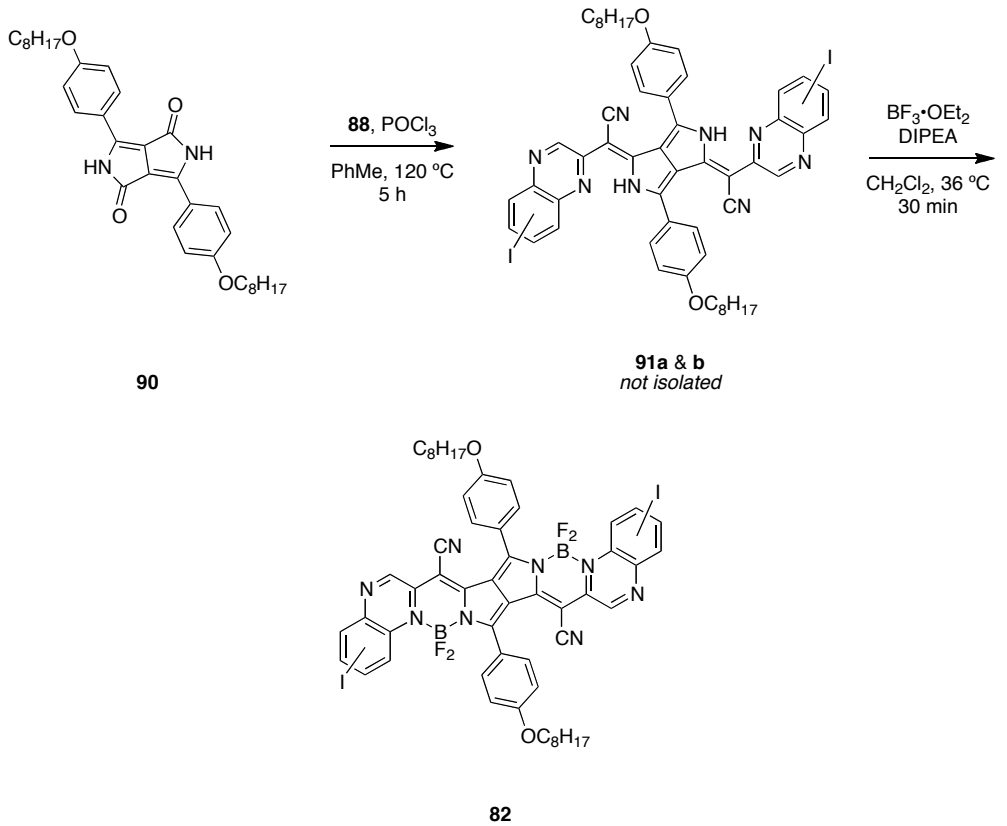

90

91a & **b**
not isolated

82

To a suspension of DPP dye **90** (222 mg, 0.407) was added either isomer of **88** (300 mg, 1.02 mmol) and $POCl_3$ (303 μL, 3.25 mmol). The mixture was refluxed for 5 h. The mixture was cooled to 25 ºC and the solvent was removed under reduced pressure. The residue was digested in methanol, filtered, and washed with copious amounts of methanol to yield **91** in sufficient purity for chelation step, 336 mg of semi-pure **91a** was obtained and 315 mg of **91b**. **91a.** MS (ESI) calcd for $C_{54}H_{51}I_2N_8O_2$ $\{M\text{-}H\}^-$ 1097.22, found 1097.41.

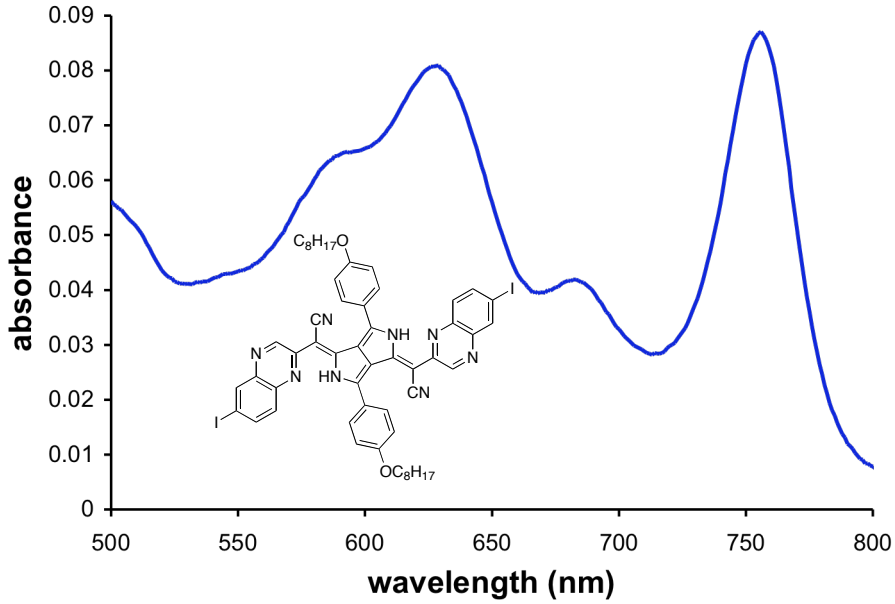

To either isomer of **91** dissolved in CH_2Cl_2 was added Hunig's base. The mixture was stirred at 25 ºC for 30 min and BF_3•OEt_2 was added. The reaction was refluxed for 30 min and then cooled to 25 ºC. To the mixture was added 10 mL of water and the mixture was stirred vigorously for 10 min. The layers were separated and the organic layer was washed twice with 10 mL water and once with 10 mL brine. The organic layer was dried over $MgSO_4$, filtered, and the solvent was removed under reduced pressure. The residue was purified by flash silica chromatography eluting with CH_2Cl_2 and the solvent was removed under reduced pressure to yield **82** as a reddish shiny residue, in the case of **82a** 11 mg (3 % - 2 steps) was isolated, and **82b** 12 mg (3 % - 2 steps). It is noteworthy that solubility of the products is poor, especially for **82b** to the point that routine ^{1}H was arduous (see text). HPLC analysis performed on silica column, 4.6 x 150 mm, eleuting with CH_2Cl_2 at 1 mL/min. **82a.** ^{1}H NMR (500 MHz, $CDCl_3$) δ 9.27 (s, 2H), 8.53 (m, 2H), 8.32 (d, *J* = 9.5 Hz, 2H), 8.02 (m, 2H), 7.71-7.64 (m, 4H),

7.11-7.00 (m, 6H), 3.99 (t, J = 6.5 Hz, 4H), 1.78 (q, J = 8.0 Hz, 4H), 1.57-1.25 (m, 20H), 0.88 (t, J = 7.0 Hz, 6H). HRMS (MALDI) calcd for $C_{54}H_{51}B_2F_4I_2N_8O_2$ $\{M+H\}^+$ 1195.2357, found 1195.2338.

82b. HRMS (MALDI) calcd for $C_{54}H_{51}B_2F_4I_2N_8O_2$ $\{M+H\}^+$ 1195.2357, found 1195.2369.

82a

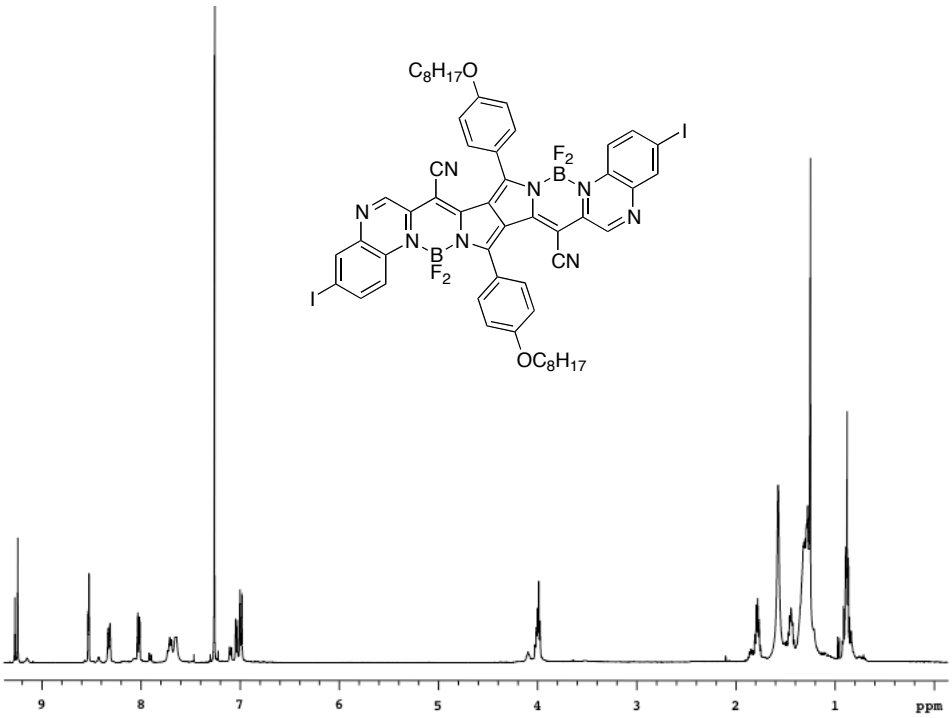
C8H17O
CN
F2
B
N
I
CN
OC8H17
9
8
7
6
5
4
3
2
1
ppm

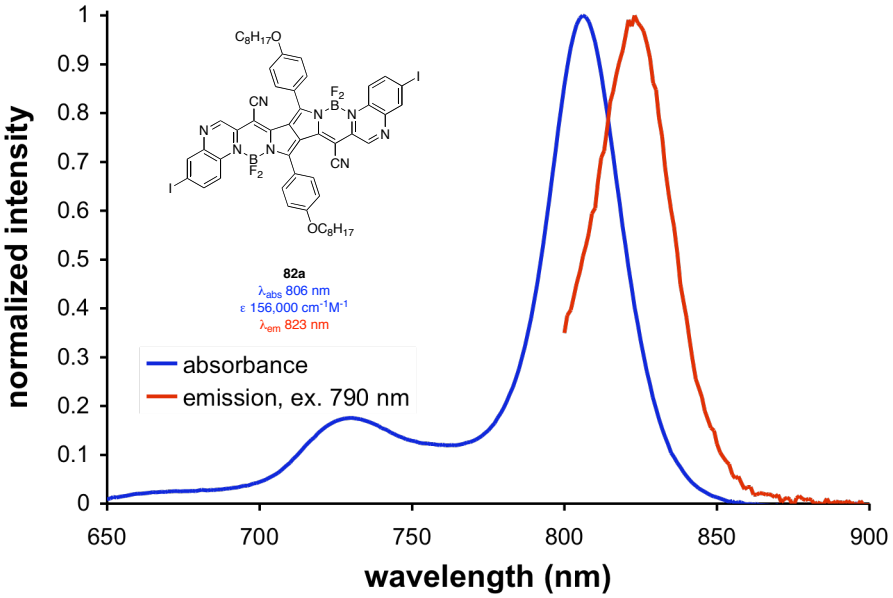
normalized intensity
wavelength (nm)
82a
λabs 806 nm
ε 156,000 cm-1M-1
λem 823 nm
absorbance
emission, ex. 790 nm

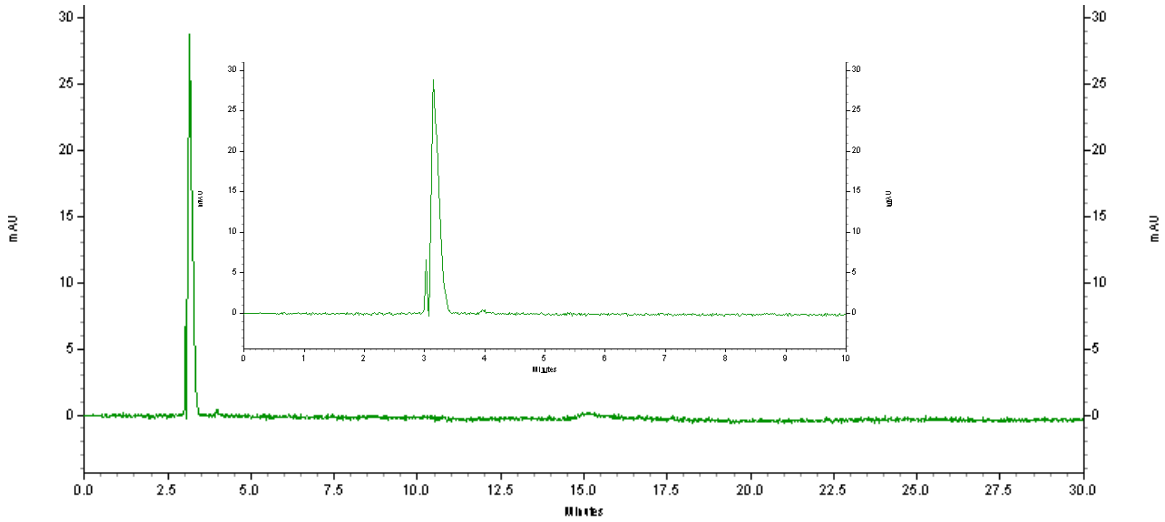
mAU
Minutes
0.0
2.5
5.0
7.5
10.0
12.5
15.0
17.5
20.0
22.5
25.0
27.5
30.0

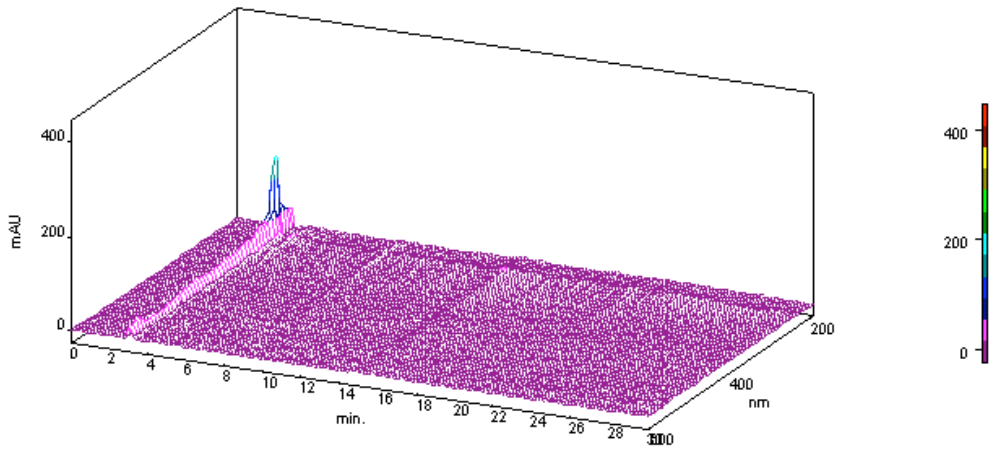
mAU
400
200
0
min.
nm
200
400

82b

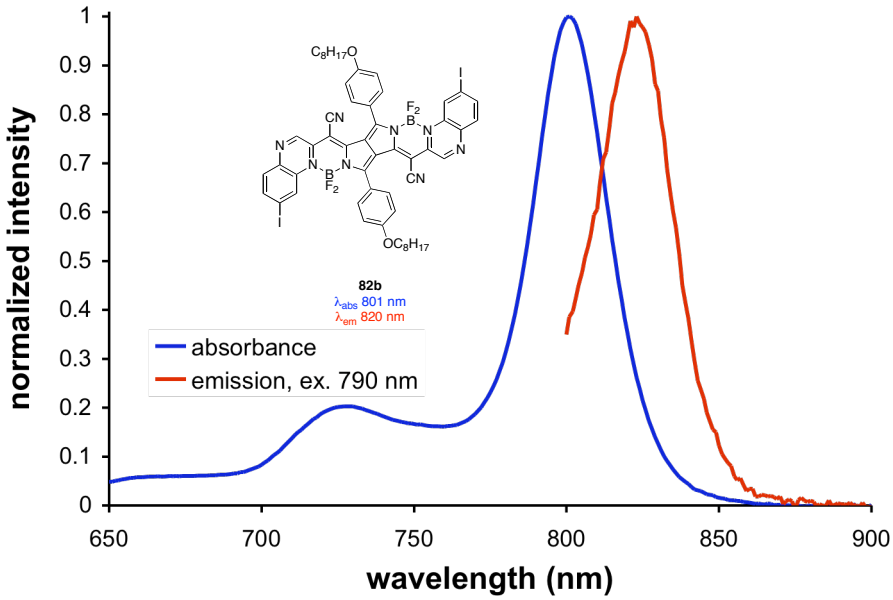
normalized intensity
wavelength (nm)
absorbance
emission, ex. 790 nm
82b
λabs 801 nm
λem 820 nm

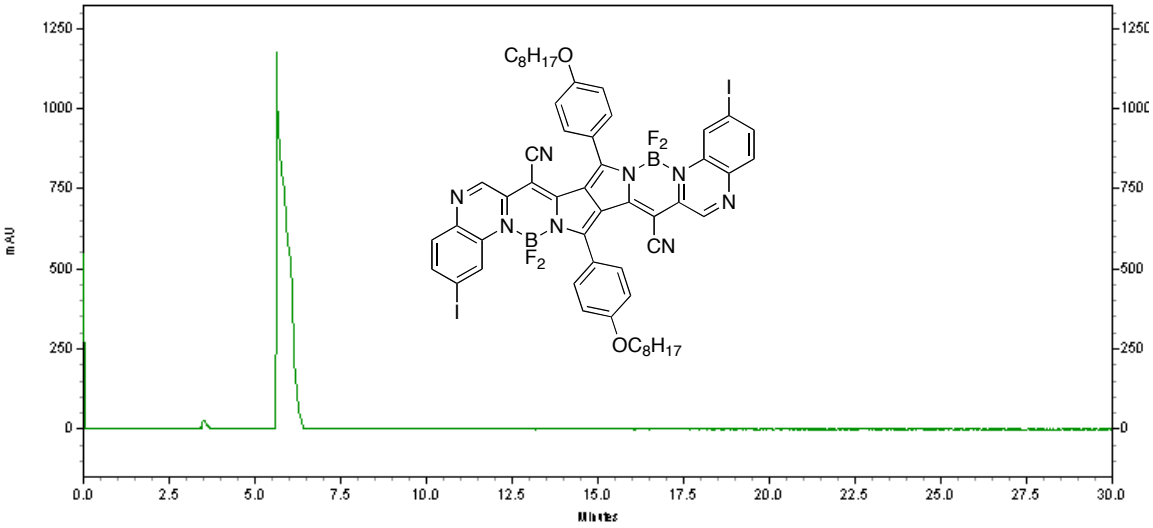
mAU
Minutes

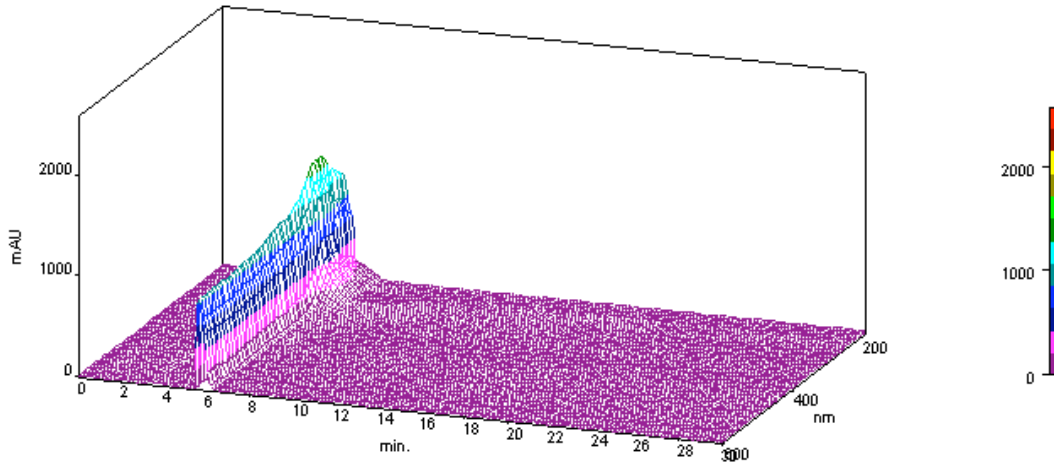
mAU
2000
1000
0
0
2
4
6
8
10
12
14
16
18
20
22
24
26
28
min.
200
400
nm
2000
1000
0

VITA

Name: Cliferson Thivierge

Address: Department of Chemistry
c/o Dr. Kevin Burgess
Texas A&M University
College Station, TX 77843-3255

Email Address: clifman@gmail.com

Education: Ph.D., Chemistry, Texas A&M University, 2011
B.S., Chemistry, Florida Atlantic University, 2005